Long Discontinuous Carbon Fibre/Polypropylene Composites for High Volume Automotive Applications

David Burn

MEng. (Hons.)

Thesis submitted to the University of Nottingham

for the degree of Doctor of Philosophy

September 2015

Abstract

The volume of fibre reinforced composites is increasing within the automotive industry, as stringent emissions legislation and consumer demands for improved fuel economy are encouraging manufacturers to reduce vehicular mass. Moreover, the falling cost of carbon fibre has meant that these composites are now being considered for semi-structural and structural components for medium-volume (+50,000ppa) applications in Euro Market Segments E and F (Jaguar XF, BMW 7 Series, Mercedes S-Class).

The use of thermoplastic matrices with carbon fibre enables cycle times of less than one minute, creating opportunities for high volume manufacture of high specific stiffness components. However, the interfacial adhesion between these materials has been shown to be poor. This thesis seeks to identify whether polypropylene combined with long, discontinuous carbon fibres at high volume fractions, are suitable for high volume, semi-structural applications within the automotive industry. In particular, fibres recovered using two different recycling methods have been considered, as a potential route for reducing future material costs.

Interfacial characterisation has been performed using the microbond method to investigate the quality of adhesion between the fibre and matrix, where the effects of sizing removal and introduction of a coupling agent have been considered. Fibre surface topology and chemistry have been examined to interpret data collected from interfacial testing, in addition to fibre strength measurements to assess the validity of the microbond method for high interface strength systems. A tow coating rig has been developed to produce partially pre-impregnated carbon fibre/polypropylene tows. The continuous coated tow has been chopped and processed into random fibre composites using non-isothermal compression moulding, and mechanical properties of the moulded panels have been characterised.

The interface strength between sized and desized (pseudo-recycled) carbon fibre and unmodified polypropylene has been found to be poor. A 295% increase in interfacial shear strength (IFSS) is observed with the addition of 2wt.% maleic anhydride to the polypropylene, between the matrix and epoxy-sized carbon fibres. An increase of up to 353% in IFSS is observed for the desized fibres. These improvements can be attributed

to chemical bonding as a result of esterification of hydroxyl groups on the carbon fibre surface, with anhydride functionalities of the coupling agent. Additionally, interactions occur between the nitrogen containing groups on the desized fibre surface and the anhydride carbonyl groups in the matrix. Surface roughness is not found to significantly contribute to interface strength. Good interfacial bonding has therefore been observed between polypropylene and sized carbon fibre due to the addition of a coupling agent at 2wt.%, which allows the low cost polymer to be combined with commercially available fibre.

Long, discontinuous carbon fibre/polypropylene composites have been characterised in this study at volume fractions that have not previously been reported. Mechanical property characterisation has shown linear increases in stiffness with increasing fibre volume fraction. The specific stiffness of carbon fibre/polypropylene ($0.45V_f$) is comparable to the carbon fibre/epoxy benchmark. A plateau is observed for both strength and impact strength above volume fractions of 0.25, due to increased void content. The specific strength of the long fibre carbon fibre/polypropylene system can be improved further to a certain extent, by optimising the processing conditions to minimise trapped air.

Dedicated to Valerie Barber

Acknowledgements

Contents

1.   Introduction

The use of carbon fibre composites (CFRPs) in high performance automotive applications is well established, however in high volume vehicles, composites are primarily limited to injection moulded parts that have short fibre architectures restricting their use to non-structural applications. The market for automotive CFRPs is expanding rapidly, where the compound annual growth rate is reported to be 30.6%, with an estimated value of approximately £65 million by 2017 [1]. A major driver for these changes is strict emissions targets in Europe and fuel economy targets in the US, where automotive manufacturers are looking to save up to 100kg of weight year on year. The vehicle Body-In-White (BIW) is where most savings are projected to be made [2] with current target weight reduction strategies for some major original equipment manufacturers (OEMs) presented in Figure 1-1. Clearly there are opportunities for lightweight materials that can provide sufficient properties to be used for semi-structural and structural components. Replacing traditional components with lightweight CFRP has however been limited due to a number of barriers such as the high cost of carbon fibre, uncertainty of manufacturing processes, long cycle times, disposal of End-of-Life (EoL) parts and lack of experience with composites.
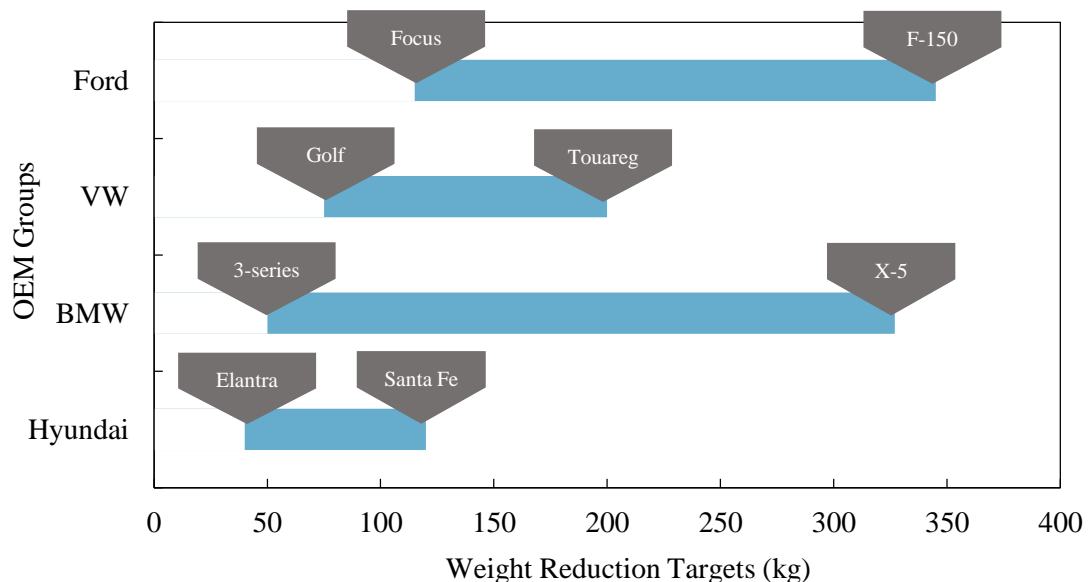
Figure 1-1 - Example of OEM weight reduction targets for vehicles across respective fleets (reproduced from Frost and Sullivan [2])

1.1   The 'Low Carbon Vehicle'

The idea of a low carbon vehicle (currently defined as a vehicle that emits less than 100g CO_2/km) has become widely adopted of late, as increased use of fossil fuels has become a concern due to critical levels of CO_2 being reached in the atmosphere, driving global warming. This coupled with industrialisation of developing countries with high population densities means that emissions must be reduced.

In the UK, The Climate Change Act (2008) was implemented to reduce all CO_2 emissions by 80% of the levels reported for the 90's, by 2050, of which the automotive sector accounts for 24% [3]. A significant amount of investment is being put into achieving these targets, where this year, the government have committed £500 million to the research and development of ultra-low emission vehicles [4]. Moreover, the European Parliament have introduced regulations (EC 443/2009) [5] to set emissions performance standards for new passenger cars to be less than 130g/km CO_2 in 2015, and to have maximum average fleet emissions of 100g/km by 2020 - only two model development cycles from now. According to recent statistics (Jan – Mar 2015 [6]), average CO_2 emissions of cars registered for the first time in the UK was 123.1g/km, marking a significant improvement from 2001 where it was approximately 180g/km [4].

Recent reductions in CO_2 emissions can be attributed to diesel and hybrid-electric vehicles gaining market share, but also more efficient petrol variants through low displacement, direct injection, supercharged engines. Despite the fact that emissions have become an increasingly pertinent issue, the last 25 years has seen total car weight increase as consumers drive expectation for higher levels of safety, comfort and technology as well as expecting more economical vehicles, without sacrificing build quality. Figure 1-2 shows the relationship between vehicle weight and fuel efficiency. A clear trend is seen between fuel efficiency and vehicle weight, where diesels currently perform higher than petrol engines (hybrids have not been included).

Given the trends seen between CO_2 emissions, fuel efficiency and vehicle weight, it is evident that both consumer and legislation requirements could be met by reducing vehicle mass. A reduction in weight of 100kg corresponds to a reduction in fuel

consumption of approximately 0.3 – 0.5 litres/100km and a reduction in CO_2 emissions of 8 – 11g/km [7]. As a consequence of reducing vehicle mass, engine, transmission and brake size can also be reduced and therefore provide improvements in fuel economy, as well as responsiveness under acceleration, braking and cornering.
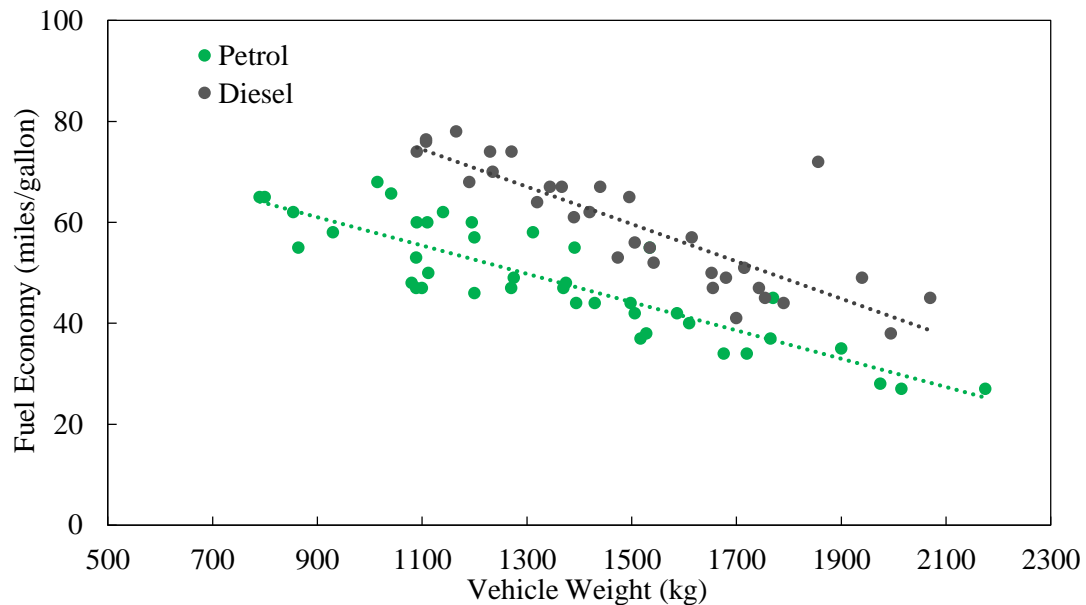
Figure 1-2 - Fuel economy as a function of vehicular weight for common new petrol and diesel vehicles (compiled from manufacturers data available through parkers.co.uk)

1.2   Polymer Composites

Polymer composites offer the potential for weight saving as they exhibit high specific properties (mechanical performance per unit weight) compared to other engineering materials, as well as offering other advantages such as greater design flexibility and parts integration, reduced tooling and assembly costs, enhanced corrosion resistance and higher specific energy absorption [8]. A composite material is composed of two primary constituents; the reinforcing phase, which for polymer composites is typically glass, carbon or natural fibres, and the matrix which serves to hold the reinforcement in place as well as distributing load [9]. A variety of materials are available for composite manufacture (Figure 1-3) and control over the combination of the constituents allows tailoring of the mechanical properties, and therefore component optimisation for specific loading scenarios.

Polymer Composites

Polymer matrices are divided into two groups; thermosetting or thermoplastic. Thermosetting polymers are manufactured through curing which creates a 3-dimensional cross-linked structure, where polymer chains are linked to each other through chemical bonds. Thermoplastic polymers are composed of linear polymer chains that are held together by weak intermolecular forces, which allow the polymers to be reshaped at elevated temperatures. Due to the cross-linked nature of thermosetting polymers, they offer excellent thermal properties, high dimensional stability and excellent surface finish characteristics. However the cross-linked structure means that these polymers cannot be recycled easily, as unlike thermoplastics, they cannot be remoulded at elevated temperatures. Thermoplastic polymers therefore have a significant advantage over thermosetting matrices as they can be re-melted and reprocessed several times, and do not require curing, enabling them to be processed much faster (10's of seconds rather than 10's of minutes).

Composite Structure
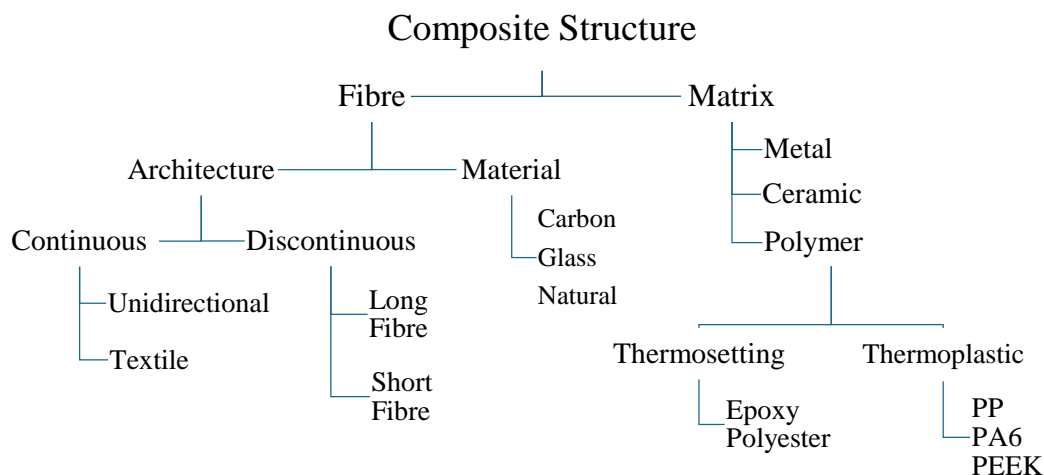
Figure 1-3 - Structure of composite materials

To fully realise the properties of the reinforcement, there must be strong (chemical) bonding to the matrix, which allows optimum transfer of load between the fibres. The mechanical performance of a composite is therefore largely dictated by the quality of the interface between fibre and matrix. During manufacture of high performance fibres, such as carbon and glass, the fibre is coated with a sizing agent that is specifically designed to optimise this interface as well as protect the brittle fibres from damage during subsequent handling and processing [10]. CFRPs are primarily used in

applications that require significant weight savings or increased stiffness, as they are 30% lighter than glass fibres and exhibit 4 times the stiffness [9]. It is reported that an optimised continuous carbon fibre composites (CFRP) can achieve a 75% mass reduction over steel, 40% over aluminium and 50-60% over glass fibre composites [11].

1.3 Carbon Fibre Composites in the Automotive Industry

Carbon fibre composites are an excellent candidate for vehicular mass reduction, however they are generally confined to low volume, high performance applications in the automotive industry as the matrix material requires long curing cycles and the fibre costs are prohibitive. Advances in thermosetting resin cure systems has meant that the cycle time for CFRPs has been greatly reduced, with BMW producing medium volume CFRP intensive body structures for their i3 and i8 vehicles. High-Pressure Resin Transfer Moulding (HP-RTM) is used to produce CFRP parts for both vehicles, where cycle times are limited by polymer cure (5 minutes) and demoulding (10 minutes). Production rates are currently 36,500 per annum for i3 vehicles [12].

High performance CFRPs primarily use thermosetting matrices, which have significantly lower viscosities than thermoplastic matrices, allowing better penetration into the compacted fibre bundles and enhanced fibre encapsulation. Nevertheless, increasing interest has grown for high performance carbon fibre/thermoplastic composite materials (CFRTPs) due to vastly reduced cycle times, opening up possibilities for high volume manufacture. Moreover CFRTPs exhibit higher chemical resistance and impact properties as well as enhanced recyclability and 'infinite' shelf life over CFRPs [13]. Cycle times of less than 1 minute have been reported [14] (where less than 8 minutes is considered state of the art for thermosetting composites [15]) and although capital investment costs are increased due to higher processing temperatures and pressures required, automotive OEMs are primarily concerned with volume part price.

The demand for high volume carbon fibre parts has been demonstrated by the number of automotive OEMs that have formed partnerships with companies that have composite expertise. One of the more notable examples is the partnership between

General Motors (GM) and Teijin, developing Teijin's Sereebo CFRTPs for use in high volume automotive applications. The partnership formed in 2011 with an electric passenger cell concept, announcing that they were developing CFRTP parts by compression moulding with a 60 second cycle time. Table 1-1 presents the extent to which OEMs and carbon fibre manufacturers are looking to bring carbon fibre composites into the high volume automotive industry.

The primary focus of these collaborations is to overcome barriers that are currently limiting the use of carbon fibre composites. The main challenge to the adoption of carbon fibre composites is cost, where CFRP parts are approximately 10 times more expensive to produce than comparable steel parts [8]. The cost of carbon fibre is continually decreasing as the use of alternative precursors is explored and demand for carbon fibre increases, it is estimated that a cost of approximately £7/kg [16] for carbon fibre will fully enable its use as a replacement for existing materials.

Collaborators	Notes	Date
BMW, SGL	Stake holding to manufacture carbon fibre and carbon fibre fabrics for the i3 and i8	Oct 09
Toyota, Toray, Fuji	Collaboration to supply Toyota and Fuji Heavy with CF for automotive hood and roof applications	Oct 10
Daimler, Toray	Manufacture and marketing of CFRP using Toray's High cycle RTM	Jan 11
Audi, Voith	Development and automated production of composite materials for automotive use	Feb 11
Audi, Quickstep	Develop manufacturing solutions for the cost effective volume production of automotive composite parts	Nov 11
GM, Teijin	Develop carbon fibre composite technologies for potential use in high-volume GM vehicles, using carbon fibre reinforced thermoplastics	Dec 11
Toray, Gordon Murry Design	Develop mass production techniques for thermoplastic CFRP in the vehicle main structure	Feb 12
Ford, DowAksa	Establishment of an economic source of automotive grade carbon fibre and develop component manufacturing methods for high-volume automotive applications	Mar 12
Zoltek, Magna	Partnership to develop low-cost carbon fibre sheet moulding compound (SMC) for the automotive industry	Mar 12
Cytec , Jaguar Land Rover	Develop designs, materials and manufacturing concepts for the cost-effective use of composites materials for automotive structures	Aug 12
BASF, Tencate	Development, production and commercialization of thermoplastic composite materials suitable for high-volume vehicle production	Oct 12
BASF, SGL	Development of reactive polyamide system and tailored sizing for automotive applications	Oct 12
Faurecia, Fraunhofer ICT	Engineering and prototypes for advanced industrial processes for composites for applications in the automotive field	Nov 12
Dieffenbacher, KrausseMaffei, Audi	High Pressure RTM parts for structural automotive components	Apr 13

Henkel, Benteler	Collaboration to design and manufacture composite leaf springs for Volvo XC90	Aug 13
Toray, Zoltek	Toray completes purchase of Zoltek - manufacturer of large tow carbon fibre for automotive industry	Mar 14
Cytec, EPL	Develop automated manufacturing processes for low cost hybrid, structural thermoplastic composite automotive components	Apr 14
Toyota, AZL	Development of production technologies for lightweight components	Jun 14
SABIC, Kringlan	Development of first carbon fibre thermoplastic composite wheel	Jun 14
Cytec, Dralon	Establish the production of large tow industrial-grade carbon fibre for automotive applications	Jul 14
Tesla, GS Caltex	GS Caltex to supply Tesla Motors with long carbon fibre thermoplastic material	Aug 14
AML, Gurit	Gurit to supply carbon fibre based exterior Class-A automotive body panels	Jan 15
Ricardo, AEC	Development of composite body, chassis and other structural components to the automotive industry	Feb 15
Hexion, Sogefi	Design and manufacture of a composite suspension coil for Audi	Mar 15

Table 1-1 - List of notable collaborations aiming to introduce CFRP into the high volume automotive market

1.4   Discontinuous Fibre Composites

The use of discontinuous fibre composites (DFCs) has the potential to lead to significant cost savings over continuous fibre composite (CFC) parts as automated manufacturing methods can be more easily employed, eliminating the need for labour-intensive production often associated with CFCs. Moreover, high levels of automation lead to more consistent part quality and reduced cycle times, therefore lending these composites to high volume manufacture processes.

Discontinuous fibre composites (DFCs) have been used in the automotive industry for decades, most commonly in the form of sheet moulding compounds (SMCs) and injection moulded components. SMCs enable higher volume fractions (and therefore mechanical properties) to be used over injection moulded compounds as they have a heterogeneous mesoscale architecture where single fibres are bundled together into 'tows', which consist of several thousand fibres (Figure 1-4). Despite having higher mechanical properties than injection moulded composites, glass fibre SMCs are primarily used for cosmetic applications as they tend to be heavily filled with calcium carbonate to achieve 'Class A' surface finishes and allow high levels of flow in the mould. Nevertheless, these materials have been popular for automotive manufacturers as they offer lightweighting potential, excellent surface finish and corrosion resistance

whilst maintaining total cost parity with metals that are currently used [17]. Carbon fibre SMCs have been developed for structural automotive applications, but due to high fibre volume fractions and low filler content require high mould coverage levels due to limited flow. These composites still allow much higher part complexity than CFCs, for example Lamborghini utilise carbon fibre SMCs for manufacture of their inner monocoque chassis, and suspension control arms of the Sesto Elemento [18], achieving part complexities that cannot be realised with continuous fibre composites .
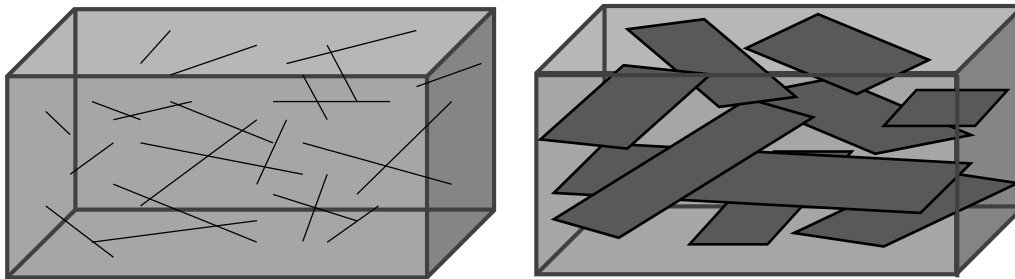
Figure 1-4 – Microscale architecture single fibre composite (left) and mesoscale architecture composite (right), where each tow (represented by the shapes inside the cube) consists of thousands of filaments, greatly increasing packing efficiency.

Glass mat thermoplastics (GMTs), which consist of chopped glass in a polypropylene matrix, are the thermoplastic equivalent to SMCs and are also widely used in the automotive industry for parts ranging from front end modules, underbody shields and instrument-panel carriers. More recently in-line compounding systems that integrate compounding and moulding processes together to produce long fibre thermoplastics (LFTs) have gained interest. This process allows the moulder to combine fibre, matrix (usually glass fibre and polypropylene) and any additives at the press, which are mixed and fed as a shot into compression moulding equipment. Through careful design of the extruder used to mix the compound, fibre lengths of up to 25mm can be maintained [19], greatly increasing mechanical performance.

Currently in the automotive industry, thermoplastics are primarily coupled with glass fibre and as a result, applications are limited by stiffness requirements. Carbon fibres have been trialled for LFT processes with polyamide 6 [20] and although significant improvements were made over glass fibre composites produced in the same way, high levels of fibre breakage occurred due to the lower failure strain compared to glass,

reducing mechanical performance. A gap in mechanical performance therefore exists between thermoplastic DFCs and CFCs. High performance thermosetting DFCs such as HexMC offer mechanical properties within this region (see Appendix B), however the material cost is significantly higher than other DFCs and cure cycles are typically 4 – 8 minutes, longer than required for mass manufacture.

The necessity for short cycle times and increased demand for recyclability due to government legislation on the disposal of end-of-life automotive parts has prompted significant interest in thermoplastic composite materials. Combined with discontinuous fibres, complex 3D geometries can be realised as well as enabling automated processing, greatly reducing costs associated with the manufacture of CFCs.

1.5   Theme of work

The research presented here has been carried out as part of the 'Towards Affordable closed-loop Recyclable Future Low Carbon Vehicle' project, a collaborative EPSRC funded programme between 8 UK universities, with over 40 personnel involved. It is envisioned that the future low carbon vehicle will be a mass-optimised multi-material concept. This part of the project is focussed on advanced polymer matrix composites for lightweight vehicle structures.

The use of carbon fibre allows access to mechanical properties that no other commercially available fibre can achieve. Significant interest in this fibre has been shown by the automotive industry and increased demand as well as alternative precursor development is gradually reducing the cost to a point where it can be economically used for high volume manufacture. Polypropylene was chosen as the matrix material as it is the most commonly used thermoplastic in the automotive industry, accounting for 32% of all automotive polymers and therefore has the necessary infrastructure in place for high volume manufacture [21]. The primary concern with carbon fibre/polypropylene is that the interface strength between the fibre and matrix is weak, however the widespread use of polypropylene in glass fibre composites has demonstrated that excellent bonding can be achieved. Recent studies by Wong et al. [22] investigating short recycled carbon fibres and polypropylene has indicated that the interface can be significantly increased with the addition of a coupling

agent, but it is unclear how these materials will interact at high fibre loadings required for enhanced mechanical performance.

The aim of this thesis is to investigate whether low cost polypropylene is suitable for use with discontinuous carbon fibre at high volume fractions. The intended application is for semi-structural automotive components, where there is an opportunity for materials that possess mechanical properties between short fibre composites, used for non-structural applications, and continuous fibre composites, used for structural applications.

To achieve mechanical properties suitable for semi-structural parts, a heterogeneous architecture is required where fibres are bundled together into tows to improve packing and therefore access higher volume fractions. A carbon fibre tow coating line was developed (Section 3.3) to enable polypropylene to be coated on continuous fibre tows, as appropriate commercial materials were not available at the volume fractions required. During coating the tow was spread by rollers to ensure intimate contact between the fibre and matrix to aid subsequent processing. Adjustments in coating parameters allowed the fibre volume fraction to be varied as well as the potential to introduce a coupling agent to improve the bond between fibre and matrix. The interfacial strength was investigated at the microscale using the microbond test method (Chapter 4), where the aim was to determine the effect of coupling mechanisms between the fibre and matrix on interface strength. Fibre chemistry and topology were subsequently characterised (Chapter 5) to explain differences in interface strength observed during microscale testing.

Finally, the microscale work was correlated with mechanical testing at the macroscale (Chapter 6), with investigation into the effect of micromechanical bonding on failure mechanisms in discontinuous fibre thermoplastic composites. Mechanical data was compared to a number of benchmarks to assess the performance and suitability of these materials for semi-structural automotive applications. The findings of this thesis will add to the knowledge of low cost, high performance thermoplastic composites for automotive applications and demonstrate that these materials can be part of an optimised multi-material vehicle in the future.

The combination of mesoscale carbon fibre architecture and thermoplastic matrix at volume fractions appropriate for semi-structural automotive applications has not been reported previously. Moreover, the use of polypropylene as a matrix material for carbon fibre has not been widely investigated due to the disparity in cost, with research currently limited to short recycled fibres. This study therefore investigates the ultimate performance this matrix can achieve.

2. Literature Review

2.1 Discontinuous Fibre Composites

The mechanical properties of discontinuous fibre composites (DFC) are controlled by the physical properties of the constituent materials and also their distribution within the composite. In terms of the material architecture, parameters such as volume fraction, fibre length and tow size dictate the ultimate composite properties and therefore require optimisation. Fibre volume fraction has arguably the most significant influence on mechanical performance, but is limited by the packing efficiency of the fibres, which is a function of fibre dimensions and orientation [23], demonstrated in Figure 2-1. Knowledge of interactions between these parameters is therefore essential for attaining the maximum mechanical performance. A review of some of the more critical parameters is given here.
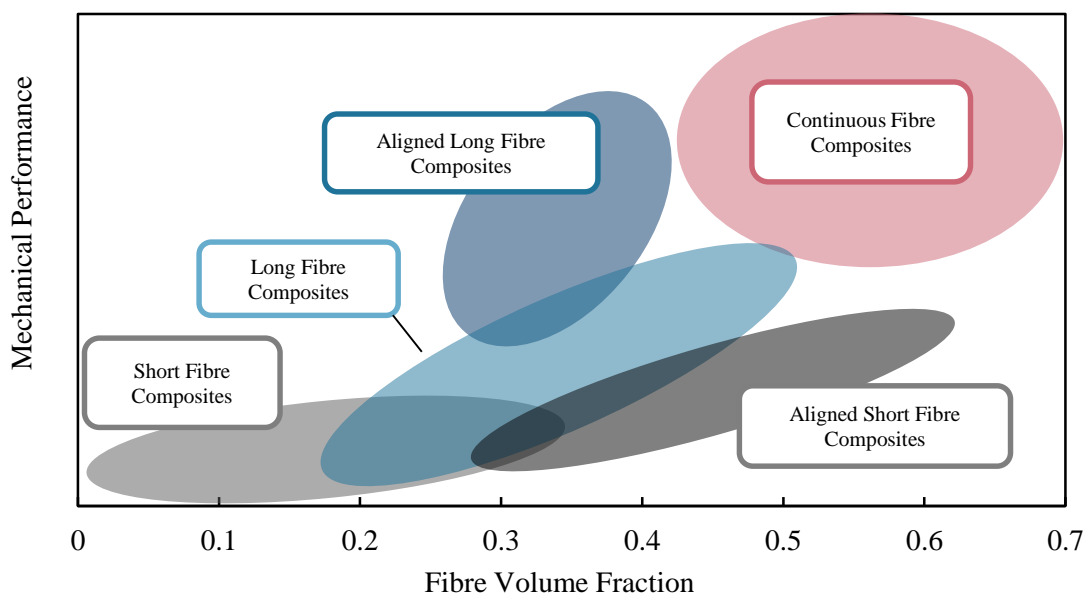
Figure 2-1 - Mechanical performance as a function of fibre volume fraction for different DFC architectures, with quasi-isotropic woven composites included for reference. Balloons represent approximate levels of performance for each composite architecture, based on references in Appendix F

2.1.1 Random Fibre Composites

For most DFCs the fibres are randomly oriented within the matrix to provide an isotropic material. Some work has focussed on investigating alignment of discontinuous fibres to achieve higher volume fractions and therefore realise increased

performance [24]–[28], but good fibre alignment is very difficult to achieve at high manufacturing rates and therefore was not considered during this work. For random composites the fibre orientation can be divided into two architectures, 2D random and 3D random, shown schematically in Figure 2-2. For 3D random architectures, primarily associated with injection moulding manufacturing routes, the fibres are oriented in the x-y-z plane and have fibre lengths less than the thickness of the composite. These composites comprise shorter fibres ($< 5mm$ [29]) and lower volume fractions ($< 0.2V_f$ [9]) than other discontinuous fibre composites, in order to maintain a suitably low viscosity to aid processing of the injected material.
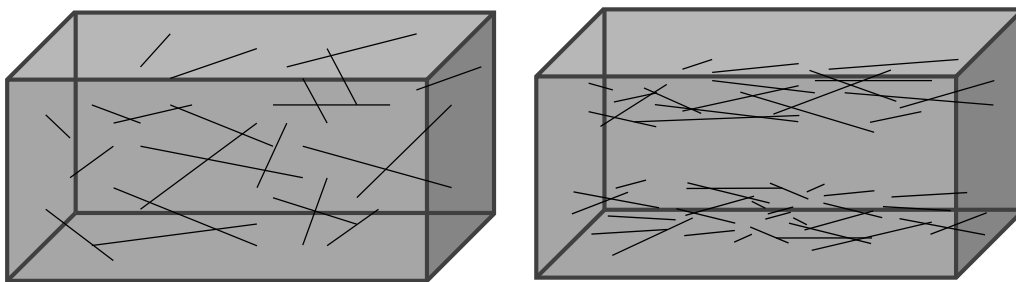
Figure 2-2 - Single fibre random architectures, 3-dimensional - where fibres lie in the x-y-z plane and (right) 2-dimensional - where fibres lie in the x-y plane

For 2D random architectures, the fibres are oriented in the x-y plane and the fibre length and volume fraction are only limited by the physical dimensions of the part and stacking of the fibres. Common examples of 2D architectures are Sheet Moulding Compounds (SMC) and Glass Mat Thermoplastics (GMT), available commercially in sheets, where charges are cut from the material and stacked in a compression moulding tool to form the part.

2.1.2 Fibre Volume Fraction

For a unidirectional continuous fibre composite, the fibre volume fraction (V_f) can theoretically be as high as 0.9, however fibre packing is often irregular and as such the practical limit is approximately 0.7 [9]. For random DFCs, achievable volume fractions are limited to approximately 0.3 for microscale (single fibre) architectures [30], where single filaments are randomly distributed within the composite, and 0.5 for mesoscale (bundled fibres) architectures [31], where unidirectional fibres are tightly packed into bundles that are randomly distributed within the composite. The achievable volume

fraction therefore limits the application of the material, and as such restricts these microscale architecture composites to non-structural applications. For use as semi-structural components, new materials must be able to compete with high performance discontinuous GMTs and SMCs, where mesoscale architectures are required to obtain high volume fractions necessary for enhanced mechanical performance.

For random fibre composites, tensile modulus has been experimentally shown to increase linearly with volume fraction up to approximately 0.5, with good agreement observed between analytical predictions and modulus for microscale architectures [32]–[34]. Tensile strength displays a similar trend, however at higher volume fractions the trend is non-linear, due to a number of mechanisms including; higher void content [35], fibre breakage, increased stress concentrations as a result of more fibre ends [36] and reduced stress transfer efficiency due to small fibre spacing [23]. The onset of this deviation is dependent on both the fibre and matrix properties, for example the strength of glass fibre/polypropylene has been shown to plateau at approximately 0.2 - 0.25Vf [35], [36], whereas for glass fibre/epoxy, strength has been shown to increase linearly with volume fraction up to 0.5V_f [37], after which it becomes non-linear due to the mechanisms described above. This suggests that the higher viscosity of thermoplastic matrices may reduce the maximum achievable volume fraction further, with fibre infiltration issues becoming more apparent at higher volume fractions. Carbon fibres appear to be less susceptible to this phenomena as a plateau in strength was not observed for carbon fibre/polypropylene [38] or carbon fibre /polyamide 12 [34], which indicates that more optimised packing of smaller diameter fibres may reduce defects seen at higher volume fractions.

One of the main advantages of thermoplastics over thermosets is that they behave in a ductile manner and exhibit superior energy absorption properties allowing progressive failure compared to the catastrophic failure shown by brittle materials. However, introduction of fibres into a thermoplastic matrix restricts polymer chain mobility, and sites of stress concentration are increased, resulting in decreased strain to failure. Reductions in strain-to-failure of 25% have been reported for fibre volume fractions of 0.08, and up to 50% for volume fractions of 0.19 in glass fibre/polypropylene [35]. Greater reductions have been observed for more brittle fibres, where an increase of fibre

volume fraction from 0.02 – 0.04 for carbon fibre/polypropylene resulted in a 92% reduction in strain to failure [39].

Despite large reductions in strain-to-failure as a consequence of increased fibre loading, impact strength has been reported to increase linearly with increasing volume fraction [40],[41], however some reports for glass fibre/polypropylene have shown that deviations are experienced at higher volume fractions, which are attributed to similar mechanisms reported for strength [36], [38]. Compared to continuous fibre composites, DFCs are able to absorb more energy due to complex crack paths caused by fibres arranged in multiple orientations [42]. It therefore follows that as volume fraction increases, further energy is dissipated as more fibres are out of plane with each other. Glass fibres composites have shown to be more efficient in absorbing energy than carbon fibre, where the addition of glass fibre to a carbon fibre/epoxy system improved the impact strength 3-fold [43].

2.1.3 Fibre Length

To obtain the maximum reinforcing potential in a DFC, the fibres must be above the critical length (or critical aspect ratio), which is the minimum length at which the centre of the fibre can realise its ultimate tensile strength, when the matrix is at maximum shear stress [9]. High performance discontinuous fibre composites are often comprised of fibre tows – or large groups of fibres bundled together, usually ranging from 1,000 (1k) to 48,000 (48k) filaments per bundle, primarily to aid handling and subsequent processing [44]. It has been shown that carbon fibre tows, like individual fibres, exhibit a critical length [45]. As the bundle diameter is much larger than the individual fibres, the critical bundle length is much larger than the critical fibre length. To be able to transfer the maximum tensile stress to a bundle, the bundle length must therefore be orders of magnitude longer than the fibre critical length.

It is worth noting that critical lengths exist for a number of mechanical properties, analytical models have been developed for modulus, tensile strength and impact strength by Cox [46], Kelly-Tyson [47] and Cottrell [48] respectively. However the critical fibre length for these models do not tend to coincide. Work by Thomason et al. [49] has shown that the optimum aspect ratio for stiffness is greater than 100, whereas

strength is greater than 1000 and impact strength is maximum at approximately 250 and decreases thereafter. The fibre length, and therefore tow length, are critical parameters in determining the transfer of stress between the matrix and fibre.

The mode of failure of a composite is somewhat determined by the relationship between the fibre length and critical length. Below the critical length (for a given fibre diameter) fibres pull out of the matrix material, as the shear force at the interface is less than the tensile force required to cause failure and fibres above the critical length fragment into shorter fibres [50].

For static loading scenarios it is more practical to have fibres that are as short as possible, but still remain above the critical length to maintain optimum composite properties [45]. Additionally using shorter fibre lengths also allows higher part complexity, increased homogeneity and provides a better surface finish when compared to longer fibre composites [51]. In terms of strength, increasing the length of a fibre increases the probability of the fibre containing a flaw, which acts as a stress concentration, reducing the composite strength. The probability of a fibre containing a flaw can be modelled statistically using a Weibull distribution [52]. This method was developed for uniaxial stress states on relatively brittle materials, where one flaw would cause catastrophic failure [53]. It has been widely used for describing composite failure, and although thermoplastics offer higher strain to failures than traditional thermosets such as epoxy, this is often not translated to the composite, as the fibres inhibit large matrix deformations [54].

Strength has been found to increase with fibre length for polypropylene reinforced with chopped carbon fibre tows, with increases of 80% and 90% for modulus and strength respectively, for lengths increasing from 0.5 and 10mm [55]. Similar observations were found for carbon fibre/polybenzoxazine, however a 55% decrease in strength was observed for an increase of fibre length from 17 – 27mm [56]. Above the critical length, modulus is relatively insensitive to fibre length, however complex interactions between fibre length and bundle size mean that tensile strength is significantly affected for mesoscale architectures. Shorter fibre lengths lead to more fibre ends per volume, and therefore an increase in the number of stress concentrations. Longer fibre lengths however, statistically contain more flaws and subsequently reduce mechanical

properties [45]. Optimisation is therefore required to tailor mechanical properties to specific load scenarios.

Analytical models based on the work by Cottrell [48] have been used to model the effect of fibre length on impact strength, where summations of contributions due to sub- and supercritical fibre lengths result in an optimum value for impact strength, either side of which strength rapidly decreases. There is little experimental evidence to verify this for polymer composites however, with concerns that its development from unidirectional metallic composites may not be applicable to these random materials [41]. Increases in impact strength with increasing fibre length have been reported for glass fibre/polypropylene over the range of 0 – 12mm, with values starting to plateau at around 5mm [41]. The critical length of this system was calculated to be 2mm, however no reductions in strength were witnessed above this value. Increases have also been reported for carbon fibre/polypropylene [55] and carbon fibre/epoxy [57] for ranges 0.5 – 10mm and 25 – 50mm respectively, however in contrast to glass fibre/polypropylene, no plateau in strength was recorded for either material.

The critical fibre length for impact behaviour is therefore higher than previously thought and it may then be possible to extract higher properties from these composites if longer lengths are used. There is still a need to optimise the fibre architecture to tailor the composite mechanical properties for in-service load scenarios.

2.1.4 Tow Size

One of the main considerations for the choice of tow size for discontinuous composite manufacture is cost, with lower filament count tows being more expensive than high filament counts. Over recent years, the price of carbon fibre has seen a decrease, which has somewhat narrowed the difference in cost, however defining actual costs is difficult as the price of carbon fibre is sensitive to market variations [51]. The primary reason for the higher cost of smaller tow sizes is that the throughput is significantly lower. The same floor space is required to produce a 1k tow as is needed for a 24k tow, therefore production rates for smaller tow sizes are much lower in comparison.

Discontinuous Fibre Composites

Due to the disparity in cost, small tows are primarily used in aerospace applications and automotive composites typically utilise tow sizes of 24k filaments or greater [58]. As more carbon fibre is being used for automotive products, as well as other market sectors, there has been an increase in large tow products available. It is expected that by 2020 the global production of large tow sizes (>24k) will be in excess of 53,000 metric tonnes – accounting for almost a third of all carbon fibre production [59]. Attempts have been made to split large tows into smaller tows to circumvent some costs associated with small tow production. Ford [60] have been successful in splitting a 50k tow into 25k and 10k tows for use in SMC materials. They found that the tensile strength of resultant SMC coupons was increased by 292% by reducing the tow size from 50k to 10k.

Stress concentrations occur at bundle ends due to differences in stiffness between the fibre and matrix, large tows have therefore been shown to reduce strength in composites as the synchronisation of a large number of fibre ends act as failure initiation sites [61]. Rondeau et al. [31] noted a reduction in strength for large tows and explained that fibre tows are analogous to large diameter fibres. As the tow size, and therefore aspect ratio gets larger, a longer fibre is needed to realise the full mechanical performance of the tow. Moreover, the number of bundle ends per unit volume is simultaneously reduced with increasing tow length, further improving strength due to reduced stress concentrations.

Increasing tow size affects the distribution of fibre in a composite, for the same volume fraction, smaller tows distribute more homogeneously inside the composite. Variations in areal density of up to 80% have been found for increasing carbon fibre tow size from 6 to 24k, however tensile properties were largely unaffected due to high levels of filamentisation (natural splitting of large tows as a result of chopping) which increased homogeneity and therefore offset reduction in mechanical properties caused by increasing tow size [62]. Filamentisation increases with tow size and decreases with level and type of sizing agent, as well as fibre length [63], however it can significantly increase preform loft and therefore restricts achievable volume fractions due to reduced packing efficiency and permeability [62], [64].

Homogeneity and isotropy of discontinuous fibre composites are significantly affected by the material architecture. To achieve the highest volume fraction, fibres must be packed efficiently, where the most optimum configuration is seen for unidirectional composites. For random DFCs higher volume fractions are achieved by bundling fibres into tows, with larger tow sizes leading to increased heterogeneity. As a result, variations in fibre distribution and mechanical properties can be expected, with coefficient of variance values reported as high as 44% for carbon fibre/epoxy tensile properties [62].

2.1.5 Fibre/Matrix Interface Considerations

The interface between fibre and matrix in discontinuous composites is important as the matrix material at the fibre/matrix interface is responsible for stress transfer between the fibres, which directly affects the mechanical performance [65]. Failure morphology is also determined by the interfacial strength; where very high interface strengths result in low toughness, brittle failures and very low interface strengths produce tough, but weak composites that are largely governed by the properties of the matrix [66].

Tailoring of the interface is largely determined by a number of surface properties such as; functional groups, surface microstructure, morphology and surface energy [67]. Many authors have been able to improve interfacial characteristics by modifying these with surface treatments and coatings. Removal of sizing from carbon fibre has been shown to improve interfacial performance with higher temperature thermoplastics, as the polar thermoplastic matrices show little chemical affinity to the thermoset optimised sizing [68]. However, complete removal of the sizing leads to problems with handling and filamentisation of the fibre tow during processing. To improve adhesion between thermoplastics and carbon fibre, specially formulated sizings are available, but currently only from Teijin and SGL for their dedicated automotive customers. There is a wide range of literature available that investigates the effect of different sizing formulations to increase compatibility between thermoplastics and carbon fibre via increased mechanical and chemical interactions [69]–[72], but these are unlikely to gain significant interest from commercial carbon fibre suppliers as they develop their own proprietary formulations. It is possible that thermoplastic compatible sizing formulations may receive greater interest as larger volumes of fibre are recycled, and

therefore require resizing to aid handling and processing [73]. However the focus here is on current modifications made to existing commercially available materials.

A number of authors have reported on chemical treatments to promote adhesion between the fibre and matrix, with common examples including fibre oxidation [74], heat treatment [75] and plasma treatment [76] – a comprehensive review of carbon fibre surface modifications can be found in the work by Sharma et al [77]. Applying treatments to the fibre can change many of the physical-chemical surface properties needed to increase adhesion between fibre and matrix. To obtain the most significant increase in interface strength for thermoplastic matrices, both the fibre and matrix should be modified simultaneously [78]. This is due to the nonpolar nature of the surface of carbon fibre and thermoplastics [79], where weak intermolecular forces and frictional forces typically form the majority of adhesion between fibre and thermoplastic matrix [80], [81]. Modification of the fibre surface can lead to chemical bonding for thermosetting matrices or polar interactions in thermoplastic matrices, such as hydrogen bonding and Lewis acid-base interactions [65].

There are many methodologies for characterising the change in the fibre surface properties after treatment; X-ray Photoelectron Spectroscopy (XPS) and Fourier Transform Infrared Spectroscopy (FT-IR) for both functional groups and surface chemical composition [79], [82], [83], Scanning Electron Microscopy (SEM) and Atomic Force Microscopy (AFM) for surface morphology measurements [84], [85], contact angle measurements for wettability and surface energy analysis [86], [87] and Brunauer-Emmett-Teller (BET) theory for adsorption techniques used to quantify specific surface area [65], [88]. Although these methods give some insight into the chemistry that occurs at the interface, mechanical performance data is still required to assess how each of the treatment affects the resultant composite.

2.1.6   Conclusions

For random 2D DFCs, increasing volume fraction has been shown to improve the composite mechanical properties. The literature suggests that a critical volume fraction exists, which is a function of fibre packing efficiency and polymer viscosity, above which there is a plateau – or in some cases a decrease, in modulus and strength

properties. This critical volume fraction is approximately $0.25V_f$ for glass fibre/polypropylene systems and in excess of $0.3V_f$ for comparable carbon fibre/polypropylene systems. Strain to failure is significantly decreased with very small fibre loadings, however impact testing studies still showed an increase in strength with fibre volume fraction. The range of volume fractions in the reviewed literature was primarily between 0 and 0.3, indicative of the material architecture where single filaments are randomly dispersed in the matrix. A performance gap exists between these homogenous architectures and isotropic continuous fibre composites, where fibre tows may be able to provide sufficient increases in volume fraction to bridge between them.

The tow size should be tailored for each specific application as there is a trade-off between cost and performance. For this study a 12k tow count was selected primarily due to availability, but also to allow a relatively homogeneous distribution of fibre within the composite, which is critical for discontinuous fibre composites at this scale. XPS, SEM, AFM and optical microscopy, will be used here to characterise the surface chemistry and morphology of the fibres and composite. The use of these techniques provides analysis at multiple scales, which is critical here for examining the features at the macroscale (composite level), mesoscale (tow level) and microscale (fibre level).

The critical length for DFCs is an important characteristic as almost all of the literature reviewed showed increases in mechanical properties with fibre length. Strength tended to decrease above the critical fibre (or bundle) length, due to a greater number of flaws present in longer fibres. Impact properties seemed to be most significantly improved by increasing fibre length, which contradicts some analytical models that suggest that there is an optimum length, above which properties decrease. Consideration of fibre length to coupon size has also been shown to be significant, as fibres that can span the width or length of the tested coupon are likely to give erroneous results.

The fibre/matrix interface for carbon fibre and thermoplastics has been widely discussed in the literature, however commercial carbon fibre is currently coated with sizing optimised for thermosetting polymers. It is unclear whether the thermosetting sizing greatly affects the bond between carbon fibre and thermoplastics, as without modification, they do not form chemical interactions. The effect of sizing and polymer modification will therefore be investigated to determine the compatibility between the

fibre and matrix. Surface treatments will not be considered here as refinement of a treatment process was outside the scope of this study. Moreover, the use of surface treatments further increases raw material cost.

.

2.2 Interfacial Testing Methods for Carbon Fibre Composites

The short beam shear test is the most common method for characterising the interfacial behaviour between fibres and matrix due to simple sample preparation and data collection. However it is criticised because it does not induce true shear in the component [89] and the ductility of thermoplastic matrices can inhibit delamination, invalidating the test [90]. Therefore alternative testing methods are required that involve more complex geometries, making macroscale interface testing less attractive.

Microscale characterisation of the interface between fibre and matrix has become increasingly important as the number of material combinations has significantly increased over the last few decades. In the literature a number of methods have been used to evaluate the interface for fibre reinforced composites, however there is large debate over the repeatability of data between institutions and testing methods as no standard test method exists [91]. Some of the more widely used methods are discussed here.

2.2.1 Micro-composite Testing Methods

2.2.1.1 Single Fibre Pull-Out Test (SFPO)

For the single fibre pull-out test, a fibre is embedded in a polymer matrix with one end free of the matrix and attached to a small load tensile testing machine. The length of fibre inside the matrix is below the critical length, to ensure that the fibre pulls out of the matrix, as opposed to breaking. As the fibre is loaded in tension, the force and displacement are recorded, with the apparent interfacial shear stress (IFSS) being calculated from the maximum force using Equation 2-1. Due to the large scatter in data produced from the SFPO test [92], a large number of samples (typically 20 or more) need to be tested to obtain a statistically representative IFSS.

$$\tau_{app} = \frac{F_{max}}{\pi D_f l_e}$$

Equation 2-1 - Calculation of the apparent interfacial shear strength (τ_{app}) for the SFPO test, where F_{max} is the maximum force recorded, D_f is the fibre diameter and l_e is the fibre embedded length

The IFSS is therefore an approximate mean shear stress calculation based on the shear lag model developed by Cox [46] (further detail including derivation is given by Nairn et al. [93]) and assumes a constant shear stress distribution along the interface. Whilst this is known to be an oversimplification [94], this method has been widely used to characterise the interface strength of a number of fibres and matrices [95].

Sample preparation is more difficult for thermoplastics as they are solid at room temperature, and great care must be taken to ensure sample preparation is consistent and repeatable for all tested samples [96]. To simplify preparation and reduce measurement errors associated with the fibre embedded length and therefore increase repeatability, the microbond test has been developed as an alternative to the SFPO test.

2.2.1.2 Microbond Test

The microbond test [97] has been used to establish the interfacial behaviour between different fibre/matrix combinations such as carbon fibre/epoxy [98], glass fibre/polypropylene [91], carbon fibre/polypropylene [22] and carbon fibre/polyphenylene sulphide [99]. A number of authors have performed FE analysis on experimental parameters, such as knife edge separation, fibre free length and droplet geometries, to investigate methods for reducing data scatter [100]–[104].

The test is performed by forming a droplet of polymer onto a single carbon fibre. A number of different methods have been employed in the literature [91], [105]–[107]. Once the droplet is formed, one of the free ends of the fibre is attached to a tensile testing machine and the droplet is constrained from moving vertically by using two rigid knife edges that contact the droplet on the meniscus [91]. As the fibre is pulled in tension, shear is induced at the interface and eventually the interface fails, the test is shown schematically in Figure 2-3.

A typical microbond force-displacement plot is shown in Figure 2-4. A similar trace is obtained for SFPO tests described in the previous section. At location 1, the curve is relatively linear and the fibre and matrix behave in a linear-elastic manner. At location 2 the fibre starts to debond from the matrix through interfacial crack propagation [108], and this has been described as the debond force [109]. The force then continues to increase with crack length until location 3, where the crack propagation becomes unstable and the fibre fully debonds from the matrix [110]. Location 4 corresponds to the residual frictional force of the matrix on the fibre. The apparent interfacial shear strength is calculated in the same way as the SFPO test using Equation 2-1.
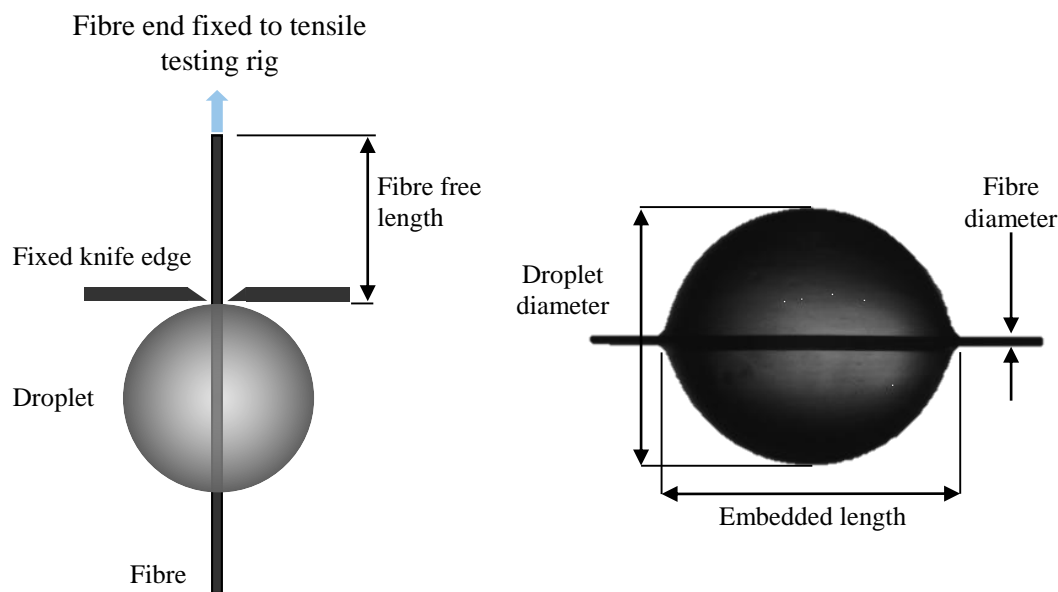
Figure 2-3 - Schematic of microbond test set-up (left) and microdroplet viewed by optical microscopy (right)

There is debate in the literature as to whether the assumptions for the calculation of IFSS are valid for the systems tested [110]. The deformation associated with debonding is assumed to be elastic, although some authors have noted that plastic deformation can occur for thermoplastic systems [111], potentially invalidating results. The calculation for IFSS also assumes that the stress along the interface is constant, but FEA modelling has shown that this is an oversimplification [112]. Nevertheless, the microbond test method is a useful method for determining interface strength and is less labour intensive than the SFPO test, and is therefore more practical in that it allows a large number of repeats to be carried out, which can reduce some of the uncertainty in the data analysis.
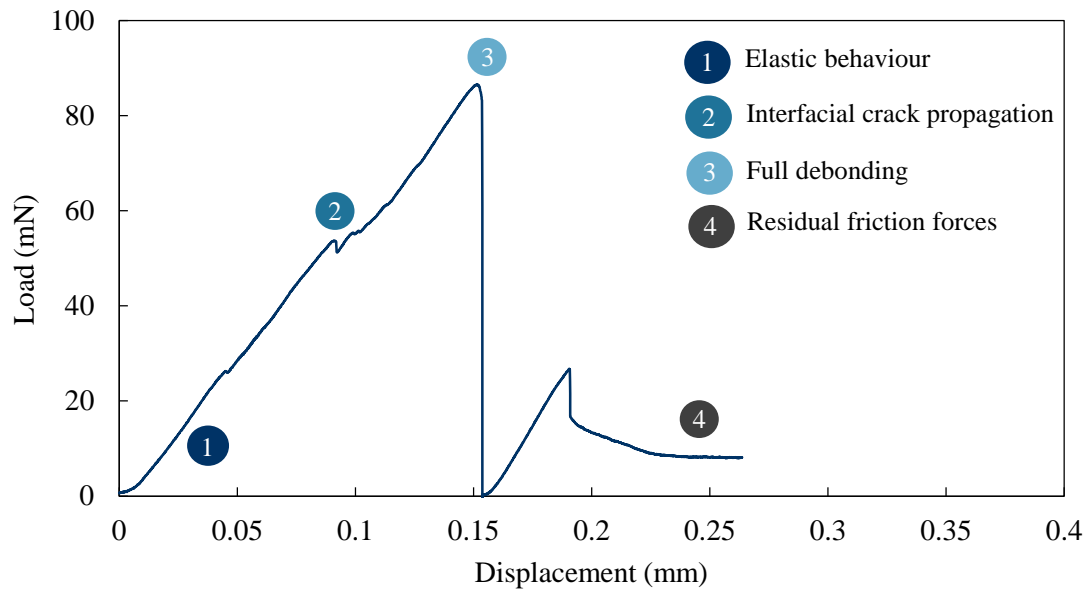
Figure 2-4 - Microbond force-displacement plot demonstrating processes that occur during the microbond test

2.2.1.3   Single Fibre Fragmentation Test

The single fibre fragmentation test (SFF) is an interface characterisation method introduced by Kelly and Tyson [47] and has been adopted for a number of studies as it affords relatively simple specimen preparation and ease of testing [113]. This test method has also been recognised as being able to provide information on failure modes within composites and how these relate to macroscale mechanical properties [114].

The test is performed by embedding a single fibre into a polymer matrix, which is typically moulded as a dogbone specimen [115]. A load is applied to the dogbone and tensile stress is transferred to the fibre through interfacial shear stress. As the load is increased, the strain in the fibre will reach the failure strain and the fibre fractures. The specimen is continuously loaded and the fibre continues to break into smaller lengths. Once the fibre becomes too short to break any further, a saturation state is reached and the test is stopped. [113]. The apparent interfacial shear strength is calculated using Equation 2-2, which is based on the constant shear model developed by Kelly and Tyson [47]. Assumptions are that the fibre behaves elastically and there is perfect adhesion between fibre and matrix adhesion

Micro-composite Testing Methods

$$\tau_{app} = \frac{\sigma_f D_f}{2l_c}$$

Equation 2-2 - Calculation of apparent interfacial shear strength (τ_{app}), where σ_f is the fibre tensile strength, D_f is the diameter of the fibre and l_c is the critical length of the fibre

The critical length can be determined through Weibull analysis [116], although it is usually calculated using Equation 2-3, which is based on semi-empirical analysis of the data developed by Ohsawa et al.[117].

$$l_c = \frac{4}{3}\bar{l}$$

Equation 2-3 - Calculation of the fibre critical length (l_c), where $\bar{l}$ is the average fragment length

Calculation of the critical length from Equation 2-3 assumes that the fibre fragment length distribution is symmetrical, however this is rarely the case [113]. Moreover, phenomena such as shear yielding of the matrix, interfacial debonding and transverse matrix cracking are also reported to take place during the test [118], [119], which makes using the constant shear model highly inaccurate for this procedure. Aside from its limitations, the constant shear model is still often used due to ease of calculation.

A number of authors have tried to improve data reduction [120]–[123] and model the test using finite element analysis and numerical simulations to better understand processes that are occurring during the test such as stress field distribution [122], matrix cracking [119], debond propagation [124] and local yielding of the matrix [125], but still there is little consensus on the best practice for calculation of the interfacial shear strength using this method.

Deng et al. [126] report the IFSS using the SFF test for a carbon fibre/epoxy system (T700S/Araldite-F). The authors state the average interfacial strength based on the modified Kelly Tyson model (Equation 2-2 combined with Equation 2-3) in the form:

$$\tau_{app} = K\frac{\sigma_{f(\bar{l})}D_f}{2\bar{l}}$$

Equation 2-4 - Calculation of IFSS for single fibre fragmentation test, where K is a constant and $\sigma_{f(l)}$ is the fibre strength at average fragment length

In equation 2-4, K is generally set to ¾, however other researchers have found K to be 0.699-1.000, depending on Weibull shape parameter for fibre strength [127]. Values of 30 – 50MPa have been reported for K values between 0.75 – 1 [126].

2.2.1.4   Micro-indentation Test

First proposed by Mandell et al. [128], the micro-indentation test uses a standard micro-indentation hardness tester to apply a force to the centre of a fibre to push it through the sample [129]. For thicker samples, the fibre is pushed into the matrix (commonly called the push-in test) and for thin samples the fibre is pushed through the matrix and out of the other side (push-out test). The advantage of this test is that it simulates the conditions of a 'real' composite in that residual thermal stresses, effect of adjacent fibres and morphology of the matrix are taken into account [129], moreover the sample doesn't need special preparation other than being polished for microscopic examination [130]. The push-in test is far easier to prepare than the push-out test as the preparation of very thin slides (approximately 50µm [131]) is difficult and therefore limits the test to composites with high stiffness, low interfacial adhesion and large fibre diameters [132]. Therefore only the push-in test will be considered here.

To calculate the interface strength a fibre end, perpendicular to the surface of the matrix, is loaded by the standard pyramid indentor which displaces the fibre below the surface of the containing matrix, and a linear relationship is obtained in the form [131]:

$$u_{fibre} = \frac{F}{\pi r n E_f}$$

Equation 2-5 - Relationship between the fibre displacement, u_{fibre}, and applied force, F, where r is the radius of the fibre and E_f is the fibre Young's modulus

where

$$n^2 = \frac{2G_m}{E_f \ln(\frac{R_e}{r})}$$

Equation 2-6 - Calculation of variable n, where G_m is the matrix shear modulus and R_e is the distance from the tested fibre to the ring of adjacent fibres

The interfacial shear stress is then calculated from the maximum shear stress at the onset of debonding by:

$$\tau_{crit} = \frac{nF_{crit}}{2\pi r^2} = \frac{n}{2}\sigma_f^{crit}$$

Equation 2-7 - Calculation of interfacial shear stress at debond, τ_{crit}, where σ_f^{crit} is the axial stress at the cross-section of the fibre at debonding

A complication arises from using standard micro-hardness indentors, as with small diameter fibres such as carbon, indentor positioning is difficult and further to this, the fibre can be easily split by the indentor during testing [132]. Another issue is that for fibre reinforced polymers, the compliance of the matrix during testing can affect the results and errors therefore become more significant for ductile matrices [133].

Much like the other interfacial testing methods, analytical and finite element studies have been carried out to assess whether the simplistic shear-lag model used to calculate the interfacial shear stress is appropriate. Aside from simplifications inherent in using the shear-lag model, for example assuming perfect hexagonal packing of fibres and elastic deformation of the matrix [134], one of the issues faced by the test method is that the debonding loads can be significantly affected by the local fibre volume fraction around the tested fibre [135]. Corrections to debonding loads have been suggested based on fibre diameter and average distance to adjacent fibres [136], however the measurement of the average distance to adjacent fibres is somewhat equivocal and the addition of FEA complicates the procedure further. Some success has been found with current analytical models (Equation 2-7) for large fibre spacing [131],

2.2.1.5   Conclusions

A comparison of the results obtained using different interfacial testing methods is given in Table 2-1. Unsurprisingly, there is a large range of values given for the carbon fibre/epoxy system studied (AS4/EPON 828). As thermoplastic matrices are much more ductile than the epoxy used for those tests, it is likely that calculation of the interfacial shear strength will be further complicated. Of the tests investigated, the short beam shear method appears to have the simplest preparation method, however the induced failure is mixed-mode including components of tension and compression as

well as shear and is therefore not suitable for testing with ductile matrices, such as polypropylene.

Of all the microscale methods, the microbond test appears to be one of the most widely used and affords relatively simple sample preparation and data reduction. Small changes in adhesion can be detected by this method and direct comparison can be drawn with data available in the literature for a carbon fibre/polypropylene system, therefore this interfacial testing method will be used here.

Test Method	Test Type	Apparent Interfacial/ Interlaminar Shear Strength (MPa)
Short-beam shear test (ILSS)	ILSS	84
Iosipescu shear test	ILSS	95.6
Single-fibre pull-out test	IFSS	88
Microbond test	IFSS	50.3
Single-fibre fragmentation test	IFSS	65.8
Micro-indentation test	IFSS	68.3

Table 2-1 - Comparison of interfacial and interlaminar shear strengths obtained from macro and micromechanical test methods, complied from [42], [137]

2.2.2 Experimental Parameters Affecting the Microbond Test

As discussed in the previous section, the difficulty in interpreting the interface between fibre and matrix means that a number of different approaches to modelling the microbond test have been demonstrated in the literature. Important information about factors that affect repeatability can be extracted from FEA simulations if modelled appropriately. Differences in scale between the droplet and the interface (approximately 0.5µm for carbon fibre [138]) mean a mesh of equally sized elements cannot be used. To resolve this the fibre, interface and droplet are modelled as different surfaces (each with their own mesh) and joined them using tied contact pairs, which essentially restricts the surfaces from slipping against or moving away from each other and greatly reduces computing time [102]. During FE analysis, the droplet is sheared away from the fibre along the interface. Progressive damage can be modelled using cohesive contact surfaces, however as the fibre beneath the droplet needs to be unconstrained to replicate the test, numerical errors occur in analysis as the droplet is debonded. To

prevent this, contact behaviour can be added between the droplet and knife edges using cohesive contact without damage [139].

2.2.2.1 Blade Separation

The blade separation (also referred to as: blade opening/positioning, vice angle and knife edge positioning) determines where contact between the droplet and blades occurs. For larger separations the blades contact the droplet further away from the fibre near the middle of the droplet and for smaller separations the blade makes contact with the droplet near the meniscus. According to the literature the resulting IFSS is relatively insensitive to the blade separation, but the stress distribution is greatly affected [102], [103], [140], [141].

The stress distribution has been modelled using FE analysis for 2D and 3D systems, however 2D analysis is limited as it models the blades as a circular opening and assumes the droplet is axisymmetric. 2D and 3D models provide similar results for the stress states away from the droplet, however at the blade edges, the 2D model only captured an average of the peak stress that was found for 3D modelling [100]. It has been suggested that the optimum blade separation is approximately 2 times the fibre diameter apart [142], where narrower separations lead to higher shear stresses at the interface, which may result in premature interface failure [143]. For blade separations greater than double the fibre diameter, the stress distribution has been shown to be relatively insensitive to blade separation [144], however extensive matrix cracking has been found as a result of larger blade openings, leading to cohesive failure in the matrix as opposed to interfacial failure [142].

2.2.2.2 Test Speed

As mentioned previously no standard exists for the microbond test, it is up to the user to decide the appropriate parameters to conduct an effective test. As polymers are highly strain rate sensitive, it seems logical that there should be a set test speed for this method, however almost all the literature cites different test speeds (ranging from 0.001 – 500mm.min^{-1} [104], [145]), rendering result comparison difficult. For glass [111] and aramid fibre/epoxy stems [105], ranges of 0.05 to 100mm.min^{-1} have been tested in the literature. Apparent IFSS was found to increase by approximately 75% between 0.05

and 2mm.min^{-1}, with decreases of 55% reported for test speeds up to 100mm.min^{-1}. Slower test speeds are recommended for carbon fibre than glass to avoid fibre breakage [146], where 0.03 – 0.25mm.min^{-1} have been used for carbon fibre/epoxy [98], [147], [148] and approximately 1mm.min^{-1} has been used for carbon fibre/thermoplastics [22], [149], [150].

2.2.2.3   Fibre Free Length

The fibre free length (L_f) is the distance between the top of the polymer droplet and where the fibre is gripped. It is generally recommended that L_f is minimised and kept constant for each sample tested, however little explanation has been given for this. Details of L_f may be explained by some of the literature covering the single fibre pull-out test which was widely used before the microbond test was developed. For this method, the fibre free length has been suggested to be as small as possible due to the increase of surface flaws and fibre strain with increasing L_f [139], [151]. To achieve the maximum yield from prepared samples, lower fibre free lengths ensure that the tensile strength of the fibre is sufficiently high to allow the interface to debond. Additionally it has been suggested that fibre free lengths of above a few millimetres can eliminate the purely frictional part of the pull-out curve [137]. Fibre free lengths of 0.03 – 10mm have been reported for carbon fibre/thermoplastic systems [74], [152], [153], where the length should be kept constant to minimise the effects of stored elastic energy on the initiation and propagation of interface failure [154].

2.2.2.4   Droplet Formation

For fibre/matrix combinations with strong interfacial adhesion, chemical bonding, (where compounds in the fibre and matrix are joined by strong covalent bonding), is the dominant mechanism in stress transfer. However for low adhesion systems, for example polypropylene and carbon fibre, the interface strength is an order of magnitude lower and physical bonding, (where fibre and matrix are weakly bonded by forces of attraction such as Vander Waal's and coulombic forces), is much more dominant. The difference in thermal expansions between fibre and matrix causes compressive residual stresses on the fibre during cooling which increases interfacial friction. The effect of these residual stresses has been shown to account for 25 – 70% of the IFSS in glass fibre/polypropylene [141], [155] and is dependent on the droplet forming temperature

[81] and testing temperature. Reductions in IFSS of 69% have been reported between test temperatures of 0 and 40ºC for glass fibre/polypropylene [155]. Therefore careful control of both forming and testing temperature must be maintained to ensure consistent results.

2.2.2.5   Conclusions

Characterisation of the interface between carbon fibre and commodity/engineering thermoplastics via the microbond test has had relatively little investigation. These materials will become increasingly important as the cost of carbon fibre decreases through recycling methods and fabrication through alternative precursors, especially for automotive applications where a cost/performance ratio is more important than for the aerospace industry. A number of parameters affect the microbond method, which need to be controlled to allow for repeatable testing.

Blade separation should be approximately 2 fibre diameters apart to prevent premature interface failure due to high local shear stress concentrations at the knife edges, as well as minimising the risk of cohesive matrix failure associated with larger separations. The interfacial shear stress is significantly affected by test speed due to the strain-rate sensitivity of the polymer, with speeds of 1mm.min^{-1} used for carbon fibre thermoplastic systems in the literature. Fibre free length should be minimised to attain higher fibre strengths due to a reduced number of flaws on the surface. The same fibre free length should be maintained for all tests in order to reduce effects of fibre elastic deformation on the initiation of interface failure. Free lengths of 0.03 – 10mm have been successfully used for carbon fibre/thermoplastics. Finally, droplet formation temperature and test temperature should be kept constant for all sample preparation, as interfacial friction due to compressive residual stresses has been shown to significantly affect interfacial shear strength.

2.3   Processing of Long Discontinuous Fibre Thermoplastic Composites

Due to the high viscosity of thermoplastics compared to thermosetting polymers, conventional processing routes associated with composite fabrication may not be suitable. Figure 2-5 shows different processing methods and material formats for

thermoplastic composites as a function of volume fraction. The method in which fibre and matrix are brought together for processing defines the maximum achievable volume fraction and also impacts the cycle time length. For higher performance products with a fibre volume fraction greater than 0.35, intermediate products are often used that either already have some consolidation between fibre and matrix, or that intersperse the matrix within the fibre to minimise the melt flow distance of the polymer [156]. Some common intermediate products are reviewed here.

Part Property Classification									
Non-Structural				Semi-Structural			Structural		
Fibre Volume Fraction (%)									
10	15	20	25	30	35	40	45	50	55 +
Long Discontinuous Material Formats									
	GMT								
BMC		SMC						ASMC	
Thermoplastic Composite Processing									
LFT Pellets						Prepreg			
Film Stacking						Commingled			
				Coated Fibre					
				Liquid (In-Situ Polymerisation)					

Figure 2-5 - Part property classification, material formats available and processing routes as a function of volume fraction for thermoplastic composites processing

2.3.1 Intermediate Products

A variety of commercial intermediate products are available for both thermosetting and thermoplastic composites. The most commonly used intermediate format for thermoplastics are pellets containing short, aligned fibres, which are typically processed by injection moulding. As discussed previously these composites are limited by low strengths as a result of low volume fractions and short fibre lengths. Injection moulded parts are therefore limited to cosmetic automotive parts and will not be discussed further here.

2.3.1.1 Commingled Fibres

Fibre commingling is where the polymer, in continuous filament form, is brought together and interspersed within the fibre tow (Figure 2-6), minimising the melt flow distance to around 20 - 40µm [157]. Continuous reinforcement fibres can be commingled with polymer yarns in a variety of processes and have the advantage of

maintaining a high flexibility compared to other intermediate products [158], enabling complex geometries to be formed more easily. It is unclear however how the integrity of the yarn would be affected by chopping for a discontinuous fibre preform. Common methods include using a compressed air-jet to push the thermoplastic yarn into the continuous carbon tow and stretch breaking fibres with thermoplastic yarn, where the latter is subsequently spun (using textile spinning techniques) into a continuous commingled yarn. Stretch breaking maintains a high level of fibre strength as it breaks the fibres at the weakest point, with reductions of no more than 10% observed for carbon fibres [157]. The air-jet intermingling process is popular as the process speed is twice as fast as other commingling methods [159], however care must be taken in optimising the air pressure to minimise damage whilst still providing adequate blending between the two fibres. For both methods volume fractions of up to 0.6 are routinely possible [160].
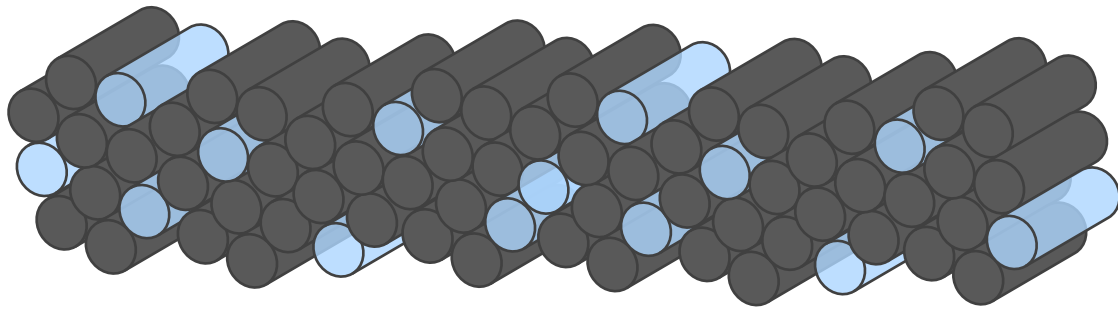
Figure 2-6 - Schematic of commingled fibres, where the grey filaments represent the reinforcing phase and the blue filaments represent the matrix (in fibre form).

Composites manufactured from continuous commingled fibres have been shown to have comparable properties to analogous continuous fibre composites. A unidirectional commingled carbon fibre/polyetheretherketone (CF.PEEK) composite showed an equivalent tensile modulus and 15% reduction in strength compared to unidirectional pre-impregnated CF/PEEK composite [161]. Woven composites manufactured from carbon fibre/polyamide 12 (CF.PA12) have also demonstrated equivalent mechanical properties to commercial carbon fibre/thermosetting and thermoplastic composites [162]. Additionally CF.PA12 has proven to be suitable for high volume manufacture processes, where cycle times of 10 seconds per mm part thickness have been reported [163], although tensile properties were 15% lower than reported for compression moulding with a cycle time of 10 minutes [162].

A number of commercially available products exist for commingled fibres, due to the simple mixing of reinforcement and matrix fibres. GF/Polypropylene (PP) 'Twintex' from OCV Reinforcements, France and CF/Polyamide (PA12) manufactured by EMS Chemie, Switzerland and Schappe Techniques, France are the most widely used products for glass and carbon fibre respectively.

2.3.1.2   Coated Fibre

A number of different methods exist for fibre coating and like commingled fibres, create an intermediate product with a specific volume fraction that can be easily processed into a finished part. In contrast to commingled fibres, the intermediate product is much stiffer as the fibres are encased in a polymer. Melt impregnation, powder impregnation and solution impregnation methods for fibre coating are discussed here.

Melt Impregnation

Melt impregnation involves pulling a continuous tow of fibre through a bath of molten polymer, which is usually fed via an extruder and kept at constant temperature. The tow is pulled over a series of offset pins which help push the molten polymer into the fibre. After passing through the melt bath, the coated tow is pulled through a die which controls the volume fraction (typically up to 0.35 is achievable [164]) and the coated tow is then cooled and hauled off. Due to the high viscosity of semi-crystalline thermoplastics, direct melt impregnation is difficult and often impregnation is slow [165], furthermore high impregnation pressures force filaments in the tow to become more densely packed, reducing the permeability of the fibres [166]. Another key consideration for melt impregnation is melt stability of the polymer. It is imperative that it does not degrade due to thermal oxidation during processing, or further downstream by heating during moulding [167].

Variations of the melt impregnation method have been developed to improve efficiency and quality of the process. In one case, the polymer is forced through narrow slots in the impregnation pins, as opposed to being pulled through a bath, this induces shear thinning in the polymer to aid impregnation into the fibre bundle [168]. Another process (DRIFT [169]) reduces viscous drag in the melt bath by driving the impregnation pins

as well as using convex bars to improve tow spreading. Melt impregnation quality is usually dictated by the number of impregnation pins, however as the number of pins increases the tension is increased in the tow and is therefore limited by the fibre tensile strength [169]. The tension is also influenced by pulling speed and therefore quality is usually compromised for higher throughput. The DRIFT process reduces the tension in the tow and therefore allows high line speeds of 20-60m.min^{-1} [8] . Despite improving the impregnation quality however, the volume fraction is still limited to around 0.35.

Even with advances in melt impregnation processing, other processing methods are generally preferred due to lower processing costs, greater selection of materials and higher achievable volume fractions.

Powder Impregnation

Powder impregnation routes can be classified as either wet or dry. Dry powder impregnation involves pulling a continuous tow through a bath of powder, which can be agitated, fluidised or charged to aid dispersion [170], [171], after which it is usually then passed through a scraper to remove any excess powder on the surface. For wet powder impregnation, the tow is passed through a carrier liquid containing suspended powder particles. The amount of carrier liquid that coats the fibre can be controlled by capillary forces that act when the tow is pulled out of the bath and therefore the volume fraction can be controlled [172]. The tow is subsequently dried in a continuous oven and the process thereafter is identical to dry powder, where the powder is tacked to the tow by heat, cooled and hauled off.
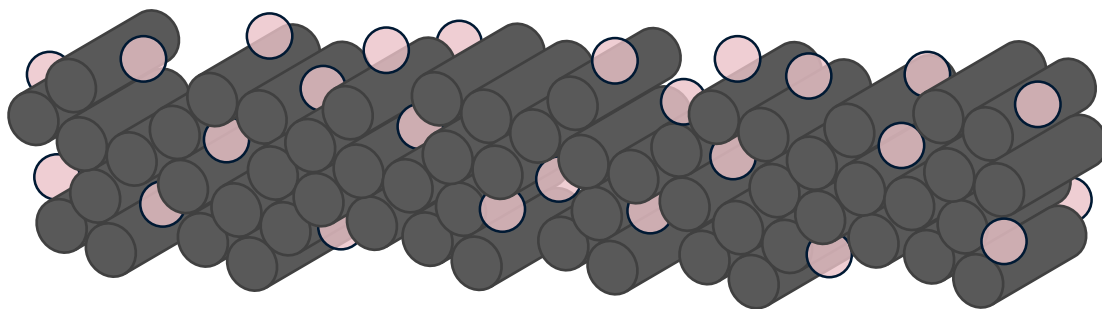

Figure 2-7 –Structure of powder impregnated tows, where the grey filaments are the fibres and pink spheres are polymer particles. Small particle sizes are required to allow powder particle impregnation into the fibre bundle

Carbon fibres are particularly well suited to powder impregnation as the tows can be easily spread due to the low comparative amount of sizing that holds the filaments together [173]. Powders of similar diameter to the fibres have been shown to be the most effective in coating [166], however processing polymer powders to these diameters is expensive and typically diameters of around 15 - 150µm are used [174].

Powder impregnation is a common technique to produce tapes with thermoplastics that are difficult to process due to high viscosity [166]. The volume fraction range for powder coating is typically between 0.5 – 0.6, significantly higher than that of melt impregnation [174]. The coated tow is then heated using infrared heaters, which have a spectral bandwidth (3 - 5µm for long wave emitters [175]) similar to that for polymer absorption (3.2 -3.6µm for most polymers due to carbon-hydrogen bond content [176]), making the polymer powder 'tacky', sticking it to the tow. The coated tow is subsequently cooled and hauled off. In other variations of the process, the tow can be preheated when it enters the powder to aid powder pick-up [171].

For powder impregnation, line speeds of up to 10m.min^{-1} have been shown to be possible whilst maintaining a good level of impregnation [177], however void content increases with increasing line speed. As the produced tape is an intermediate material and requires subsequent consolidation, the impact of consolidation level on void content in the resultant composite is not clear. Unlike melt impregnation, a heated bath is not required to keep the thermoplastic molten (which uses a higher amount of energy). Therefore the viscosity of the polymer system is negated, making impregnation a function of powder particle size. Impregnation time is reduced as it takes place by polymer flow parallel to the fibres, where permeability is around one order of magnitude higher than in the perpendicular direction to the fibres [156].

The main disadvantage with powder processes is that it can be difficult to control the amount and distribution of powder that is deposited on the tow [178]. This is exacerbated in dry powder processes as smaller particle size powders may agglomerate, leaving areas of dry fibre during coating, which has been found to be a significant effect between a particle size of 53µm for PEEK [179]. The most significant cost of powder impregnation is processing powders to the desired particle size. Due to the ductile nature of thermoplastics cryogenic milling is required to obtain small particle

diameters, where high operating costs are incurred due to the use of liquid nitrogen [180].

Solution Impregnation

In solution impregnation thermoplastic polymers, primarily amorphous, are dissolved in a solvent, significantly reducing the viscosity. This process can prevent the need for polymers to be processed at high temperatures (although some solvents require moderate heating to allow dissolution) therefore negating the risk of thermal degradation of the polymer above its melting temperature. There are however a number of problems associated with solution impregnation; often environmentally hazardous solvents are used [181], complete removal of the solvent can be difficult, potentially causing volatile emissions during moulding [83] and only a limited number of polymers can be dissolved in solvents and therefore are also susceptible to chemical degradation in service parts [174].

Despite the disadvantages, fabrication of tapes using this method can be successful when the correct matrix material is specified. Volume fractions of around 0.6 can be achieved [182]; TenCate's 'Cetex' (CF/Polyetherimide(PEI)) product is a common example produced by this method and has a nominal volume fraction of 0.59. Typical line speeds for solution impregnation are between 3 and 4.5m.min^{-1} [183], somewhat lower than other processing techniques.

2.3.1.3 Conclusions

All of the aforementioned intermediate products are currently produced commercially, showing that consistent and high quality material formats are achievable. Commingled fibres show the most potential due to high fibre volume fractions and lower risk of thermal degradation to the polymer, as it has received one less thermal cycle than the other processes. However it is unclear how the integrity of the commingled bundle would be maintained after chopping into discrete lengths as filamentisation of the yarn and therefore dispersion of the fibre and matrix is a concern.

Melt impregnation is unlikely to be a good candidate system as the volume fraction is limited compared to other processes, and risk of polymer degradation is higher than

other processes. Solution impregnation is limited since only a small number of polymers can be used. Whilst high volume fractions are achievable, this processing route naturally limits the chemical resistance of the final composite. Both wet and dry powder impregnation routes are likely to be good candidate systems as they are capable of running at moderate line speeds and are not restricted by the high viscosity polymers. Additionally carbon fibre is well suited to powder impregnation as tows are easily spread, allowing greater take-up of the polymer.

2.3.2 Consolidation Methods

Consolidation is a crucial step in part manufacture for thermoplastic composite materials, its purpose is to remove voids, increase fibre and matrix contact, and finally to solidify and crystallise the polymer, the latter when semi-crystalline polymers are used [184]. Conventional composites processing methods such as autoclave curing and resin transfer moulding (RTM) are generally not suitable or optimised for thermoplastic composites processing, therefore thermoplastic forming techniques have been adapted to allow manufacture of these parts. Some developments have been made in increasing fibre length for injection moulding, and pellets with long fibres (10 – 50mm [185]) are widely available, however during processing, significant fibre attrition occurs and the resultant fibre length is in the region of 2-3mm [29].

Consolidation methods for high-volume manufacturing of thermoplastic composites can generally be divided into two main groups; thermoforming or compression moulding. An exception to this however is reactive processing, or in-situ polymerisation, where low viscosity prepolymers are polymerised in the mould with the fibres, in a similar way to resin transfer moulding for thermosetting composites - Cyclics CBT resins are a commercial example of matrices used for this process. The polymerisation process is a relatively lengthy process (approximately 30 minutes [186]) and therefore cannot compete with thermoforming and compression moulded processes unless used for large or thick parts [187]. Additionally, only a limited number of polymers are currently available to be polymerised in-situ [188]. Due to the long cycle times, this process will not be looked at in detail here, a comprehensive review of reactive processing is given by van Rijswijk et al. [189].

2.3.2.1   Thermoforming

Thermoforming is a process derived from thermoplastic component manufacture; where a pre-impregnated fabric (prepreg) is clamped and heated to its softening point (below T_m) using infrared heaters. Once the prepreg is at the correct temperature, the material is draped over, or forced onto a single sided mould where it is held until it cools (Figure 2-8). Thermoforming can be used to create very large parts (for example boat hull cores [27]), and typically only a single sided tool is needed, greatly reducing costs. However, all the parts produced need trimming due to the initial clamping of the material, which means there is some wasted material, and parts are limited in complexity due to the draping method used for this process.
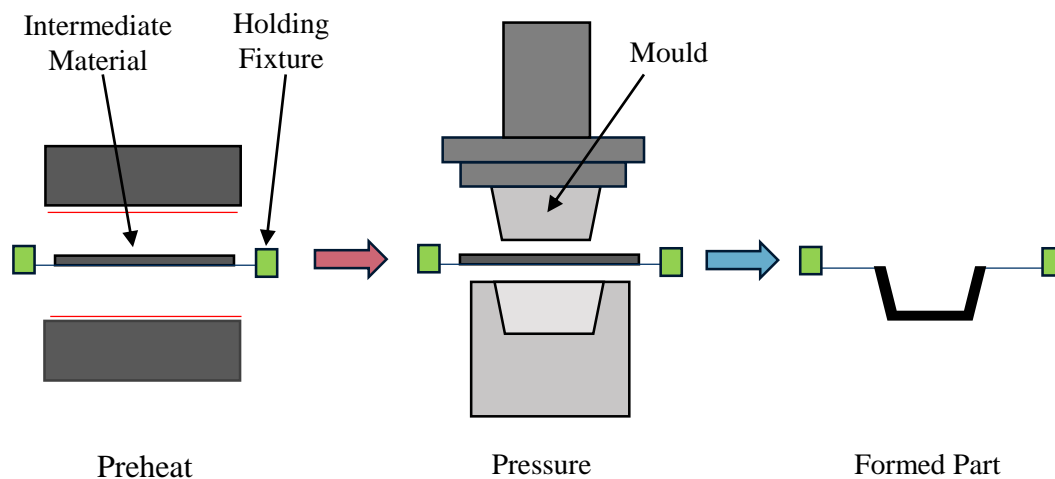
Figure 2-8 - Schematic of the thermoforming process

The state-of-the-art of this process is Fiberforge RELAY [190]. This process uses automated tape laying and subsequent thermoforming to produce thermoplastic parts in less than 3 minutes. The company currently license their technology and rely on carbon fibre/thermoplastic tape from suppliers such as TenCate, Ticona and Baycomp. The process currently has a maximum part size of 2 x 2m, but joining technologies for thermoplastics means that the applications are not limited.

Due to the material draping needed, a certain amount of integrity is needed to hold the material. This therefore limits thermoforming to fabric prepregs and continuous fibre products.

2.3.2.2   Compression Moulding

Compression moulding is the most widely used forming method for high performance discontinuous fibre thermoplastic composites. A pre-shaped charge (such as an SMC) or a mixture of fibres and resin is placed into a female mould cavity, the cavity is usually heated, but for thermoplastic composite manufacturing it is not unusual to pre-heat the material and transfer it into a 'cold' mould (where the mould temperature is below the T_g of the thermoplastic) to reduce cycle times. The female and male mould are closed together and pressure is applied, the tool is then either cooled to solidify the material, or the mould is already cool enough to quench the material in the mould. The advantage of compression moulding is that the thermoplastic matrix is heated to above its T_m, resulting in material flow which is advantageous for parts with higher complexity. The parts produced usually need trimming due to polymer flow out of the shear edges (flash gap) present on most compression moulding tools.

To aid fast processing times, a number of authors [184], [191]–[193] have considered non-isothermal compression moulding (NI-CM) routes, where the material, typically net-shape [194] is preheated and the tool is kept at a 'cold' temperature during moulding (Figure 2-9). The advantage of the non-isothermal process is that the tool is not thermally cycled, which saves large amounts of energy and therefore operating costs, and as consequence short cycle times are realised (approximately 10 seconds/mm of part thickness [163]), which make this method suitable for high volume manufacture of parts. Parts of comparable quality can be made using NI-CM [184] and it is therefore likely to be the more suitable manufacturing method for this study, a review of processing parameters that affect composite consolidation and performance is outlined below.

The initial process for NI-CM is preheating the material (charge) in an oven before forming and consolidation. The preheating process for NI-CM is important as the material must be heated through the thickness to the correct temperature, but also must not be allowed to degrade on the surfaces, which will be at the required temperature for a longer duration than the core. For NI-CM, polypropylene is heated to around 210 – 230°C depending on the fibre type [195]–[197]. Thermoplastics that are held above their melting temperature begin to degrade after prolonged exposure to heat. Figure

2-10 shows the decrease in molecular mass of a glass fibre/polypropylene composite for different preheating temperatures and preheat times. The decrease in molecular mass is a representation of degradation of a polymer. The author has chosen an arbitrary molecular mass, below which the composite is considered to be significantly degraded.
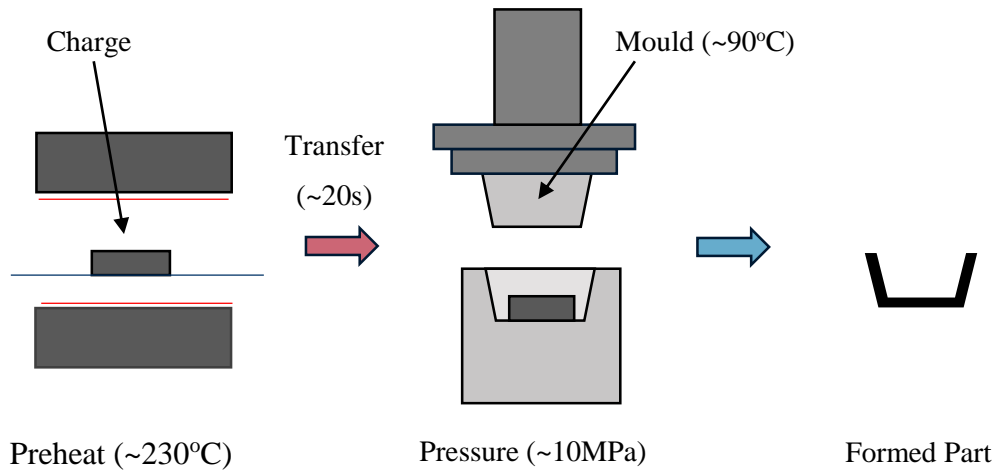
Figure 2-9 – Schematic of the non-isothermal compression moulding process. Similar to the thermoforming process (Figure 2-8) however for discontinuous fibre charges, more flow is possible, allowing more complex geometries to be formed. Typical processing parameters shown in brackets for polypropylene composite mouldings.

Figure 2-10 shows that increasing the preheating temperature by only 10°C (from 210°C to 220°C) causes degradation to occur over 200 seconds earlier. As short cycle times are required for this process, the above is used to determine the maximum operating conditions for a given material. For the optimum temperature (220°C), the composite can be held for over 5 minutes before degradation occurs. As the oxidative degradation process is both a function of time and temperature, it provides an upper limit to the processing window available for preheating. The preheat time is governed by the part thickness, but may also be affected by air contained within the preform due to loft [198]. If the loft is high, heat penetration into the centre of the preform will be increased and therefore the preheat temperature may need to be reduced to prevent degradation. To minimise these effects, pre-consolidation can be used. Santulli et al. [199] used heated rollers to apply a pressure of 4.5MPa to the preform for 1 second after preheating the material at 200°C for 1 minute.

The preheat temperature has been shown to be a significant parameter for tensile strength, where increases of 65% have been reported for GMTs from 170 – 240°C

[200], however tensile modulus was largely unaffected. The optimisation of mechanical properties with preheat temperature has shown that tensile and flexural strength both increase with increasing temperature over the ranges studied [201], [202]. This has been linked to decreased part thickness due to reduced polymer viscosity and therefore void content reduction [194].
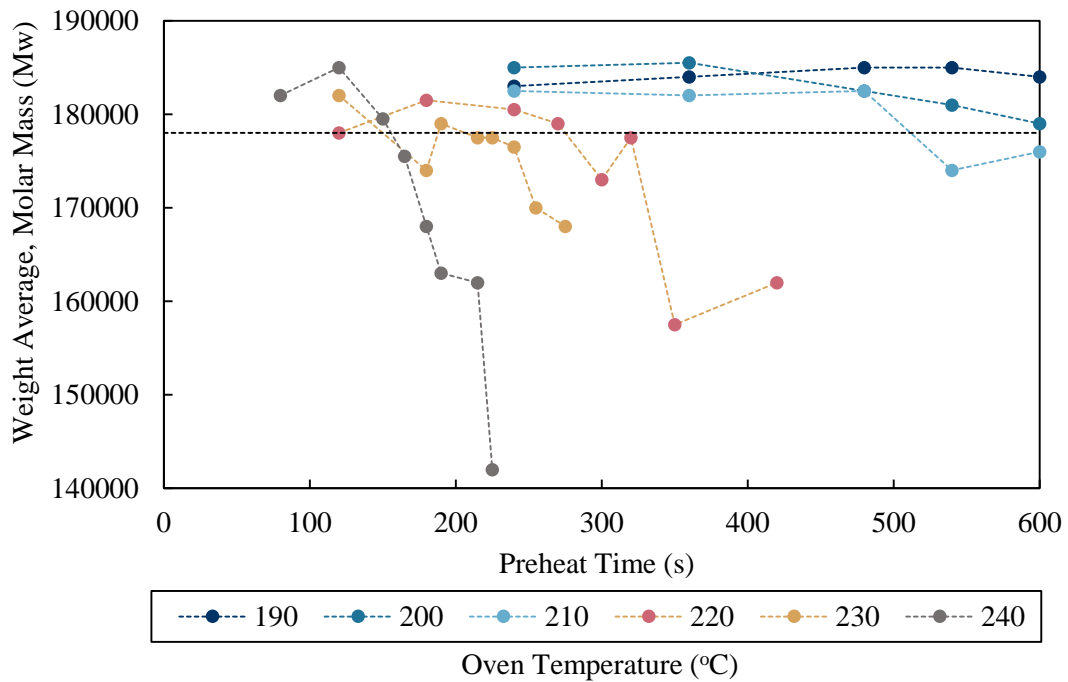
Figure 2-10 - Degradation of polypropylene during preheating of GMT. Data below black dotted line indicates degradation has occurred in the polymer. (Figure reproduced from Wakeman et al. [185])

Transferring the preheated material to a press is not seen as a significant factor for thermoplastic composite processing due to the insulation by the outer layers of the preform. Typical transfer times range between 15 – 90 seconds, with commercial processes using robotics to automate the transfer process [185]. The rate of closure, coupled with the tool temperature have been shown to be more critical for the formation of a well consolidated and low void content composite. When the material is transferred to the tool the bottom surface cools first (with cooling rates of up to 50°C per second [193]) and the outer skin of the composite is rapidly quenched. It is suggested that increasing the temperature of the bottom of the mould half to 90°C (as opposed to 80°C [185]) reduces the cooling rate of the bottom of the polypropylene when it is first introduced to the mould, allowing for tool closure time [164]. Tool closure speeds are typically between 10-100mm s^{-1} [203], ensuring the temperature differential across the

part is minimised and preventing solidification of the material before the mould is filled [204]. Approach speeds, where the top of the material is not in contact with the top tool surface, should be as fast as the equipment allows and are usually in excess of 425mm.s^{-1} [205].

The tool temperature governs the effective cooling rate of the composite and therefore directly affects cycle time. Typical NI-CM tool temperatures for moulding polypropylene composites are approximately 20 - 80°C [174]. The tool temperature dictates the length of time at which the core of the material is at low viscosity and for increasingly complex geometries both the tool temperature and closure rate should be increased to allow prolonged material flow time [200]. Additionally increases in fibre dominated properties such as tensile, flexural and compressive performance can be achieved for higher tool temperatures [163], [201], although the quality of surface finish has been reported to be reduced [200]. Crystallisation during rapid cooling of semi-crystalline thermoplastics is reported to be a key effect in the bonding of the matrix and fibres, with faster cooling rates leading to lower crystallinities and therefore improved matrix dominated properties, such as strain to failure and impact strength [184].

To aid fibre encapsulation by the polymer and to reduce void content, pressure is applied to the composite during processing. It is desirable, as with temperature, to use lower pressures to reduce capital costs. However relatively high pressures are needed for NI-CM; for example for a CF.PA12 commingled composite, a pressure of 4.2 MPa was used [163]. Optimum pressures are more difficult to determine than preheat temperatures and are much more dependent on the matrix properties. As a comparison, polypropylene composites require pressures of up to 20 MPa [185] during moulding, which is mainly attributed to the viscosity of PP being in the order of 10^3Pa.s, compared to PA12 with a viscosity of approximately 10^2 Pa.s. For discontinuous fibre products, such as GMTs and SMCs, the material is designed to flow in the mould, enabling production of more complex shapes than fabric architectures. To induce material flow, the pressure required is therefore higher than that needed for fabric prepregs and is a function of part complexity. For a simple planar part made from GMT, pressures of around 5 MPa are needed [200], but for a complex shape where large draw is needed, such as a door cassette, up to 40 MPa might be required [197]. Whilst closing speed is linked to removal of the majority of trapped gases during initial consolidation, the

pressure, and time at pressure, are significant factors for reducing the void content of the final part.

The time at pressure is a significant parameter as final void content reduction occurs by diffusion into the matrix, where polypropylene is capable of dissolving 15 times its own volume of air [206]. Void content reductions of 85% have been observed for GMT by increasing the time at pressure from 5 to 40 seconds [200]. Time at pressure has been shown to be the most significant factor for mechanical properties of GMT materials, where an increase from 10 to 50 seconds resulted in a 23% increase in flexural strength [202].

2.3.2.3 Conclusions

There is a large body of research on the rapid processing of glass fibre/polypropylene composites. Non-isothermal compression moulding is the most suitable process as it allows fast manufacture (sub 1 minute cycle times) of long discontinuous fibre thermoplastics composites, whilst maintaining fibre length and tow integrity. The optimisation of processing parameters is important for the successful moulding of these composites, with preheating temperature and time at pressure dominating the mechanical properties of the final component. Definition of the onset of polymer degradation for the system used in this study will be vital to maximise the processing conditions and therefore mechanical properties. Further optimisation of the processing parameters is outside the scope of this study and composites will be produced in accordance with data gathered from this literature review on similar glass fibre/polypropylene systems.

Processing Parameter	Value
Preheat Time	240 seconds
Preheat Temperature	230 oC
Mould Temperature (top)	90 oC
Mould Temperature (bottom)	90 oC
Mould Pressure	10 MPa
Time at Pressure	300 seconds
Transfer Time	~30 seconds
Closure Rate	100 mm.second^{-1}

Table 2-2 - Processing parameters chosen to manufacture CF/PP composites based on literature review

3. Experimental Methodology

3.1 Materials

Datasheets for all the materials used in this study are given in Appendix B.

3.1.1 Fibre

T700SC-60E 12k tow carbon fibre, supplied by Toray Co., was primarily used as the composite reinforcement, as it is widely used in commercial automotive applications. Toray T700SC-50E and unsized 12k AS4 carbon fibre, supplied by Hexcel, Duxford, UK were also used for tow coating rig commissioning to assess the effect on fibre spreading, properties are given in Appendix B.

For microbond testing (Chapter 4), pseudo-recycled fibres were produced to simulate pyrolysis and solvolysis recycling methods. To simulate the pyrolysis recycling process, the virgin T700 fibres were heated in a furnace at 550°C for 10 minutes [207] and subsequently put in a ultrasonic cleaner water bath for 30 minutes, before being dried at 80°C for a week (referred to as CFP fibres). To simulate the solvolysis recycling process, 2g of virgin T700 carbon fibre were soaked in $100cm^3$ of acetone for a week at room temperature. The fibres were then washed three times using fresh acetone, and then refluxed in $200cm^3$ of boiling tetrahydrofuran (THF) for 72hrs. The fibres were washed a further three times with fresh THF, and then dried at 80°C for a week (referred to as CFS fibres).

3.1.2 Matrix

An isotactic homopolymer polypropylene (PP), Sabic 576P (Sabic Europe B.V., Netherlands), was used for both microbond and macroscale experiments. The polymer was supplied as pellets, however to allow coating on the tow coating rig, a powder was required. Cryogenic milling was used to produce the powdered polymer, processed by Goonvean Fibres (Honiton, UK) to a maximum particle size of 90μm (average 65μm).

A developmental powdered epoxy system, DLS 1776 (Hexcel, Duxford, UK), was used as a benchmark thermosetting polymer as it could be melted and cured in a similar manner to the thermoplastics, making it suitable for use on the tow coating rig (Section 3.3).

3.1.3 Coupling Agent

A maleic anhydride grafted polypropylene coupling agent, G3015 (Eastman, UK), was supplied in granular form and was processed into a powder using a ceramic grinder at ambient temperature. In all cases the coupling agent was mixed with the polypropylene at 2wt.% based on work carried out previously by Wong et al. [22].

3.1.4 Commercial Benchmark Materials

A carbon fibre/epoxy advanced sheet moulding compound, HexMC (Hexcel, Duxford, UK), was used as a commercial discontinuous thermosetting benchmark. It consisted of 50 x 8mm fibre bundles with a fibre volume fraction of 0.57 and areal weight of 2000gsm. The material was moulded as a net-shape charge and processed for 10 minutes at 120°C to cure.

A pre-impregnated carbon fibre/PEEK tape, AS4/APC-2 (Cytec Industrial Materials, Heanor, UK), with a nominal volume fraction of 0.61 was used as a discontinuous thermoplastic benchmark by chopping the tape into 25mm lengths. The chopped fibre was randomly distributed within the mould tool and heated to 380°C where it was held for 10 minutes before cooling and demoulding.

3.2   Characterisation Methods

Standard mechanical property characterisation methods used in this study (tensile, flexural and impact testing) can be found in Appendix C.

3.2.1 Differential Scanning Calorimetry

Differential Scanning Calorimetry (DSC) is a thermo-analytical method to measure the amount of energy that is absorbed or released from a sample as it heated, cooled or held isothermally. DSC was used in this thesis to characterise the oxidation induction time

of polypropylene, which is the time taken to reach the onset of thermo-oxidative degradation.

A TA Instruments Q2000 DSC was used to heat the virgin polypropylene at 10°C/min over the range of 190 – 240°C in accordance with ISO 134A. A small sample (10 - 15mg) of polypropylene powder was heated to the set-point temperature under a nitrogen atmosphere to prevent oxidative degradation. The temperature was then held isothermally at the set-point for 3 minutes to reduce the effect of any transient temperature variations on the recorded data. After 3 minutes the gas supply was switched to air, whilst being held isothermally. As the polypropylene sample degraded an exothermic reaction occurred, and the onset time for this reaction (from the initial introduction of air) was measured. 5 samples were taken at each set-point temperature and an average was taken to obtain an oxidation induction time for each set point temperature.

3.2.2 Microbond Test Method

The method for producing carbon fibre/polypropylene microbond samples was based on work by Yang et al. for glass fibre/polypropylene [96]. The PP pellets were heated on a hot plate set to 200ºC to melt the polymer. The residence time on the hot plate was less than 2 minutes to ensure there was no risk of polymer degradation. Tweezers were then used to pull the molten polymer into a long fibre, the diameter of which was not controlled, and could be varied by pulling at different rates from the hot plate. The long PP fibres were subsequently cut into shorter lengths to allow easier manipulation. Single carbon fibres were suspended from a backlit panel to assist with viewing, where a small amount of tape was needed on the end of each fibre to keep it in tension whilst preparing the samples. To attach the polymer fibre to the suspended carbon fibres, an open knot was made with the polymer fibre using two pairs of precision tweezers. This knot could then be positioned around the carbon fibre and the polymer fibre ends pulled to secure it in place. The embedded length and droplet diameter are a function of the volume of polymer added, so could be controlled by cutting the loose ends of the knot and by changing the polymer fibre diameter.

The droplets were formed in a nitrogen-purged oven for the non-degraded samples and under atmospheric conditions for the degraded samples. Once enough samples had been made, they were transferred to an oven on a specially prepared mesh to form the droplets. The degraded microdroplets were formed at 220°C for 5 minutes. The non-degraded microdroplets were heated under a nitrogen atmosphere for the whole heating and cooling cycle. Again the samples were heated to 220°C, and held at temperature for 5 minutes.

A different method was used to prepare the carbon fibre/epoxy samples. The epoxy used was B-staged, in a state of partial cure where full cross-linking occurs through the addition of heat and pressure at a later stage of processing. To further aid processing, this epoxy was able to be melted below its curing temperature, which allowed it to be pulled into fibre without curing. The epoxy was much more brittle than PP, which prevented it from being tied onto the carbon fibre. A soldering iron was used to apply heat (without touching) to an epoxy strand, making it coil around the fibre to secure it in place. These samples were transferred to a preheated oven at 125°C to cure for 23 minutes in accordance with previous work carried out by Bond [138].

Once the microdroplets had been produced in the oven, the individual fibres were mounted to card tabs using Araldite and left for 4 hours to cure. The card tabs allowed the fibre to be easily aligned in the loading direction as well as ensuring the fibre free length was kept constant between tests. Once the adhesive had cured the samples were viewed under an optical microscope and the embedded length, droplet diameter and fibre diameter were measured using ImageJ software. Finally, excess card was removed from around the fibre and a hole was punched in-line with the fibre to facilitate attachment to the tensile testing equipment

The card tabs were suspended from the punched hole, on a steel hook attached to a 10N load cell of an Instron tensile testing machine (Model 3342). A fixture (as used by Yang et al. [96]) comprising two knife edges, which were movable by micrometer heads, constrained the droplet vertically. The knife edge separation could be finely controlled by the micrometers and was kept constant for each test. Positioning of the knife edges was aided by the use of a stereo microscope at x45 magnification.

The knife edge separation was 14µm and the test was carried out at a constant rate of 0.1mm.min^{-1} in accordance with findings from the literature. Non-axisymmetric samples and samples that failed by fibre failure were not included in the results. After testing, the samples were re-examined under a microscope to check pure debonding had occurred and for re-measurements of the embedded length. Approximately 20 tests were used to obtain the IFSS value for each sample.

3.2.3 Fibre Strength Measurements

Single fibre tensile testing was used to measure the tensile strength of the as-received carbon fibre and pseudo-recycled fibres to determine whether any damage had been introduced into the fibre during sizing removal. The test was carried out in accordance with ISO 11566. Single carbon filament were extracted at random from a larger fibre tow and glued to polymer tabs using a UV curable epoxy resin. 30 - 35 samples were manufactured for each fibre type to provide high confidence limits, with approximately 80-90% of these samples being successfully tested.

A specimen was mounted to a micro-tensile testing machine and gripped at each end of the fibre. The fibre diameter was measured by a laser micrometer to allow calculation of the fibre tensile strength from the fibre cross-sectional area and recorded load. The gauge length of the fibre was kept constant at 25mm. A 5N load cell (range: 0.1 – 5N, resolution: 10^{-4}N) was used to load the specimen at a crosshead speed of 1mm.min^{-1} until the fibre failed. The fibre tensile strength was calculated using Equation 3-1

$$\sigma_f = \frac{F_{max}}{A_f}$$

Equation 3-1 - Calculation of the fibre tensile strength from the maximum force (F_{max}) and the cross sectional area of the fibre (A_f)

A software package, UvWin, was used to record the force-displacement data. The tensile strength of the fibres was automatically calculated in accordance with ISO 11566. Weibull analysis was subsequently used to characterise the fibre strength, which is a widely used method for this procedure [116], [208], [209]. The general three-parameter model (Equation 3-2) was simplified to a two-parameter model by assuming

that σ_{th}, the threshold stress (where $P_{(\sigma)} = 0$ for $\sigma < \sigma_{th}$) is equal to zero for brittle materials [210] (further details are given in Chapter 5).

$$P_{(\sigma)} = 1 - exp\left[-\delta V \left(\frac{\sigma - \sigma_T}{\sigma_0}\right)^m\right]$$

Equation 3-2 - Equation describing the 3 parameter Weibull distribution, where $P_{(\sigma)}$ is the probability of fibre failure, δV is the change in volume, σ is the applied stress, σ_{th} is the threshold stress, σ_0 is the Weibull scale parameter and m is the Weibull shape parameter

A probability estimator (Equation 3-3) was used to calculate the probability of fibre failure ($P_{(\sigma)i}$) for the ith strength. N was the number of samples tested, which were sorted into ascending order and assigned a rank value (i), and α and β were statistical parameters that are commonly set to $\alpha = 0.5$ and $\beta = 0$ [208]. These values were used because they have been shown to give a less biased value of the shape parameter for a sample size of less than 50 specimens [210].

$$P_{(\sigma)i} = \frac{i - \alpha}{N - \beta}$$

Equation 3-3 - Probability estimator for Weibull analysis to calculate the probability of fibre failure for the ith strength

As single fibre testing was carried out over one gauge length, Equation 3-2 was rearranged to give Equation 3-4, in the form $y = mx + c$, where the Weibull parameters σ_0 and m were estimated using a linear least squares regression analysis.

$$ln\left[-ln\left(1 - P_{(\sigma)}\right)\right] = m.\,ln(\sigma) - m.\,ln(\sigma_0)$$

Equation 3-4 - Rearrangement of Weibull three parameter model, into a two parameter model and arranged in the form $y = mx + c$

3.2.4 Surface Roughness Measurements

Atomic force microscopy (AFM) was used to characterise the topology of the carbon fibres. A glass slide was used as the substrate for the carbon fibres. Two strips of Araldite were applied along the top surface of the slide at the extremities of the longest edges, which allowed a large section in the middle (with no adhesive) for the carbon fibres to be analysed. Single fibres were then extracted at random from the fibre bundles

and laid perpendicular to the applied resin. The ends of the fibre were gently pulled to ensure that the fibre was straight and that it was in direct contact with the glass slide. The adhesive was cured at room temperature for 4 hours according to the manufacturer's data.

A Veeco Dimension 3000 SPM system atomic force microscope (AFM) was used to measure the surface topology of the fibres. The AFM was used in tapping mode with a scan area of 2 x 2µm measured for each sample. 12 scans were carried out for each fibre type, with 2 scans per fibre, using the same parameters but in different locations. An open-source analysis package (Gwyddion) was used to analyse the output and calculate the roughness values. The background of the fibre was removed by a 2nd order polynomial algorithm and the roughness values were calculated using a moving average calculation.

3.2.5 Surface Composition Measurements

Surface chemical composition measurements were characterised by X-ray photoelectron spectroscopy (XPS). Samples were prepared by covering a 25.4mm diameter disc with adhesive tape and placing longitudinal strips of carbon tow ensuring that the disc was completely covered. To minimise surface contamination, the tow was extracted from an unexposed region of the bobbin and kept in foil. Once the tow was fixed to the disc, excess fibre was removed using compressed air.

XPS analysis was performed using a Kratos AXIS Ultra DLD photoelectron spectrometer equipped with an Al kα X-ray source at 1486.6 eV. All spectra were recorded at a 90° take-off angle, with pass energies of 80eV (resolution 0.5eV/step) and 20eV (resolution of 0.2eV/step) to obtain the survey spectra (0 – 1400eV) and high resolution spectra for the C1s peaks respectively. The surface atomic composition was calculated using Casa XPS software with Kratos sensitivity factors. Curve fitting of the XPS high resolution spectra was carried out using a Gaussian-Lorentzian product function with a Shirley type background. A G/L mix of 0.5 was used for all peaks except the main graphitic peak, where a G/L mix of 0.8 was used to fit the asymmetric graphitic feature [211], [212].

3.3 Tow Coating Rig Commissioning

A carbon fibre tow coating rig was designed and manufactured to produce combinations of polymers and fibres at different fibre volume fractions as these materials were not available commercially. The rig consisted of four sections and was designed to be modular so that each section could be moved or adjusted easily to optimise the coated tow output. The first section (Figure 3-1a) consisted of a number of static bars through which the fibre was passed to increase tension and spread the fibres laterally, increasing surface area. The static bars could be adjusted both vertically and horizontally, with eyelets at the front enabling multiple tows to be processed simultaneously.

Tow spreading has been used frequently in the literature [213], [214] and in commercial systems (Sigmatex SigmaST and Oxeon TeXtreme) for unidirectional and woven composite pre-pregs. For these applications it is used to achieve a lower crimp angle and therefore produce composites with straighter fibres. This enhances the mechanical properties in both compression and tension as well as decreasing the weight by removing resin rich areas near the fibre cross-overs. The purpose for spreading here was to reduce the polymer melt flow distance by reducing the height of the fibre bundles and allow more intimate contact between the fibres and matrix, improving impregnation during consolidation and reducing cycle times [215]. Once the fibre tow was spread slightly and tensioned, it was passed through a vibrating powder tray (Figure 3-1b).
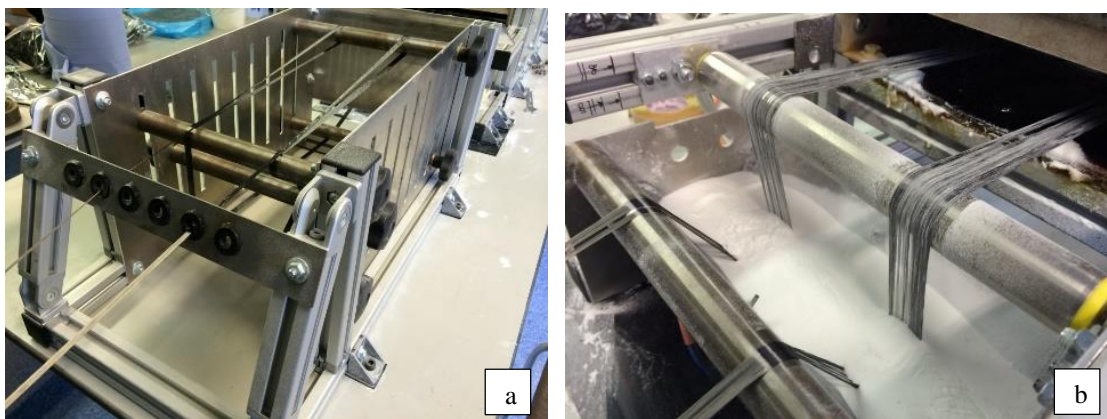

Figure 3-1 – Spreading section of the tow coating rig (a) consisting of a number of static bars to increase tension and spread the fibre bundles. Power tray section (b) showing spreading and coating of the fibres with polypropylene powder.

The vibrating powder tray was filled with a polymer powder and fluidised by two electric DC motors with variable speed control mounted on either side of the tray. The fluidisation of the powder allowed the fibre tow to pass through the powder tray without significantly increasing the tension or causing fibre breakage. After coating, the polymer was melted in the heating section (Figure 3-2) which used two ceramic 650W medium-wave infrared heaters. These heaters were chosen as the polymers used here have spectral absorption curve peaks between 3 and 4µm (a similar wavelength to the output of the infrared heaters), ensuring the polymer was heated efficiently. Whilst the polymer was being melted, it was forced into the fibre tow by two free rotating rollers to improve consolidation. The rollers shown towards the front of Figure 3-2 allowed the polymer to be preheated and the rollers at the back were spring loaded consolidation rollers that forced the polymer into the tow. The spring compression could be adjusted to allow modification of pressure on the tow.
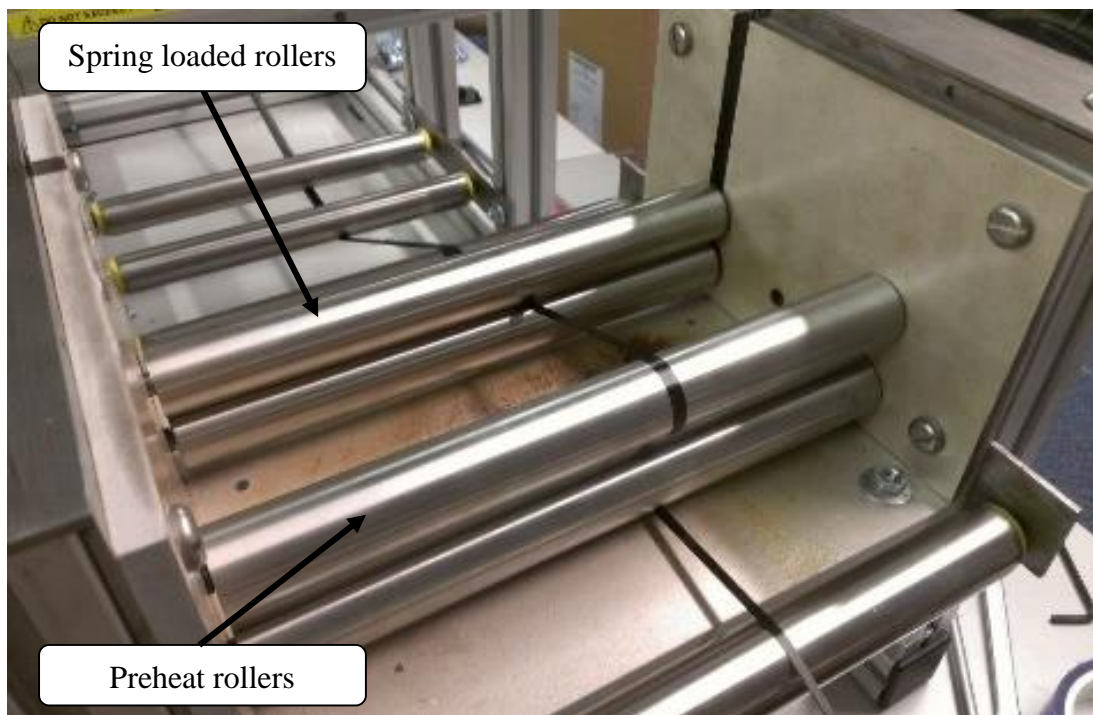
Figure 3-2 - Heating section of tow coating rig showing preheat and consolidation rollers to ensure maximum impregnation of the polymer into the tows (heaters and side insulation removed for photo)

The coated fibre tow was cooled and rewound onto a bobbin for further processing in the final section of the rig. A three-phase AC motor, in conjunction with an inverter, was used to pull the tow through the rig and control the rotational speed. A 50:1

reduction gearbox was attached to the motor shaft to give a range of rotational speeds suitable for tow coating. The line speed was set by the motor speed and the diameter of the bobbin, which were chosen to give speeds ranging from $0 - 10 \text{m.min}^{-1}$.

3.3.1 Fibre Spreading Measurements

For the tow to be spread effectively, the tension had to be high enough to force the fibres to roll over each other and push outwards to the sides (see Figure 3-3). To quantify the tension induced by the static bars, different roller placements were tested, Figure 3-4 and Figure 3-5 show the two configurations that were used. Each configuration had 3 variants that assessed the effect of modifying the angle between each roller and the distance between them.
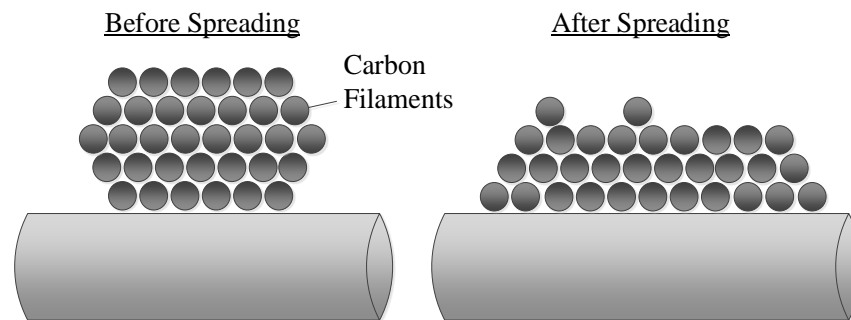
Figure 3-3 - Simplified schematic of spreading induced in fibre tows during processing through tow coating rig
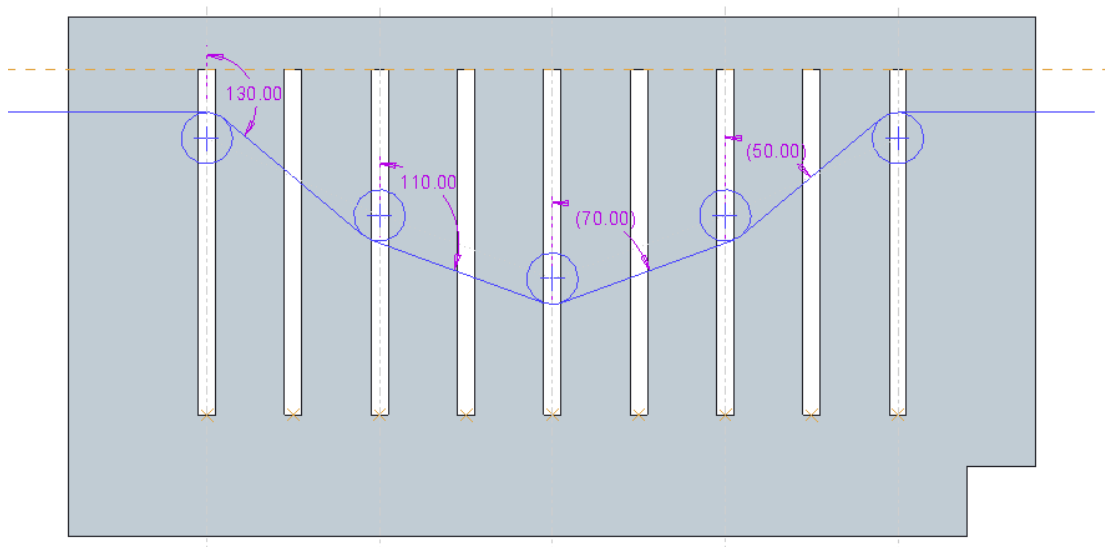
Figure 3-4 - View from the side of the spreading section of the rig showing static bar positions (circles) and path of fibre for Configuration 1 used for tension measurement experiments. Angles displayed in purple were modified to produce different contact lengths and total distance between bars.
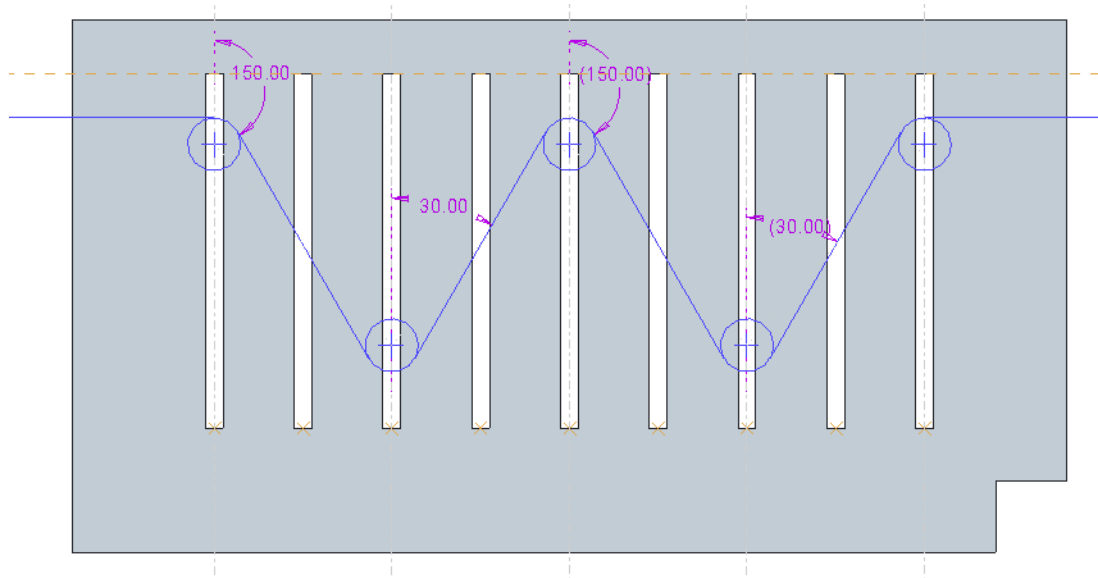
Figure 3-5 - View from the side of the spreading section of the rig showing static bar positions (circles) and path of fibre for Configuration 2 used for tension measurement experiments. Angles displayed in purple were modified to produce different contact lengths and total distance between bars.

The contact length was calculated as the length that the tow was in contact with the rollers for each set-up and total distance was calculated as the sum of the free lengths of tow measured between each roller. Increasing contact length and total distance both resulted in an increase in tension, as increasing contact length effectively increases the friction in the system. To assess the effectiveness of the spreading section, the fibre tow was initially run through the rig without coating.

The tow width was recorded using a video camera with a rule mounted directly above, but not touching the fibre. The sample rate was every 20 seconds (over a 20 minute period) with a 0.5mm margin of error. The tow width was measured for each configuration tested and was found to increase with tension (and therefore contact length and total distance). The results are presented in Figure 3-6. Irfan et al. [214] measured the effect of roller angle (α) and distance (L) on the tow width and compared it to a calculated parameter, $L\cos\alpha$. The authors found that the tow width increased with increasing L and decreasing $\cos\alpha$, which is in agreement with the results reported here as decreasing $\cos\alpha$ would effectively lead to a higher contact area on the rollers.
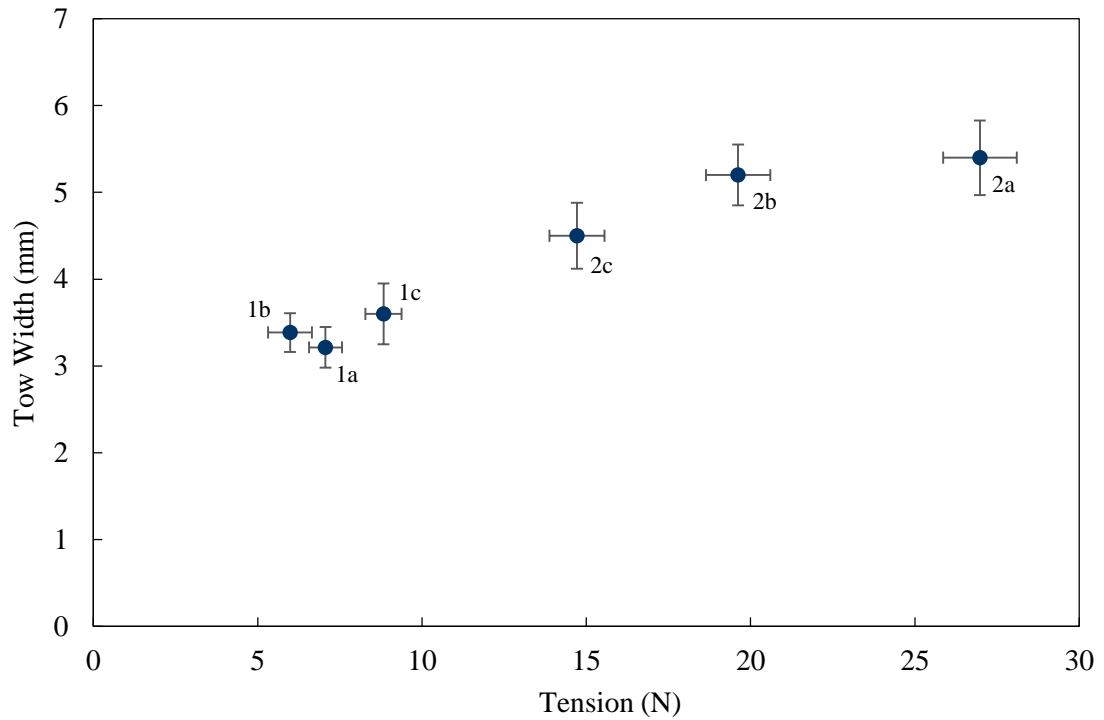
Figure 3-6 - Relationship between tow tension and tow width for the tension measurement experiments with experimental configuration shown next to each set of data. (error bars indicate standard deviation).

Configuration	Measurement	Bar 1-2	Bar 2-3	Bar 3-4	Bar 4-5
1a	Fibre Exit Angle	130	110	70	50
	Distance	130.2	106.4	106.4	130.2
1b	Fibre Exit Angle	130	120	60	50
	Distance	130.2	115.5	115.5	130.2
1c	Fibre Exit Angle	140	120	60	40
	Distance	155.3	115.5	115.5	155.3
2a	Fibre Exit Angle	150	30	150	30
	Distance	199.8	200.3	200.3	199.8
2b	Fibre Exit Angle	140	40	140	40
	Distance	155.3	155.9	155.3	155.9
2c	Fibre Exit Angle	130	50	100	50
	Distance	130.2	130.9	130.9	130.2

Table 3-1 - Fibre exit angles and distances between static bars used for the configurations shown in Figure 3-6.

3.3.2 Volume Fraction Optimisation

To commission the rig, a number of tests were performed to verify that the tow was consistent and of an acceptable volume fraction. A nominal fibre volume fraction of

0.45 was chosen so that moulded composites would have suitable properties for semi-structural automotive applications. Since the volume fraction relies on the fibre surface area available, the width of the tow (after spreading) was a major consideration for the minimum volume fraction that could be achieved. To assess the range of achievable volume fractions, a developmental epoxy powder (Section 3.1.2) system was used for convenience. The epoxy melted at 65°C and cured at 120° C which meant that trials could be run at low temperatures compared to the thermoplastics and that subsequent processing and moulding would be easier. The volume fraction was measured by chopping the continuous coated tow into 1m lengths and measuring the mass. As negligible fibre was lost during processing, the mass of polymer could be determined and the volume fraction was calculated from Equation 3-5.

$$V_f = \frac{v_f}{v_f + \left(\frac{m_p}{\rho_p}\right)}$$

Equation 3-5 – Calculation of the fibre volume fraction (V_f) from the discontinuous impregnated tape. Where v_f is the volume of fibre (calculated from the linear density), and m_p and ρ_p are the mass and density of the polymer respectively

The effect of material and processing parameters on the tow volume fraction were investigated for commissioning of the tow coating rig and are outlined in the following sections

3.3.2.1   Effect of Fibre Sizing

Fibre sizing is extremely important for technical fibres as it aids handling and provides protection to the fibre, as well as improving the interfacial bond between the fibre and polymer system. Three fibre sizing levels were trialled here (I. unsized, II. 60E - 0.3% epoxy sizing and III. 50C - 1% epoxy sizing). Figure 3-7 shows issues caused with the unsized fibre during coating and as a result, no data was collected from the trial as excessive fibre breakage occurred, making it unsuitable for processing. The 60E fibre was able to be processed more successfully and with the experimental set-up gave a volume fraction of 0.51 ± 0.04. The low level of sizing allowed the fibre to spread and very minimal fibre breakage occurred during processing. The 50C fibre was noticeably much stiffer than the 60E fibre and fibre spreading was reduced due to the higher proportion of sizing, resulting in an average volume fraction of 0.70 ± 0.04. Fibre twist

appeared to be reduced for the 50C fibre, but the low spreading and consequently high volume fraction meant that the 60E was chosen.
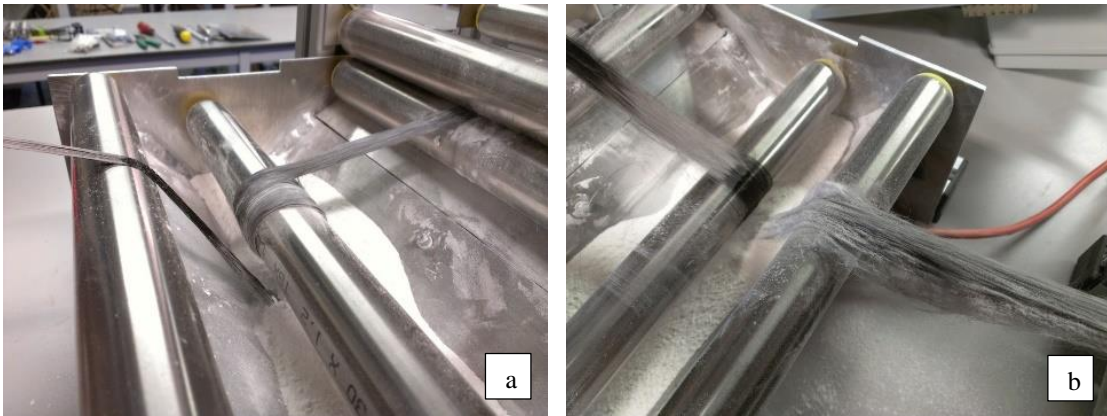
Figure 3-7 - Issues caused in the vibrating powder tray section whilst using unsized fibre. a) Unsized fibre wrapping around rollers, b) excessive powder pick-up and fibre breakage

3.3.2.2   Effect of Powder Tray Vibration Level

The level of vibration could be modified through control of the two variable speed DC vibration motors. Vibration levels of 30%, 50%, 70%, 85% and 100% (percentage of motor output) were tested to assess the effect of vibration on the volume fraction. At lower vibration levels, the polymer powder was not able to be fluidised fully and holes in the powder formed behind the tow path. This caused higher variability in the coated tow output and consequently a higher volume fraction. Additionally the tension was greatly increased by the loss in fluidity of the powder and large amounts of fibre breakage occurred when processed for longer periods of time. Figure 3-8 shows the effect of vibration level on the coated tow volume fraction. An optimum vibration level was found at 85% power where the vibration was strong enough to fluidise the powder, but not too excessive that it would cause powder to detach from the tow and to fall back into the powder tray.

3.3.2.3   Roller Configuration

In the powder tray section two rotating rollers were required to guide the fibre through the powder for coating, three configurations of the top roller position were trialled to investigate changes in volume fraction. A schematic of the roller positions is shown in Figure 3-9, where each position defined the angle at which the fibre exited the powder

tray. Position 1, 2 and 3 corresponded to exit angles of -30°, 0° and 30° respectively (where 0° was vertical).

Figure 3-8 - Effect of powder tray vibration level on tow fibre volume fraction (black dotted line represents the target volume fraction, error bars indicate standard deviation)
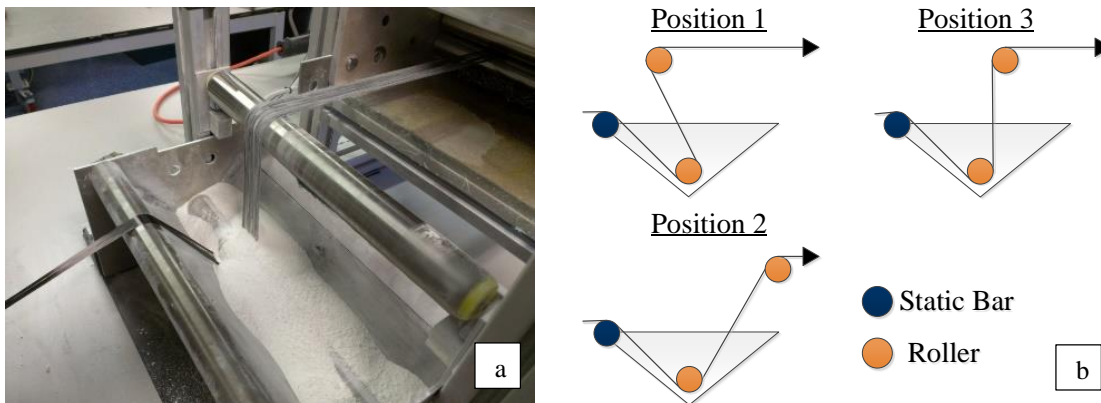
Figure 3-9 - Powder tray rollers required for coating a) and schematic of roller positions trailled to modfiy the exit angle of the fibre b)

Position 1 (-30°) produced the highest volume fraction of the tested configurations (0.58 ± 0.08). As the fibre passed through the powder tray, the top surface appeared to have a thicker coating than the bottom and as the fibre was directed at -30°, the top surface was therefore inverted as it left the tray. Powder from the inverted top surface of the fibre was easily detached from the fibre due to the vibration, causing an increase in volume fraction. Increasing the angle of fibre leaving the powder tray decreased the

volume fraction as the top surface of the fibre became less inverted, retaining the powder on the surface. Position 3 (30°) gave the lowest volume fraction 0.45 ± 0.06, but had a high variability as the fibre acted like a conveyor belt pulling lumps of powder out of the powder tray. Position 2 (0°) appeared to give a consistent coating, whilst maintaining a reasonably low volume fraction 0.48 ± 0.03 compared to the first position.

3.3.2.4   Line Speed

The line speed was an important parameter as it defined the throughput for the rig. The motor inverter was set to speeds of 6, 8, 10, 12 and 14 which corresponded to line speeds of 2.2, 3, 3.8, 4.6 and 5.4m.min^{-1} respectively. The line speed was calculated by dividing the bobbin circumference by the time taken for the bobbin to complete 1 rotation. The bobbin was recorded using a video camera, and the line speed was an average of the values recorded. The results of the line speed tests are presented in Figure 3-10. Overall there was an increase in volume fraction from 2.2 - 5.4m.min^{-1}, with acceptable volume fractions being produced from 2.2 - 4.6m.min^{-1} (0.39 ± 0.03 to 0.44 ± 0.03 respectively). It was observed that the width of the tow decreased slightly through the spreading section of the rig at higher line speeds, increasing the volume fraction.
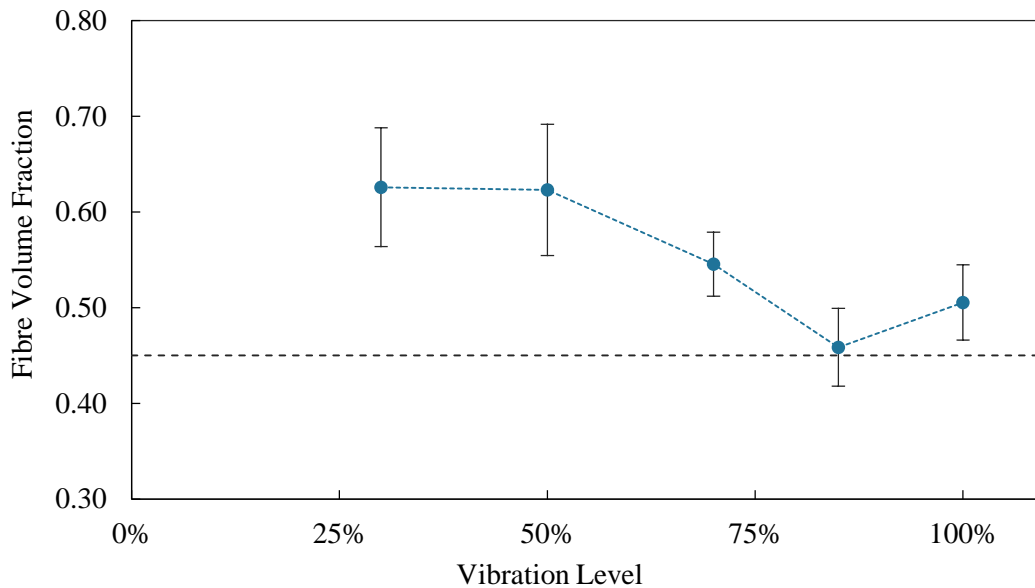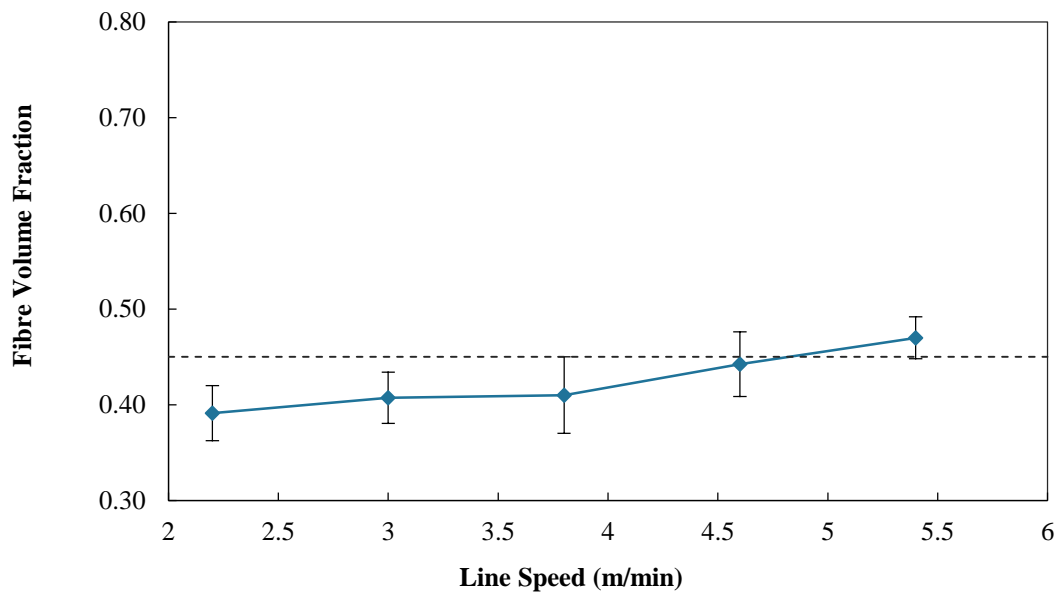

Figure 3-10 - Effect of tow coating rig line speed on tow fibre volume fraction (black dotted line represents the target volume fraction, error bars indicate standard deviation)

Based on the above experiments the optimised conditions for tow coating were; a tow tension of approximately 15N achieved using configuration 2c of the spreading section, vibration level of 85%, roller position 2 and a line speed of 3.8m.min^{-1} The combination of these parameters provided the most consistent output with an acceptable volume fraction range. Although higher tensions, and therefore spreading was achievable, the configuration that gave approximately 15N was chosen. This was due to fibre breakages downstream caused by further increases in tension when the fibre passed through the vibrating powder tray. Similarly for line speeds of 4.6 and 5.4m.min^{-1}, a number of issues occurred in the heating section causing stoppages in production, so a line speed of 3.8m-min^{-1} was chosen.

3.3.3 Heating Requirements

The heaters were specified for a number of thermoplastic polymers to allow processing of polypropylene and enable use of the rig for subsequent projects. Figure 3-11 shows the minimum power requirements for the thermoplastic matrices. The energy required to melt each thermoplastic was calculated using Equation 3-6; for amorphous thermoplastics (PC and PEI) the heat of fusion was 0 as there was no phase change in the polymer at the melting point. This meant that a much lower power was required for melting the amorphous polymers compared to the semi-crystalline thermoplastics.
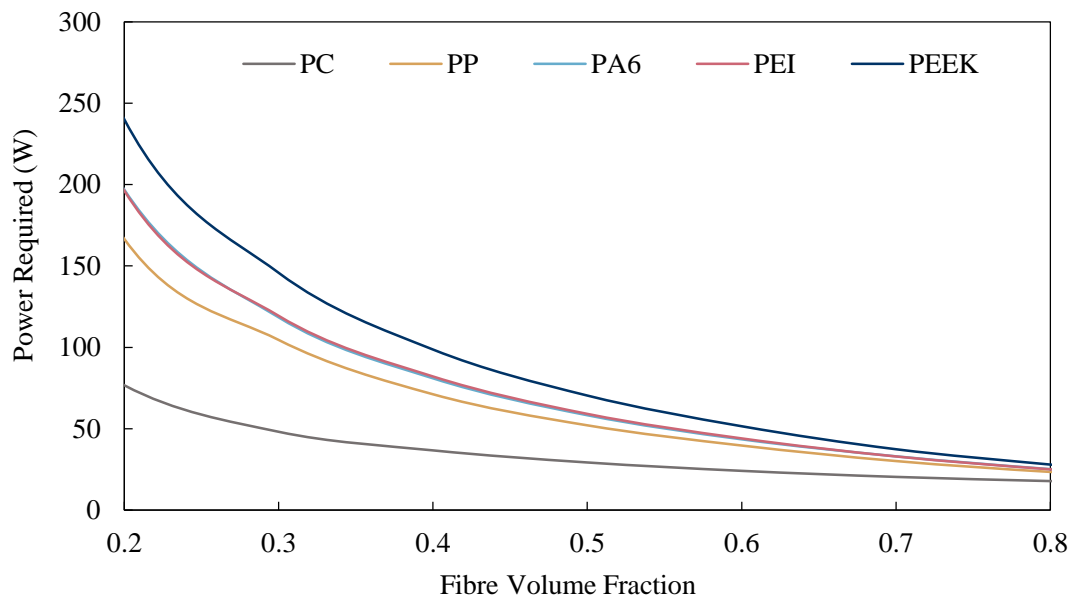
Figure 3-11 - Heating power requirements for various thermoplastic polymers with increasing fibre loading for a line speed of 10m/min

$$Q = mC\delta T + m\delta H^{o}_{fus}$$

Equation 3-6 - Calculation of the energy required to melt each polymer (Q), where m is the mass of the polymer, C is the specific heat capacity, δT is the change in temperature (ambient to the polymer melt temperature) and δH^{o}_{fus} is the heat (or enthalpy of fusion)

The T700 fibre had a linear mass of 0.8g.m^{-1} and the mass per metre of the polymer was calculated based on the volume fraction required. The power was calculated for a 10m.min^{-1} line speed and an oven length of 300mm, which meant that approximately 0.5m of polymer per tow needed to be melted every second. As multiple tow processing was desired to increase throughput, the power required was then multiplied to specify the heaters. Figure 3-12 shows the effect of introducing more tows, using PEEK as the coating material, with the horizontal lines corresponding to the heater power outputs.

Using PEEK to coat the fibre was the most demanding for the heating requirements. Two 650W heaters were specified for the heating section to account for heating losses and also ensure that the heaters weren't run at maximum capacity for prolonged periods of time.
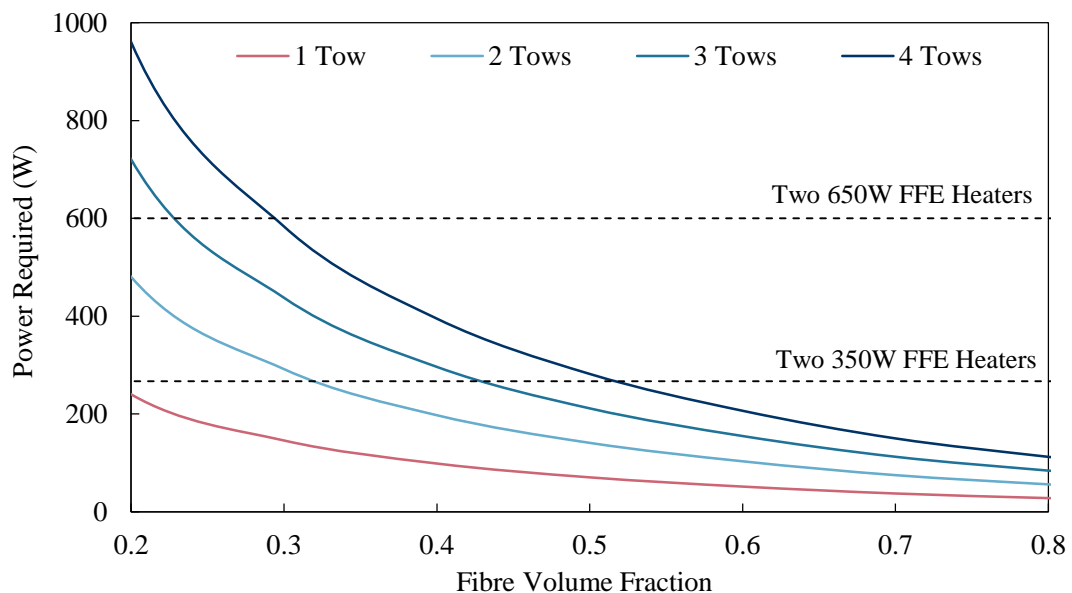
Figure 3-12 - Heating requirements for multiple tows with PEEK. Dotted lines represent the maximum power output that the ceramic heaters could apply to the heated area

3.3.4 Coated Fibre Quality

The coated tow was examined under SEM to determine the quality of coating and whether the fibre had been sufficiently encapsulated. As expected, the epoxy matrix used for commissioning showed good wetting of the fibres and consistent coverage over the tow when viewed using SEM. Figure 3-13 shows micrographs of the CF.PP samples. The high viscosity of the polymer inhibited wetting into the fibre bundles and the spreading of the polymer was not consistent across the surface. The polymer also seemed to push the fibres apart instead of flowing in between them. After initial investigations into the wet-out of the fibre, the consolidation pressure was increased in the heating section of the tow coating rig. Figure 3-14 shows the micrographs for the CF.PP with additional consolidation pressure. The added pressure improved the wetting of the fibre surface and the fibres were noticeably stiffer when extracted from the rig.
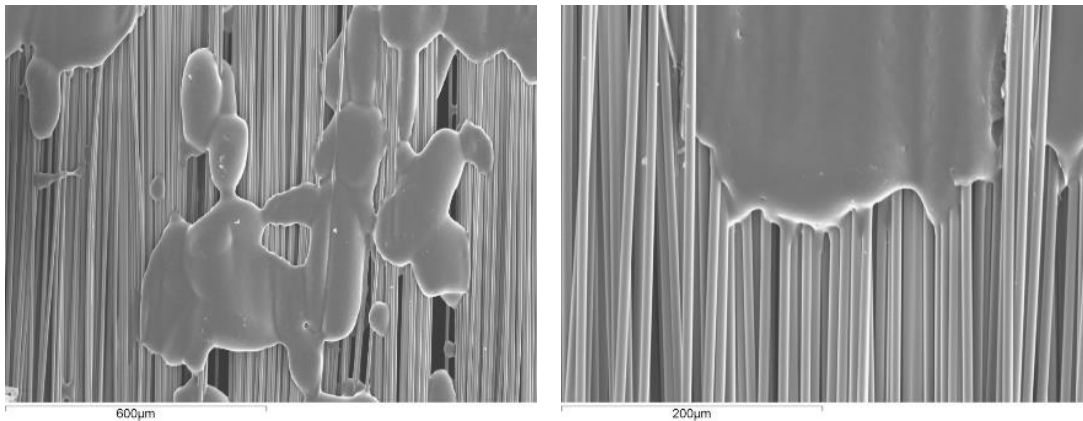
Figure 3-13 - SEM micrographs of carbon fibre tow coated with polypropylene, showing little impregnation into the fibre tow
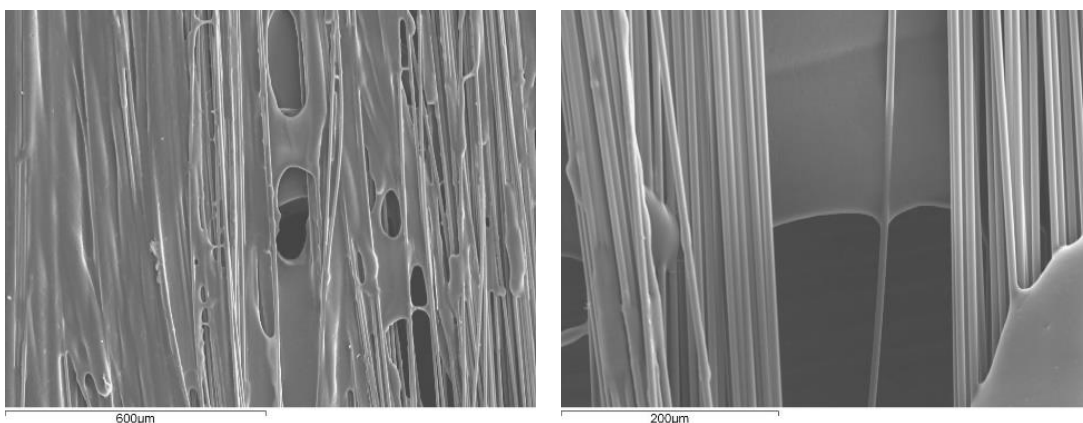
Figure 3-14 - SEM micrographs of carbon fibre tows coated with polypropylene using additional consolidation pressure in the heating section, demonstrating good impregnation into the fibre bundles

3.4   Discontinuous Fibre Processing

To process the continuous coated tow into discontinuous chips for composite manufacture, the tow was chopped into 25mm lengths. Approximately 650g (500m) of coated tow was required for each panel. After the fibres had been chopped, it was found that the bulk factor of the material was very high, primarily due to fibre curvature induced by the rewinding bobbin.

To remove the loft, the fibres were preformed into a series of mats which could then be stacked easily into the tool. A 406 x 406mm square compression moulding tool fitted to a 160T Daniels upstroke press was used for moulding all the panels. The coated fibres were divided into 10 layers of equal mass to ensure that an even fibre areal density was achieved during preforming. To reduce fibre alignment at the edges of the preforms, the coated fibre was laid out over approximately 420mm square onto a high temperature release film. The coated fibre stack was inserted between two aluminium plates and transferred to a press (Daniels 160T downstroke) at 200°C and 0.1MPa for 5 minutes. After removing the preform from the press, net-shape preforms were stamped out using a 400mm square cutting forme (S&W cutting formes, Nottingham, UK) which was loaded into a press with the preforms at ambient temperature. Figure 3-15 shows the coated fibre stack before and after preforming

Figure 3-15 - Preforming for 406mm square parts. Fibre stack before preforming (left) and fibre stack after preforming (right)

3.4.1 Moulding Procedure

The literature review identified that non-isothermal compression moulding was a suitable processing method for these composites, the moulding process was as follows. Preforms were stacked between two polished steel plates that acted as a carrying

medium and were transferred to a press at 230°C to preheat the material. It should be noted that the literature suggests using infra-red heating to preheat the material, however initial trials showed that preheating was faster and more consistent using conductive heating. Thermocouples were placed in the bottom middle and top layers to monitor the temperature during the heating cycle, the results are presented in Figure 3-16. The time to set point temperature was approximately 4 minutes at which point, the stack (including the steel plates) were transferred to the compression moulding tool. The press was closed at a speed of 100mm.s^{-1} and a pressure of 10MPa was applied for 5 minutes to consolidate the part. Figure 3-17 shows a typical carbon fibre/polypropylene panel moulded using this procedure.
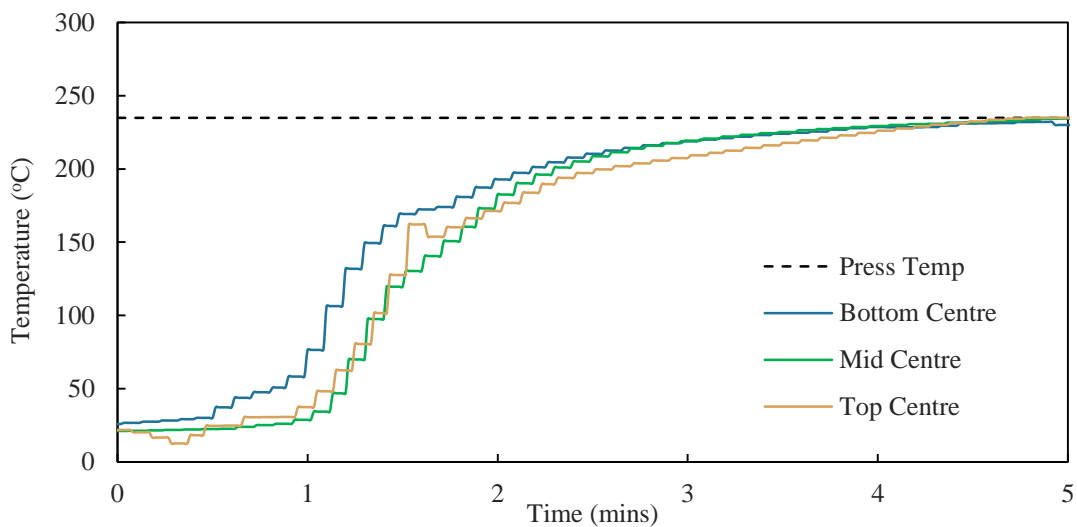
Figure 3-16 - Press preheat temperature profile for top, middle and bottom of preform stack

Figure 3-17 - Carbon Fibre/Polypropylene panel moulded at 0.45V_f manufactured using NI-CM for this study

4. Interface Characterisation Using the Microbond Test

4.1 Introduction

The mechanical performance of the composite at the macroscale is significantly influenced by the microscale interface which governs the stress transfer capability of fibre reinforced composites. The microbond test method was used to characterise the interfacial strength between carbon fibre and polypropylene, as the literature had indicated that the affinity of these materials was poor. This method was chosen as sample preparation is relatively simple (see Section 3.2.2), it allows detection of small changes in interfacial strength, and is widely used so comparisons can be drawn to other data in the literature. The aim of this study was to investigate the interfacial adhesion between carbon fibre and polypropylene and assess whether improvements could be made, which may enhance macroscale performance.

One of the main issues with using carbon fibre is that commercially available tows are coated in sizing, which is formulated to increase chemical bonding between the fibre and thermosetting polymers. It was identified from the literature that polar high temperature thermoplastics had higher interface strengths when the epoxy compatible sizing was removed [68]. To test this theory the sizing was removed by two methods which simulated pyrolysis and solvolysis (CFP and CFS respectively) recycling technologies currently used for carbon fibre. The first objective was therefore to simultaneously investigate the effect of sizing removal and compatibility with pseudo-recycled fibres on the interface strength, as it was identified that recycling technologies for carbon fibre will significantly reduce the cost of the material in the future.

The second objective was to investigate enhancement in the interface strength through the addition of a maleic anhydride coupling agent. This coupling agent was chosen as it is well known that maleic anhydride can significantly increase IFSS between glass fibre and polypropylene, where increases of 25 – 110% have been reported for these systems [96],[216]. Additionally a recent study between recycled carbon fibre and polypropylene reported 100-200% increases in IFSS [22]. The use of this coupling agent for sized carbon fibre and polypropylene has not been previously reported. Despite advances in thermoplastic-compatible sizing agents for carbon fibre, these

niche products command a much higher price than epoxy compatible counterparts. Significant cost savings can be realised if the adhesion between standard commercial carbon fibres and polypropylene can be improved.

The final objective of this study was to investigate the effect of polymer degradation on the interface strength using the microbond test. It has recently been suggested that preparation of microbond samples should be conducted under an inert atmosphere as the risk of polymer degradation is high when prepared under atmospheric conditions. Thermo-oxidative degradation has been shown to have a significant effect on the IFSS for glass fibre/polypropylene systems with up to 70% reductions in IFSS observed after only 4 minutes at 220°C, and complete degradation after 6 minutes [217]. Moreover, analysis of the recorded values in a recent paper on recycled carbon fibre/polypropylene appeared to be very low (6.5MPa [22]) compared to values reported for glass fibre/polypropylene systems (10 - 25MPa [96]), despite using a coupling agent.

Due to differences in data recorded between institutions as a result of different testing equipment and methodology, a carbon fibre/epoxy (CF.EP) benchmark was used to compare values against data reported in the literature and therefore validate the experimental setup. Samples were produced using virgin fibre (with epoxy sizing) only. It was found that the CF.EP benchmark had an IFSS of 45.8MPa ± 4.6, which was within the range of other values reported for similar systems [212], [218], [219], and therefore supports comparison of subsequent results collected here. As an additional verification of acceptable droplet production, the embedded lengths were plotted against the droplet diameter [220]. A linear fit through the origin confirms good droplet formation, as shown by the results in Appendix E. A summary of the data recorded for all interfacial shear strength testing is given in Table 4-1.

4.2 The Effect of Fibre Sizing

Sizing is applied to fibres to improve handling and provide protection during transport and processing [10], but is also optimised to enhance adhesion between the fibre and matrix, either through superior wetting properties or chemical bonding [221]. In this study, the commercially applied sizing on the carbon fibre was optimised for

thermosetting matrices, in particular epoxy, so chemical interaction between the sizing and thermoplastic polymer was not expected [81].

Sample	IFSS (MPa)		Successful Tests	Total Tests	Yield
	X	s			
CF.PP (degraded)	3.4	1.2	31	32	0.97
CF.PP (non-deg)	8.0	2.2	35	37	0.95
CFP.PP	8.3	1.8	25	30	0.83
CFS.PP	10.6	1.0	21	25	0.84
CF.mPP	31.6	4.8	26	86	0.30
CFP.mPP	35.9	2.6	16	51	0.31
CFS.mPP	36.2	2.9	22	47	0.46
CF.Epoxy (benchmark)	45.9	4.6	17	67	0.25

Table 4-1 - Summary of interfacial shear strengths and yield (successful tests/total tests) for all microbond data

Two types of force-displacement plot (Figure 4-1) were observed for the samples tested in this section and are indicative of low interface strength systems (the titles 'Type 1' and 'Type 2' etc. were chosen arbitrarily). The 'Type 1' plot was observed for almost all of the low interface strength samples and was characterised by a sharp drop in load at interfacial failure, directly followed by a constant load reading which is reported to be proportional to the friction of the droplet sliding along the fibre (dynamic friction) [106], [133]. The residual force was found to correlate reasonably well to the embedded area of the droplet indicating that thermal residual stresses, caused by the mismatch in thermal expansions during cooling, were relatively constant for all the samples [222]. Further investigation was outside the scope of this study.

The 'Type 2' plots have been reported to be caused by residual polymer left on the fibre surface after debonding [91]. This however indicates that failure is due to cohesive matrix failure, where cracks propagate through the bulk matrix as opposed to along the interface, and not interfacial debonding. Samples that exhibited the Type 2 plots were inspected under SEM and no residual polymer was found. As this plot was associated with low interface strengths, it was attributed to a progressive interface failure rather than a cohesive matrix failure.

Figure 4-2 shows the embedded area versus peak load plot for virgin carbon fibre/polypropylene microbond samples (VCF.PP) as well as samples with the fibre sizing removed (CFP.PP and CFS.PP). Linear regression through the origin was used to analyse trends, and generally, the scatter in the data was relatively large, with R^2 values between 0.58 and 0.66. These values are however representative of data recorded for this method and (assuming the experimental set-up was unchanged – see Section 2.2.2) can be caused by a number of factors such as microscopic heterogeneities on the surface of the fibre [223], changes in contact conditions due to variations in droplet size [106] and small variations in test temperature [224].

R^2 values of 0.60 – 0.73 could be achieved by not forcing the data through the origin – and have been similarly reported elsewhere [91], [99], [106]. For the purposes of data reduction here, the shear stress along the interface was assumed to be constant [144], and therefore the regression lines were fitted through zero in accordance with Equation 2-2 (Section 2.2.1.2). It should be noted that the assumption of a constant shear stress along the interface is a simplification of the stress profile, where FEA analysis has shown large peaks in stress in the vicinity of the knife edges [100], [102]. Nevertheless, the assumption of constant shear stress is valid for the average interfacial shear stress calculation as it is a close approximation of the average stress along the fibre during testing.
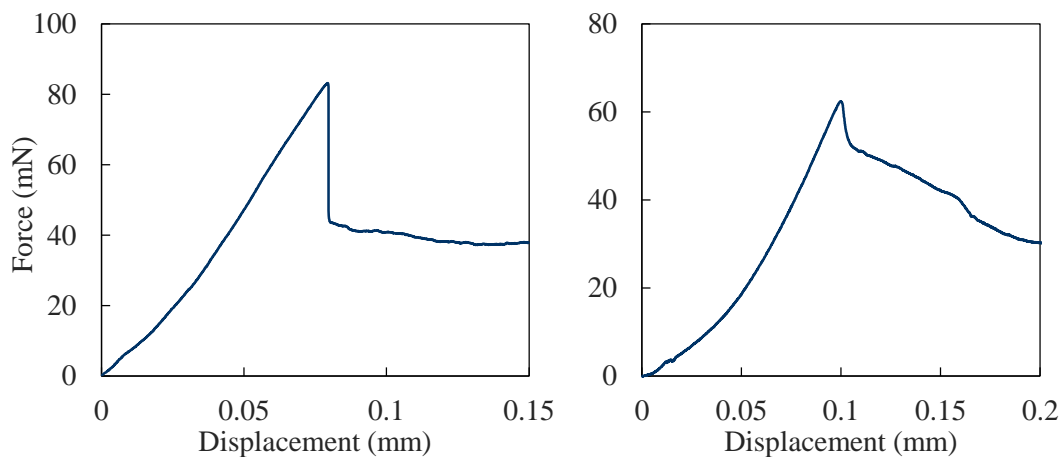
Figure 4-1 - Typical force-displacement traces observed from microbond testing of low interface strength systems; 'Type 1' (left) interfacial debonding followed by constant dynamic friction and 'Type 2' (right) interfacial debonding followed by decreasing dynamic friction
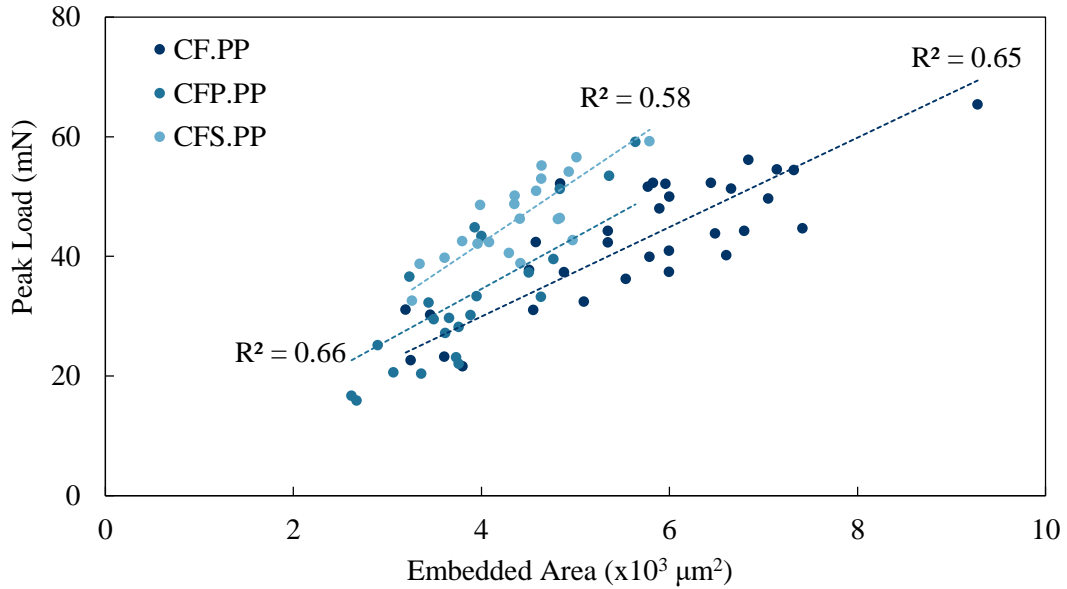
Figure 4-2 - Peak force vs. embedded area plot for VCF, CFP and CFS with unmodified PP

Removing the epoxy sizing by pyrolysis (CFP) and solvolysis (CFS) both resulted in an increase in IFSS (gradient of regression line). The CFP.PP and CFS.PP samples exhibited a 4% and 32% increase in IFSS respectively over the VCF.PP (non-degraded). Mechanical and physical interactions between the fibre and matrix accounted for most of the interface strength, due to the absence of chemical bonding as a result of both the carbon fibre surface and polypropylene being nonpolar [81]. The increase in IFSS seen for sizing removal may be attributed to the sizing acting as a weak layer between the two interfaces (fibre-sizing and sizing-polymer) [225], preventing intimate contact between the fibre and polymer. The removal of sizing has been shown to increase the interface strength (~5%) between carbon fibres and allyl bisphenol A modified bismaleimide (BMI), which although a thermosetting polymer, does not have optimum surface functionality to bond with the sizing [226].

Large differences in IFSS were also observed between the CFP.PP and CFS.PP samples, with the CFS.PP showing a 28% increase over the CFP.PP samples. Clearly the method of sizing removal had a significant effect on the surface of the fibre and the increase seen may be due to incomplete removal of sizing, which has been shown to lead to higher IFSS values due to changes in surface topology [226]. Increases in surface roughness are believed to be beneficial to increasing interface strength due to mechanical interlocking of the polymer on the fibre. However it is usually seen as a

product of fibre surface treatments which may also simultaneously increase surface energy and functional groups [84], [227], [228], resulting in increases for IFSS. Song et al. [229] isolated the effect of surface roughness on the IFSS for CF.EP by lightly etching the fibres in aqueous ammonia. The authors recorded improvements of up to 56% in IFSS due to increased roughness and therefore overall surface area available for contact with the fibres.

4.3   The Effect of Maleic Anhydride

The IFSS values recorded for CF with unmodified PP ranged from 3.4MPa to 10.6MPa, which were significantly lower than 45.9MPa recorded for the CF.EP system. The addition of maleic anhydride improved the IFSS for all CF.PP systems under investigation. An example of a typical force-displacement plot recorded from samples with maleic anhydride introduced is given in Figure 4-3. The 'Type 3' plot (again arbitrarily chosen) shows similar characteristics to the Type 1 plot reported in the previous section, however at interfacial debonding the load reduces to zero. The load then partially recovers before another smaller drop observed, due to a change in friction from static to dynamic and the force eventually reaches a plateau value which is proportional to the dynamic friction [110].

The region of zero load immediately after debonding is caused by release of strain in the fibre, coupled with the fibre undergoing Poisson's shrinkage at high strain values [133]. This resulted in the fibre contracting whilst the droplet was sliding at low friction, causing the droplet to 'jump' a section of the fibre [96]. Gaps of up to 60μm were recorded between final debonding and resumed contact of the knife edges, which made it difficult to tell if the fibre or the interface has failed. The CF.EP samples and all the samples with the maleic anhydride coupling agent displayed the Type 3 f-d plot which is reported to be indicative of a high interfacial shear strength system [110], [230].

Figure 4-4 shows a plot of the peak force as a function of embedded area for the VCF.PP and VCF.mPP. Introducing the coupling agent at 2%wt. showed a clear increase in gradient as well as a reduction in data scatter. The IFSS of the VCF.PP (non-degraded) system was increased by 295%, from 8.0MPa ± 2.2 to 31.6MPa ± 4.8, which was attributed to chemical bonding at the interface as result of the functional groups

introduced by the maleic anhydride [231]. Figure 4-5 shows SEM micrographs taken from CF.EP (benchmark), CF.mPP and CF.PP microdroplet samples respectively. The increase in interface strength due to the addition of the maleic anhydride coupling agent resulted in a change in failure at the contact point with the knife edges. Failure of the CF.mPP specimens was similar to the CF.EP specimens, with a small part of the meniscus becoming detached from the droplet after debonding. Figure 4-6 shows higher magnification images of the menisci for the CF.EP and CF.mPP samples.
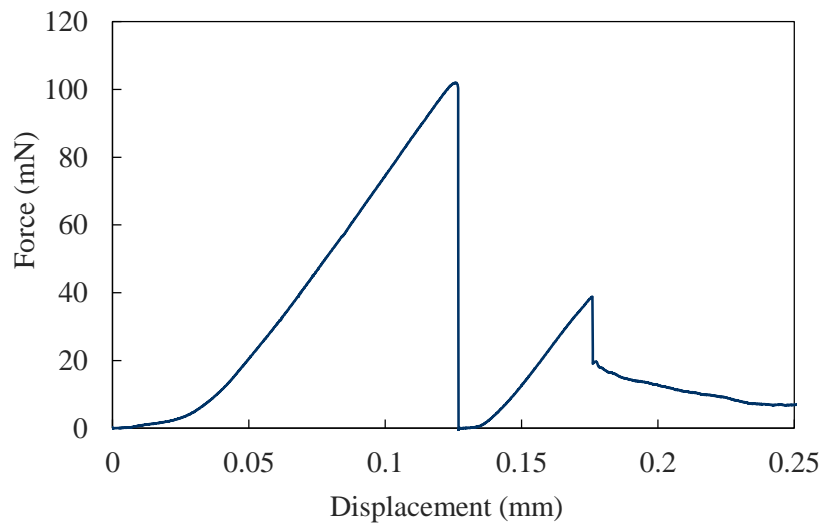
Figure 4-3 – 'Type 3' force-displacement plot observed for all high interface strength systems tested in this study
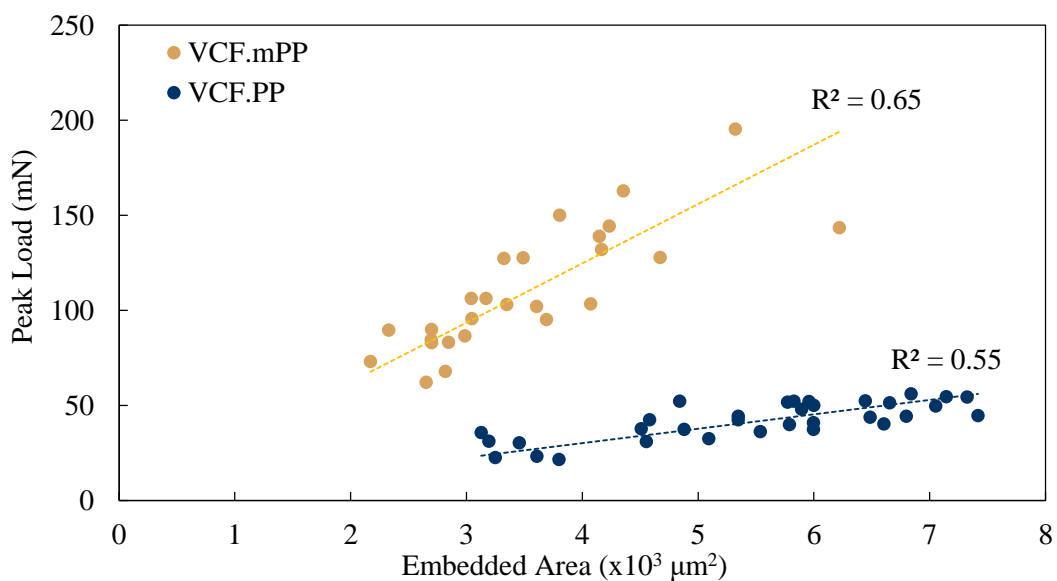
Figure 4-4 - Peak force vs. embedded area plot for CF.PP, with and without maleic anhydride
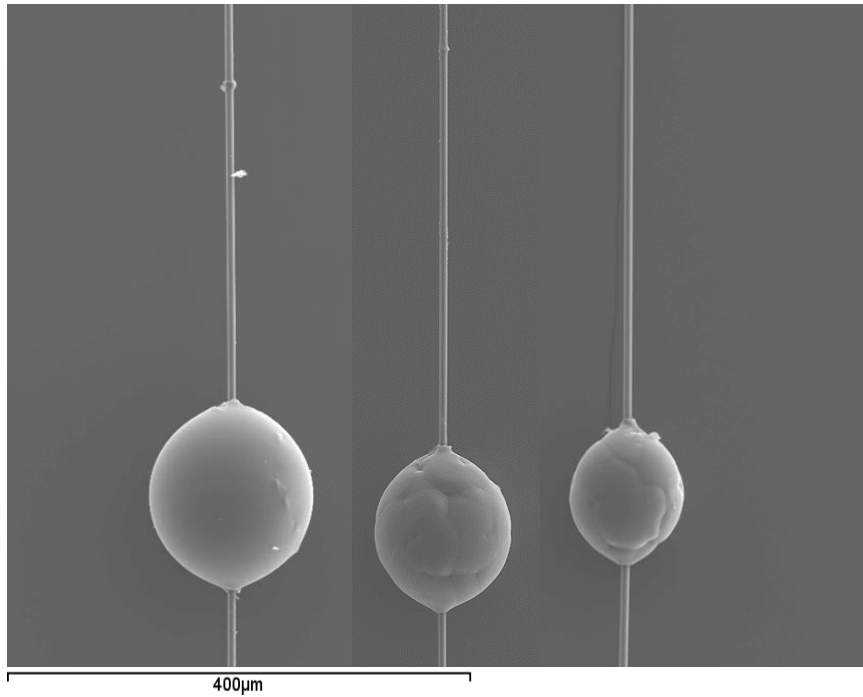
Figure 4-5 - SEM micrographs of (left) a debonded CF.EP microdroplet with detached meniscus (middle) CF.mPP microdroplet also with detached meniscus and (right) CF.PP microdroplet without a detached meniscus
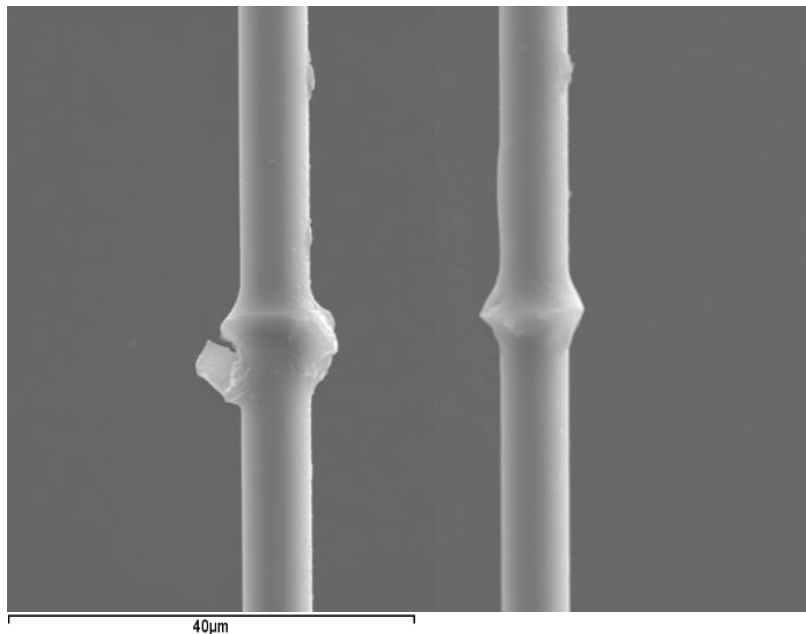
Figure 4-6 - SEM micrographs of the meniscus from (left) a CF.EP microdroplet and (right) a CF.mPP microdroplet, both after debonding

There was no discernible difference in the shape of the residual meniscus between the two samples and no signs of ductile behaviour for the CF.mPP samples. This suggested that the brittleness of the polypropylene in the interface region was increased, where plastic deformation was restricted by the cross-linked structure of the maleic anhydride.

The coupling agent is known to migrate to the fibre surface during the formation of composites [231],allowing chemical bond formation with the fibre and therefore simultaneously increasing the bond strength, and promoting the brittle failure characteristics seen here.. This effect is not observed at the macroscale for polypropylene as maleic anhydride concentrations of up to 10wt.% have been reported to have no effect on the bulk mechanical properties [232].

The presence of the meniscus remaining on the fibre after debonding raises the issue that the failure may not be completely interfacial, and therefore may partly be due to matrix cracking. No remains of polymer were found along the debonded region however, which suggests that apart from the meniscus, the failure mechanism was interfacial. In any case, the effect of matrix cracking in the meniscus region has been shown to have negligible effect on the final pull-out force, and therefore interfacial shear strength [142]. The embedded lengths were therefore corrected for samples that showed meniscus failure, measured by optical microscopy after testing.

The modified PP was also combined with the CFP and CFS fibres to assess the compatibility of mPP with the bare carbon fibre surface. The peak load vs. embedded area plot is presented in Figure 4-7. Compared to the samples with no coupling agent the data scatter was lower, indicating that microbond samples were less sensitive to small changes in the fibre surface when the coupling agent was added. The interface strength increased by 349% and 353% to 35.9MPa ± 2.6 and 36.2MPa ± 2.9 (compared to the VCF.PP samples) for the CFP.mPP and CFS.mPP samples respectively. Statistically there was no discernible difference between the CFS.mPP and CFP.mPP systems, given the level of experimental variation. Both the CFS.mPP and CFP.mPP samples outperformed the VCF.mPP by approximately 14-15%, however such large improvements seen for all the samples with mPP demonstrated that chemical bonding was possible between the commercial sizing agent as well as the bare carbon fibre surface.
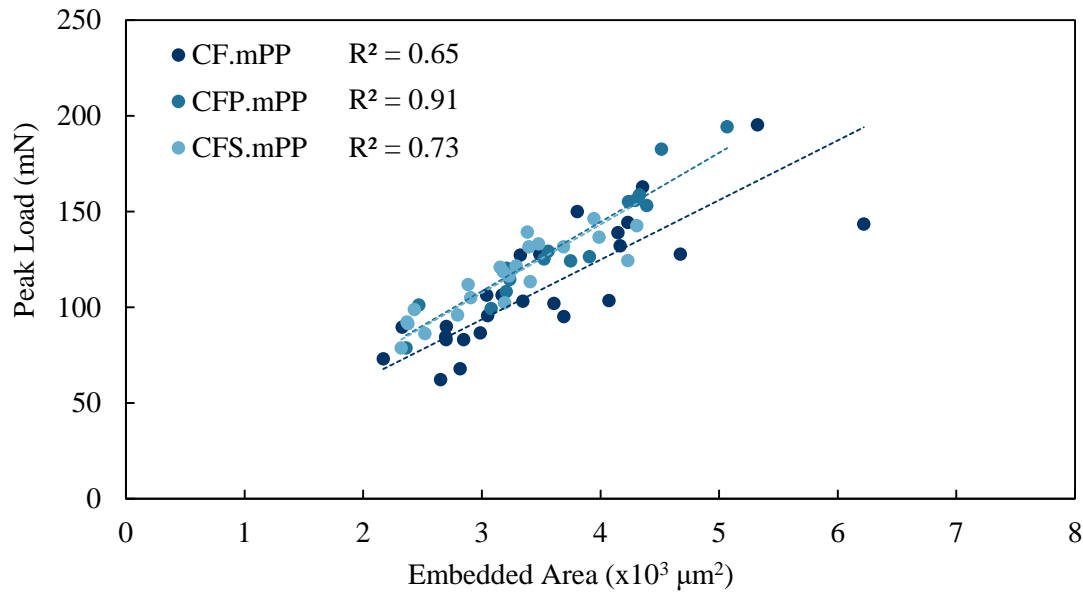
Figure 4-7 - Peak force vs. embedded area plot for all fibre types with modified polypropylene (CF.mPP, CFP.mPP and CFS.mPP)

Figure 4-8 - Peak load vs. embedded area plot for CFS.mPP and CF.EP shows the CFS.mPP data plotted with CF.EP, demonstrating the significant improvement in interface strength for the carbon fibre/polypropylene samples. For these systems with higher interface strengths it became increasingly difficult to test a sufficient range of embedded lengths, as small changes had a large effect on the peak load and consequently tensile stress in the fibre. For the high interface strength systems the tensile stress in the fibre (calculated from peak load divided by fibre cross-sectional area) was found to be 60 - 80% of that reported in the manufacturer's datasheet (4900MPa). The strength achieved on the datasheet is not achievable in practice through single fibre testing as the manufacturer's test procedure uses resin-encased tows as opposed to single fibres. Nevertheless, this gave some uncertainty to the value of IFSS and indicated that the IFSS values recorded were a lower bound result of the true interfacial shear strength for these systems.

The consequence of measuring higher interface strength systems was that a higher percentage of tests resulted in fibre failure before interfacial debonding could occur. Figure 4-9 shows the relationship between interfacial shear strength and the 'yield' (tests that failed by interfacial failure, divided by total tests performed). The lowest yield was found for the CF.EP samples, where only 1 in 4 tests were successful and a total of 67 samples were tested to obtain enough data to reasonably determine the IFSS.

Similar yields were found for the modified polypropylene systems which made this test method extremely inefficient for measuring high IFSS values.
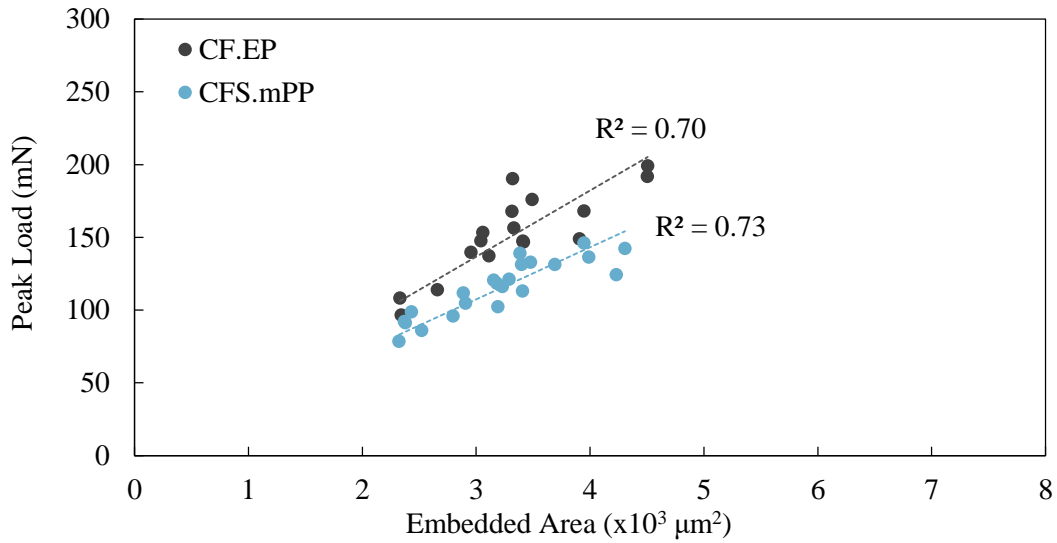
Figure 4-8 - Peak load vs. embedded area plot for CFS.mPP and CF.EP
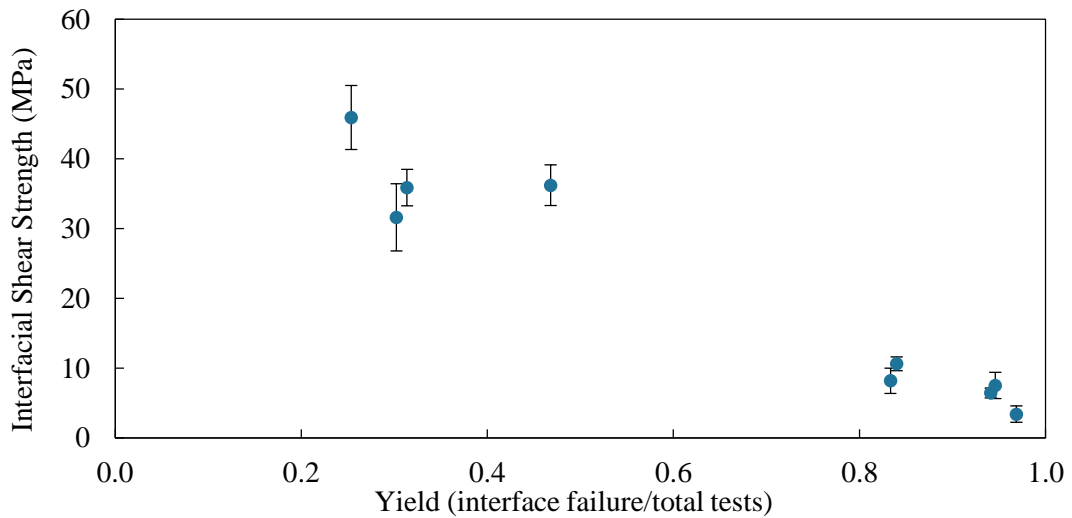
Figure 4-9 - Relationship between yield and interface strength (error bars are standard deviation)

Despite a large number of samples resulting in fibre failure, an acceptable number (approximately 20) were able to be tested to allow data reduction for all of the systems. The combination of adding a coupling agent and removing the epoxy sizing yielded the highest IFSS, where the effects of adding the coupling agent were more significant than removing the sizing agent. The addition of the coupling agent brought the IFSS values

for the CF.PP system close to values reported in the literature and observed here for carbon fibre/epoxy [212], [218], [219].

The improvement in IFSS from the addition of maleic anhydride was much higher than values reported in the literature for a similar system. Wong et al. [22] investigated the effect of maleic anhydride on the IFSS for recycled carbon fibre/polypropylene. The authors found a maximum increase of 197% with the addition of 8%wt G3015 maleic anhydride, however this was from 2.36MPa to 7.00MPa, lower than even the VCF.PP investigated here. Whilst the carbon fibre (T600SC-60E) and polypropylene (100-GA12) grades used were different to the current study, the values reported were approximately 80% lower than the values reported here, using the same microbond test. Polypropylene is sensitive to oxidation, which can cause mechanical degradation [217]. Samples for the current study were all prepared under nitrogen to avoid oxidative degradation. The following section investigates the sensitivity of the IFSS to environmental conditions during sample preparation, in order to explain the discrepancy between the current data set and the literature.

4.4   The Effect of Matrix Degradation

Differential scanning calorimetry was used to measure the oxidation induction time (OIT) of the polypropylene used in this study. At the point of degradation, polypropylene exhibits an exothermic reaction [233] which can be monitored using this method. Further details of the methodology were given in Section 3.2.1. Figure 4-10 shows the effect of temperature on the OIT for the polypropylene used in this study (blue) and another commercially available polypropylene (green). Clearly there was a significant difference in the OITs recorded for the two polymers, which was due to an anti-oxidant package added to the polypropylene in this study [234]. Additives are often used to improve thermal properties, but are seldom mentioned in material datasheets as they are proprietary to the manufacturer. Even with the use of an anti-oxidant package, the polypropylene was still susceptible to degradation at elevated temperatures, at 220ºC the OIT was approximately 3 minutes. To ensure the degradation process had initiated in the degraded microbond samples, they were prepared at this temperature for 5 minutes. Further details of the droplet formation methodology was described in Section 3.2.2.
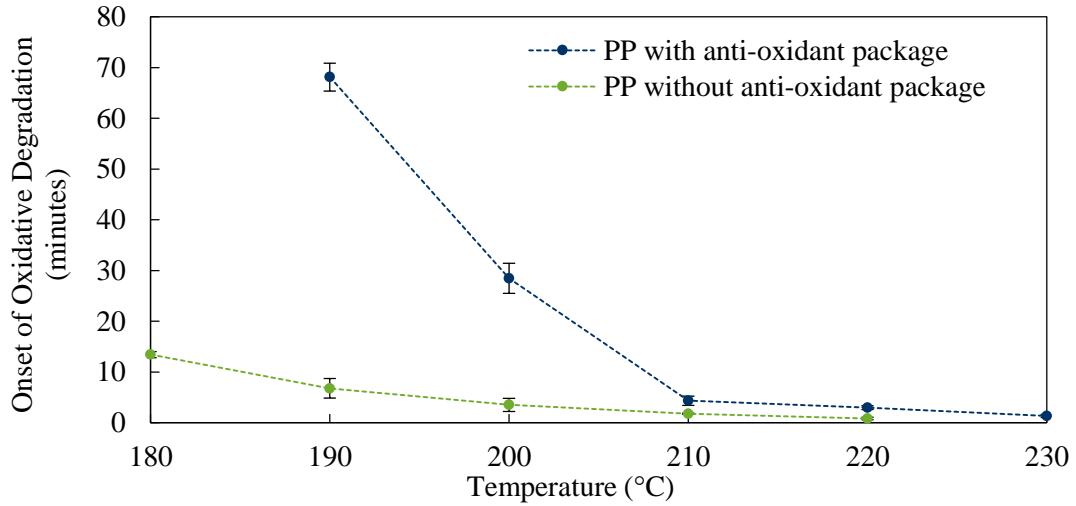
Figure 4-10 - Oxidative induction time for polypropylene, with and without stabilisation packages to prevent thermo-oxidative degradation (blue line corresponds to the polypropylene used in this study, and green line to another commercial available grade)
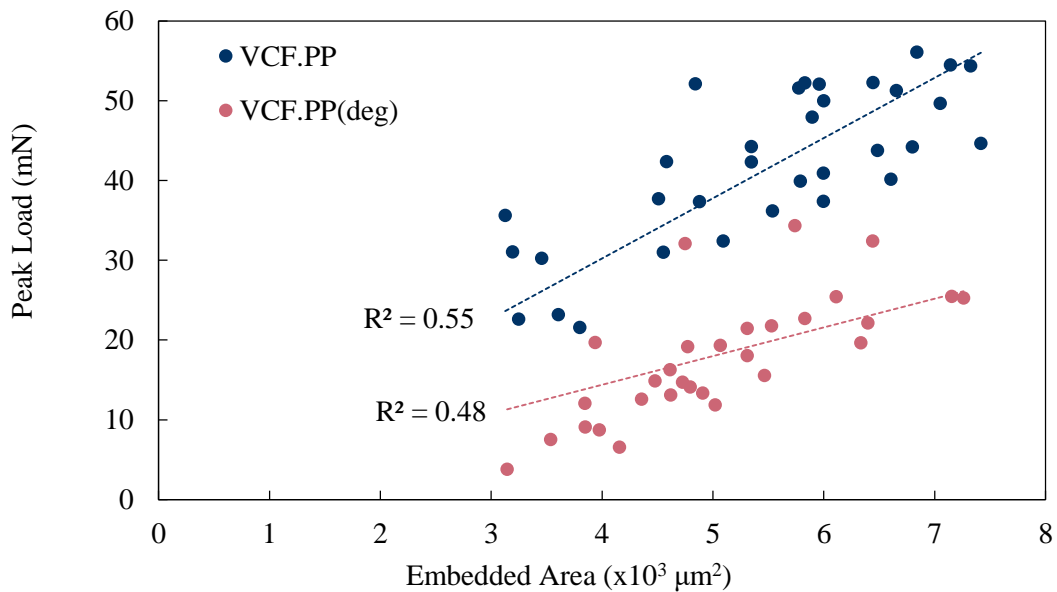
Figure 4-11 - Peak force vs. embedded area plot for degraded and non-degraded CF.PP samples

Figure 4-11 shows the peak force versus embedded area plot for the degraded and non-degraded VCF.PP samples. The degraded samples had an IFSS of 3.4MPa ± 1.2, similar to that found in [22], equating to a 58% reduction compared to the non-degraded samples (8.0MPa ± 2.2). Data scatter was observed to be higher in the degraded system, shown by the poor linear regression fit through the origin ($R^2 = 0.48$). On inspection of the data, droplets with large diameters appeared to have a higher than expected IFSS and droplets with smaller diameters had a lower than expected IFSS. This was caused

by the larger surface area-to-volume ratio of the smaller droplets [217], where a higher level of degradation occurred in the smaller droplets, since a greater percentage of the polymer was exposed to oxygen per unit time.

Chain scission is the primary mechanism of degradation for thermo-oxidative deterioration [235], where the polymer chain effectively separates, reducing the molecular weight. It is well known that a reduction in molecular weight leads to undesirable attributes such as embrittlement [236] and reduction in crystallinity [217]. The effect of which is extensive deterioration in mechanical performance [237], with decreases in crystallinity reportedly accounting for up to 70% of the IFSS for GF.PP due to significant reductions in compressive radial stress at the interface [155]. Figure 4-12 shows the difference in surface topology as observed by SEM of typical degraded and non-degraded polypropylene microbond samples after testing. The degraded sample had a rough and pitted surface, which is a common phenomenon referred to as 'chalking' in polymer degradation [238]. The non-degraded sample had a smooth surface with visible spherulite boundaries formed during crystallisation.

Figure 4-13 shows a magnified view of the menisci for the two samples. The meniscus was not present for the degraded sample and was also not found on the fibre, which suggests that embrittlement in the polymer had occurred and the meniscus fragmented during testing. In contrast, the non-degraded sample showed almost no signs of being tested, with only a small plastic deformation to the right of the fibre where the knife edge was in contact. Interestingly, optical microscopy was also able to identify the effects of degradation, with small changes in colour and opacity noticed. Figure 4-14 compares optical micrographs of the degraded and non-degraded samples. The changes were however very slight between the samples and it would be difficult to notice the degradation without a side-by-side comparison, indicating that it may be hard to monitor whether samples have degraded using optical microscopy. Exposing the polypropylene to elevated temperatures, even for a very short period of time, had a significant impact on the degradation of the polymer and therefore the interfacial properties. It is therefore recommended that a batch of samples are screened by SEM to check for signs of degradation, such as chalking, before testing or that droplet formation is carried out in an inert atmosphere.
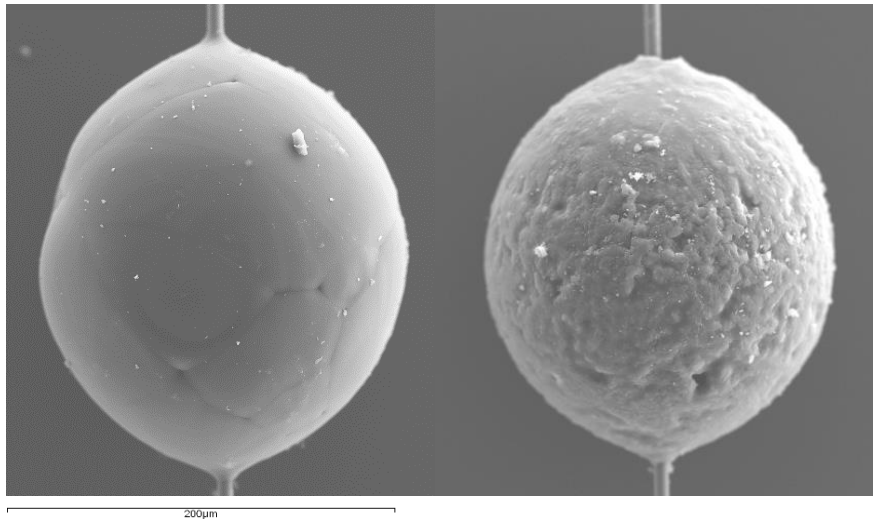
Figure 4-12 - SEM images of non-degraded (left) and degraded (right) microbond samples after testing
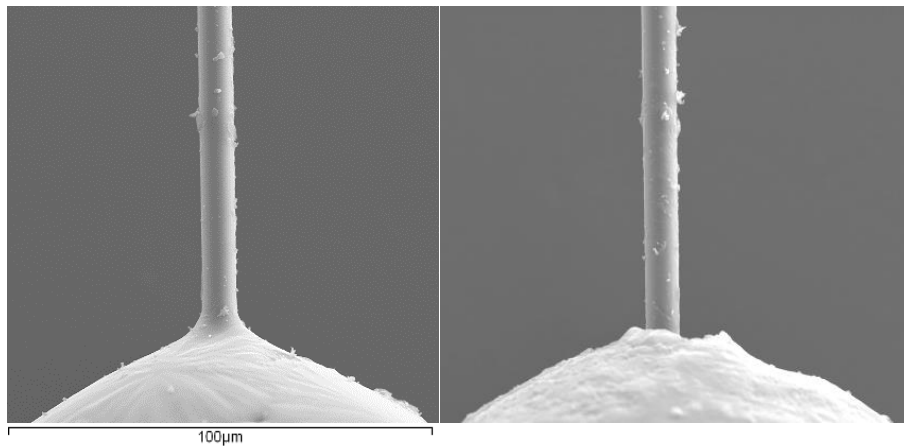
Figure 4-13 - High magnification SEM images of menisci of non-degraded (left) and degraded (right) microdroplets presented in Figure 4-12
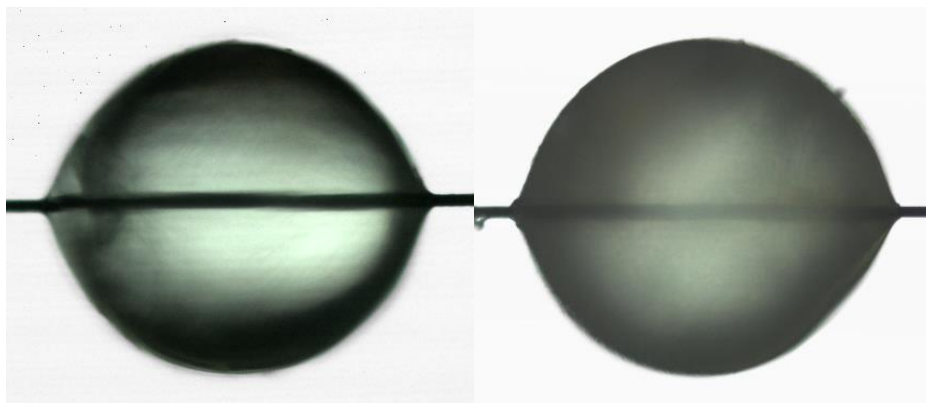
Figure 4-14 - Optical microscopy images of non-degraded (left) and degraded (right) microbond samples prior to testing. This highlights the difficulty in identifying degradation from visual observation at this scale.

4.5 Conclusions

The objective of this study was to investigate the adhesion between carbon fibre and polypropylene. The importance in understanding interactions at the microscale was paramount, as ultimately these properties affect the macroscale mechanical performance. The removal of fibre sizing by pyrolysis yielded a 4% increase in the IFSS, and sizing removal by solvolysis increased the IFSS by 33%. The addition of maleic anhydride had the largest effect on the IFSS, with a 295% increase over the base polymer for the virgin fibres and 349% and 353% increase for the CFP and CFS samples respectively. The combination of removing sizing by solvolysis and the addition of the coupling agent yielded the highest IFSS value of 36.2MPa ± 2.9, which is approaching the shear strength of the polymer - the theoretical maximum IFSS value that can be achieved. The excellent adhesion between carbon fibres with epoxy compatible sizing and modified polypropylene has not been reported before, and indicated that fibres with this sizing are appropriate for use with thermoplastic matrices. This is pertinent as carbon fibres are almost exclusively sized for use with thermosetting matrices, where thermoplastic sized fibres will add further material cost due to limited market volumes in comparison with CFRPs.

The value of the IFSS for the maleic anhydride modified samples was much higher than other values reported for similar systems in the literature, which suggests that other authors may have tested samples that have degraded during droplet formation. Matrix degradation is therefore a key factor in interface strength measurements, where the IFSS was 135% higher for samples prepared under nitrogen, compared with those prepared under atmospheric conditions. The oxidation induction time was measured for polypropylene and revealed that degradation occurred after less than 3 minutes at typical sample processing temperatures.

From the IFSS tests it was identified that surface roughness may contribute to the interface strength. Residual stresses formed during droplet formation were not responsible for changes in interface strength because all samples were prepared at the same temperature. For the higher interface strength systems chemical bonding was the dominant mechanism, however it was unclear why the interface strength was higher for the desized fibres. Additionally, a significant reduction in yield was observed for the

higher IFSS systems, despite the recorded tensile stresses in the fibre being lower than the manufacturer's strength data. This suggested that the microbond method may not be able to detect higher interface strength values and as a consequence, the data for carbon fibre with modified polypropylene may be lower bound results.

The next chapter investigates the effect of surface roughness and chemical interactions on the interfacial shear strength to explain the difference in data recorded in this study. Additionally fibre strength measurements were taken to assess whether reductions in yield were a consequence of reduced strength compared to the manufacturer's data, and the implications this would have on using the microbond test method for these systems.

5. Microscale Fibre Characterisation and Effect on the Microbond Test

5.1 Introduction

Fibre and matrix interaction at the microscale is extremely complex and drawing conclusions from work in the previous section on the microbond test required further analysis. Fibre strength characterisation was employed to investigate whether damage had occurred to the fibres during sizing removal to account for a higher proportion of tests resulting in fibre failure for high interface strength systems. Surface roughness measurements were taken to assess whether changes in fibre surface topology were responsible for changes to the interfacial shear strength due to mechanical interlocking, which was believed to be a significant factor for samples that did not form chemical interactions. Finally, functional groups present on the surface of the fibre were also analysed and the effect of fibre surface chemistry on the interfacial shear strength was investigated.

5.2 Fibre Strength Characterisation

5.2.1 Weibull Analysis

Figure 5-1 shows the Weibull plots for data recorded from the single fibre tensile test using two-parameter unimodal Weibull analysis. The linear regression lines represent the strength distribution for each system and characteristic strengths were calculated at $\ln[-\ln(1/(1 - P_f))] = 0$. The two-parameter model is commonly simplified for the analysis of brittle fibres [239]–[241] and was preferred over the general three-parameter model due to greatly reduced complexity in data analysis. Moreover, it has been shown that the iteration required to obtain the best correlation of data for three-parameter analysis may lead to unrealistic results [242]. All of the plots showed good agreement between experimental data and Weibull distribution, with values close to others reported in the literature for carbon fibre at a 20mm gauge length [84], [209], [243]–[245]. The characteristic strength is very sensitive to the gauge length used for single fibre tensile testing (SFTT), and a number of authors have performed scaling analyses to allow extrapolation of data to lengths that are difficult to test [241], [246]–[248]. In this study, a single gauge length of 20mm was investigated as it was approximately

equal to the effective fibre length for microbond testing in the previous chapter, and allowed relatively easy preparation of samples compared to shorter lengths. The Weibull parameters obtained are summarised in Table 5-1.
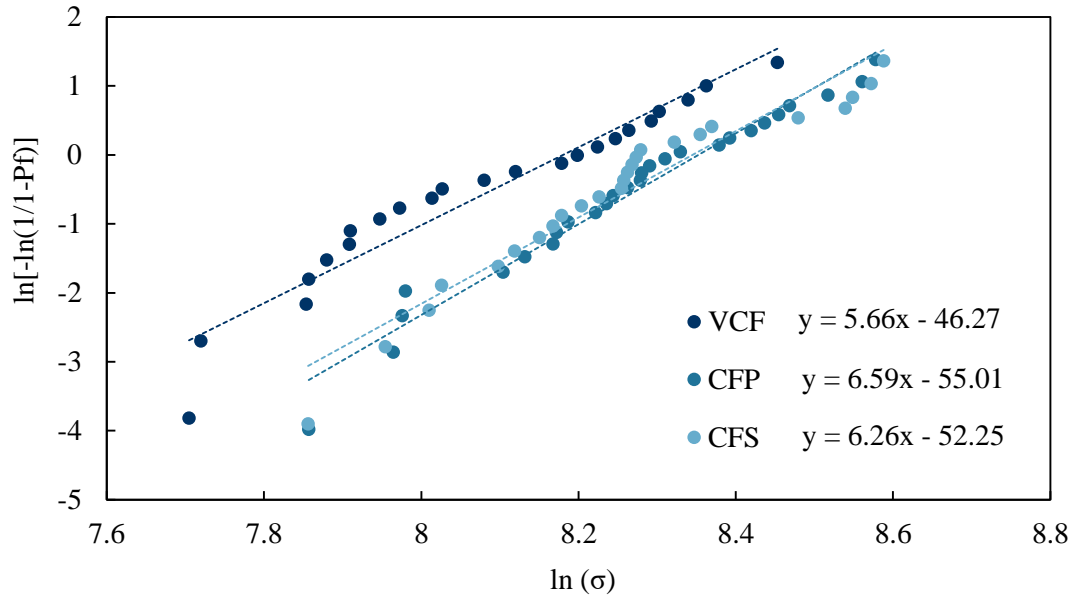
Figure 5-1 - Weibull coordinate plot for single fibre tensile testing for the three fibre treatments used in this study

Fibre	Fibre tensile strength (GPa)		Shape parameter	Characteristic Strength (GPa)	Samples
	avg	st dev			
VCF	3.3	0.69	5.66	3.57	23
CFP	3.96	0.72	6.59	4.24	27
CFS	3.91	0.76	6.26	4.21	25

Table 5-1 - Single fibre strength data obtained from single fibre tensile testing and Weibull parameters

For the Weibull plots (Figure 5-1) the lower strength region was not well defined by the least squares regression analysis, which appeared to be a common issue arising from fitting carbon fibre data with a unimodal Weibull distribution [246], [247], [249]. According to Beetz [239] and more recently Zinck et al. [242] fibre strength analysis is likely to be bimodal due to multiple types of defects present on the surface of fibre. For bimodal systems, there are low and high strength defects, with the former arising from surface damage during handling [247] and the latter due to fibre defects formed during heat treatment processes during fibre manufacture [240]. Fibres with tensile strengths below 2GPa were extremely difficult to extract from the fibre bundles due to the low

strength defects described above. This meant that the lower region of the bimodal distribution would not be well represented unless a significant number of samples were tested [208]. Moreover, it was assumed that similar difficulties in fibre extraction (of fibres with the low strength defects) would occur for the microbond test and therefore the lower strength region was not of direct interest for this study.

A unimodal two-parameter Weibull analysis was therefore used here, which has been shown to provide similar values to the three-parameter model when tested at a single gauge length [250]. Although the samples size studied was relatively small (23 - 27 samples) it has been shown in the literature that the statistical validity of the data obtained from this sample size is sufficient for this type of analysis [246].

The distribution of the fibre strengths is shown in Figure 5-2 as a cumulative distribution function. The manufacturer's data for the tensile strength of carbon fibre was 4900MPa (38% higher than the characteristic strength value obtained for the VCF) As discussed previously, the manufacturer's test method (TY-030B-01) measures the strength of a carbon fibre tow encased in epoxy resin and is therefore likely to be much larger than strengths recorded here using single fibre tensile testing. Increases of 18-19% in characteristic strength were observed for the CFP and CFS fibres and the Weibull modulus was also increased over the VCF by 16 and 11% respectively, showing that the spread of the data was reduced in these samples. The Weibull moduli recorded agreed well with other data in the literature (approximately 4.5-10 [147], [240], [244], [251]), although the VCF fibre tended towards the lower end of reported vales.

On inspection of the breaking loads recorded for the SFTT, there was a marginal increase for the CFP and CFS fibres (7 - 8%) over the VCF fibre, from 110mN ± 27 to 118mN ± 19 and 119mN ± 25 respectively. This indicated that the sizing on the as received fibres may have slightly skewed the results as it increased the apparent diameter of the fibre, but didn't necessarily contribute to the fibre strength. Moreover, the CFP and CFS fibres had on average a 0.2μm smaller diameter than the as received fibres, which was significant as the sizing layer on the fibre has been reported to be an order of magnitude smaller than this [87], suggesting that some of the outer layer of the carbon fibre may have become detached during sizing removal or subsequent washing.

To assess the extent of outer layer removal from the fibre, the sizing layer thickness was estimated. Fibre and sizing densities were taken as 1800 and 1250kg/m^3 respectively, the fibre diameter (including sizing) was 7µm, linear mass of the T700 tow was 800g/1000m for a 12000 filament tow, with 0.3%wt. of sizing. Using these values the sizing thickness was calculated to be approximately 80nm, which suggests that 120nm of fibre was removed from the surface for the CFP and CFS fibres.
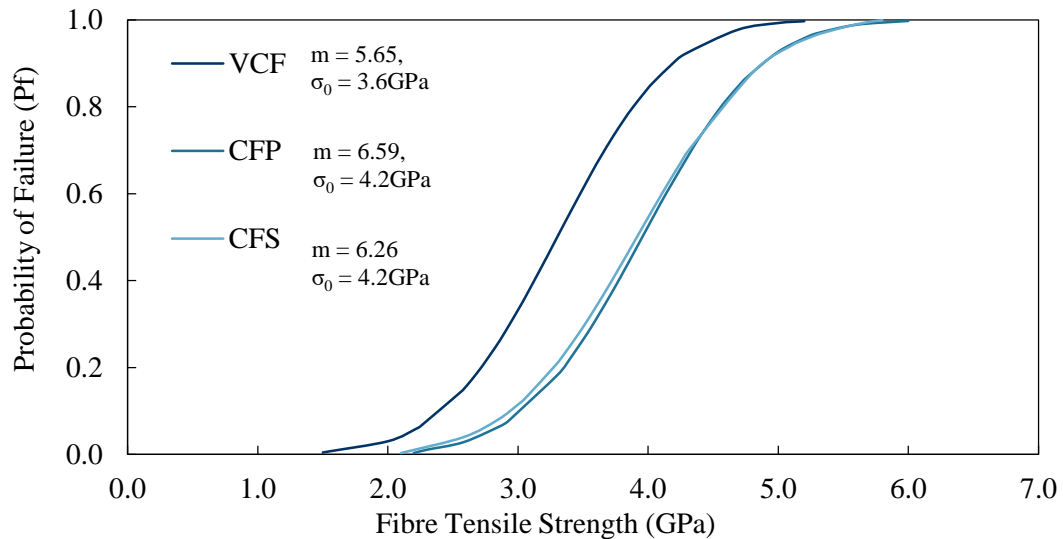
Figure 5-2 - Probability of fibre failure based on fibre tensile strength plotted as a cumulative distribution function

Highly oriented graphitic planes are formed on the outer surface of carbon fibre by heat treatment during manufacture [252]. As heat treatment increases, these basal planes become increasingly thick and aligned [253], which improves the fibre tensile modulus, but may reduce tensile strength [252]. In the core the graphitic structure is much more irregular and as heat treatment increases, bonding between these dissimilar layers decreases leading to reductions in tensile strength [253]. This highly aligned outer layer of carbon fibre, typically 1.5µm [252], is relatively weak [133], [254], and removal of this layer therefore increases the tensile strength [255] and has been shown to improve the interface strength in carbon fibre/epoxy [256]. It has also been suggested that the removal of the outer layer removes surface flaws, which may increase tensile strength properties [255], however the similarity in shape of the curves in Figure 5-2 suggests that there was no change in failure mechanism. As only approximately 120nm of the surface layer was removed from the fibre, this may not be enough to remove the effects of the critical surface flaws.

Partial removal of this outer layer may then be the explanation for the CFP.mPP and CFS.mPP microbond samples showing improvements in IFSS over the VCF.mPP samples. As the fibre strength was found to be higher for the two desized fibres, higher interface strengths could be tested, which may suggest that the average IFSS for the VCF.mPP was a lower bound result, as stronger interfaces couldn't be tested due to fibre breakage. The agreement between the increases in characteristic strengths compared with the increases seen in IFSS, between the three fibres respectively, certainly support this hypothesis. Additionally, the reduction in data scatter from the VCF to the desized fibres may also be explained by an increased range of embedded lengths available due to the increase in fibre strength.

5.2.2 Implications of Fibre Strength on the Microbond Test

By quantifying the fibre strength for the three fibre permutations that have been used, the theoretical maximum embedded length could be calculated for a known interface strength using Equation 5-1. Figure 5-3 shows the microbond data collected for the VCF fibre with maleic anhydride added to the polypropylene (CF.mPP), the dotted line represents the theoretical maximum embedded area that could be produced for tests to result in interface failure, as opposed to fibre failure. The fibre strength values used here were the characteristic strength values calculated from the Weibull analysis. The theoretical maximum embedded area shows good agreement with the experimental data, with almost all of the data points for interfacial failure occurring before the maximum theoretical embedded area, with a significant number of fibre breakages after.

$$L_e < \frac{\sigma_0 D_f}{4\tau_{app}}$$

Equation 5-1 - Relationship between the embedded length and maximum tensile strength of the fibre, where L_e is the embedded length, σ_0 is the characteristic fibre strength, D_f is the fibre diameter and τ_{app} is the apparent interfacial shear strength

Figure 5-4 shows the relationship between embedded length and interfacial shear strength for the fibre strengths recorded from the single fibre tensile test. Clearly as the interface strength of a fibre/matrix system increases, the range of available embedded lengths decreases, which reduces the reliability of the value of IFSS obtained from linear regression. The range of suitable embedded lengths for testing with carbon fibre

is shown in the figure by the vertical lines, ranging from 90µm to 300µm. Droplets with embedded lengths of less than 90µm were extremely hard to prepare due to the small amount of polymer needed, and droplets with embedded lengths of over 300µm were often non-axisymmetric. The theoretical maximum embedded length was approximately 200µm for interface strengths of 35MPa, therefore the range of available embedded lengths was effectively halved, explaining the reduction in yield at higher values observed in the previous chapter.
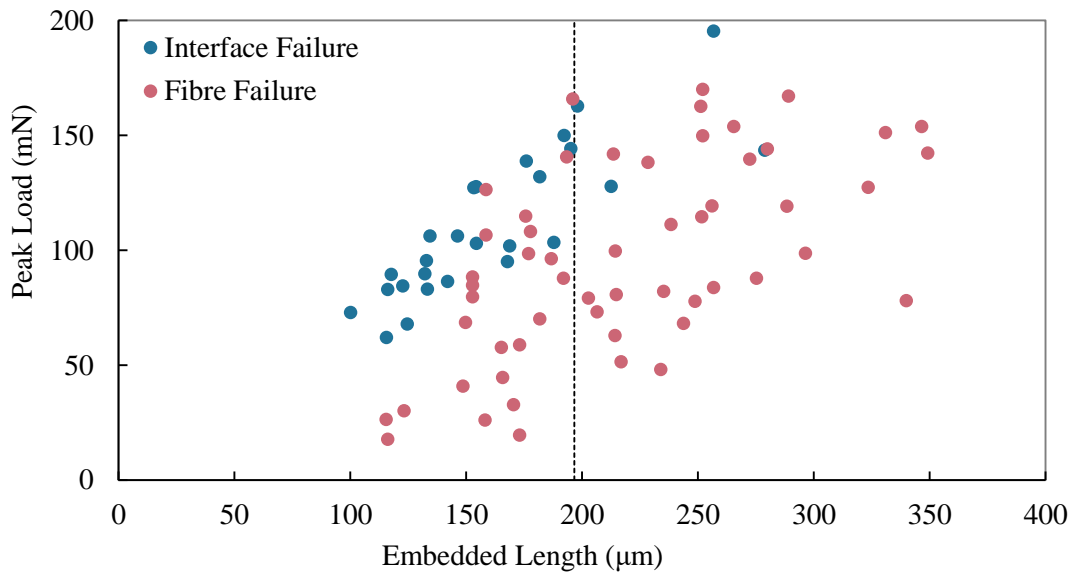
Figure 5-3 - Microbond test data for CF.mPP with theoretical embedded length limit. Fibre failure indicates that the fibre failed before the interface.
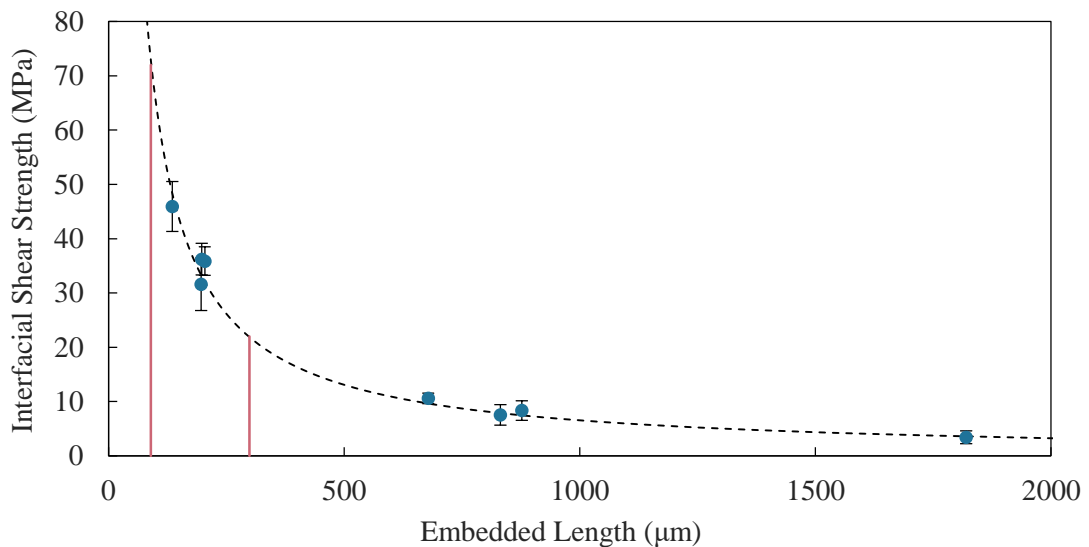
Figure 5-4 - Maximum theoretical embedded length for a given IFSS based on data obtained from microbond testing. The red bounds indicate the range of practical droplet sizes available for carbon fibre and polypropylene

5.2.3 Conclusions

The single fibre tensile test was used to characterise the fibre tensile strength and investigate the effect of fibre strength on the microbond test results, as well as assessing the validity of the test for higher interface strength carbon fibre/polypropylene systems. Increases in fibre strength were observed for the CFP and CFS fibres over the VCF fibres and were attributed to the removal of the sizing layer, which acted to increase the diameter of the fibre, but not significantly contribute to the tensile strength. Additionally approximately 8% (120nm) of the highly oriented graphitic outer layer of fibre was also removed, which has been shown to increase tensile strength in carbon fibres. On inspection of the cumulative distribution functions of the three fibre types there was no significant change in shape, which suggests that the increase in strength seen for the CFP and CFS fibres was not flaw driven. Therefore the partial removal of the outer layer of the fibre was not enough remove critical surface defects.

The fibre strength data was used to characterise the maximum theoretical embedded length for each fibre type and analysis of fibre and interface breaking loads agreed well with the theoretical values. The yield of samples was compared with the interface strength and showed a linear trend of decreasing yield with increasing IFSS, supporting the hypothesis that the higher interface strength systems tested here were either at the maximum or slightly higher than the maximum that this method could measure. This then suggests that the data for the VCF.mPP, CFP.mPP and CFS.mPP may be lower bound results, as approximately 70% of the tests resulted in fibre failure. To form consistent axisymmetric droplets, the maximum embedded length range was approximate 90-300µm, and investigation of the relationship between IFSS and embedded length showed that to obtain a range of lengths that would allow reasonable data reduction, the maximum IFSS that could be tested for carbon fibre/polypropylene was approximately 20-30MPa. Although it is possible to test systems with higher interface strengths, the confidence in the IFSS value will decrease as only a limited range of embedded lengths can be tested, additionally sample preparation would be extremely laborious.

5.3 Fibre Surface Characterisation

5.3.1 Atomic Force Microscopy

The surface roughness of each fibre permutation was characterised using AFM, further details of the experimental procedure were given in Section 3.2.4. The fibre topology was investigated as interfaces without chemical coupling rely on mechanical interlocking as a mechanism for stress transfer. AFM was capable of resolving nanoscale features and therefore able to detect changes in roughness due to striations or other asperities on the surface. The results from the AFM measurements are summarised in Table 1-1. The root mean square roughness R_{RMS} and mean roughness R_a are typically similar in value, however R_{RMS} is affected more by large peaks in the data. The VCF fibre had the largest percentage increase between R_a and R_{RMS} values, suggesting that the surface was the least uniform, additionally it also displayed the largest maximum height (44 and 57% higher than CFP and CFS fibres respectively). Inspection of the fibre surface topology showed that there were often large features present on the surface of the VCF fibre, two of the more extreme cases are presented in Figure 5-5.

	Fibre Type		
	CF	CFP	CFS
RMS roughness, R_{RMS} (nm)	15.5	5.9	4.0
Mean roughness, R_a (nm)	11.5	4.5	3.1
Max Height (nm)	77.5	45.3	43.4
Scan size (µm)	2x2	2x2	2x2

Table 5-2 - Results from AFM on the surface roughness characteristics of the three fibre treatments

As the topology was scanned, data was simultaneously collected on the phase lag between the drive signal-to-AFM cantilever and the actual cantilever oscillation. Changes in phase lag between the two signals have been reported to be caused by differences in material elastic modulus and have therefore been used to distinguish between dissimilar materials [257]. Further interpretation of the physical meaning of the changes in phase lag was extremely difficult however, as mechanical and physical properties such as viscoelasticity and adhesion simultaneously contribute to the results [258]. Figure 5-6 shows phase lag images for two samples shown in Figure 5-5. There was almost no change in phase lag for the larger features present on the surface which

would indicate that they were likely to be similar, if not the same composition as the sizing present on the rest of the fibre.

Figure 5-5 - AFM imaging of large features present on the VCF fibre surface
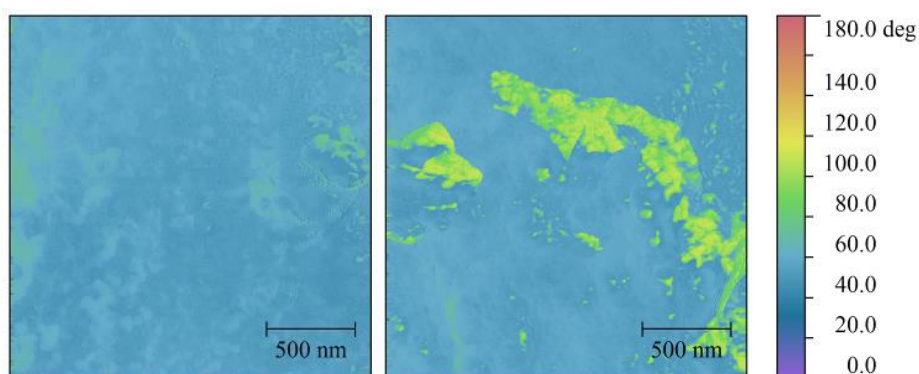
Figure 5-6 - Phase lag plots obtained from AFM corresponding to images shown in Figure 5-5

The origin of the lumps of sizing present on the fibres was due to sizing tearing during extraction of fibres, resulting in a large layer left on the fibre surface. The small change in phase lag at the feature edges, shown in Figure 5-6, was attributed to an increased apparent stiffness of the material caused by a sharp increase in gradient of the surface [259]. A number of topology scans of the VCF fibre revealed that the thickness of the sizing was very uneven in some areas, leading to a higher overall roughness.

The CFS fibres had the second highest surface roughness and maximum height values, Figure 5-7 shows two surface profiles from the AFM measurements. Interestingly, the surface of the CFS fibres appeared to have striations along the length, which was

surprising as striations are not common on the surface of unsized T700, they are typically associated with lower modulus fibres such as T300 [65], [229]. Based on the fibre diameter reduction for the CFP and CFS fibres discussed in the previous section, these striations may be visible due to the removal of the outer layer of the fibre – exposing the core which is formed of 'rippled ribbons' of basal planes [253]. These features increased the surface roughness of the fibre by 18% over the CFP fibre. The corresponding phase maps (Figure 5-8) showed that there was no significant change in phase across the surface of the fibre, indicating that the sizing was removed fully and no contamination was present on the surface.
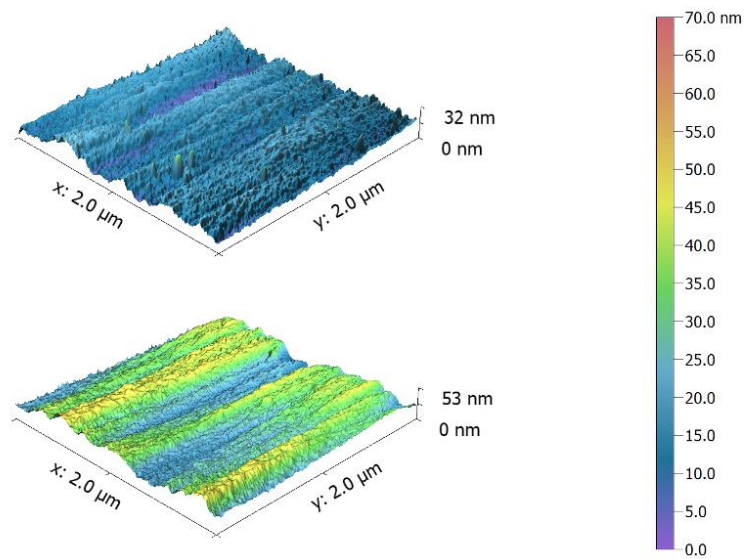
Figure 5-7 - AFM imaging of the features present on the CFS fibre surface
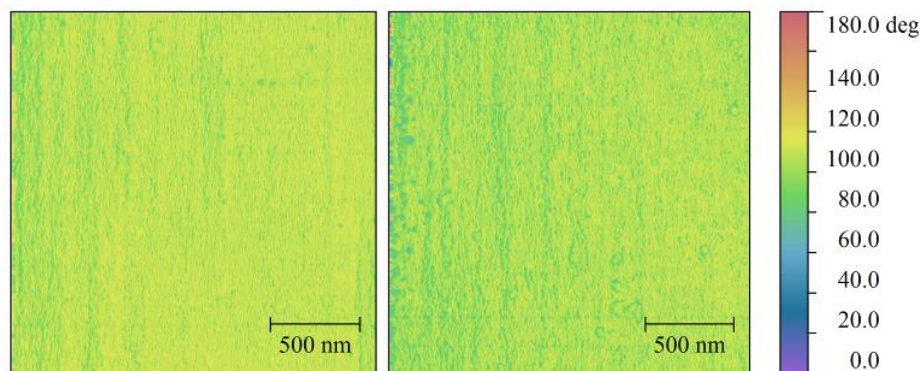
Figure 5-8 - Phase maps obtained from AFM corresponding to images shown in Figure 5-7

In contrast to the CFS samples, the CFP samples had the lowest roughness, and did not display any striations along the surface of the fibre. The topology images showed that in most cases the fibre surface was relatively homogeneous, however there were some

larger features present on a few of the samples (Figure 5-9) which may have accounted for the slightly higher change in R_{RMS} compared to the CFS fibre. The features on the surface of the CFP fibres were much smaller in size than that found on the VCF fibres, and on inspection of the phase lag images these features had a relatively large change in phase (Figure 5-10), which indicated that they were not likely to be the same material as the fibre surface. It has been reported that char forms on the surface due to thermal decomposition of the epoxy sizing from pyrolysis treatments [260], however these products would be of a much larger magnitude than shown on the AFM phase lag plot. Due to the changes in diameter recorded for the desized fibres and the difference in surface morphology compared to the CFS fibres, it was proposed that these features were fragments of aligned graphitic outer layer of fibre that hadn't been completely removed.
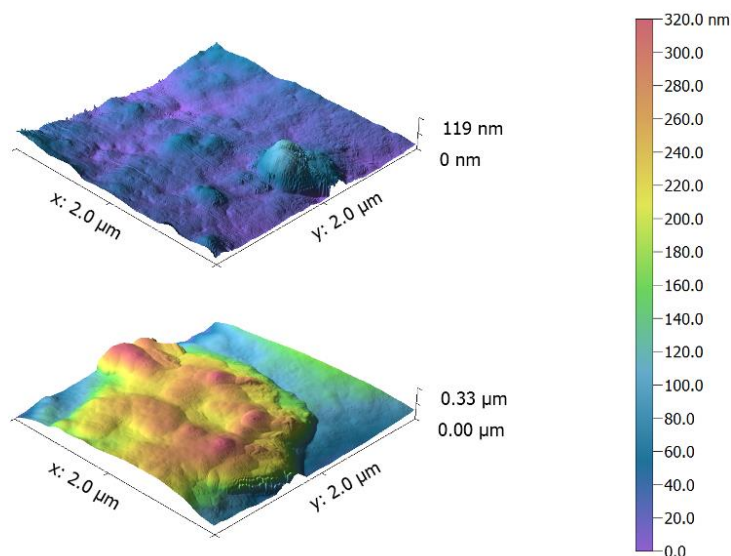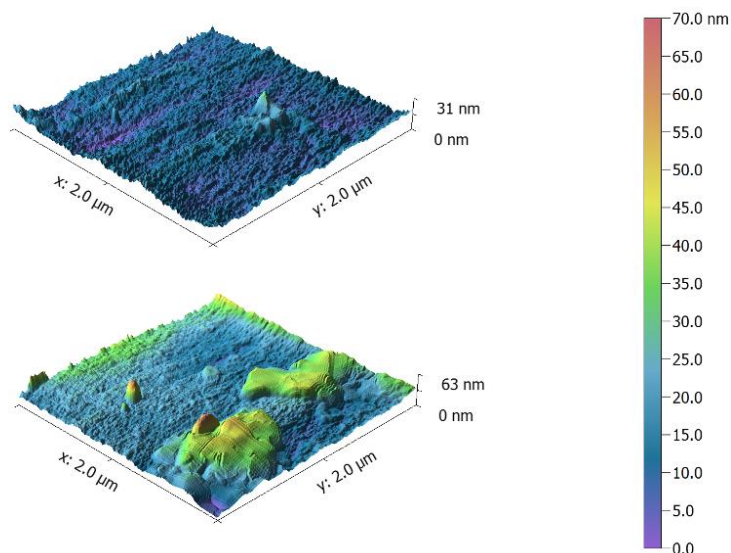

Figure 5-9 - AFM imaging of the features present on the CFP fibre surface
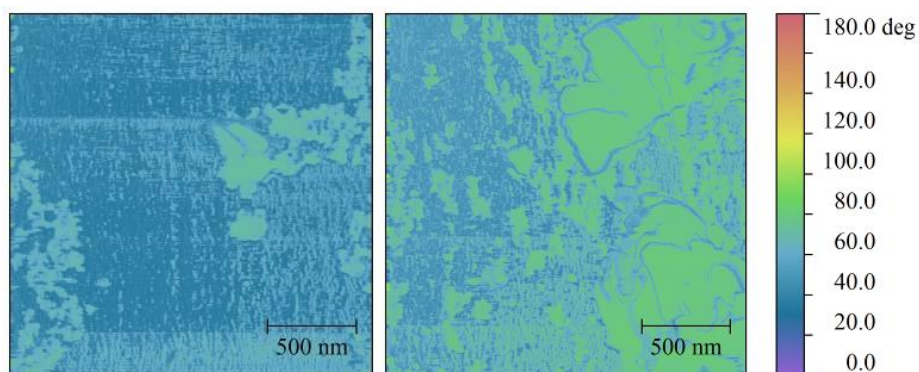
Figure 5-10 - Phase maps obtained from AFM corresponding to images shown in Figure 5-9

5.3.2 Effect of Surface Roughness on the Interfacial Shear Strength

The intermittent presence of large features on the surface of the VCF undoubtedly had an influence on the IFSS, and may explain the higher level of variability recorded for both the VCF.PP (~45% higher) and the VCF.mPP (~85% higher) microbond samples compared to the desized samples. These large variations masked the 'true' surface roughness of the sized fibres and therefore reasonable comparison to the IFSS data was difficult. Additionally these features would be unlikely to be seen for fibres in a tow, as they were created by extracting fibres from the bundles. Samples with large surface features were subsequently excluded from the analysis to investigate the surface roughness for the uniformly coated fibres. Although the reliability of the data was slightly reduced, due to the reduced number of samples, it was observed that the VCF fibres had a surface roughness of 3.38nm, which was in agreement with other data in the literature for virgin T700SC fibres [261].

For both the low and high interface strength systems, the IFSS increased with the surface roughness. Between the VCF and CFS, there was a 57% increase in surface roughness and a 33% increase in IFSS (VCF.PP and CFP.PP). The CFP fibre showed a 33% increase in surface roughness but only a 4% increase in IFSS. The discrepancy between the IFSS of the CFP and CFS may have been due to types of surface features seen on the fibres. Although the roughness values were similar, the CFS fibres showed consistent striations on the surface, with almost no other features present, whereas the CFP fibre displayed a relatively homogenous surface, with small features present intermittently. Small scale surface features such as striations have been shown to cause thermal stress concentrations and therefore enhance nucleation of the polymer on the fibre surface [81]. This may lead to improved mechanical interaction between the fibre and matrix and explain the increase in IFSS seen for the CFS over the CFP samples.

The effect of the removal of sizing was observed to have the most significant effect on the IFSS values as it has been shown to be a weak layer that effectively prevents direct interaction between the fibre and matrix [262]. The tearing of sizing seen from AFM images indicated that the sizing layer was soft and therefore may have relieved some of the compressive residual stresses formed during cooling [263], which accounts for a significant proportion of the IFSS in low interface strength systems [155], [264].

Surface roughness was certainly a factor for interfacial strength, although only small changes were observed, so the significance was likely to be low [265]. It was however believed to be of greater importance for the lower interface strength systems.

In the higher interface strength systems, the surface roughness was less likely to have a significant influence over the IFSS results, as chemical interactions were observed to be an order of magnitude greater for microbond testing. Therefore the correlation with the surface roughness data was presumably coincidental for these higher interface strength systems and other methods would be required to analyse the differences seen in IFSS. Contact angle experiments are frequently performed to characterise the wetting behaviour between materials, and have been reported to be significant factors for the interfacial strength. Components of energy are able to be separated to into dispersive and polar forces - responsible for weak and strong interactions between interfaces respectively, which allows some analysis of both low and high interface strengths. A review of data in the literature showed however that only a minority of authors were able to link (albeit loosely) the effects of surface energy to IFSS [225], [266], with other authors finding no correlation at all [79], [129], [152], [267]. X-ray photoelectron spectroscopy (XPS) is a common method for characterising surface chemistry and therefore higher interface strength systems, and was used here to interpret differences in IFSS observed between the VCF and desized fibres.

5.3.3 X-Ray Photoelectron Spectroscopy

X-ray photoelectron spectroscopy (XPS) was used to analyse the change in surface functionality due to sizing removal and the results for the VCF, CFP and CFS fibres are given in Table 5-3. Details of the procedure used as well as peak fitting can be found in Section 3.2.5. The survey spectra for VCF, CFP and CFS are presented in Figure 5-11. The VCF fibre surface was primarily composed of carbon and oxygen with trace amounts of nitrogen, silicon and sodium, potentially left from the fibre manufacturing process [207]. The desized fibres (CFP and CFS) were also mainly composed of carbon and oxygen, but had higher proportions of nitrogen, sodium and silicon compared to the VCF fibre, which was consistent with observations reported in the literature for T700 fibres [207], [221].

Fibre Type		Photopeaks			Ratios	
		C 1s	O 1s	N 1s	O/C	N/C
VCF	At (%)	76.4	22.8	0.8	0.30	0.010
CFP	At (%)	81.6	14.2	3.1	0.17	0.038
CFS	At (%)	80.6	16.0	3.4	0.20	0.042

Table 5-3 - Surface composition of VCF, CFP and CFS including oxygen to carbon and nitrogen to carbon ratios
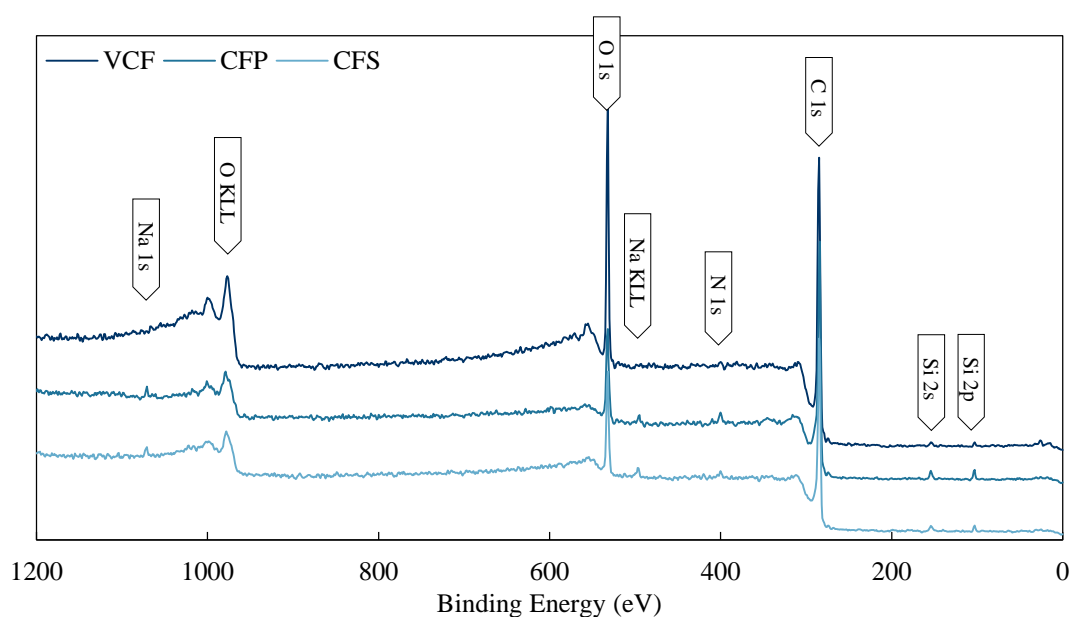
Figure 5-11 - XPS survey spectra of VCF, CFP and CFS

The oxygen to carbon ratio (O/C) was affected by sizing removal, both the CFP and CFS fibre showed lower values (ratios of 0.17 and 0.20 respectively) compared to the VCF fibre which had a ratio of 0.3. The decrease in O/C ratio and absolute values were found to be in agreement with data for virgin and desized CF literature for T700 fibres [71], [221], although the VCF seemed to be at the upper end of values reported [65], [207], [268]. The epoxy sizing is known to have a high oxygen radical content [83], and removal of the sizing therefore led to a decrease in O/C ratio and as consequence the surface activity [269]. The relative increase in nitrogen content for the CFP and CFS fibres was due to either incomplete carbonisation of the polyacrylonitrile precursor or surface treatments applied at the end of the fibre manufacturing process [270]. In either case, the increased presence of nitrogen indicated that the sizing layer had been removed to within at least 10nm, the penetration depth of the XPS analysis.

Figure 5-12 shows C 1s spectra recorded by XPS. The percentage of each functional group is presented in Table 5-4 and were estimated using curve fitting based on well-known binding energies of these groups [271]. The VCF fibre showed the highest presence of carbon-hydroxyl (C-OH) functionalities (group 2), which was likely due to the layer of sizing coating the fibre. Removal of sizing has been shown to decrease the presence of this group, whilst simultaneously increasing carboxyl functionalities (group 4) [83]. This was demonstrated from data recorded for the CFP and CFS fibres which showed a 72 and 87% decrease in groups 2 functionalities and a 179 and 243% increase in group 4 respectively. Smaller increases in carbonyl (group 3) of 32 and 42% were seen for CFP and CFS fibres respectively. These groups have been reported to be higher for fibres that have received oxidation treatments [133], which may explain the slight increase seen for the CFP samples.

Fibre		C 1s Photopeak					
		Ref	1	2	3	4	5
VCF	B.E (eV)	284.5	285.0	286.3	288.1	288.9	289.9
	%	49.0	5.4	39.0	5.0	1.4	0.2
CFS	B.E (eV)	284.5	285.0	286.3	287.8	289.1	290.0
	%	49.4	27.2	10.7	7.1	3.9	1.7
CFP	B.E (eV)	284.5	285.0	286.3	287.8	289.2	290.5
	%	51.2	30.1	5.0	6.6	4.8	2.4
Peak Assignment		Reference	C-C C-H	C-OH	C=O	COOH	O=C-O π - π^*

Table 5-4 - Percentage contribution and binding energies of C 1s photopeaks for VCF, CFP and CFS

5.3.4 Effect of Surface Composition on Fibre/Matrix Adhesion

A number of authors have studied the effect of changes in functional groups on the adhesion between fibre and matrix. It is generally believed that increased presence of oxygen functional groups such as C-OH, C=O and COOH lead to better adhesion properties as they bond to polar matrices forming ether and hydrogen bonds [67], [86]. For non-polar matrices, increasing oxygen functional groups can lead to higher surface energy and therefore better wetting [272], which leads to improvements in impregnation and therefore interfacial bond strength [273]. As the presence of these functional groups can be summarised by investigating the O/C ratio, it is logical to assume that a higher O/C ratio would lead to an increase in interfacial shear strength.
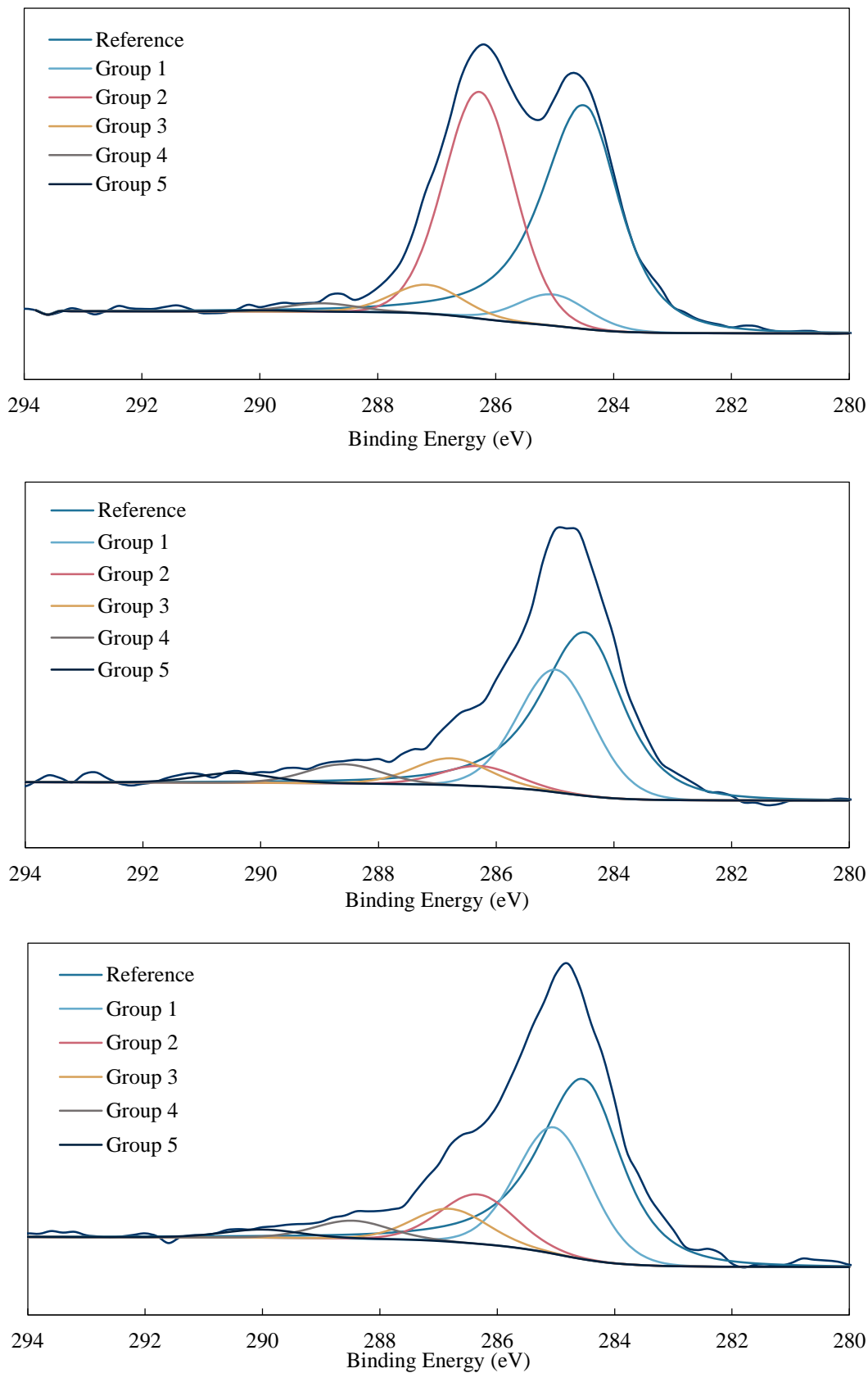
Figure 5-12 - C 1s scan for VCF (top), CFP (middle) and CFS (bottom) with peak fitting for each group (grey line represents overall CPS for C 1s photopeak)

There has however been very little agreement between this theory and experimental data. O/C ratios have been investigated between carbon fibre and a range of polar and non-polar thermoplastics, as well as thermosetting polymers [76], [207], [274], [275], with relatively little correlation found between the ratio and IFSS. Ramanathan et al. [276] suggested that the IFSS may be more dependent on the acidity or basicity of the functional group, with basic groups providing better adhesion for both CF/Epoxy and CF/PPS. Basic oxide groups are however difficult to introduce onto the fibre surface, as they are formed after cooling from heat treatments of 950°C under vacuum in an inert atmosphere [277], so are not likely to be responsible for changes in IFSS reported here.

Figure 5-13 shows the O/C ratio plotted with the interfacial shear strength for the VCF, CFP and CFS fibres with the modified polypropylene matrix. The unmodified and modified polypropylene with the three fibre types showed the same trend with increasing IFSS from VCF to CFP to CFS, however no agreement was found between the O/C ratio and IFSS for this data. Groups 3 (C=O) and 4 (COOH) are plotted against IFSS for the three fibre types in Figure 5-14, with group 4 showing good agreement with the IFSS data. The carboxylic acid group is known to form chemical bonds with high temperature thermoplastics and similar bonding was expected here through the hydroxyl moiety (-OH) of COOH to anhydride functionalities in the modified polymer.
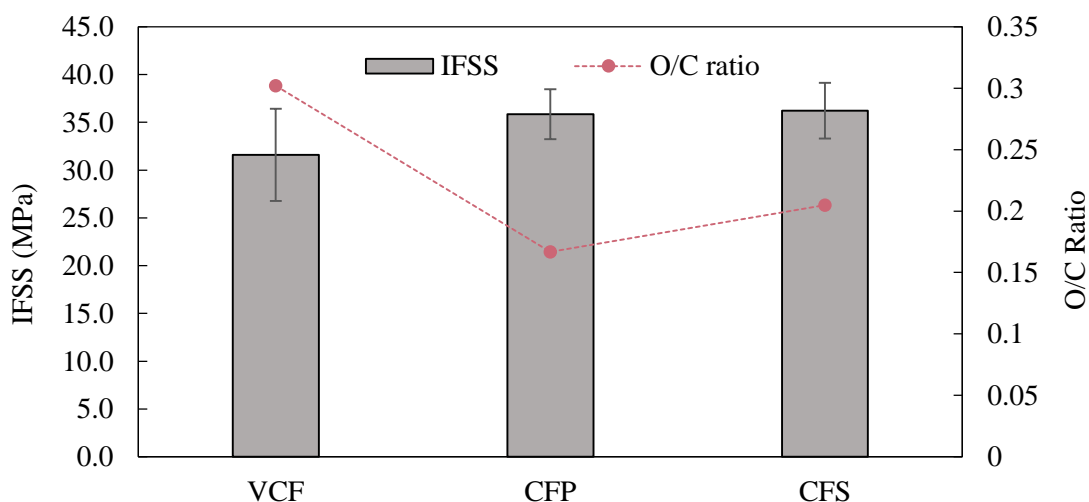
Figure 5-13 - Interfacial shear strength of carbon fibres/modified polypropylene and oxygen to carbon ratio measured using XPS

Figure 5-15 shows group 2 (C-OH) plotted against the three fibre types, showing an inverse trend to the IFSS. This indicates that carbon-hydroxyl functionalities were primarily responsible for chemical bonding at the interface for the VCF fibres. The trend seen between hydroxyl containing groups and the IFSS was due to the esterification of the anhydride functionality and hydroxyl moieties for both C-OH and COOH on the fibre surface [278]. This mechanism is known to enhance the transference of stress at the interface and improve mechanical properties [279]. These reactions significantly improved the IFSS values for all fibre types investigated in this study, however compared to the VCF, the percentage of hydroxyl groups for the desized fibres were lower and therefore cannot fully explain the difference in IFSS values.
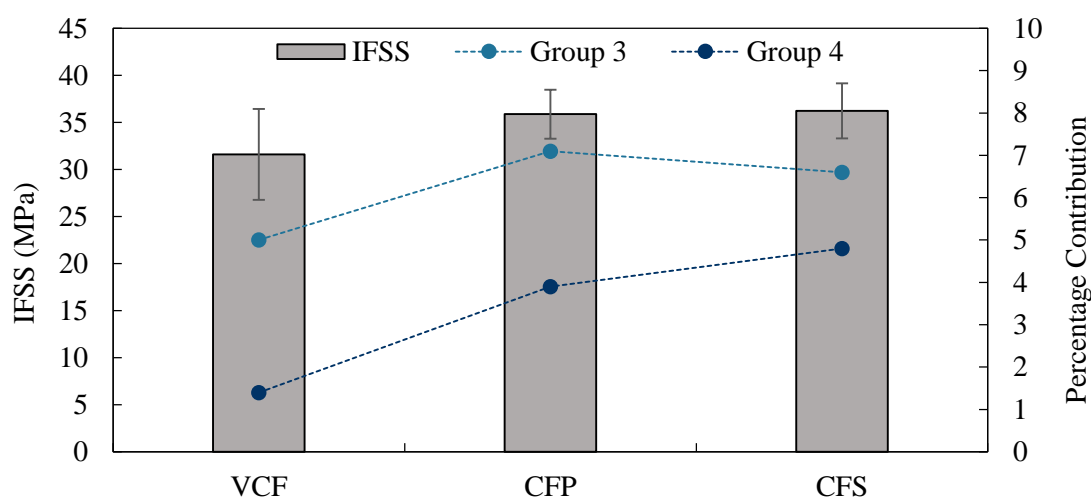
Figure 5-14 - Interfacial shear strength of carbon fibres/modified polypropylene and percentage of functional groups 3 (C=O) and 4 (COOH)

The concentration of nitrogen has been reported to correlate with interfacial bonding strength, where nitrogen-containing groups such as CONH and NO_2 are known to be fundamental to adhesion performance in thermoplastic compatible sizings [280]. Analysis of the literature has shown correlation between interface strength and increasing nitrogen content [65], [207], [275], [281], where higher concentrations led to increased IFSS values. Both the CFP and CFS samples showed increased levels of nitrogen concentration to the VCF. The nitrogen percentage is plotted against IFSS data in Figure 5-16. The IFSS data was found to correlate well with the nitrogen content, indicating that increased levels of nitrogen functionality were also responsible for increases in interface strength.

According to the literature nitrogen containing groups such as C=N, C-NH$_2$ and O-C=NH can be detected from the C1s spectra at binding energies of 286.2, 286.4, and 288.5eV [150], [226], [282], [283], corresponding to groups 2 and 4 in this study respectively. Nitrogen is known to facilitate ring opening and forming of amic acid with carbonyl anhydrides present in maleic anhydride [284]. Increases in interface strength seen for the desized fibres can therefore be attributed to further chemical bonding as a result of reactions between the coupling agent and nitrogen functionalities.
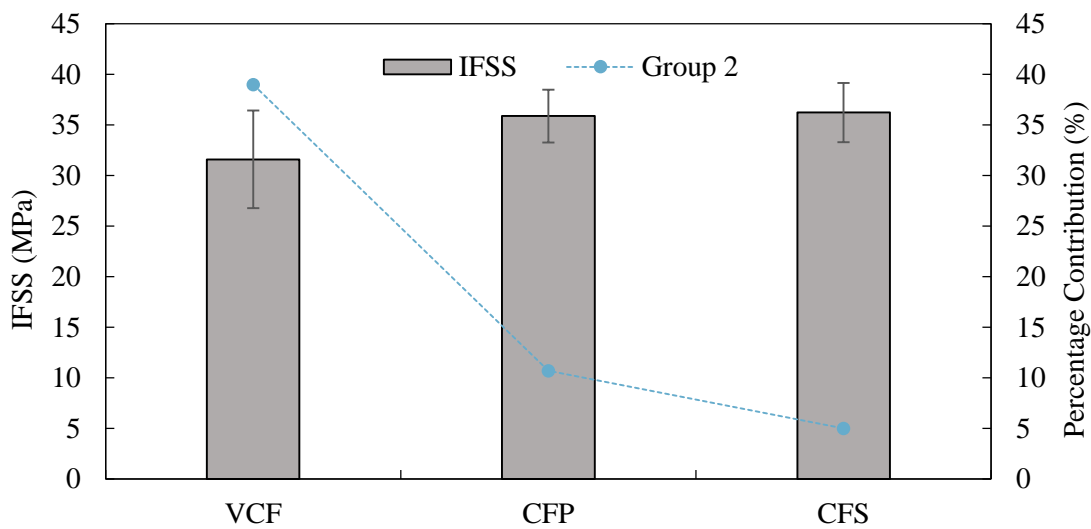
Figure 5-15 - Interfacial shear strength of carbon fibres/modified polypropylene and percentage of functional group 2 (C-OH)
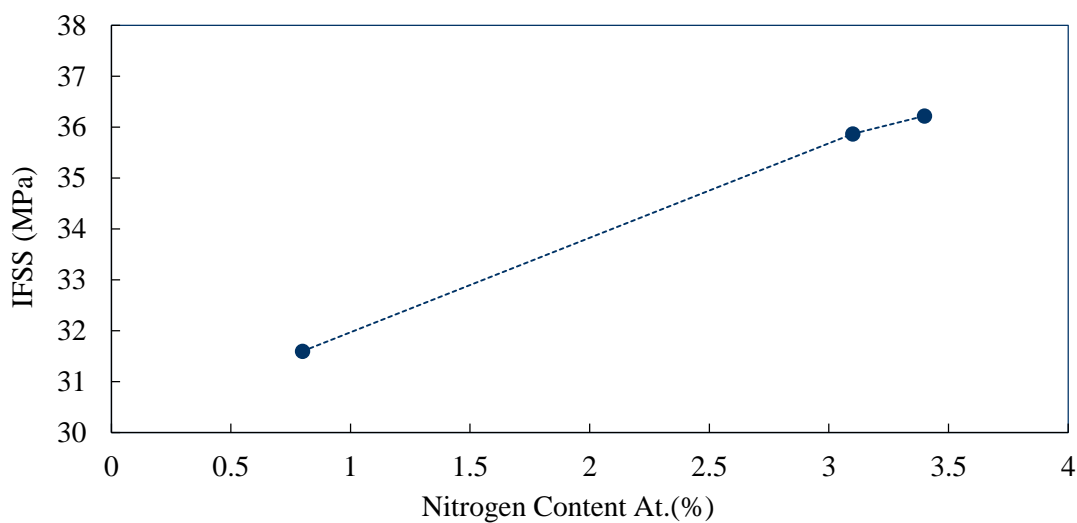
Figure 5-16 - IFSS of VCF, CFP and CFS fibres with modified polypropylene plotted as a function of nitrogen content

5.3.5 Conclusions

Data obtained from AFM showed that the surface of the VCF was very heterogeneous. Scans with large features were subsequently excluded from analysis which brought the surface roughness in line with other values reported in the literature. The CFS fibres uncharacteristically showed striations along the surface, which increased the surface roughness and therefore explained the increase in IFSS compared to the VCF and CFP samples. The IFSS showed an increasing trend with surface roughness, however it was found to be non-linear and therefore was unlikely to be the primary cause for increases in IFSS seen. It was concluded that the presence of the soft sizing layer also affected the IFSS as it prevented direct interaction between the fibre and matrix, as well as reducing radial compressive stresses formed during cooling. For the higher interface strength systems the effect of surface roughness was insignificant compared to the effect of chemical bonding, therefore surface functionality was analysed using XPS.

The surface of the VCF is primarily composed of carbon and oxygen with of both the desized fibres showing increased levels of nitrogen due to exposure of the fibre surface. The presence of nitrogen accompanied by large decreases in carbon-hydroxyl groups (C-OH) and simultaneous increases in carboxylic groups (COOH) suggested that the sizing was successfully removed for the desized fibres. The percentage of COOH and C-OH groups correlated with changes in IFSS, showing that reactions between hydroxyl moieties and the anhydride functionality in the modified polypropylene had a significant influence on the interface strength. No correlation was found between O/C ratio and interface strength, however increased levels of nitrogen observed on the desized fibres proved to positively influence the interface strength. Increases in IFSS seen for CFP and CFS over the VCF fibres may therefore be due to nitrogen-containing functionalities which have been shown to react with anhydride carbonyl groups in maleic anhydride. The interfacial properties were significantly affected by the surface characteristics of the fibre as well as modification to the matrix. Large increases in IFSS were observed through the introduction of a maleic anhydride coupling agent, with recorded values close to the shear strength of the polypropylene – the theoretical limit for interface strength, however a number of authors in the literature have reported interface strengths higher than the polymer shear and tensile strength.

6. Macroscale Performance of Carbon Fibre/Polypropylene Composites

6.1 Introduction

In the previous sections, focus has been on microscale characterisation of the interface between carbon fibre and polypropylene. This section investigates macroscale mechanical performance as well as how changes made at the microscale affect the macroscale properties and dictate failure mechanisms observed in service. While microscale testing focussed on analysis of single fibres, composites produced in this section for mechanical characterisation consisted of long, discontinuous fibre tows. This allowed investigation of a large range of volume fractions which have not been achieved previously for this material. The introduction of maleic anhydride had the most significant effect on the microscale interface, suggesting good improvements could be achieved at the macroscale. Although the desized fibres offered the highest interface strength, composites with these fibres could not be produced here using the powder impregnation method (see Section 3.3.2.1). Virgin sized fibre composites, with and without maleic anhydride were therefore manufactured to investigate the mechanical performance and failure characteristics.

6.2 The Effect of Maleic Anhydride on the Macroscale Mechanical Performance

To investigate the effect of the maleic anhydride coupling agent on the mechanical performance of carbon fibre/polypropylene composites, tensile, flexural and Charpy impact tests were performed and comparisons were made to a carbon fibre/epoxy benchmark. Table 6-1 summarises the data obtained from mechanical testing for composites moulded at $0.45V_f$.

Property	CF.PP		CF.mPP		CF.EP	
	$\overline{X}$	s	$\overline{X}$	s	$\overline{X}$	s
Tensile Modulus (GPa)	21.63	3.76	28.77	5.7	32.8	3.95
Tensile Strength (MPa)	60.13	10.13	100.82	19.51	220.57	29.7
Flexural Modulus (GPa)	13.72	1.89	18.35	3.06	19.56	1.7
Flexural Strength (MPa)	105.18	6.19	179.15	15.99	320.15	12.1
Charpy Impact (kJ/m^2)	56.37	10.96	81.93	12.5	66.1	6.07
Void Content (%)	3.47	2.12	3.34	1.29	0.36	0.12

Table 6-1 - Mechanical property data recorded for carbon fibre/polypropylene samples with and without a coupling agent, compared to a carbon fibre/epoxy benchmark all at $0.45V_f$.

6.2.1 Mechanical Testing Results

Due to the discontinuous nature of these composites, a number of fibres lie at angles to the loading direction where the maximum strength is determined by the interfacial adhesion [133]. Increases in strength were therefore expected for the improved interface composites as efficiency of stress transfer was dictated by quality of the interfacial bond. The addition of maleic anhydride increased tensile and flexural strength by 68% and 70% respectively, however significant differences in strength were observed when compared to CF.EP. The benchmark composite had 118% and 78% higher tensile and flexural strengths respectively than the CF.mPP. The carbon fibre/polypropylene samples both displayed relatively high void content compared to the CF.EP, which is known to reduce strength properties at high fibre loadings for long fibre thermoplastics [285]. Moreover, the interfacial shear strength was 45% higher for CF.EP and the unfilled tensile strength of epoxy was double that of polypropylene, so differences in strength were anticipated.

The tensile and flexural moduli were improved with the addition of maleic anhydride by 33% and 34% respectively. This was unexpected as the modulus is determined at low loads in the initial phase of the tensile or flexural test. The modulus is predominantly governed by the elastic properties of the fibre and matrix and therefore should not be significantly affected by interfacial adhesion [286]. This assumes that the matrix wets the fibres perfectly, which in practice is not true, however an improvement in modulus suggested that wetting angles between the fibre and matrix were reduced by the addition of maleic anhydride. Changes in modulus with the addition of a coupling agent are not typically seen for unidirectional composites [287], however it has been reported for DFCs [22], [79], which further compounds the importance of the interface on the mechanical properties of discontinuous fibre architectures. The tensile and flexural moduli of CF.EP were similar to that recorded for CF.mPP, displaying a 14% and 6.5% increase for the two properties respectively. The differences in moduli were primarily due to void content in the CF.mPP composites, which has been shown to account for approximately a 4% reduction in longitudinal tensile modulus (E_{11}) for

continuous carbon fibre/epoxy composites [288], [289]. The sensitivity of DFC stiffness on interfacial strength, which was observed for samples with and without maleic anhydride, indicated that the increased IFSS reported for CF.EP also contributed to the increased moduli witnessed here.

The Charpy impact strength was also improved through the addition of maleic anhydride, shown by a 45% increase from $56.4 \pm 11\text{kJ/m}^2$ to $81.9 \pm 12.5\text{kJ/m}^2$. A number of studies have suggested that a stronger interface leads to a lower impact strength, as there is larger energy dissipation through fibre pull-out, a common failure mode for weak interfaces [81], [264]. This has been demonstrated for continuous fibre composites, however it did not appear to be the case here, with similar increases reported for glass fibre/polypropylene DFCs with optimised sizing [41]. Surprisingly, the CF.EP benchmark had a higher impact strength than the CF.PP, with the CF.mPP only showing a 24% improvement over the CF.EP benchmark, highlighting that the standard geometry for Chapry testing may not be large enough to determine the impact strengths of composites with these mesoscale architectures. Nevertheless, significant improvements in all properties were demonstrated by the addition of 2wt.% maleic anhydride, most notably the tensile modulus, which was only 12% lower than a comparable CF.EP composite.

6.2.2 Failure Mechanisms

The failure mechanisms of the CF.mPP samples were determined by visual inspection as well as SEM of the failed samples, and have been compared to the CF.PP and the CF.EP benchmark samples. Figure 6-1 shows the tensile fracture sites of CF.PP, CF.mPP and CF.EP respectively, all moulded at $0.45V_f$. There was a significant difference between the CF.PP and the CF.mPP fracture sites when compared to the CF.EP. The CF.EP sample demonstrated brittle failure characteristics typical of materials with high interfacial shear strength, with almost all of the fibres still coated in epoxy resin. The planes of failure at the end of each tow were apparent from the visual inspection, whereas on the CF.PP and CF.mPP samples, there were few defined edges and the fibres had significantly less polymer surrounding them. Additionally for the CF.PP and CF.mPP samples there was evidence of fibres pulling away from the matrix, which appeared to be more prominent on the CF.PP samples. This was

particularly clear for fibres out-of-plane to the loading direction, demonstrating more ductile failure mechanisms for the CF.PP and CF.mPP samples.

Figure 6-1 – Tensile fracture sites of CF.PP (top), CF.mPP (middle) and CF.EP (bottom) all moulded at $0.45V_f$

Cracks that propagate through composites follow the least resistant paths, and in discontinuous fibre composites are impeded by discontinuities, such as fibre cross-

overs [290]. Depending on the strength of the interfacial bond between fibre and matrix, cracks will either propagate through the matrix or along the interface [264]. When the interface is weak, these interfacial cracks spread the length of the fibre and lead to fibre pull-out [291]. This was demonstrated by the CF.PP samples as the tows separated during fracture and the ends were flexible and free of matrix. Whereas the exposed tows from the CF.mPP samples were noticeably stiffer and maintained higher tow integrity, with relatively few fibres pulled away from the tows. The CF.EP fracture site was significantly different to that of the CF.PP and CF.mPP composites, with no flexibility in the exposed tows, confirming excellent adhesion between fibre and matrix.

Figure 6-2 shows SEM micrographs of tensile fracture sites for CF.PP, CF.mPP and CF.EP. In contrast to the macro images, CF.mPP and CF.EP appeared to have relatively similar fracture sites, with large amounts of matrix material present on and around the fibres. For the CF.mPP sample, there was less polymer attached to the exposed fibres than the CF.EP samples, but considerably more than was present on the fibres in the CF.PP sample. SEM confirmed interfacial failure for the CF.PP samples, as the fibres were free of matrix material, with a number of fibres pulled away from the tow, again indicating low interfacial shear strength. The addition of maleic anhydride clearly improved the interfacial adhesion between fibre and matrix with the CF.mPP samples showing large lumps of polymer still attached to the surface after testing. This demonstrated that the interface strength was large enough to promote cohesive failure in the matrix, resulting in higher strength and impact properties.

Figure 6-3 shows the difference in matrix failure between CF.mPP and CF.EP respectively. CF.EP failed in a very brittle manner, with shards of epoxy shown around the site of fracture. The interface strength was high and the matrix was brittle, therefore cracks have propagated through some of the fibre bundles leading to fibre failure. The CF.mPP sample showed higher ductility with plastic deformation clearly visible, indicating that the work of fracture was higher [292].
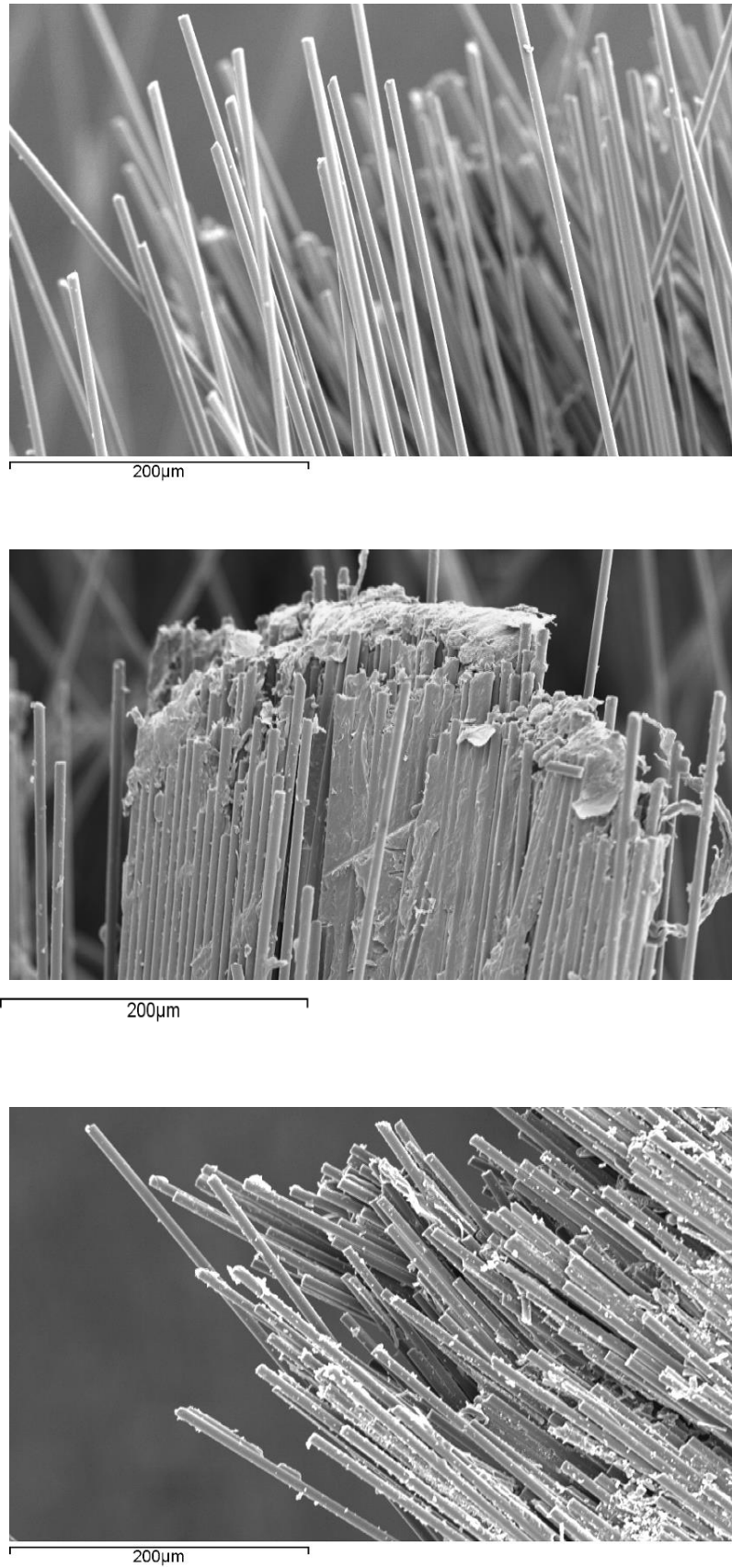
Figure 6-2 – SEM micrographs of tensile fracture sites for CF.PP (top), CF.mPP (middle) and CF.EP (bottom)
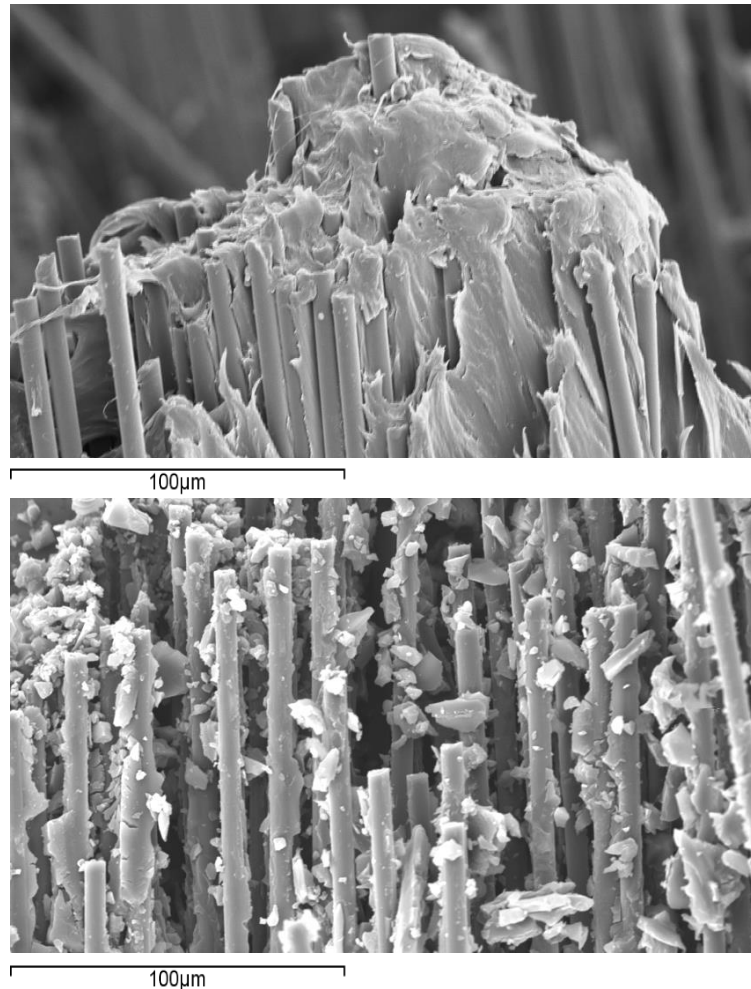
Figure 6-3 – SEM micrographs of a sample CF.mPP fracture site (top) showing matrix ductility and a sample CF.EP fracture site (bottom) where the matrix displays brittle characteristics

6.2.3 Conclusions

The effect of the addition of maleic anhydride was investigated as microscale testing had showed that the addition of the coupling agent significantly improved the interfacial shear strength. The coupling agent improved all properties that were tested, with the most marked increases seen in tensile and flexural strength. Analysis of the failure sites showed that the CF.PP had almost no matrix left on the fibre, indicating a weak interface and therefore interfacial failure. The CF.mPP samples showed some matrix left on the fibre which is characteristic of a stronger interfacial bond and therefore a mix of matrix and interfacial failure, explaining the increase in strength observed. Compared to the CF.EP benchmark, the strengths of CF.mPP were significantly lower, which was attributed to increased void content due to non-optimised processing, as well as lower interfacial and mechanical properties of PP compared to epoxy. The tensile and flexural moduli were also improved with the addition of maleic anhydride, where

CF.mPP composites showed comparable moduli to CF.EP composites, which is promising for this material considering the high volume fraction. Charpy impact strength was observed to increase with the addition of maleic anhydride, however only relatively small increases (24%) were seen over the benchmark composites, which was partially attributed to higher void content as well as effects caused by small sample/reinforcement size ratios that were required for this test method.

The failure mechanisms for CF.PP and CF.mPP were very different from CF.EP demonstrated by fracture site morphology. The CF.EP samples showed brittle fracture sites and large amounts of polymer still surrounding the fibre, indicative of high interfacial shear strength. The CF.mPP showed similar characteristics to the CF.EP sample under SEM, with matrix present on the surface of the fibre, demonstrating that the interface was strong enough to cause cohesive matrix failure. However at the macroscale, CF.mPP and more noticeably CF.PP, displayed ductile failure characteristics due to the high strain-to-failure of the polypropylene matrix. The CF.mPP samples showed comparable stiffness to the CF.EP samples and have the advantage of showing progressive failure over the catastrophic failure seen for CF.EP.

6.3   The Effect of Volume Fraction on the Mechanical Performance

The effect of volume fraction on mechanical performance was investigated to determine an optimum level of fibre content, based on lower-than-expected strengths recorded at $0.45V_f$. Tensile, flexural and Charpy impact testing were performed to characterise the mechanical properties, with density measurements taken for each sample to calculate the local fibre volume fraction and therefore normalise the test data to the nominal volume fraction. Density measurement data and corresponding property normalisation is given in Appendix D. It was identified from the literature that mesoscale architectures are prone to large variability in recorded data, and anisotropy was characterised by testing samples in both X and Y directions from the moulded plaques. An equal number of samples were tested for each direction and data presented in this section is an average of these values. The maximum percentage difference between data obtained from X and Y samples was found to be 30%, however the majority was 16% and below. The anisotropy data is given in Appendix D.

Examples of stress-strain curves for carbon fibre/polypropylene and carbon fibre/epoxy are given in Figure 6-4. It should be noted that the strain data was calculated from the crosshead displacement, as the extensometer (used to calculate modulus) was only able to measure strains up to 0.5% before it had to be removed to prevent damage. The calculated strain data is therefore likely to be larger due to the compliance of the crosshead and deformation occurring outside the gripping area [293]. Nonetheless it gives data accurate enough to observe trends between different data sets. The stress-strain relationships confirmed that the failure of the CF.mPP samples was much more progressive than the CF.EP samples.

Progressive failure was more noticeable in lower volume fraction samples, where matrix ductility was not significantly restricted by the reinforcing fibres. This was displayed by a reduction in strain-to-failure with increased fibre loading, where the CF45.mPP samples only showed approximately 20% higher failure strains than the CF.EP samples (70% lower than the virgin polypropylene). Toughness is governed by complex interactions between material architecture and properties for DFCs and therefore reductions in strain-to-failure do not necessarily lead to reduced energy absorption. The benefit of the thermoplastic matrix is that it allows progressive failure mechanisms, demonstrated here for all the CF.mPP samples, which is often preferred from a structural design standpoint.
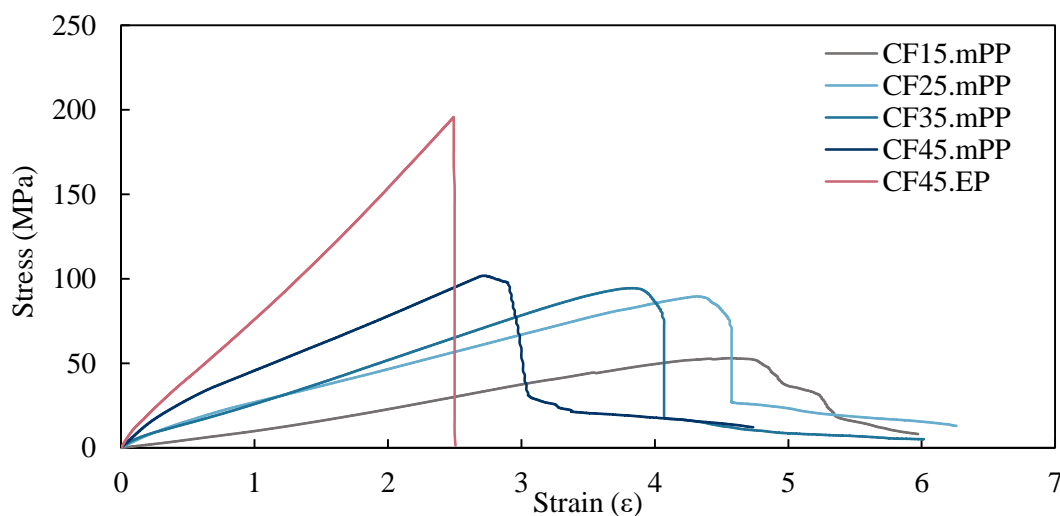
Figure 6-4 - Examples of stress-strain data recorded from tensile testing for the materials tested in this study showing the effect of variation in volume fraction.

6.3.1 Microstructural Variation

The microstructure of the composites was investigated using optical microscopy and void content was measured using image analysis software ImageJ. Figure 6-5 shows the void content as a function of volume fraction. It was expected that the void content might be high due to the high viscosity of the thermoplastic matrix, however the coated fibres appeared to reduce the melt flow distance sufficiently to provide adequate wet out. The 0.35 and $0.45V_f$ composites displayed the highest levels of void content of 3.1 $\pm$ 0.9 and 3.3 $\pm$ 1.3 respectively.

Final void content in composites manufactured by non-isothermal compression moulding (NI-CM) have been shown to be dependent on the time at pressure before demoulding [294], where it has been suggested that final void elimination is due to diffusion of the voids in the matrix [206]. The void content increased with volume fraction here, indicating that diffusion processes were longer due to the reduced content of matrix. The void content of the epoxy benchmark was 0.37% $\pm$ 0.1 at $0.45V_f$, 44% lower than the CF15.mPP, which had the lowest void content of the carbon fibre/polypropylene samples. The low void content was due to the significantly lower viscosity of the epoxy, allowing it to penetrate into small intra-bundle pores more easily. It was unlikely that voids present in the carbon fibre/polypropylene microstructure could be reduced to this level, however optimisation of the tow coating process and increased time at pressure before demoulding could reduce the porosity of the higher *Vf* composites to around 1% [294], which is generally regarded as an acceptable level of void content [295], [296]. Optimisation of the tow coating process and composite forming were outside the scope of this project, however recommendations for further work in these areas based on the findings here have been given in Section 7.1.

Figure 6-6 shows the internal microstructure of carbon fibre/polypropylene composites ranging from $0.15 – 0.45V_f$. On inspection of figures for CF15.mPP and CF25.mPP, the fibre tows were surrounded by large areas of polymer, and were not homogenously distributed within the matrix. These large groups of agglomerated bundled fibres generated high stress concentrations due to fibre end synchronisation, creating failure initiation points within the composite [297]. This has been demonstrated in high volume

fraction carbon fibre/epoxy composites [298], however it was unclear how the increased levels of ductile matrix surrounding the fibre would affect the redistribution of stresses at the bundle ends here.
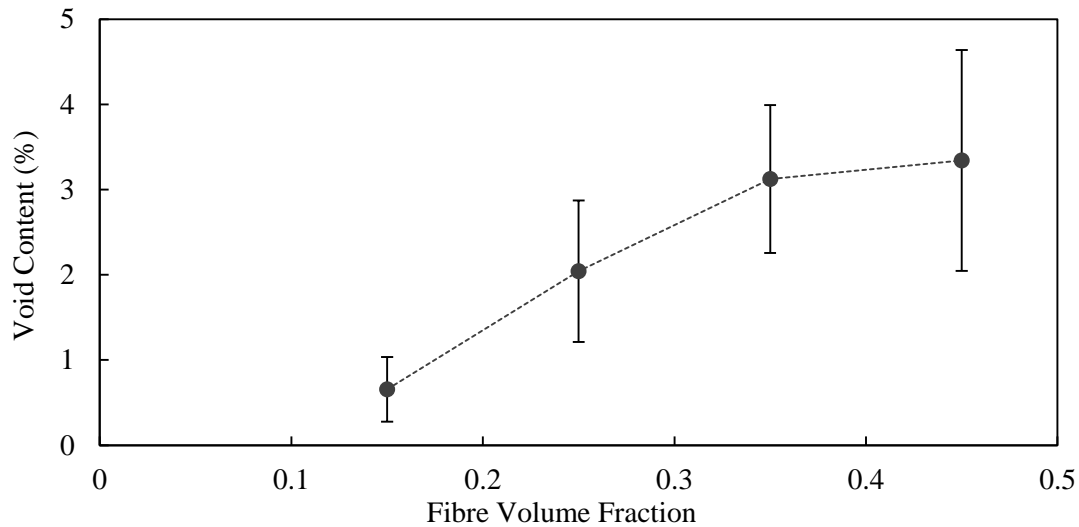
Figure 6-5 - Void content for CF.mPP samples as a function of fibre volume fraction (error bars are standard deviation)

The CF35.mPP and CF45.mPP had similar microstructures as observed by optical microscopy, where voids were confined to the edges of fibre bundles, near pockets of polymer. Voids were not widely observed in areas of high fibre concentration due to local variations in pressure within the mould. High volume fraction regions experienced the highest pressures, which subsequently reduced pressure witnessed in regions of low volume fraction. This was confirmed on inspection of the moulded panels, where slight increases in thickness were accompanied by exposed fibre on the surface of the panels, shown in Figure 6-7.

The largest areas of void content in the high V_f samples were at the mid-plane, which has been observed for NI-CM composites that have had insufficient pre-heating times [198]. There was however a large amount of material flow for these samples, which indicated that the preforms were sufficiently heated, and large longitudinal matrix flow at the mid-plane would be responsible for the elimination of most porosity [201]. Remaining voids would therefore be trapped in areas of fibre near the flow front due to reduction in volume and increased pressure of the matrix [294], as witnessed here.
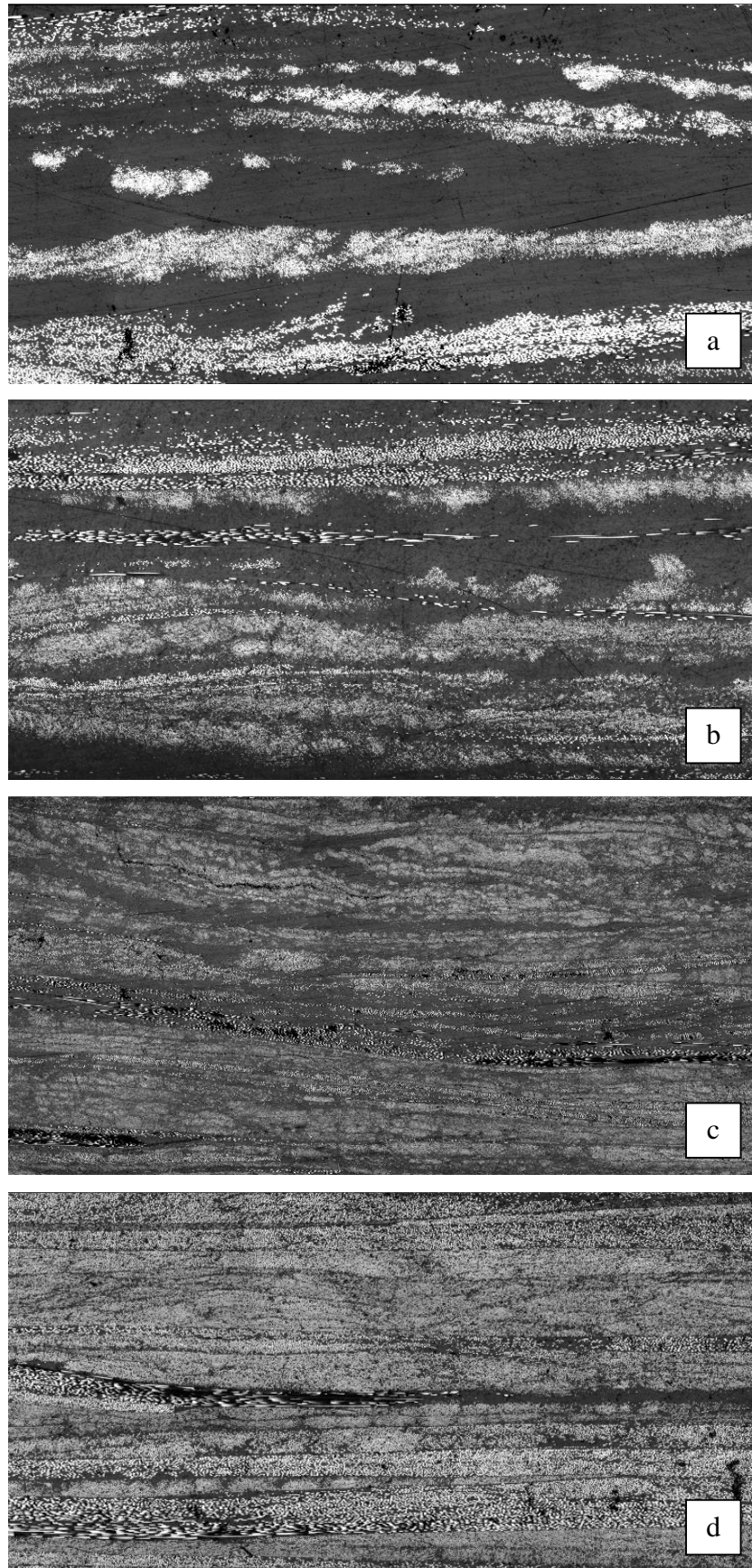
Figure 6-6 – Optical microscopy images of CF.mPP composites moulded at a) $0.15V_f$ (CF15.mPP), b) $0.25V_f$ (CF25.mPP), c) $0.35V_f$ (CF35.mPP) and d) $0.45V_f$ (CF45.mPP)

Figure 6-7 – Exposed fibres on the surface of a moulded panel due to local variations in volume fraction

6.3.2 Tensile and Flexural Modulus

The results for the tensile and flexural moduli of carbon fibre/polypropylene as a function of volume fraction are presented in Figure 6-8. It is clear that for both moduli, increasing volume fraction led to an almost linear increase in modulus. The tensile modulus showed a slight deviation away from the trend between 0.35 and 0.45V_f, accompanied by higher scatter in the data due to higher void content.
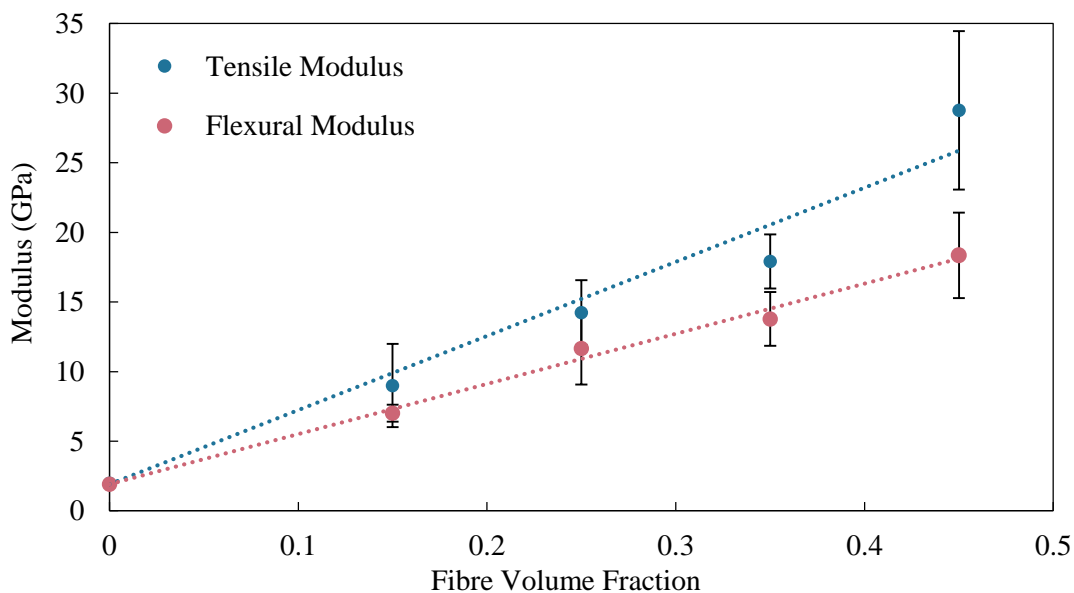
Figure 6-8 - Tensile and flexural modulus as a function of fibre volume fraction for CF.mPP

The recorded tensile moduli were compared to the Cox-Krenchel analytical model (see Figure 6-9). Assuming transverse deformations are insignificant, the fibre orientation

factor for in-plane randomly oriented discontinuous fibres is $\eta_0 = 0.375$ [9]. The fibre length efficiency factor was equal to 1 as all the fibres here were above the critical length, which in this case was 0.34mm (calculated from $lc = (\sigma_f.d_f)/\tau_{app}$). From Figure 6-9 it is clear that the experimental values fall short of the analytical predictions.

To quantify the discrepancy between the analytical model and experimental results, a bundling efficiency factor (η_b) was incorporated into the Cox-Krenchel model ($\eta_0 = 0.375$ and $\eta_l = 1$). The bundling efficiency factor was calculated as 0.56, 0.59, 0.55 and 0.71 for volume fractions 0.15 to 0.45 respectively. Apart from the deviation at 0.35 volume fraction, the bundling efficiency factor increases with volume fraction. This corroborates the findings in Figure 6-6 where, due to the nature of the bundles, fibres are not distributed evenly within the composite. At low volume fractions, these areas of high fibre content become failure initiation sites due to high stress concentrations forming at the ends of the bundles. In single fibre architecture composites, these stresses are more evenly distributed within the composite, which explains why these architectures are better predicted by the simplistic analytical models. Similarly, as the volume fraction increases, the bundle efficiency increases due to a more homogeneous distribution of bundle ends, and therefore stress concentrations, within the composite.

The Cox-Krenchel model was also used to predict the modulus for the CF.EP composite moulded at $0.45V_f$. As the material parameters were effectively the same, a theoretical value of 40.5GPa was calculated, 24% higher than the recorded data. The disparity between the analytical model and experimental results for both CF.mPP and CF.EP highlighted that this relatively simple analytical model was unable to predict basic mechanical properties for these architectures. Despite the fact that the Cox-Krenchel model is based on volume-averaged fibre and matrix moduli, which are then degraded based on statistical approximations of the effect of fibre orientation and length, it provides good approximations of modulus for homogeneous microscale architectures [299]. Additionally, the Cox-Krenchel predictions were found to be within 7% of predictions using the slightly more rigorous models developed by Halpin and Tsai [300].
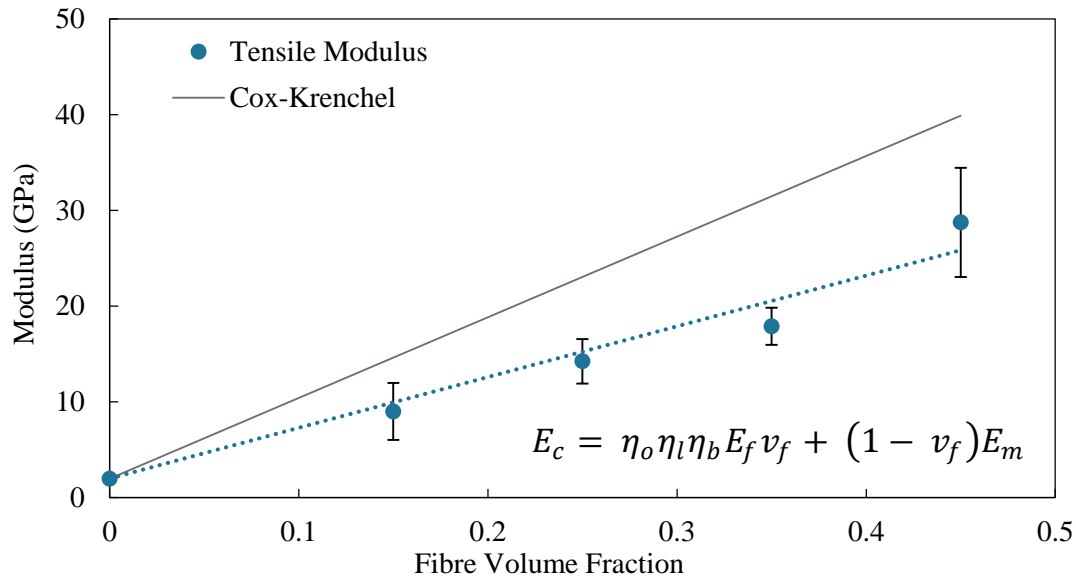
Figure 6-9 - Analytical predictions for modulus plotted against experimental data as a function of fibre volume fraction using the Cox-Krenchel model, where η_o and η_l are the fibre orientation and length efficiency factors respectively, E_f is the fibre modulus, v_f is the fibre volume fraction and E_m is the matrix modulus. (error bars represent standard deviation)

As deviations from the predicted modulus were observed over the whole range of volume fractions tested, stiffness degradation due to void content, fibre breakage and heterogeneous distribution of fibre could be ruled out. The reduction in stiffness compared to analytical predictions was therefore due to less efficient intra-bundle stress transfer combined with incomplete encapsulation of the fibres, due to the tightly packed nature of the fibre tows [64]. Moreover, these models assume perfect interfacial bonding, which has been shown in the previous sections to have a significant impact on modulus for DFCs. Single fibre architecture composites are therefore better predicted due higher permeability and consequently better fibre wet-out, even with high viscosity thermoplastics such as polypropylene.

6.3.3 Tensile and Flexural Strength

The results for the flexural and tensile strength of carbon fibre/polypropylene, as a function of volume fraction, are presented in Figure 6-10. Both tensile and flexural strength increased with increasing volume fraction, but in a non-linear manner in contrast to the moduli values. At approximately $0.25V_f$, both tensile and flexural strength properties appeared to plateau, with tensile strength only increasing by 3% between 0.25 and $0.35V_f$ and decreasing by 1% from $0.35 - 0.45V_f$. The flexural

strength showed a similar trend between 0.25 and $0.35V_f$, with only a 0.3% increase, however between 0.35 and $0.45V_f$ there was a more significant increase of 19%.
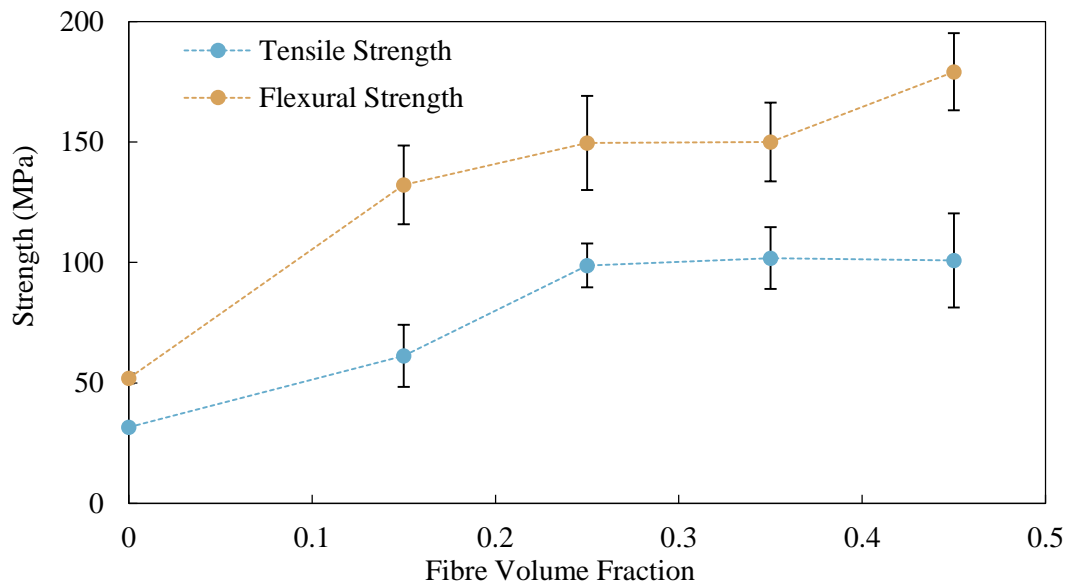
Figure 6-10 - Tensile and flexural strength as a function of fibre volume fraction for CF.mPP

The plateau in strength was due to defects caused by packing limitations [301], where void content was shown to increase. As volume fraction increases the inter-fibre spacing and stress transfer efficiency are reduced, resulting in increased risk of fibre breakage due to high local shear stresses induced during processing [23]. This effect has been observed in glass fibre/polypropylene LFTs above volume fractions of 0.1 [285], but was not displayed for carbon fibre/polypropylene LFTs, where linear increases in strength were reported up to $0.25V_f$ [38]. Due to the mesoscale architecture used here, improved packing compared to microscale architectures should lead to a saturation point at a higher volume fraction, confirming that further strength improvements could be made.

The experimental tensile strength data was compared to the Kelly-Tyson analytical model, which is an extension of the rule-of-mixtures [35]. The orientation efficiency factor is equal to $\eta_0 = 0.375$, similarly to the analytical model for modulus, and the critical length was calculated as before. The fitted efficiency factor, k, (see Figure 6-11) is controversial as it was introduced based on the overestimation of strength from the Kelly-Tyson model for discontinuous fibre composites [35], [302]. It is reported in the

119

literature that good correlation has been found for values of k=0.53 [299], however this still overestimated strength values here significantly. The analytical model was fitted to the tensile strength data recorded here using k=0.24 (Figure 6-11), similar to that found for a natural fibre/polypropylene system [302]. The figure shows that by modifying the fitted efficiency factor, the data is relatively well represented up to around $0.25V_f$. The use of a fitting factor however seemed to suggest that the analytical model was not sufficient for predicting strengths for these architectures. A fitted efficiency factor was also calculated for the CF.EP benchmark strength and was found to be k=0.35, which further highlights the inappropriateness of using this factor to fit experimental data.
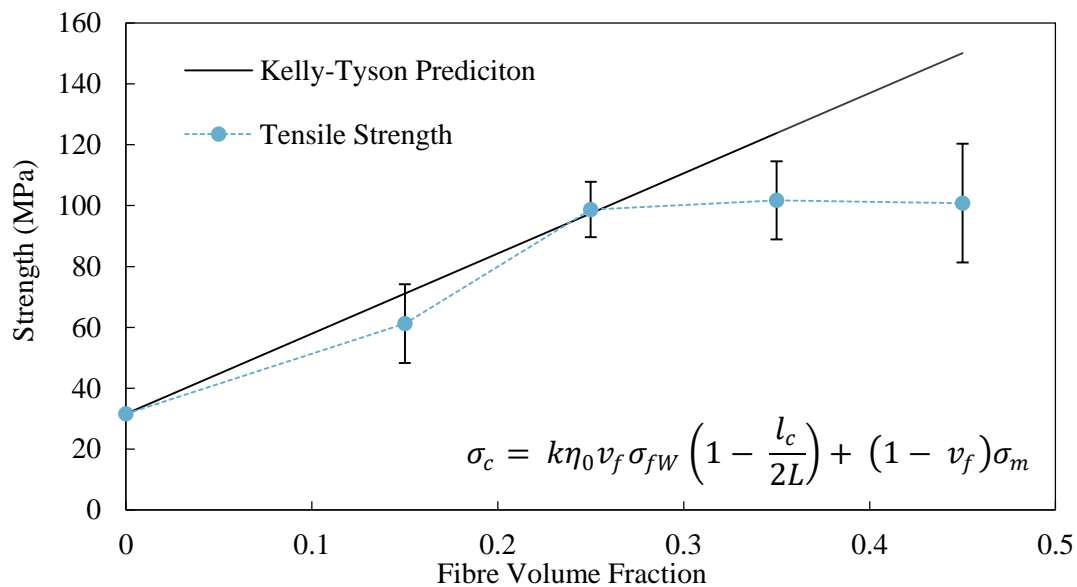
Figure 6-11 - Comparison of tensile strength data to the Kelly-Tyson analytical model, where k is the fitted efficiency factor, η_0 is the orientation efficiency factors, σ_{fW} is the strength of the fibres normalised to fibre length by a Weibull distribution function, l_c is the critical fibre length, L is the fibre length and σ_m is the matrix strength

The analytical modelling of strength using volume-averaged strengths of the constituent materials and statistical representations of fibre orientation and length was not appropriate here as a number of complex micromechanical mechanisms dictate the onset of failure for random DFCs. Whilst microscale architectures may be better predicted, failure mechanisms in heterogeneous mesoscale architectures are more dependent on tow geometry, where damage has been shown to initiate at the ends of fibre bundles aligned in the loading direction, which terminate on transverse bundles [303]. Failure is significantly influenced by fibre packing defects, which are significant

for both micro- and mesoscale architectures. This means that at higher volume fractions the relationship between strength and volume fraction is non-linear, showing that rule-of-mixture predictions are not appropriate for strength in this range.

6.3.4 Charpy Impact Strength

The results from the un-notched Charpy impact testing are presented in Figure 6-12 as a function of fibre volume fraction. As with the modulus and strength, the Charpy impact strength initially increased with fibre loading. The largest increase in impact strength (107%) was observed between 0.15 and $0.25V_f$, reaching a maximum value of $94.7 \pm 13.45\text{kJ/m}^2$ at $0.35V_f$, and subsequently decreasing by 13% from $0.35 - 0.45V_f$. Taking experimental variation into account, it appeared that there was relatively little improvement in impact strength with volume fraction above $0.25V_f$. Similar findings have been reported for a number of systems [285], [304], [305], however little explanation has been given and it was assumed that void content was not entirely responsible [306].
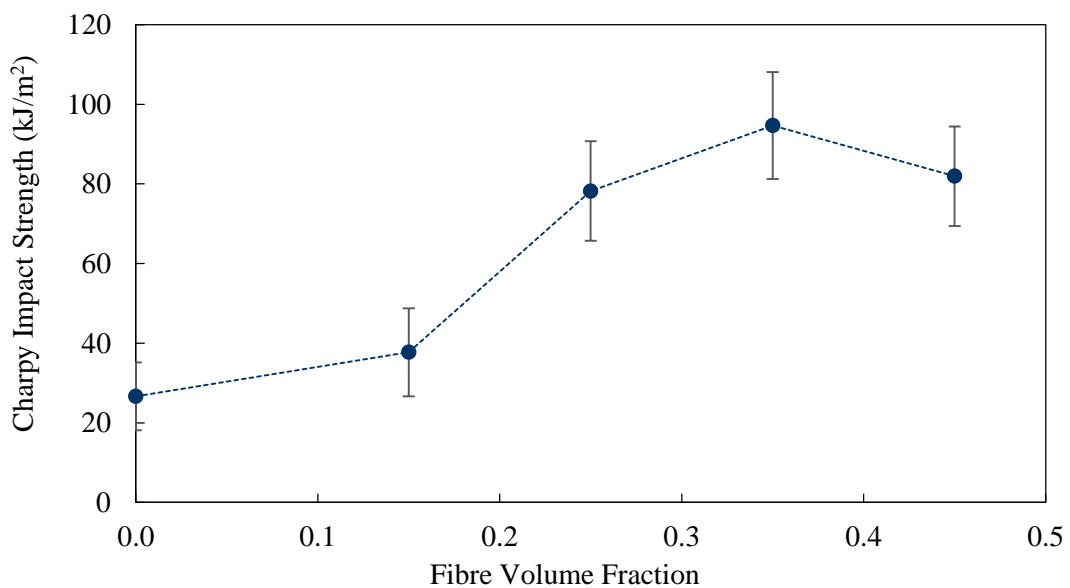
Figure 6-12 - Charpy impact data for carbon fibre/polypropylene as a function of volume fraction

It is proposed that the plateau seen for the impact strength was due to the following; firstly, impact strength in DFCs is largely matrix-dominated [182], where ductile matrices have been shown to dissipate energy through the blunting of sharp crack tips [292]. Despite fibre breakage and pull-out accounting for a large proportion of the

fracture energy, there must be sufficient matrix to transfer stresses efficiently. It is known that fibre fracture leads to stress intensification [245] and for high interface strength systems, cracks therefore propagate through the matrix, as opposed to along the interface [291]. This is exacerbated at higher volume fractions as the inter-fibre spacing is reduced and may lead to brittle failure characteristics. Additionally for the systems tested here lower fracture energies at higher volume fractions may have been observed due to the increased likelihood of fibres spanning the width of the sample, which would lead to premature failure, as stress redistribution would not have been possible.

Novak and DeCrescente [43] and Beaumont and Wells [307] have analytically described energies required for pull-out (Equation 6-1) and fibre fracture (Equation 6-2) in unidirectional composites respectively. Dividing the two equations gives the ratio of energy of pull-out to fibre fracture, which for the materials tested here gave $U_p/U_{ff} = 0.175$, demonstrating that the main mechanism of energy absorption was through fibre fracture. The ratio is very sensitive to changes in interface strength, for example, CF45.PP had a U_p/U_{ff} ratio of 0.65, much larger than that of CF.mPP, indicating that lower interface strengths lead to higher energy absorption. This however was not observed here, as the CF45.mPP had an increased impact strength of 45% over the CF45.PP samples. Moreover, it has been postulated that increases in impact strength due to increased IFSS, must be accompanied by increases in fibre strength [41]. Again this was found to be invalid as the interfacial strength was increased by matrix modification only, with identical fibres.

$$U_{po} = \frac{v_f d_f \sigma_f^2}{24\tau}$$

Equation 6-1 - Energy required for fibre pull-out, where v_f is volume fraction, d_f is the fibre diameter, σ_f is the fibre tensile strength and τ is the lesser of matrix or interface shear strength

$$U_{ff} = \frac{v_f L \sigma_f^2}{6 E_f}$$

Equation 6-2 - Energy required for fibre fracture, where L is the gauge length of the test specimen and E_f is the fibre modulus

6.3.5 Conclusions

The effect of increasing fibre volume fraction on the mechanical properties showed improvement for all of the properties tested. Tensile and flexural moduli displayed relatively linear correlation, with tensile, flexural and impact strength showing linear increases up to approximately $0.25V_f$, where the properties appeared to plateau. Void content also increased with volume fraction, with voids found in the mid-plane of the composites, close to the interface between fibre and matrix. This suggested that further reductions in void content, and therefore increases in strength, may be possible by optimisation of tow coating and moulding processes.

The plateau in strength was partly attributed to the increased void content at higher volume fractions, but also to inefficient stress transfer between fibre and matrix due to small inter-fibre spacing. The plateau in impact strength was postulated to be due to polymer constraint caused by the densely packed fibres, leading to brittle failure characteristics and therefore lower energy absorption.

Analytical models were unable to predict the behaviour of the carbon fibre/polypropylene composites due to the heterogeneous architecture, which highlights that further development of models will be required to characterise these materials. This is pertinent as there is an increasing trend in the use of long fibre reinforced thermoplastics, with many processes now looking to incorporate fibre tows to further improve performance.

6.4   Comparison of Carbon Fibre/Polypropylene to Commercial Automotive Benchmarks

In this section the mechanical properties of CF.mPP have been compared to long discontinuous glass fibre/polypropylene (GF.PP), carbon fibre/epoxy (CF.EP), carbon fibre/PEEK (CF.PEEK), HexMC (commercial CF.EP advanced SMC), Aluminium 7075-T6 (AA7075) and high strength, low alloy steel 420 (HSLA420). AA7075, HSLA420 and HexMC were chosen as they represent typical materials used in the automotive industry, with CF.PEEK chosen to represent the highest thermoplastic composite performance currently available. It was expected that the HexMC material and experimentally tested CF.EP would perform similarly, and would therefore verify

the composite production process due to the similar architectures. The comparison between all the materials is presented in Figure 6-13, with composite properties normalised to $0.45V_f$. CF.EP and CF.PEEK mechanical properties were determined experimentally in this study, further details of the manufacture of these composites was given in Section 3.1. Mechanical properties of GF.PP, HexMC, AA7075 and HSLA420 were taken from manufacturer's data sheets to compare with the experimental findings here.
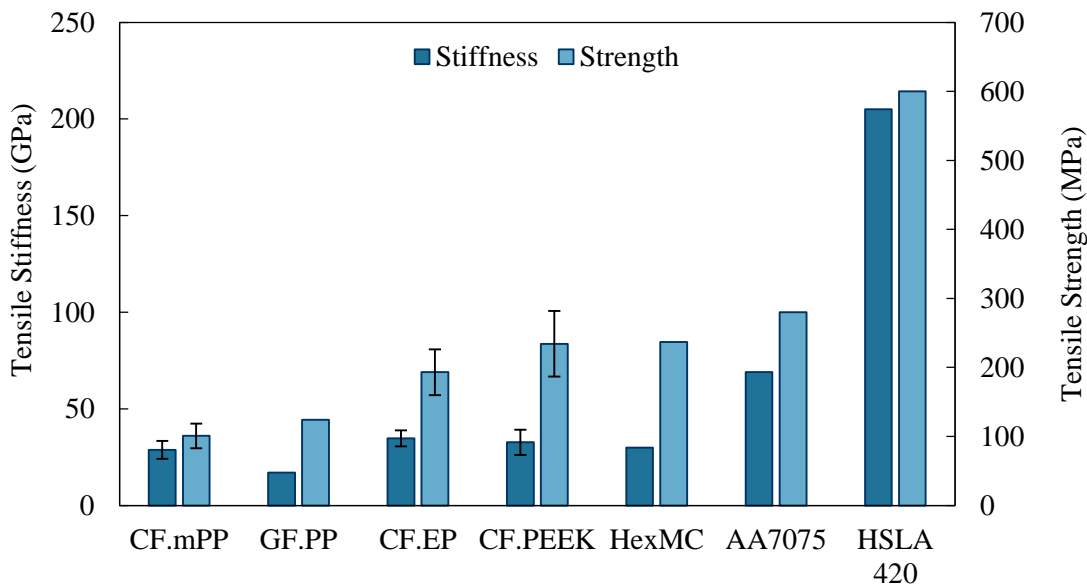
Figure 6-13 - Comparison of tensile properties of CF.mPP and various benchmark materials, composite properties for GF.PP, CF.PEEK and HexMC have been normalised to $0.45V_f$ for comparison purposes

The CF.mPP performed well compared to the other composite materials in terms of stiffness and was only 12% lower than an equivalent CF.EP composite, which had the highest stiffness of the composite benchmark materials. The tensile strength however was much lower than the other composites, 57% lower than HexMC which had the highest value. Even compared to GF.PP, which had the second lowest strength, CF.mPP was 38% lower, indicating that stress transfer between fibre and matrix was not taking place efficiently, despite the high interface strengths recorded from the microscale tests. Specific properties ($\sigma^{(1/2)}/\rho$ and $E^{(1/3)}/\rho$ – optimised indices for bending [308]) are presented in Figure 6-14 to reflect the property-to-weight ratio.

With stiffness and strength values normalised for density, it was clear that the composite materials were able to compete with metals that are currently used in the

automotive industry. Due to the low density of the polypropylene, CF.mPP exceeded the specific stiffness of all the other composite materials. This is pertinent since automotive components are typically stiffness driven, making CF.mPP a suitable candidate material. In terms of strength CF.mPP compared relatively poorly to the other composite benchmark materials, apart from GF.PP, where it was marginally higher (2%). The comparable CF.EP composite had a 23% strength increase over the CF.mPP, however it was unclear whether this was a limitation of the polypropylene matrix, interfacial bonding or inefficient stress transfer arising from the high fibre volume fraction.
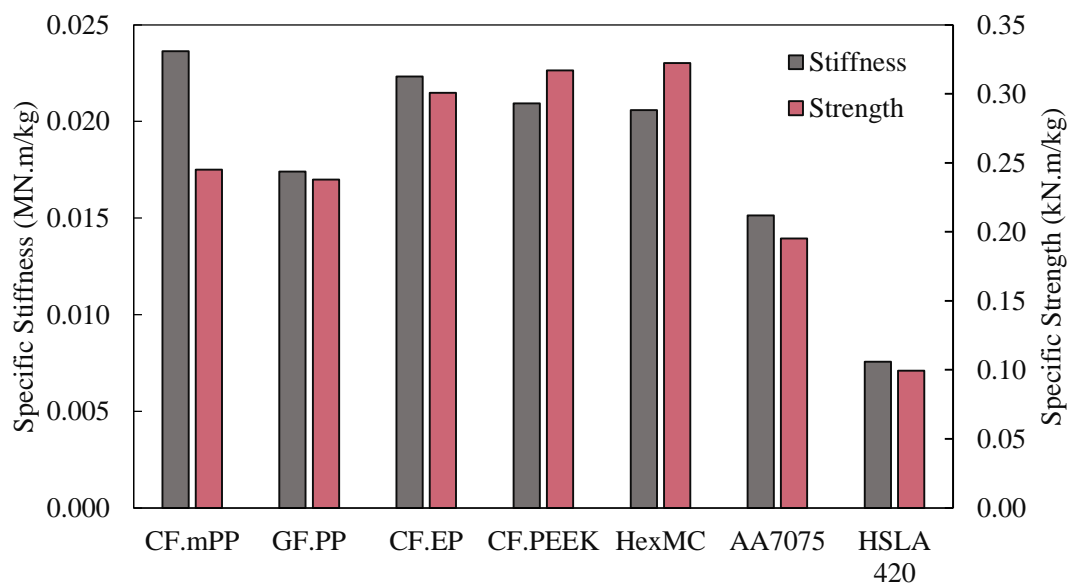
Figure 6-14 - Comparison of specific tensile properties (property/density) of CF.mPP and various benchmark materials, composite properties for GF.PP, CF.PEEK and HexMC have been normalised to $0.45 V_f$ for comparison purposes

To investigate this further, the composite data has been normalised to the base matrix stiffness and strength (Figure 6-15) to show the reinforcing effect of the fibres. The intrinsic mechanical properties of polypropylene were significantly lower than other matrices typically used for composites, with a 56% and 67% lower strength and 37% and 45% lower stiffness than epoxy and PEEK respectively. CF.mPP had the largest improvement in stiffness and similar improvements in strength compared with the other materials. The GF.PP however showed the largest improvement for strength, perhaps indicating that some further improvements could be made with the CF.mPP composite by optimisation of the interface through fibre sizing and matrix modification.

Comparison of Carbon Fibre/Polypropylene
to Commercial Automotive Benchmarks

A number of commercial 'LFT' long glass fibre/polypropylene compounds and one commercial long carbon fibre/polypropylene were compared to the CF.mPP strength and stiffness data and are presented in Figure 6-16 and Figure 6-17 respectively. According to the manufacturer's data, the sizing had been fully optimised for all of the LFT compounds to achieve maximum mechanical performance. Interestingly, even for these optimised materials there appeared to be a plateau and subsequent drop-off in tensile strength above values of approximately $0.15 - 0.25 V_f$ indicating that $0.25 V_f$ was the limit for strength using these microscopic architectures. In terms of stiffness the GF LFT compounds showed linear increases with volume fraction, however the CF LFT compound appear to plateau at around $0.25 V_f$, despite showing increased performance over the CF.mPP.
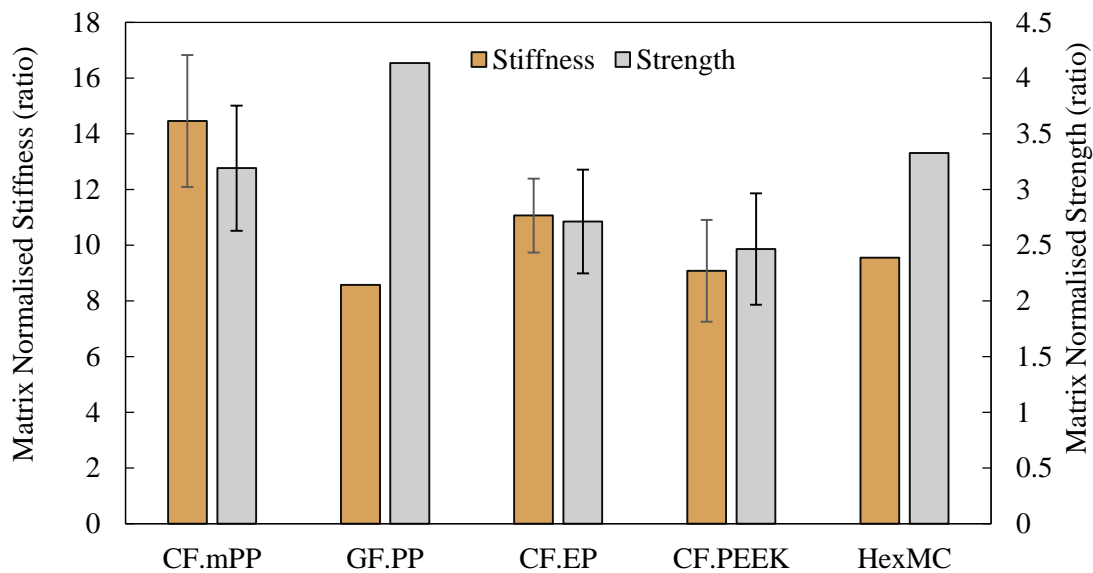
Figure 6-15 - Matrix normalised properties to show improvements made by the addition of fibres

The LFT compounds were however manufactured from long fibre pellets and injection moulded, consisting of single fibre architectures, and therefore in the final moulding would have a much more homogenous distribution of fibre compared to the CF.mPP. Furthermore, it is common for fibres to align along the flow direction for injection moulded samples, so the tensile properties are likely to be higher due to the anisotropy of the material. To demonstrate the effect of fibre architecture, a $0.17 V_f$ sample (sCF.mPP) was manufactured for this study from a carbon fibre veil, consisting of randomly oriented single carbon fibres in a polypropylene matrix with 2wt.% coupling agent, as used previously. Compared to the CF.mPP, the sCF.mPP showed a 72%

increase in tensile strength (105.7MPa) and a 5% increase in tensile modulus at $0.17V_f$, demonstrating the effect of enhanced fibre encapsulation for these composites. Further increases in volume fraction of the sCF.mPP were not possible due to inefficient fibre packing as a result of the single fibre architecture. This was also the case for the LFT materials, although with a higher volume fraction limit of around $0.33V_f$. For thermoplastic DFCs to compete with current semi-structural materials such as SMCs and metals, the fibres must be packed efficiently to allow higher fibre loadings and therefore higher mechanical properties to be realised.
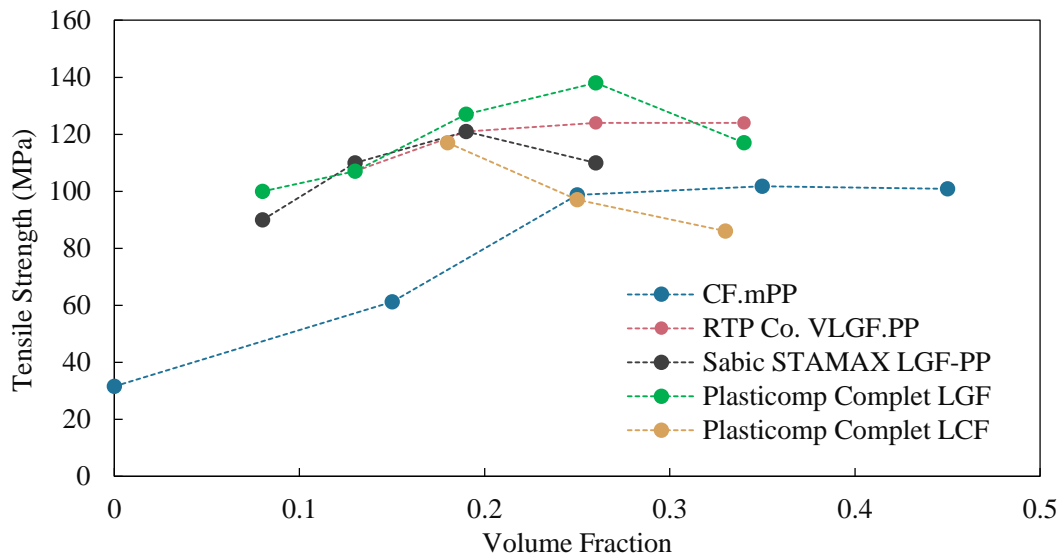
Figure 6-16 - Comparison of commercial GF.PP and CF.PP LFT compounds with CF.mPP tensile strength data
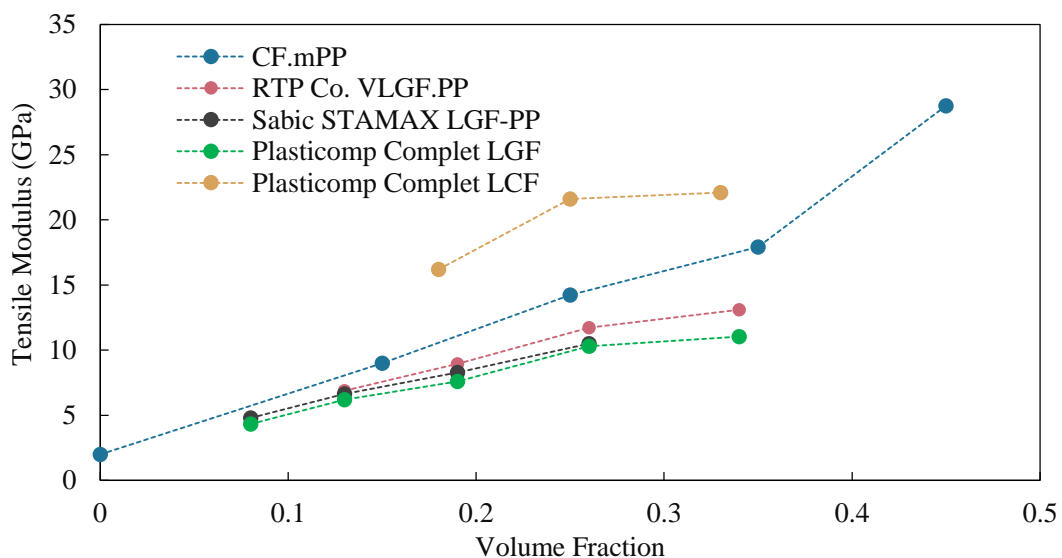
Figure 6-17 - Comparison of commercial GF.PP and CF.PP LFT compounds with CF.mPP tensile stiffness data

Figure 6-18 and Figure 6-19 shows the performance of CF.mPP to other data for carbon and glass DFCs found in the literature, continuous quasi-isotropic fibre composites have also been added for comparison. The majority of data for DFCs lies between 0.05 and $0.3V_f$, which was primarily due to microscopic fibre architectures being most common for DFCs. Above $0.25V_f$, the stiffness of CF.mPP was comparable to a number of systems tested in the literature. It is worth noting that almost all of the literature uses matrices that are both stronger and stiffer, as well as having better interfacial properties than that seen for CF.mPP. This is highlighted in Figure 6-19 for volume fractions above 0.25, where the specific strength of CF.mPP decreases. Deficits in strength may be reduced by further investigation into thermoplastic sizing in addition to optimised processing to reduce defects and improve the interface between carbon fibre and polypropylene. Between 0.35 and $0.5V_f$, there was a lack of data in the literature and therefore a performance gap was seen between DFCs and continuous fibre composites over this range. By utilising fibre tows and therefore producing DFCs with volume fractions between 0.4 – 0.5, which are not attainable for single fibre architectures, properties similar to quasi-isotropic woven composites can be achieved, but with the ability to create much more complex parts due to the enhanced flow of DFCs.
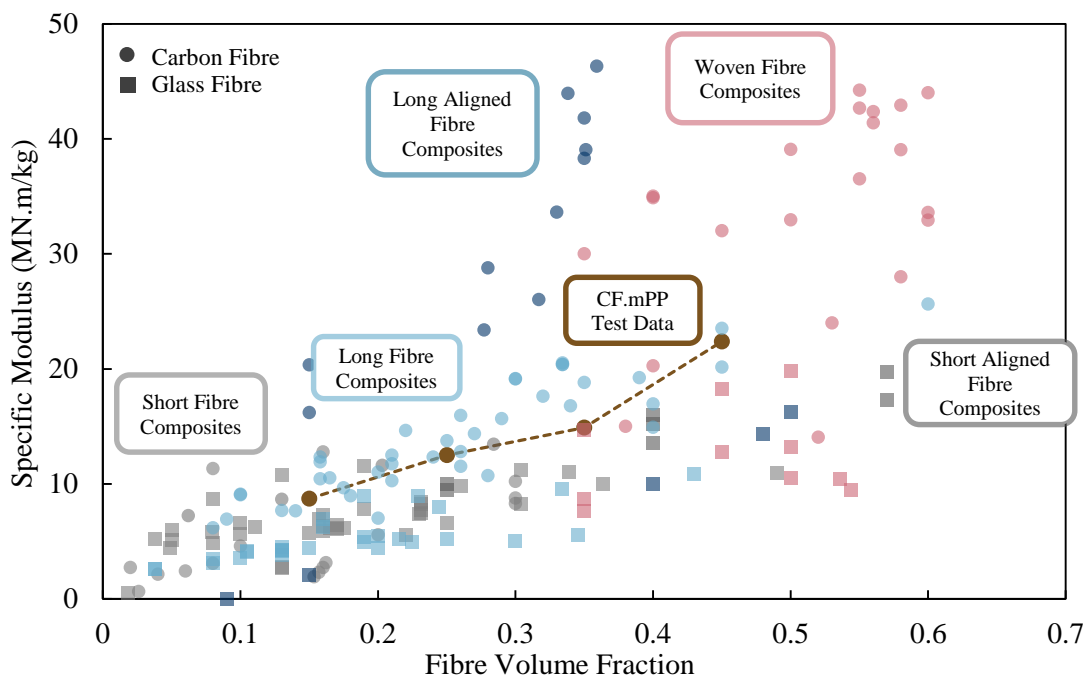
Figure 6-18 - CF.mPP specific stiffness data compared to literature values for carbon and glass DFCs (see Appendix F for table of values and references)
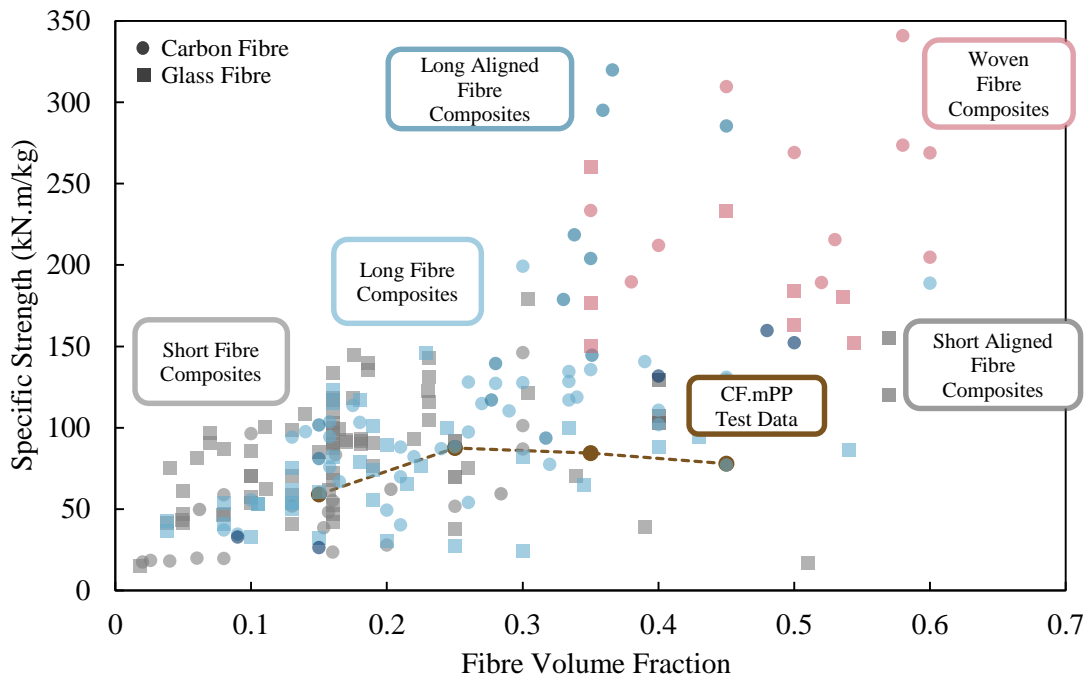
Figure 6-19 - CF.mPP specific strength data compared to literature values for carbon and glass DFCs (see Appendix F for table of values and references)

6.4.1 Conclusions

The $0.45V_f$ volume fraction CF.mPP composite was compared against commercial materials that are currently used in semi-structural and structural automotive applications. Compared to CF.EP, CF.PEEK and HexMC benchmarks the CF.mPP performed well in terms of stiffness, however the strength was lower due to porosity as a result of non-optimised processing, inefficient stress transfer due to small fibre-to-fibre spacing and intrinsically lower base matrix properties. As the density of polypropylene was much lower than the other matrix systems used for the benchmark composites, the specific bending stiffness of CF.mPP outperformed all of the composites benchmarks. The deficit in strength was somewhat reduced, however a similar GF.PP material had an increased strength compared to the CF.mPP. The GF.PP composite was modified by the manufacturer to ensure chemical coupling between the fibre and matrix and therefore it seems reasonable to assume that the reduction in strength of the CF.mPP may be partially due to an interfacial issue.

The high strength achieved by the GF.PP composites highlights that there is room for strength improvements for the CF.mPP composites. Optimisation of pre-heat time, tool temperature and time held at pressure have been shown to reduce void content to less

than 1% for glass fibre/polypropylene systems and can be used in the same way for CF.mPP to minimise the void content observed here. A plateau in strength may still be observed as there will be a saturation limit, where the inter-fibre spacing is reduced to a point where excessive fibre breakage occurs during moulding. This point is still significant however as it will allow optimisation of these composites, and define a range of mechanical properties that can be achieved. To be able to achieve higher strength properties it is likely that another thermoplastic matrix, with higher base mechanical properties, will need to be used.

Carbon fibre reinforced composites are primarily used for stiffness driven, or weight critical applications in the automotive industry, with glass fibre preferred for strength due to comparable properties at reduced cost. Therefore CF.mPP has shown to be competitive with materials that are currently used, despite polypropylene having much lower material properties than other engineering polymers. This was demonstrated by the significant improvements to the base polypropylene properties with the addition of $0.45V_f$ carbon fibre, which showed a 14-fold improvement in stiffness and 3-fold increase in strength. Interestingly, the only material that outperformed CF.mPP in terms of matrix-normalised strength was GF.PP (4-fold increase), indicating that improvements in strength are attainable with this material. This coupled with future reductions in cost of carbon fibre and the low cost of polypropylene, as well as the benefits of thermoplastic composites over thermosetting composites makes this material an interesting alternative to existing materials.

7. Thesis Conclusions

The aim of this study was to investigate whether the performance of long, discontinuous carbon fibre/polypropylene is suitable for semi-structural and structural automotive components. Due to the inherent low affinity of carbon fibre and polypropylene, a detailed understanding of the interface between the two materials was required as adhesion between the fibre and matrix dictate mechanical performance and failure characteristics.

Composite mechanical properties were compared to commercially available materials used for structural automotive applications and carbon fibre/polypropylene was found to perform exceptionally well, where the specific bending stiffness out-performed all of the benchmark materials. The strength of the composites was lower than expected, most likely due to increased void content (up to 3.3% at $0.45V_f$) and issues with fibre packing at higher volume fractions, with similar glass fibre/polypropylene composites exhibiting higher strengths. Comparison of the matrix normalised properties to a similar glass fibre/polypropylene composite indicated that further increases in strength were achievable through further optimisation of the interface and processing methods to produce the composites. Evaluation of the mechanical properties with other composites reported in the literature demonstrated that carbon fibre/polypropylene is able to bridge the performance gap between discontinuous fibre thermoplastic composites and continuous fibre composites, making these materials suitable for stiffness-driven semi-structural automotive applications.

A tow coating rig was developed to produce coated tow for composite processing, where partially consolidated tows coated in either polypropylene or epoxy could be produced between fibre volume fractions of $0.15 – 0.5$, much higher than has previously been reported for carbon fibre/polypropylene. Although the coated tow was relatively well consolidated, the high viscosity of the polypropylene prevented full penetration into the core of the bundles, in contrast to the epoxy which showed excellent wet-out. Commercial grades of polypropylene with different viscosities (melt flow index) are available, and initial trials with higher melt flow index polypropylene showed enhanced wet out during tow coating and would therefore improve consolidation during moulding. The results were not presented here as only small samples of the materials

were available for evaluation on the tow coating rig. This highlights the difficulty in obtaining suitable polymers for use on the coating rig, where the small particle sizes were only achievable through cryogenic milling, due to the high ductility of the polymer. This may negate cost benefits seen from using low cost polymers such as polypropylene and alternate methods may therefore be required to minimise the cost of the intermediate material. For the purposes of this study, the tow coating rig was beneficial as it allowed direct comparison between equivalent carbon fibre/epoxy and carbon fibre/polypropylene composites. Moreover, it allowed a range of volume fractions to be produced as well as the introduction of a maleic anhydride coupling agent, which was not possible with commercially available materials.

Interfacial characterisation was performed using the microbond test, where the effect of fibre sizing and coupling agent addition were the primary focus. The effect of the epoxy-compatible sizing on carbon fibre on the interface strength with polyolefins had not been reported previously, as the fibre sizing is often removed for interfacial testing between carbon fibre and thermoplastics. However, almost all commercially available carbon fibre is coated in epoxy-compatible sizing, so knowledge of the adhesion between the materials was essential for macroscale mechanical performance characterisation. Initial interfacial measurements between carbon fibre and polypropylene showed that the adhesion was low (8MPa), confirming that there was no chemical bonding between the materials. The addition of maleic anhydride to polypropylene significantly improved the interfacial shear strength, where a 295% (31.6MPa) increase was observed. The high IFSS reported was lower than that recorded for carbon fibre/epoxy (45.9MPa), but indicated that chemical bonding was possible between these materials and confirmed that carbon fibre/polypropylene was suitable for use in high performance composites.

Interfacial strength was also characterised between fibres that had the epoxy-compatible sizing removed, where sizing removal processes imitated two recycling methods (pyrolysis and solvolysis) for carbon fibres from EoL parts. The pseudo-recycled fibres showed further improvements in interfacial strength, with increases of 349% and 353% over virgin carbon fibre/polypropylene. The adhesion observed here between carbon fibre and maleic anhydride modified polypropylene was over 4 times higher than other values reported in the literature, and was attributed to preparation of

microdroplets under an inert atmosphere, which has previously only been used for glass fibre/polypropylene. To investigate the large increases in interface strength, functional groups on the surface of the carbon fibre were analysed using x-ray photoelectron spectroscopy (XPS). It has been reported that significant increases in interface strength can only be made through modification of both the fibre and matrix, however excellent adhesion was observed between both sized and desized fibres with the modified polypropylene. Comparison between the functional groups and interfacial strengths indicated that hydroxyl moieties (-OH) in the carbon-hyrdoxyl groups and carboxylic acid groups were responsible for the chemical bonding with anhydride functionalities in the modified polypropylene for virgin fibres and pseudo-recycled fibres respectively. Increases in IFSS observed for the pseudo-recycled fibres over the virgin fibres were due to reactions between nitrogen-containing functionalities and anhydride carbonyl groups on the fibre surface, which indicated that further improvements in interfacial properties can be achieved through the use of sizings with reactive nitrogen functional groups.

Despite the microbond test method being widely used for the measurement of interface strength, no standard method has been developed and large variations in data are often observed. During testing of the high interface strength systems used in this study, it was identified that a significant number of tests were resulting in fibre breakage, as opposed to interfacial failure. Analysis of tensile stresses developed during testing for the high interface strength systems showed that the fibres were subjected to 60 - 80% of their tensile strength, according to the manufacturer's datasheet. Approximately 80% of the tests resulted in fibre failure for these systems, which prompted an investigation into the fibre strength. Single fibre tensile testing was performed at a gauge length of 25mm (similar to the length used for microbond testing) and the characteristic strength value was found to be 3570MPa for the virgin fibres, 27% lower than the manufacturer's data. This meant that for the higher interface strength tests, the tensile strength of the fibre was often exceeded, explaining the significant reduction in yield seen. Analysis of the fibre strength allowed calculation of a theoretical range of embedded lengths and corresponding interface strengths that were appropriate to test for carbon fibre/polypropylene. To ensure reliable data reduction, a range of 150 – 200µm in embedded length should be characterised and therefore the maximum IFSS that could be tested was approximately 20 - 30MPa (for carbon fibre/polypropylene). This

therefore indicated that the results obtained for the higher interface strength systems were lower bound values, as higher interfacial strengths could not be tested due to excessive fibre breakage.

7.1   Recommendations for Further Work

The work of this thesis has demonstrated that carbon fibre/polypropylene composites can achieve equivalent stiffness properties to carbon fibre/epoxy, however strength properties were lower than expected. Optimisation of the non-isothermal compression moulding process was outside of the scope of this project, and as a consequence, increased void levels were observed for higher volume fraction composites. An efficient method for determining the effects of processing parameters on the response of a system can be carried out using Design of Experiments analysis, where preheat temperature, mould temperature, moulding pressure and time at pressure should, at minimum, be investigated as variables. The response should be strength, where flexural strength may provide easier data collection due to more compact specimen size, and void content should be avoided due to difficulties in obtaining an absolute value unless a significant number of samples are examined.

The tow coating rig was able to produce relatively well impregnated coated tows, however the high viscosity of the polypropylene still limited the extent to which the fibre bundle could be penetrated. Increased costs associated with producing the powdered polymer suggested that this coating method was not the most economical processing route, therefore indicating that another process should be developed. From the literature, commingled fibre intermediate products showed promise, however the integrity of the hybrid yarn may be lost when the fibre is chopped, resulting in poor distribution of polymer and high levels of loft. Carbon fibre/PEEK intermediate products are currently manufactured using solvent impregnation and this method may be suitable, providing that an appropriate solvent can be found for polypropylene. Currently polypropylene is only able to be dissolved in a limited number of solvents that require high temperature processing to allow dissolution of the polymer. The main advantage of this process is that dissolution significantly reduces the polymer viscosity, allowing better tow penetration, and mechanical properties are not largely affected when the polymer is precipitated.

Development of analytical models for these heterogeneous mesoscale architectures is critical for commercial use of these products. Despite providing good approximations to microscale architectures, current models are unable to predict failure of high performance DFCs due to complex failure mechanisms and interactions between fibres in the fibre bundles. Additionally, variability is much higher for these architectures, which further compounds the difficulty in predicting the mechanical properties. To be used as a replacement for well-defined materials such as aluminium and steel, the properties must be able to be adequately modelled and failure initiation must be able to be predicted. The continued reduction in cost of carbon fibre will no doubt accelerate analytical property characterisation, where integration of these models into CAD design tools will enable true optimisation of parts using these materials.

Appendices

A. Publications

D.T. Burn, L.T. Harper, M. Johnson, N.A. Warrior, L. Yang, J. Thomason *"The influence of coupling agent, fibre sizing and matrix degradation on the interfacial shear strength between carbon fibre and polypropylene"* 16th European Conference on Composite Materials, ECCM16, 2014, Seville, Spain.

D.T. Burn, L.T. Harper, M. Johnson, N.A. Warrior, L. Yang, J. Thomason *"Characterisation of the interfacial strength between carbon fibre and polypropylene using the microbond test"* Submitted to Composites Science and Technology

D.T. Burn, L.T. Harper, M. Johnson, N.A. Warrior *"The effect of volume fraction on the mechanical performance of long fibre discontinuous carbon fibre/polypropylene composites with heterogeneous architectures"* Journal of Thermoplastic Composite Materials (awaiting submission)

B. Materials

Sabic 576P Polypropylene

Properties	Unit	Datasheet	Experimental	Test Method
Polymer Properties				
Melt Flow Rate (MFR)				ISO 1133
at 230ºC and 2.16kg	g/10min	19		
at 230ºC and 5kg	g/10min	58		
Density	kg/m^3	905		ISO 1183
Mechanical properties				
Tensile test				ISO 527
Tensile Strength	MPa	30	31.6	
Strain-to-Failure	%	700	11[a]	
Flexural test				ASTM D790
Flexural Modulus	GPa	1.9	1.9	
Izod Impact Notched				ISO 180/4A
at 23ºC	kJ/m^2	2.5		
Charpy Impact Notched				ISO 179
at 23ºC	kJ/m^2	2.5	26.64[b]	
Hardness Shore D	-	71		ISO 868
Thermal Properties				
Heat Deflection Temperature				
at 1.80 MPa (HDT/A)	ºC	53		ISO 75/A
at 0.45 MPa (HDT/B)	ºC	98		ISO 75/B

Table B-1 - Properties of Sabic 576P according to manufacturer's datasheet and compared to experimental results where applicable (a - reduction in strain-to-failure due to compression moulding process, b – Un-notched Charpy impact strength)

Eastman G3015 Maleic Anhydride

Property	Unit	Datasheet	Test Method
Polymer Type		MAPP	
Acid Number	mg KOH/g	15	
Ring and Ball Softening Point	°C	156	
Penetration Hardness	dmm	<1	ASTM D 5
Viscosity, Brookfield			
at 125°C		Solid	
at 190°C	cP	18,000	
Molecular Weight		47,000	

Table B-2 - Properties of Eastman G3015 Maleic Anhydride from manufacturer's datasheet

Hexcel DLS 1776 Epoxy (Developmental System)

Properties	Unit	Experimental	Test Method
Tensile Test			BS EN 2747-1
Tensile Modulus	GPa	3.3	
Tensile Strength	MPa	65	
Strain-to-failure	%	2.5	
Poisson's Ratio		0.38	
Compression Test			ISO 604
Compressive Modulus	GPa	7.5	
Compressive Strength	MPa	316	
Strain-to-failure	%	4.2	
In-Plane Shear Test			ASTM D7078
Shear Modulus	GPa	2.1	
Shear Strength	MPa	32.8	
Strain-to-failure	%	1.7	
Density	kg/m^3	1181	

Table B-3- Mechanical properties of the developmental epoxy systems provided by Hexcel. (Mechanical testing performed by M.D. Bond [138])

Toray T700SC Carbon Fibre

Property	Unit	Datasheet	Test Method
Fibre Properties			
Tensile Test			TY-030B-01
Tensile Modulus	GPa	230	
Tensile Strength	MPa	4900	
Strain-to-Failure	%	2.1	
Density	kg/m^3	1800	TY-030B-02
Filament Diameter	µm	7	
Yield	g/km	800	TY-030B-03
Sizing Type & Amount	Type (%)	50C (1.0)	TY-030B-05
		60E (0.3)	
Functional Properties			
CTE	$\alpha.10^{-6}/°C$	0.38	
Specific Heat	Cal/g.°C	0.18	
Thermal Conductivity	Cal/cm.s.°C	0.0224	

Table B-4 - Properties of Toray T700SC carbon fibre for both sizing levels used in this study from the manufacturer's datasheet

Cytec APC-2/AS4 CF.PEEK Tape

Properties	Unit	Datasheet	Experimental	Test Method
Tensile Test				ISO 527
Tensile Modulus (0)	GPa	138	52.5	
Tensile Modulus (90)	GPa	10.3	38	
Tensile Strength (0)	MPa	2070	325	
Tensile Strength (90)	MPa	86	300	
Strain-to-failure	%	1.45	2.3	
Poisson's Ratio		0.3	-	
Flexural Properties				ISO 14125
Flexural Modulus	GPa	124	40.4	
Flexural Strength	MPa	2000	675	

Table B-5 - Mechanical properties of Cytec APC-2/AS4 CF.PEEK tape, datasheet values based on unidrectional composite at $0.6V_f$, experimental data based on discontinuous fibre composite also at $0.6V_f$

Hexcel HexMC C/2000/M77

Properties	Unit	Datasheet	Test Method
Tensile Test			ASTM D3039
Tensile Modulus	GPa	38	
Tensile Strength	MPa	300	
Flexural Test			ASTM D790
Flexural Modulus	GPa	30	
Flexural Strength	MPa	500	
Areal Weight	g/m^2	2000	
Fibre Volume Fraction		0.57	
Fibre Length	mm	50	
Density	kg/m^3	1550	

Table B-6- Properties of HexMC for a 4mm thick moulded plate from manufacturer's datasheet

C. Testing Methodology

All of the specimens produced for the following test methods were according to the moulding procedure given in Section 3.4.1, and were cut to shape using a bandsaw with 18tpi carbon steel Duratec blades. Specimens were cut in both the X and Y directions of the moulded panels to characterise anisotropy effects (Appendix D). The edges of the specimens were subsequently sanded using wet and dry paper, from 400 to 1200 grit.

Tensile Testing

Tensile testing was carried out in accordance with ISO 572-4/2/2. A modified Type 2 specimen was used, where the length and width of the specimen were 150mm and 25mm respectively, with 75mm spacing between the grips. All specimens had a nominal thickness of 3mm. The test speed was 2mm.min^{-1} in accordance with the standard for qualification tests, and were carried out in a temperature controlled environment, maintained at 23°C. A clip on extensometer was used to measure the initial strain of the material for calculation of the modulus, and was removed at 0.5% strain to avoid damage. At least 10 specimens were tested for each sample, where specimens that failed at the grips were discarded from analysis.

Flexural Testing

Flexural testing was carried out in accordance with ISO 14125/I/2. Three-point bending was used to characterise the flexural properties, where support radii, R_1 and R_2, were 5 $\pm$ 0.2mm and 2 $\pm$ 0.2mm respectively. The specimen type was Class I, which is recommended for discontinuous fibre reinforced thermoplastic composites. The nominal sample thickness was 3mm, so the specimen geometry was adjusted in accordance with Annex A.1 and A.2 of the standard. Therefore the specimen dimensions were 60x25x3mm (lxwxh), with a span of 48mm. Testing was carried out under a controlled temperature environment at 23°C and at least 10 specimens were tested for each sample at a test speed of 2mm.min^{-1}.

Charpy Impact Testing

Charpy impact testing was carried out in accordance with 179-1/2/f/U. The samples were unnotched and the blow direction was flatwise. The specimen type was Type 2 in accordance with the standard for long-fibre reinforced materials, with dimensions of 75x15x3mm (lxwxh), where a width of 15mm is recommended for coarse microstructures. A span of 60mm was used. The striking velocity for the equipment was $3.46m.s^{-1}$ and the gravity reading was determined to be 0.05J, which was used to correct the readings as detailed in ISO 13802. At least 10 specimens were tested for each sample, and testing was carried out under a controlled temperature environment at $23^{o}C$.

D. Density and Anisotropy Measurements

Density measurements were performed using a Mettler Toledo XSE Analytical Balance in conjunction with a Mettler Toldeo density measurement kit. Specimen mass was measured in air and distilled water at 23ºC, where adjustments could be made for variations in temperature of either of the fluids. The density was calculated from the analytical balance software. The specimens were cut from the ends of the tensile samples that had been held in the grips, where the extracted specimen dimensions were 10x25x3mm. It was found that the grips had imprinted dimples into the surface of the specimens during testing, so the samples were lightly sanded to remove the features before density measurements were taken. Two samples were tested from every tensile testing specimen, with three repeats taken for each sample.

The data recorded for both ends was averaged to obtain an average density for each specimen, where the coefficient of variance was found to be approximately $0.5 - 2\%$ in most cases. The volume fraction of the specimen was then calculated based on the fact that the composite density is a volume weighted average of the fibre and matrix density, given by Equation D-1:

$$V_f = \frac{\rho_c - \rho_m}{\rho_f - \rho_m}$$

Equation D-1 - calculation of composite volume fraction based on the recorded composite density (ρ_c) and the fibre and matrix densities (ρ_f and ρ_m)

From the calculated density the strength and stiffness values were normalised to the nominal volume fraction, which assumed that there was a linear relationship between the properties. Table D-1 shows the average values recorded for each of the CF.mPP samples.

Sample	Volume Fraction		Strength		Modulus	
	$\overline{X}$	CoV (%)	$\overline{X}$	CoV (%)	$\overline{X}$	CoV (%)
CF15.mPP	0.14	5.2	55.43	20.2	8.03	25.5
CF25.mPP	0.25	4.4	98.08	10.1	14.2	17.6
CF35.mPP	0.34	2.8	96.64	10.6	17.6	11.8
CF45.mPP	0.43	0.9	96.17	18.2	27.4	18.9

Table D-1 - Global fibre volume fraction data obtained from density measurements of tensile test specimens

Interestingly, the coefficient of variance decreased with increasing volume fraction, which was due to more homogeneous fibre distribution in the higher volume fraction samples. All of the volume fractions recorded were within 0.02 of the nominal volume fraction, which allowed reliable normalisation of the data to the nominal values. Figure D-1 shows the strength and stiffness data respectively plotted against the volume fractions determined from the density measurements. These figures also highlight the variability of the recorded data, and despite having the lowest CoV for volume fraction, the CF45.mPP showed high levels of variability compared to CF25.mPP and CF35.mPP.
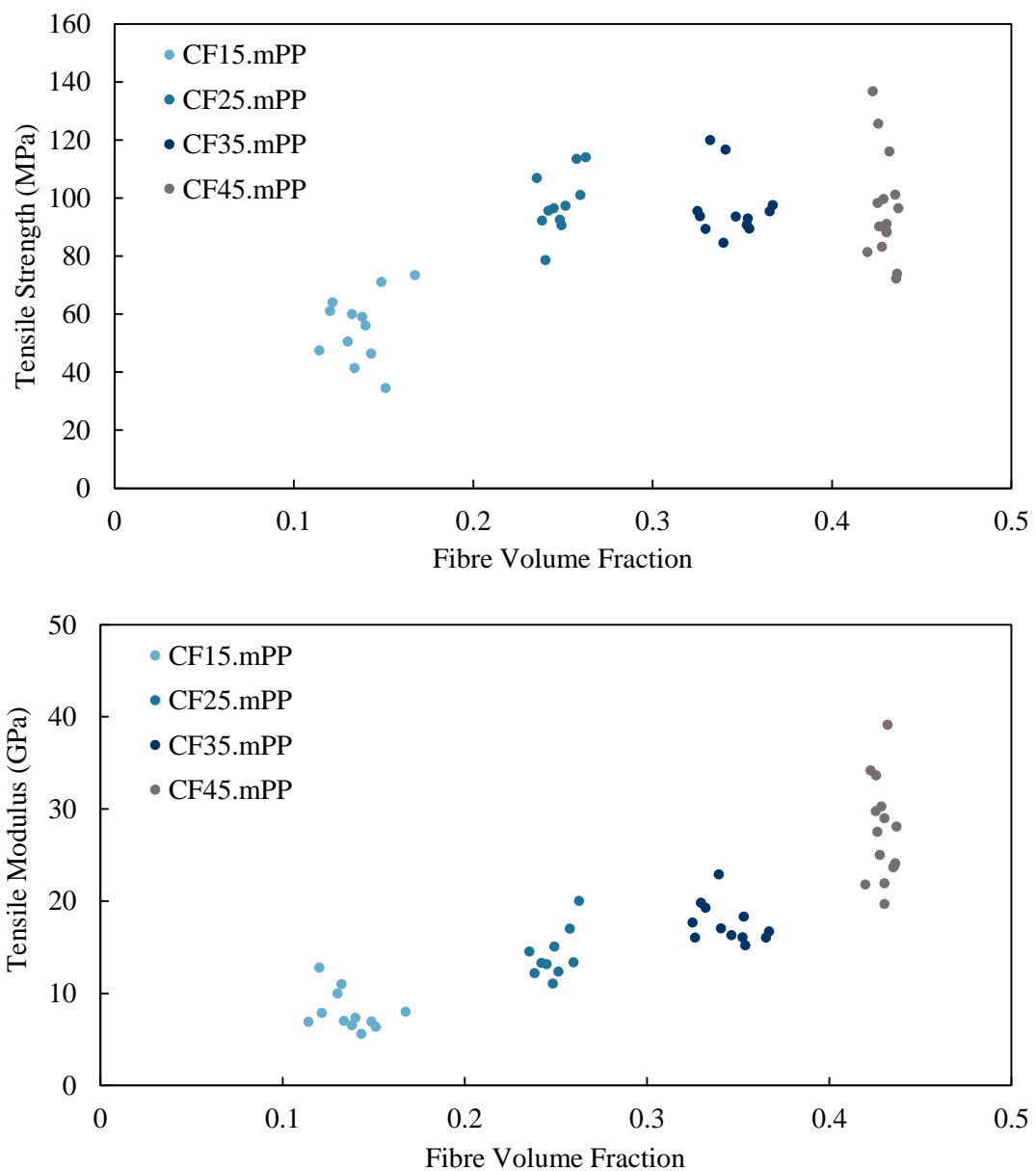
Figure D-1 – Tensile strength data (top) and tensile modulus data (bottom) plotted against calculated volume fraction from density measurements

Appendix D – Density and Anisotropy Measurements

The level of anisotropy was also investigated for the tensile test data by extracting specimens from both the X and Y directions of the moulded panels and the data is given in Table D-2.

Sample	Stiffness (GPa)			Strength (MPa)		
	X	Y	X/Y	X	Y	X/Y
CF15.mPP	9.5	8.5	1.1	69.2	53.3	1.3
CF25.mPP	14.3	14.2	1.0	99.7	98.2	1.0
CF35.mPP	18.4	17.2	1.1	108.4	93.5	1.2
CF45.mPP	33.0	25.9	1.3	117.2	89.8	1.3
CF45.PP	24.5	19.8	1.2	63.1	55.4	1.1
CF45.EP	38.1	32.8	1.2	256.8	220.6	1.2

Table D-2 - Anisotropy data recorded from tensile testing

The X/Y values show the degree of anisotropy for the samples, with a value of 1 corresponding to an isotropic laminate. The highest levels of anisotropy were found for the CF45.mPP data, which agrees with high levels of variability also reported for these specimens. The CF15.mPP also showed high levels of anisotropy, which was due to poor distribution of fibres in the composite at low volume fractions. This was largely unavoidable due to the mesoscale architectures used, although an increase of volume fraction to 0.25 resulted in an almost perfectly isotropic panel. As the fibres were distributed by hand orientation bias could not be completely removed, despite using a number of methods to minimise it. By averaging the values recorded from each plane, the pseudo-isotropic mechanical properties were obtained and this data was reported in Chapter 6.

E. Microbond Analysis

One of the methods for analysing the quality of droplet formation for the microbond test, was to plot the embedded length against the droplet diameter, where linear regression should accurately model the data and pass through the origin. The degraded CF.PP sample, not shown here, appeared to have reasonable agreement between the droplet diameter and embedded length, however when it was plotted, the R^2 value was 0.75, much lower than seen for the non-degraded systems. This implies that this quick screening method is useful for detecting degradation in microbond samples.
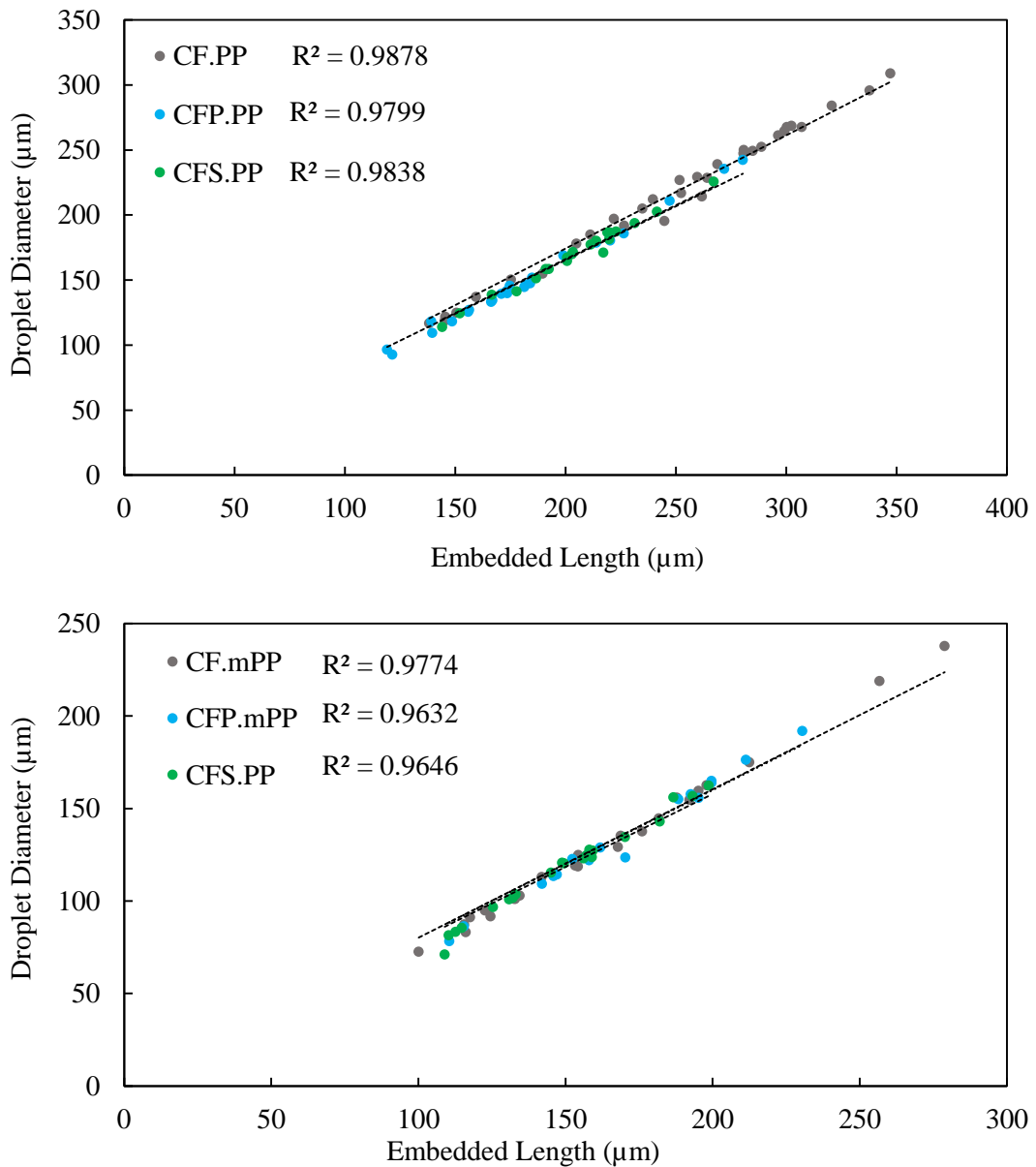
Figure E-1 – Droplet diameter vs. embedded length plots for samples without maleic anhydride (top) and samples with maleic anhydride (bottom)

F. Material Properties of Discontinuous Fibre Composites

Class	Fibre	Matrix	Vf	Modulus GPa	Strength MPa	Density g/cm3	Ref
Short Fibre	Glass	PA6	0.05	6.2	50	1.21	[40]
			0.10	7.2	90	1.28	
			0.15	7.8	115	1.35	
			0.22	8.1	135	1.45	
		PA6	0.07	-	112	1.24	[309]
			0.16	-	137	1.37	
		PP	0.05	-	60	0.98	
			0.13	-	79	1.12	
		PP	0.08	5.0	49	1.03	[38]
			0.16	6.9	49	1.17	
			0.25	8.7	50	1.32	
		PA6,6	0.16	8.7	123	1.37	[310]
			0.17	8.9	126	1.38	
			0.18	8.5	164	1.39	
		PBT	0.05	6.0	59	1.36	[311]
			0.11	9.0	90	1.44	
			0.19	12.0	118	1.54	
			0.34	19.0	122	1.73	
			0.49	21.0	-	1.92	
		PP	0.08	6.0	48	1.03	
			0.16	8.0	72	1.16	
			0.36	15.0	-	1.50	
		PA6	0.18	-	201	1.39	[312]
			0.19	-	190	1.40	
		PP	0.10	-	61	1.07	
			0.10	-	57	1.07	
		PBT	0.18	-	142	1.53	
			0.18	-	137	1.53	
		PA6,6	0.16	-	183	1.37	[24]
		PA6	0.16	-	162	1.37	
		ABS	0.16	-	134	1.30	
		PET	0.16	-	152	1.57	
		PC	0.16	-	130	1.43	
		PVC	0.16	-	113	1.56	
		PSU	0.16	-	127	1.45	
		PS	0.16	-	88	1.29	
		PE	0.16	-	63	1.20	
		PP	0.16	-	55	1.17	
		PA6	0.30	13.0	191	1.57	[24]
			0.23	12.1	193	1.47	
			0.23	11.0	154	1.47	
			0.30	17.6	282	1.57	
			0.23	12.3	210	1.47	
			0.23	11.3	170	1.47	

		PP	0.04	5.0	40	0.96	[35],
			0.08	9.0	90	1.03	[49]
			0.13	12.0	110	1.12	
			0.19	14.0	110	1.22	
			0.26	13.0	100	1.33	
			0.39	-	60	1.55	
			0.51	-	30	1.75	
		PP	0.13	3.1	66	1.12	[286]
			0.13	3.0	45	1.12	
		PA6	0.04	-	90	1.20	[304]
			0.06	-	100	1.23	
			0.07	-	120	1.24	
			0.11	-	130	1.30	
			0.14	-	145	1.34	
			0.16	-	160	1.37	
		PP	0.02	0.5	14	0.93	[313]
	Carbon	PP	0.08	11.0	57	0.97	[38]
			0.16	13.3	58	1.04	
			0.25	14.5	58	1.12	
		PEEK	0.10	6.2	130	1.35	[314]
			0.30	12.0	211	1.44	
		PP	0.15	2.0	40	1.04	[315]
		PPMA	0.16	2.4	50	1.04	
		PP/EP	0.16	3.4	90	1.08	
		PPMA/EP	0.16	2.9	25	1.06	
		PP	0.03	0.6	17	0.92	[313]
		PP	0.02	2.5	16	0.92	[316]
			0.04	2.0	17	0.94	
			0.06	2.3	19	0.95	
			0.08	3.0	19	0.97	
			0.20	6.0	30	1.08	
		PC	0.30	12.1	120	1.38	[72]
			0.30	14.1	140	1.38	
Short Aligned Fibre	Glass	Epoxy	0.25	-	110	1.58	[24]
			0.40	-	183	1.77	
			0.25	-	145	1.58	
			0.40	26.9	190	1.77	
			0.40	24.1	230	1.77	
			0.57	34.5	240	2.00	
			0.57	39.3	310	2.00	
	Carbon	ABS	0.06	8.0	55	1.10	[57]
			0.13	10.0	60	1.15	
			0.20	14.0	75	1.21	
			0.28	17.0	75	1.26	
Long Fibre	Glass	PP	0.18		140	1.20	[317]
		PA6	0.16	8.5	168	1.37	[318]
		PA6,6	0.16	9.5	158	1.37	
		PP	0.30		115	1.40	[319]
			0.40		138	1.56	
			0.54		155	1.80	
		PP	0.13		60	1.12	[320]

Appendix F – Material Properties of Discontinuous Fibre Composites

Fibre	Matrix					Ref
	ABS	0.15		78	1.29	
	PA6	0.16		112	1.37	
	PET	0.18		126	1.59	
	PP	0.10	3.8	35	1.07	[36]
		0.15	5.1	37	1.15	
		0.20	5.5	38	1.23	
		0.25	6.8	36	1.32	
		0.30	7.0	34	1.40	
	PP	0.04	2.5	41	0.96	[49]
		0.11	4.5	57	1.07	
		0.13	4.7	69	1.12	
		0.04	2.5	35	0.96	
		0.08	3.2	42	1.03	
	PP	0.11	4.4	57	1.07	
		0.13	5.0	60	1.12	
		0.19	6.5	68	1.22	
		0.35	8.2	95	1.47	
	PP	0.19	6.0	90	1.22	[197]
		0.13	4.7	85	1.13	
		0.08	3.5	55	1.02	
	PBT	0.22	8.3	104	1.59	
	PET	0.23	7.8	120	1.57	
	PC	0.20	7.6	124	1.39	
	PP	0.19	10.9	123	1.22	
	PA6	0.23	13.1	214	1.47	
	PP	0.13	4.2	55	1.10	
Carbon	Epoxy	0.21	14.0	55	1.36	[51]
		0.24	17.0	120	1.38	
		0.25	19.0	122	1.38	
		0.27	20.0	160	1.39	
		0.29	22.0	155	1.40	
		0.30	27.0	180	1.41	
	Epoxy	0.08	8.0	48	1.29	[321]
		0.21	16.0	120	1.36	
		0.34	24.0	170	1.43	
		0.39	28.0	205	1.46	
	Epoxy	0.09	9.0	45	1.30	[62]
		0.21	17.0	95	1.36	
		0.32	25.0	110	1.42	
		0.45	30.0	195	1.49	
	Epoxy	0.26	16.0	75	1.39	[322]
		0.35	27.0	195	1.44	
	PET	0.13	11.0	135	1.43	[323]
		0.18	14.0	165	1.45	
		0.26	19.0	190	1.48	
		0.14	11.0	140	1.44	
		0.18	13.0	150	1.45	
		0.28	16.0	190	1.49	
	PP	0.10	9.0	55	0.99	
		0.17	11.0	70	1.05	

			0.22	16.0	90	1.09	
			0.26	18.0	110	1.13	
		PA12	0.10	10.0	155	1.11	[34]
			0.20	13.0	200	1.18	
			0.30	24.0	250	1.26	
		Epoxy	0.20	9.5	67	1.36	[303]
			0.40	24.8	149	1.46	
			0.40	21.8	162	1.46	
		PPS	0.16	14.7	107	1.41	[324]
			0.16	16.8	133	1.41	
			0.16	17.4	146	1.41	
			0.33	30.5	174	1.49	
			0.33	30.3	200	1.49	
			0.33	30.3	191	1.49	
Long Aligned Fibre	Glass	Epoxy	0.50	31.0	290	1.91	[325]
			0.48	27.0	300	1.88	
			0.65	28.0	110	2.10	
		PA12	0.40	17.0	225	1.71	
		PE	0.15	3.0	38	1.45	
		BMI/EP	0.09	-	45	1.37	
	Carbon	Epoxy	0.32	36.9	133	1.42	[322]
			0.35	56.1	208	1.44	
			0.34	62.8	312	1.43	
			0.33	47.9	255	1.42	
			0.36	66.7	425	1.44	
			0.37	74.5	462	1.44	
		Epoxy	0.45	80.0	425	1.49	[26]
		PC	0.15	21.0	105	1.30	[28]
			0.28	32.0	160	1.37	
		Epoxy	0.42	80.0	800	1.47	[26]
			0.56	116.0	1500	1.55	
		Epoxy	0.55	119.0	1211	1.54	[326]
		Epoxy	0.35	60.0	650	1.44	[327]
		PA	0.55	130.0	1696	1.49	[325]
		Epoxy	0.60	161.0	2625	1.57	
			0.20	63.0	535	1.25	
			0.55	119.0	1211	1.54	
		PPS	0.57	136.0	1500	1.59	
		PEI	0.50	100.0	1100	1.53	
		Epoxy	0.55	115.0	1509	1.54	
		PES	0.49	99.0	1000	1.57	
		Epoxy	0.55	110.0	710	1.54	
			0.35	55.0	293	1.44	
		PP	0.15	21.0	105	1.03	[28]
			0.28	33.0	160	1.15	
Continuous Fibre	Glass (QI)	PBT	0.54	18.8	302	1.99	[328]
			0.54	20.6	356	1.98	
	Glass (0/90)	PP	0.35	13.0	256	1.70	[185]
	Glass (bal. twill)		0.35	13.0	265	1.50	
	Glass (4/1)		0.35	22.0	390	1.50	
	Glass (UD)		0.45	31.0	790	1.70	

	PET	0.50	37.6	870	1.90	
Glass (0/90)		0.50	25.0	310	1.90	
Glass (6HS)	PA6,6	0.45	23.0	420	1.80	
Glass (8H)	PEI	0.50	20.0	350	1.90	
Carbon (5HS)	PA12	0.56	60.0	620	1.45	[163]
Carbon (0/90)	PA6	0.40	28.3	296	1.40	[90]
		0.50	48.1	393	1.46	
		0.60	50.2	410	1.52	
	PA6,6	0.60	51.2	312	1.52	
Carbon (0/90)	PP	0.38	-	234	1.23	[329]
		0.35	-	282	1.21	
	HDPE	0.53	-	330	1.53	
	PET	0.58	-	441	1.61	
	Epoxy	0.45	-	461	1.49	
Carbon (5HS)	PA12	0.58	62.9	788	1.47	[162]
	Epoxy	0.60	69.0	625	1.57	
	PEI	0.58	62.3	544	1.60	
Carbon (plain)	Epoxy	0.55	56.3	659	1.54	
	PA66	0.55	66.0	880	1.49	
Carbon (NCF)	Epoxy	0.40	51.0	597	1.46	[303]
		0.40	51.2	656	1.46	

References

[1] Frost & Sullivan Report, "Supply Chain Analysis of the Automotive Carbon Fiber Composites Market," 2011.

[2] Frost & Sullivan Report, "Global Analysis of Weight Reduction Strategies of Major OEMS," 2009.

[3] UK Parliament, "Climate Change Act 2008," pp. 1–103, 2008.

[4] The Society of Motor Manufacturers and Traders, "New Car CO2 Report 2015," 2015.

[5] "Regulation (EC) No 443/2009 of the European Parliament and of the Council," *Official Journal of the European Union*, no. L140, 2009.

[6] Department for Transport, "Vehicle Licensing Statistics: Quarter 1 (Jan - Mar) 2015," 2015.

[7] G. Belingardi, "Lightweight Design of Vehicle Body a Contribution Toward Greener Environment," *Acta Technica Corviniensis*, vol. 7, pp. 49–54, 2014.

[8] U. K. Vaidya, *Composites for Automotive, Truck and Mass Transit: Materials, Design, Manufacturing*, 1st ed. DEStech Publications Inc., 2011.

[9] D. Hull and T. W. Clyne, *An Introduction to Composite Materials*, 2nd ed. Cambridge University Press, 1996.

[10] J. L. Thomason and L. J. Adzima, "Sizing up the interphase : an insider's guide to the science of sizing," *Composites Part A: Applied Science and Manufacturing*, vol. 32, pp. 313–321, 2001.

[11] D. Brosius, "Carbon Fiber: The Automotive Material of the Twenty-First Century Starts Fulfilling the Promise," *3rd Annual Society of Plastic Engineers Automotive Composites Conference and Exposition*, pp. 1–7, 2003.

[12] J. Sloan, "BMW Leipzig: The Epicenter of i3 Production," *Composites Technology*, pp. 15–21, Jun-2014.

[13] P. Das, J. Ravine, C. Pung, and U. Vaidya, "Enhancing the Surface Finish of LFT Compression Molded Parts via Application of Surface Film," in *Composites and Polycon 2007*, 2007, pp. 1–8.

[14] A. Burkhart and D. Cramer, "Continuous-fibre reinforced thermoplastic tailored blanks," *JEC Composites Magazine*, vol. 43, no. 22, pp. 41–43, 2006.

[15] P. Malnati, "Sub-8-Minute Cycle Times on Carbon/Epoxy Prepreg," *Composites World*, pp. 28–30, Jan-2015.

[16] J. Rowe, *Advanced Materials in Automotive Engineering*, 1st ed. Elsevier, 2012.

References

[17]   V. P. McConnell, "Not Just Another Road Trip," *Reinforced Plastics*, vol. 55, no. 5, pp. 18–23, Sep. 2011.

[18]   P. Feraboli, F. Gasco, B. Wade, S. Maier, R. Kwan, W. Salmon, A. Masini, L. Deoto, and M. Reggiani, "Lamborghini 'Forged Composite®' Technology for the Suspension Arms of the Sesto Elemento," 2010.

[19]   F. Henning, H. Ernst, R. Brüssel, G. Co, O. Geiger, W. Krause, and F. Institut, "LFTs for automotive applications," *Reinforced Plastics*, no. February, pp. 24–33, 2005.

[20]   K. Rohan, T. J. Mcdonough, V. Ugresic, E. Potyra, and F. Henning, "Mechanical Study of Direct Long Fiber Thermoplastic Carbon/Polyamide 6 and its Relations to Processing Parameters," *Zoltek Report*, pp. 1–24, 2015.

[21]   M. Biron, *Thermoplastics and Thermoplastic Composites*, 2nd ed. Oxford: William Andrew, 2012.

[22]   K. H. Wong, D. Syed Mohammed, S. J. Pickering, and R. Brooks, "Effect of coupling agents on reinforcing potential of recycled carbon fibre for polypropylene composite," *Composites Science and Technology*, vol. 72, no. 7, pp. 835–844, Apr. 2012.

[23]   D. U. Shah, P. J. Schubel, P. Licence, and M. J. Clifford, "Determining the Minimum, Critical and Maximum Fibre Content for Twisted Yarn Reinforced Plant Fibre Composites," *Composites Science and Technology*, vol. 72, no. 15, pp. 1909–1917, 2012.

[24]   L. A. Goettler, "Mechanical Property Enhancement in Short-Fiber Composites Through the Control of Fiber Orientation During Fabrication," *Polymer Composites*, vol. 5, no. 1, pp. 60–71, 1984.

[25]   L. T. Harper, T. A. Turner, J. R. B. Martin, and N. A. Warrior, "Fiber Alignment in Directed Carbon Fiber Preforms - Mechanical Property Prediction," *Journal of Composite Materials*, vol. 44, no. 8, pp. 931–951, Sep. 2009.

[26]   H. Yu, K. D. Potter, and M. R. Wisnom, "A novel manufacturing method for aligned discontinuous fibre composites (High Performance-Discontinuous Fibre method)," *Composites Part A: Applied Science and Manufacturing*, vol. 65, pp. 175–185, Oct. 2014.

[27]   S. Pimenta, S. T. Pinho, and P. Robinson, "Micromechanics of Recycled Composites for Material Optimisation and Eco-Design," in *ICCM18*, 2011, pp. 1–6.

[28]   M. H. Akonda, C. A. Lawrence, and B. M. Weager, "Recycled carbon fibre-reinforced polypropylene thermoplastic composites," *Composites Part A: Applied Science and Manufacturing*, vol. 43, no. 1, pp. 79–86, Jan. 2012.

[29]   F. Henning, H. Ernst, R. Brüssel, O. Geiger, and W. Krause, "LFTs for automotive applications," *Reinforced Plastics*, no. February, pp. 24–33, 2005.

[30]   K. K. Chawla, *Composite Materials: Science and Engineering*, 2nd ed. Springer Science & Business Media, 2013.

[31]   R. Rondeau, S. Reeve, and G. Bond, "The Effect of Tows and Filament Groups on the Properties of Discontinuous Fiber Composites," in *44th International SAMPE Symposium and Exhibition*, 1999, pp. 1449–1460.

[32]   J. L. Thomason, "The influence of fibre length, diameter and concentration on the modulus of glass fibre reinforced polyamide 6,6," *Composites Part A: Applied Science and Manufacturing*, vol. 39, no. 11, pp. 1732–1738, Nov. 2008.

[33]   B. F. Blumentritt, B. T. Vu, and S. L. Cooper, "Mechanical properties of discontinuous fiber reinforced thermoplastics. II. Random-in-plane fiber orientation," *Polymer Engineering & Science*, vol. 15, no. 6, pp. 428–436, 1975.

[34]   F. Van Hattum and S. Van Breugel, "LFT: the future of reinforced thermoplastics?," *Reinforced Plastics*, vol. 45, no. 6, pp. 42–44, Jun. 2001.

[35]   J. L. Thomason, M. A. Vlug, G. Schipper, and H. G. L. T. Krikort, "Influence of fibre length and concentration on the properties of glass fibre-reinforced polypropylene : Part 3 . Strength and strain at failure," *Composites Part A*, vol. 27, pp. 1075–1084, 1996.

[36]   N.-J. Lee and J. Jang, "The effect of fibre content on the mechanical properties of glass fibre mat/polypropylene composites," *Composites Part A: Applied Science and Manufacturing*, vol. 30, no. 6, pp. 815–822, Jun. 1999.

[37]   R.E. Lavengood, "Strength of Short-fibre reinforced composites," *Polymer Engineering and Science*, vol. 12, no. 1, pp. 48–52, 1972.

[38]   S.-Y. Fu, B. Lauke, E. Mäder, C.-Y. Yue, and X. Hu, "Tensile properties of short-glass-fiber- and short-carbon-fiber-reinforced polypropylene composites," *Composites Part A: Applied Science and Manufacturing*, vol. 31, no. 10, pp. 1117–1125, Oct. 2000.

[39]   N. G. Karsli and A. Aytac, "Effects of maleated polypropylene on the morphology, thermal and mechanical properties of short carbon fiber reinforced polypropylene composites," *Materials & Design*, vol. 32, no. 7, pp. 4069–4073, 2011.

[40]   A. Hassan, R. Yahya, A. H. Yahaya, A. R. M. Tahir, and P. R. Hornsby, "Tensile, Impact and Fiber Length Properties of Injection-Molded Short and Long Glass Fiber-Reinforced Polyamide 6,6 Composites," *Journal of Reinforced Plastics and Composites*, vol. 23, pp. 969–986, 2004.

[41]   J. L. Thomason and M. A. Vlug, "Influence of fibre length and concentration on the properties of glass fibre-reinforced polypropylene: 4. Impact properties," *Composites Part A: Applied Science and Manufacturing*, vol. 28, no. 3, pp. 277–288, Jan. 1997.

[42]   B. Harris, *Engineering Composite Materials*, 2nd ed. IOM, 1999.

[43]   R. C. Novak and M. A. DeCrescente, "Impact Behaviour of Unidirectional Resin Matrix Composites Tested in the Fiber Direction," in *Proceedings of Composite Materials: Testing and Design (Second Conference)*, 1972, pp. 311–323.

[44]   A. A. Watts, *Commercial Opportunities for Advanced Composites*, 1st ed. ASTM International, 1980.

References

[45]   L. T. Harper, T. A. Turner, N. A. Warrior, and C. D. Rudd, "Characterisation of Random Carbon Fibre Composites from a Directed Fibre Preforming Process: The Effect of Fibre Length," *Composites Part A: Applied Science and Manufacturing*, vol. 37, no. 11, pp. 1863–1878, Nov. 2006.

[46]   H. L. Cox, "The elasticity and strength of paper and other fibrous materials," *British Journal of Applied Physics*, vol. 72, pp. 72–79, 1952.

[47]   A. Kelly and W. R. Tyson, "Tensile Properties of Fibre-Reinforced Metals: Copper/Tungsten and Copper/Molybdenum," *Journal of the Mechanics and Physics of Solids*, vol. 13, pp. 329–350, 1965.

[48]   A. H. Cottrell, "Strong Solids," in *Proceedings of the Royal Society of London. Series A, Mathematical and Physical Sciences*, 1964, vol. 282, no. 1388, pp. 2–9.

[49]   J. L. Thomason and M. A. Vlug, "Influence of fibre length and concentration on the properties of glass fibre-reinforced polypropylene: 1. Tensile and flexural modulus," *Composites Part A: Applied Science and Manufacturing*, vol. 27, no. 6, pp. 477–484, Jan. 1996.

[50]   S.-J. Park and M.-K. Seo, *Interface Science and Composites*, 1st ed. Academic Press, 2011.

[51]   G. Kirupanantham, "Characterisation of discontinuous carbon fibre preforms for automotive applications," University of Nottingham, 2013.

[52]   W. Weibull, "A Statistical Theory of Strength of Materials," *Ingeniorsvetenscapskademien Handlingar*, vol. 151, pp. 1–29, 1939.

[53]   J. A. Holmberg, "Application of Weibull Theory To Random-Fibre Composites," *Composites Science and Technology*, vol. 54, pp. 75–85, 1995.

[54]   S. D. Bartus and U. K. Vaidya, "Performance of long fiber reinforced thermoplastics subjected to transverse intermediate velocity blunt object impact," *Composite Structures*, vol. 67, no. 3, pp. 263–277, Mar. 2005.

[55]   F. Rezaei, R. Yunus, and N. A. Ibrahim, "Effect of fiber length on thermomechanical properties of short carbon fiber reinforced polypropylene composites," *Materials & Design*, vol. 30, no. 2, pp. 260–263, Feb. 2009.

[56]   K. S. S. Kumar, C. P. R. Nair, and K. N. Ninan, "Effect of Fiber Length and Composition on Mechanical Properties of Carbon Fiber-Reinforced Polybenzoxazine," *Polymers for Advanced Technologies*, vol. 19, no. April, pp. 895–904, 2008.

[57]   G. C. Jacob, J. M. Starbuck, J. F. Fellers, and S. Simunovic, "Effect of fiber volume fraction, fiber length and fiber tow size on the energy absorption of chopped carbon fiber-polymer composites," *Polymer Composites*, vol. 26, pp. 293–305, 2005.

[58]   M. Schwartz, *New Materials, Processes, and Methods Technology*, 1st ed. CRC Press, 2005.

[59]   J. Sloan, "Market Outlook: Surplus in carbon fiber's future," *High Performance Composites*, Mar-2013.

[60] D. Houston and D. Wagner, "Advanced Materials and Processing of Composites for High Volume Applications," in *Automotive Composites Consortium (ACC)*, 2012, pp. 1–21.

[61] K. Johanson, L. T. Harper, M. S. Johnson, and N. A. Warrior, "Heterogeneity of discontinuous carbon fibre composites: Damage initiation captured by Digital Image Correlation," *COMPOSITES PART A*, 2014.

[62] L. T. Harper, T. A. Turner, N. A. Warrior, J. S. Dahl, and C. D. Rudd, "Characterisation of Random Carbon Fibre Composites from a Directed Fibre Preforming Process: Analysis of Microstructural Parameters," *Composites Part A: Applied Science and Manufacturing*, vol. 37, no. 11, pp. 2136–2147, Nov. 2006.

[63] L. T. Harper, T. A. Turner, and N. A. Warrior, "Fiber Alignment in Directed Carbon Fiber Preforms − A Feasibility Study," *Journal of Composite Materials*, vol. 43, no. 1, pp. 57–74, 2009.

[64] A. Endruweit, L. T. Harper, T. A. Turner, N. A. Warrior, and A. C. Long, "Random discontinuous carbon fibre preforms: Permeability modelling and resin injection simulation," *Composites Part A: Applied Science and Manufacturing*, vol. 39, pp. 1660–1669, 2008.

[65] K. K. C. Ho, H. Quan, and A. Bismarck, "Carbon Fiber: Surface Properties," in *Wiley Encyclopedia of Composites*, 2012, pp. 182–193.

[66] D. Chung, *Carbon Fibre Composites*, 1st ed. Butterworth-Heinemann, 2012.

[67] L.-G. Tang and J. L. Kardos, "A Review of Methods for Improving the Interfacial Adhesion Between Carbon Fiber and Polymer Matrix," *Polymer Composites*, vol. 18, no. 1, pp. 100–113, 1997.

[68] P. Mitschang, M. Blinzler, and A. Wöginger, "Processing technologies for continuous fibre reinforced thermoplastics with novel polymer blends," *Reinforced Plastics*, vol. 63, no. 14, pp. 2099–2110, Nov. 2003.

[69] Y. Luo, Y. Zhao, Y. Duan, and S. Du, "Surface and wettability property analysis of CCF300 carbon fibers with different sizing or without sizing," *Materials & Design*, vol. 32, no. 2, pp. 941–946, Feb. 2011.

[70] I. Giraud, S. Franceschi-Messant, E. Perez, C. Lacabanne, and E. Dantras, "Preparation of aqueous dispersion of thermoplastic sizing agent for carbon fiber by emulsion/solvent evaporation," *Applied Surface Science*, vol. 266, pp. 94–99, 2013.

[71] H. Yuan, S. Zhang, and C. Lu, "Surface Modification of Carbon Fibers by a Polyether Sulfone Emulsion Sizing for Increased Interfacial Adhesion with Polyether Sulfone," *Applied Surface Science*, vol. 317, pp. 737–744, 2014.

[72] C. Ozkan, N. Gamze Karsli, A. Aytac, and V. Deniz, "Short carbon fiber reinforced polycarbonate composites: Effects of different sizing materials," *Composites Part B: Engineering*, vol. 62, pp. 230–235, 2014.

References

[73]   G. Oliveux, L. O. Dandy, and G. A. Leeke, "Current Status of Recycling of Fibre Reinforced Polymers: review of technologies, reuse and resulting properties," *Progress in Materials Science*, vol. 72, pp. 61–99, 2015.

[74]   A. Bismarck, M. E. Kumru, B. Song, J. Springer, E. Moos, and J. Karger-Kocsis, "Study on surface and mechanical fiber characteristics and their effect on the adhesion properties to a polycarbonate matrix tuned by anodic carbon fiber oxidation," *Composites Part A: Applied Science and Manufacturing*, vol. 30, no. 12, pp. 1351–1366, Dec. 1999.

[75]   S. Wang, Z.-H. Chen, W.-J. Ma, and Q.-S. Ma, "Influence of heat treatment on physical–chemical properties of PAN-based carbon fiber," *Ceramics International*, vol. 32, no. 3, pp. 291–295, 2006.

[76]   M. A. Montes-Morán, F. W. J. van Hattum, J. P. Nunes, A. Martínez-Alonso, J. M. D. Tascón, and C. A. Bernardo, "A study of the effect of plasma treatment on the interfacial properties of carbon fibre–thermoplastic composites," *Carbon*, vol. 43, no. 8, pp. 1795–1799, Jul. 2005.

[77]   M. Sharma, S. Gao, E. Mäder, H. Sharma, L. Y. Wei, and J. Bijwe, "Carbon fiber surfaces and composite interphases," *Composites Science and Technology*, vol. 102, pp. 35–50, 2014.

[78]   E. Pisanova and S. Zhandarov, "Adhesive Interactions in Interphases: Competition Between Acid-Base and Diffusion Mechanisms," in *Proceedings of 12th International Conference on Composite Materials*, 1999, pp. 5–9.

[79]   C. Unterweger, J. Duchoslav, D. Stifter, and C. Fürst, "Characterization of carbon fiber surfaces and their impact on the mechanical properties of short carbon fiber reinforced polypropylene composites," *Composites Science and Technology*, vol. 108, pp. 41–47, 2015.

[80]   J. Karger-Kocsis and T. Bárány, "Single-polymer composites (SPCs): Status and future trends," *Composites Science and Technology*, vol. 92, pp. 77–94, Feb. 2014.

[81]   S. Mukhopadhyay, B. L. Deopura, and R. Alagiruswamy, "Interface Behavior in Polypropylene Composites," *Journal of Thermoplastic Composite Materials*, vol. 16, no. 6, pp. 479–495, Nov. 2003.

[82]   H. S. Lee, S. Kim, Y. J. Noh, and S. Y. Kim, "Design of microwave plasma and enhanced mechanical properties of thermoplastic composites reinforced with microwave plasma-treated carbon fiber fabric," *Composites Part B: Engineering*, vol. 60, pp. 621–626, Apr. 2014.

[83]   S. H. Han, H. J. Oh, and S. S. Kim, "Evaluation of fiber surface treatment on the interfacial behavior of carbon fiber-reinforced polypropylene composites," *Composites Part B: Engineering*, vol. 60, pp. 98–105, Apr. 2014.

[84]   J. Xie, D. Xin, H. Cao, C. Wang, Y. Zhao, L. Yao, F. Ji, and Y. Qiu, "Improving carbon fiber adhesion to polyimide with atmospheric pressure plasma treatment," *Surface and Coatings Technology*, vol. 206, no. 2–3, pp. 191–201, Oct. 2011.

[85]   S. Y. Kim, S. J. Baek, and J. R. Youn, "New hybrid method for simultaneous improvement of tensile and impact properties of carbon fiber reinforced composites," *Carbon*, vol. 49, no. 15, pp. 5329–5338, Dec. 2011.

[86]   U. Zielke, K. J. Huttinger, and W. P. Hoffman, "Surface-Oxidized Carbon Fibers: IV. Interaction With High-Temperature Thermoplastics," *Carbon*, vol. 34, no. 8, pp. 1015–1026, 1996.

[87]   H. Yuan, S. Zhang, C. Lu, S. He, and F. An, "Improved interfacial adhesion in carbon fiber/polyether sulfone composites through an organic solvent-free polyamic acid sizing," *Applied Surface Science*, pp. 4–9, Apr. 2013.

[88]   S. Chand, "Carbon fibers for composites," *Journal of Materials Science*, vol. 35, no. 6, pp. 1303–1313, 2000.

[89]   F. Rosselli and M. H. Santare, "Comparison of the Short Beam Shear (SBS) and Interlaminar Shear Device (ISD) tests," *Composites Part A*, vol. 28A, pp. 587–594, 1997.

[90]   E. Botelho, "Mechanical behavior of carbon fiber reinforced polyamide composites," *Composites Science and Technology*, vol. 63, no. 13, pp. 1843–1855, Oct. 2003.

[91]   L. Yang and J. L. Thomason, "Interface strength in glass fibre–polypropylene measured using the fibre pull-out and microbond methods," *Composites Part A: Applied Science and Manufacturing*, vol. 41, no. 9, pp. 1077–1083, Sep. 2010.

[92]   L. Teuber, H. Fischer, and N. Graupner, "Single fibre pull-out test versus short beam shear test: comparing different methods to assess the interfacial shear strength," *Journal of Materials Science*, vol. 48, no. 8, pp. 3248–3253, Jan. 2013.

[93]   J. A. Nairn, "On the use of shear-lag methods for analysis of stress transfer in unidirectional composites," *Mechanics of Materials*, vol. 26, pp. 63–80, 1997.

[94]   W. Beckert and B. Lauke, "Critical discussion of the single-fibre pull-out test: does it measure adhesion?," *Composites Science and Technology*, vol. 57, no. 97, pp. 1689–1706, 1998.

[95]   D. Francis and C. Ward, "The Single-Fibre 1 : Review and Interpretation," *Composites Part A: Applied Science and Manufacturing*, vol. 27A, pp. 597–612, 1996.

[96]   L. Yang and J. L. Thomason, "Development and application of micromechanical techniques for characterising interfacial shear strength in fibre-thermoplastic composites," *Polymer Testing*, vol. 31, no. 7, pp. 895–903, Oct. 2012.

[97]   B. Miller, U. Gaur, and D. E. Hirt, "Measurement and Mechanical Aspects of the Microbond Pull-Out Technique for Obtaining Fiber/Resin Interfacial Shear Strength," *Composites Science and Technology*, vol. 42, no. 1, pp. 207–219, 1991.

[98]   Y. D. Huang, L. Liu, J. H. Qiu, and L. Shao, "Influence of ultrasonic treatment on the characteristics of epoxy resin and the interfacial property of its carbon fiber composites," *Composites Science and Technology*, vol. 62, pp. 2153–2159, 2002.

References

[99] B. Liu, Z. Liu, X. Wang, G. Zhang, S. Long, and J. Yang, "Interfacial shear strength of carbon fiber reinforced polyphenylene sulfide measured by the microbond test," *Polymer Testing*, vol. 32, no. 4, pp. 724–730, Jun. 2013.

[100] G. Pandey, C. H. Kareliya, and R. P. Singh, "A study of the effect of experimental test parameters on data scatter in microbond testing," *Journal of Composite Materials*, vol. 46, no. 3, pp. 275–284, Oct. 2011.

[101] A. Hodzic, S. Kalyanasundaram, A. E. Lowe, and Z. H. Stachurski, "Geometric Considerations in the Experimental and Finite Element Analyses of the Microdroplet Test," in *12th International Conference on Composite Materials*, 1999.

[102] J. T. Ash, W. M. Cross, D. Svalstad, J. J. Kellar, and L. Kjerengtroen, "Finite element evaluation of the microbond test: meniscus effect, interphase region, and vise angle," *Composites Science and Technology*, vol. 63, no. 5, pp. 641–651, Apr. 2003.

[103] H. Heilhecker, W. Cross, R. Pentland, C. Griswold., J. J. Kellar, and L. Kj, "The Vice Angle in the Microbond Test," *Journal of Materials Science Letters*, vol. 19, pp. 2145–2147, 2000.

[104] B. Morlin, L. M. Vas, and T. Czigany, "Investigation of fiber/matrix adhesion: test speed and specimen shape effects in the cylinder test," *Journal of Materials Science*, vol. 48, no. 8, pp. 3185–3191, Jan. 2013.

[105] A. Straub, M. Slivka, and P. Schwartz, "A study of the effects of time and temperature on the fiber/matrix interface strength using the microbond test," *Composites Science and Technology*, vol. 57, no. 8, pp. 991–994, Jan. 1997.

[106] Z. Liu, X. Yuan, A. J. Beck, and F. R. Jones, "Analysis of a modified microbond test for the measurement of interfacial shear strength of an aqueous-based adhesive and a polyamide fibre," *Composites Science and Technology*, vol. 71, no. 13, pp. 1529–1534, Sep. 2011.

[107] L. Gonon, A. Momtaz, and D. Van Hoyweghen, "Physico-Chemical and Micromechanical Analysis of the Interface in a Poly(Phenylene Sulfide)/Glass Fiber Composite - A Microbond Study," *Polymer Composites*, vol. 17, no. 2, pp. 265–274, 1996.

[108] C.-H. Liu and J. A. Nairn, "Analytical and experimental methods for a fracture mechanics interpretation of the microbond test including the effects of friction and thermal stresses," *International Journal of Adhesion and Adhesives*, vol. 19, no. 1, pp. 59–70, Feb. 1999.

[109] S. Zhandarov, E. Pisanova, E. Mader, and J. A. Nairn, "Investigation of Load Transfer Between the Fiber and the Matrix in Pull-out Tests with Fibers Having Different Diameters," *Journal of Adhesion Science and Technology*, vol. 15, no. 2, pp. 205–222, 2001.

[110] S. Zhandarov, "Characterization of fiber/matrix interface strength: applicability of different tests, approaches and parameters," *Composites Science and Technology*, vol. 65, no. 1, pp. 149–160, Jan. 2005.

[111] P. Zinck, H. D. Wagner, L. Salmon, and J. F. Gerard, "Are Microcomposites Realistic Models of the Fibre/Matrix Interface? II . Physico-chemical Approach," *Polymer*, vol. 42, pp. 6641–6650, 2001.

[112] J. T. Ash, L. Kjerengtroen, W. M. Cross, and J. J. Kellar, "Estimation of the True Interfacial Shear Strength for Composite Materials with the Microbond Test," in *Proceedings of the ASME 2013 International Mechanical Engineering Congress and Exposition*, 2013.

[113] D. Tripathi and F. R. Jones, "Single fibre fragmentation test for assessing adhesion in fibre reinforced composites," *Journal of Materials Science*, vol. 3, pp. 1–16, 1998.

[114] L. T. Drzal and M. Madhukar, "Fiber-matrix adhseion and its relationship to composite mechanical properties," *Journal of Materials Science*, vol. 28, pp. 569–610, 1993.

[115] P. J. Herrera-Franco and L.T. Drzal, "Comparison of Methods for the Measurement of Fibre/Matrix Adhesion in Composites," *Composites*, vol. 23, no. 1, pp. 2–27, 1992.

[116] J. Andersons, R. Joffe, M. Hojo, and S. Ochiai, "Fibre fragment distribution in a single-fibre composite tension test," *Composites Part B:Engineering*, vol. 32, pp. 323–332, 2001.

[117] T. Ohsawa, A. Nakayama, M. Miwa, and A. Hasegawa, "Temperature Dependence of Critical Fiber Length for Glass Fiber-Reinforced Thermosetting Resins," *Journal of Applied Polymer Science*, vol. 22, no. 11, pp. 3203–3212, 1978.

[118] P. Feillard, G. Desarmot, and J. P. Favre, "A Critical Assessment of the Fragmentation Test for Glass/Epoxy Systems," *Composites Science and Technology*, vol. 49, no. 2, pp. 109–119, 1993.

[119] A. C. Johnson, S. A. Hayes, and F. R. Jones, "The role of matrix cracks and fibre/matrix debonding on the stress transfer between fibre and matrix in a single fibre fragmentation test," *Composites Part A: Applied Science and Manufacturing*, vol. 43, no. 1, pp. 65–72, 2012.

[120] A. C. Johnson, S. A. Hayes, and F. R. Jones, "Data reduction methodologies for single fibre fragmentation test: Role of the interface and interphase," *Composites Part A: Applied Science and Manufacturing*, vol. 40, no. 4, pp. 449–454, 2009.

[121] T. Lacroix, R. Keunings, M. Desaeger, and I. Verpoest, "A new data reduction scheme for the fragmentation testing of polymer composites," *Journal of Materials Science*, vol. 30, pp. 683–692, 1995.

[122] D. Tripathi, C. Fangping, and F. R. Jones, "A Comprehensive Model to Predict the Stress Fields in a Single Fibre Composite," *Journal of Composite Materials*, vol. 30, no. 14, pp. 1514–1538, 1996.

[123] L. Zhou, J. K. Kim, C. Baillie, and Y. W. Mai, "Fracture Mechanics Analysis of the Fibre Fragmentation Test," *Journal of Composite Materials*, vol. 29, no. 7, pp. 881–902, 1995.

References

[124] E. Graciani, V. Mantič, F. París, and J. Varna, "Numerical analysis of debond propagation in the single fibre fragmentation test," *Composites Science and Technology*, vol. 69, pp. 2514–2520, 2009.

[125] P. W. . van den Heuvel, B. Hogeweg, and T. Peijs, "An Experimental and Numerical Investigation into the Single-Fibre Fragmentation Test: Stress Transfer by a Locally Yielding Matrix," *Composites Part A*, vol. 28A, pp. 237–249, 1997.

[126] S. Deng, L. Ye, Y.-W. Mai, and H.-Y. Liu, "Evaluation of fibre tensile strength and fibre/matrix adhesion using single fibre fragmentation tests," *Composites Part A: Applied Science and Manufacturing*, vol. 29, no. 97, pp. 423–434, 1998.

[127] R. B. Henstenburg and S. L. Phoenix, "Interfacial shear strength studies using the single-filament-composite test. Part II: A probability model and Monte Carlo simulation," *Polymer Composites*, vol. 10, no. 5, pp. 389–408, 1989.

[128] J. F. Mandell, J. H. Chen, and F. J. McGarry, "A Microdebonding Test for In Situ Assessment of Fibre/Matrix Bond Strength in Composite Materials," *International Journal of Adhesion and Adhesives*, vol. 1, no. 1, pp. 40–44, 1980.

[129] T. Ramanathan, A. Bismarck, E. Schulz, and K. Subramanian, "Investigation of the influence of surface-activated carbon fibres on debonding energy and frictional stress in polymer-matrix composites by the micro-indentation technique," *Composites Science and Technology*, vol. 61, pp. 2511–2518, 2001.

[130] S. Park and M.-K. Seo, "Composite Characterization," in *Interface Science and Composites*, 2011, pp. 667–669.

[131] J. M. Molina-Aldareguía, M. Rodríguez, C. González, and J. LLorca, "An experimental and numerical study of the influence of local effects on the application of the fibre push-in test," *Philosophical Magazine*, vol. 91, no. February 2015, pp. 1293–1307, 2011.

[132] G. Kalinka, A. Leistner, and A. Hampe, "Characterisation of the fibre/matrix interface in reinforced polymers by the push-in technique," *Composites Science and Technology*, vol. 57, no. 96, pp. 845–851, 1997.

[133] M. R. Piggott, "Why interface testing by single-fibre methods can be misleading," *Composites Science and Technology*, vol. 51, pp. 965–974, 1997.

[134] M. Kharrat, a. Chateauminois, L. Carpentier, and P. Kapsa, "On the interfacial behaviour of a glass/epoxy composite during a micro-indentation test: assessment of interfacial shear strength using reduced indentation curves," *Composites Part A: Applied Science and Manufacturing*, vol. 28, no. I 997, pp. 39–46, 1997.

[135] M. Zidi, L. Carpentier, and A. Chateauminois, "Development of a micro-indentation model simulating different mechanical responses of the fibre/matrix interface," *Composites Science and Technology*, vol. 61, pp. 369–375, 2001.

[136] J. F. Mandell, D. H. Grande, T. . Tsiang, and F. J. McGarry, "Modified Microdebonding Test for Direct In Situ Fiber/Matrix Bond Strength Determination in Fiber Composites," in *Composite Materials: Testing and Design (Seventh Conference)*, ASTM (1986), 1986, pp. 87–108.

[137] M. R. Piggott, "The single-fibre pull out method: its advantages, interpretation and experimental realization," *Composite Interfaces*, vol. 1, no. February 2015, pp. 211–223, 1993.

[138] M. D. Bond, "Multi-Scale Modelling of Discontinuous Carbon Fibre Reinforced Composites," University of Nottingham, 2013.

[139] M. A. Minnicino and M. H. Santare, "Modeling the progressive damage of the microdroplet test using contact surfaces with cohesive behavior," *Composites Science and Technology*, vol. 72, no. 16, pp. 2024–2031, Nov. 2012.

[140] A. Hodzic, S. Kalyanasundaram, A. Lowe, and Z. H. Stachurski, "The microdroplet test: experimental and finite element analysis of the dependace of failure mode on droplet shape," *Composite Interfaces*, vol. 6, no. 4, pp. 375–389, 1999.

[141] J. Novak, C. J. Pearce, Grassl P., L. Yang, and J. L. Thomason, "Analysis of the microbond test using nonlinear fracture mechanics," in *17th Unternational Conference on Composite Materials*, 2009, pp. 1–13.

[142] M. Nishikawa, T. Okabe, K. Hemmi, and N. Takeda, "Micromechanical modeling of the microbond test to quantify the interfacial properties of fiber-reinforced composites," *International Journal of Solids and Structures*, vol. 45, no. 14–15, pp. 4098–4113, Jul. 2008.

[143] P. J. Herrera-Franco, V. Rao, L. T. Drzal, and M. Y. M. Chiang, "Bond strength measurement in composites—Analysis of experimental techniques," *Composites Engineering*, vol. 2, no. 1, pp. 31–45, 1992.

[144] R. Day and J. V. C. Rodrigez, "Investigation of the Micromechanics of the Microbond Test Investigation of the Micromechanics of the Microbond Test," *Composites Science and Technology*, vol. 58, no. 6, pp. 907–914, 1998.

[145] X. Gao, R. E. Jensen, S. H. McKnight, and J. W. Gillespie, "Effect of colloidal silica on the strength and energy absorption of glass fiber/epoxy interphases," *Composites Part A: Applied Science and Manufacturing*, vol. 42, no. 11, pp. 1738–1747, 2011.

[146] B. Miller, P. Muri, and L. Rebenfeld, "A Microbond Method for Determination of the Shear Strength of a Fibre/Resin Interface," *Composites Science and Technology*, vol. 28, no. 1, pp. 17–32, 1987.

[147] R. L. Zhang, Y. D. Huang, L. Liu, Y. R. Tang, D. Su, and L. W. Xu, "Effect of emulsifier content of sizing agent on the surface of carbon fibres and interface of its composites," *Applied Surface Science*, vol. 257, no. 8, pp. 3519–3523, Feb. 2011.

[148] S. Kang, D. Lee, and N. Choi, "Fiber/epoxy interfacial shear strength measured by the microdroplet test," *Composites Science and Technology*, vol. 69, no. 2, pp. 245–251, Feb. 2009.

[149] L. Wenbo, Z. Shu, H. Lifeng, J. Weicheng, Y. Fan, L. Xiaofei, and W. Rongguo, "Interfacial Shear Strength in Carbon Fiber-Reinforced Poly (phthalazinone ether ketone) Composites," *Polymer Composites*, no. 1, pp. 1921–1926, 2013.

References

[150] D. Xu, B. Liu, G. Zhang, S. Long, X. Wang, and J. Yang, "Effect of air plasma treatment on interfacial shear strength of carbon fiber-reinforced polyphenylene sulfide," *High Performance Polymers*, 2015.

[151] S. Joseph, M. S. Sreekala, Z. Oommen, P. Koshy, and S. Thomas, "A comparison of the mechanical properties of phenol formaldehyde composites reinforced with banana fibres and glass fibres," *Composites Science and Technology*, vol. 62, pp. 1857–1868, 2002.

[152] M. Q. Tran, K. K. C. Ho, G. Kalinka, M. S. P. Shaffer, and A. Bismarck, "Carbon fibre reinforced poly(vinylidene fluoride): Impact of matrix modification on fibre/polymer adhesion," *Composites Science and Technology*, vol. 68, no. 7–8, pp. 1766–1776, Jun. 2008.

[153] a. Bismarck, D. Richter, C. Wuertz, and J. Springer, "Basic and acidic surface oxides on carbon fiber and their influence on the expected adhesion to polyamide," *Colloids and Surfaces A: Physicochemical and Engineering Aspects*, vol. 159, no. 2–3, pp. 341–350, Dec. 1999.

[154] K. Friedrich and H. Blumbergh, "Effects of Fiber/Matrix Adhesion on Off-Axis Mechanical Response in Carbon Fiber/Epoxy Resin Composites," *Composites Science and Technology*, vol. 3538, no. 95, pp. 317–327, 1995.

[155] J. L. Thomason and L. Yang, "Temperature dependence of the interfacial shear strength in glass-fibre polypropylene composites," *Composites Science and Technology*, vol. 71, no. 13, pp. 1600–1605, 2011.

[156] A. G. Gibson and J.-A. E. Månson, "Impregnation Technology for Thermoplastic Matrix Composites," *Composites Manufacturing*, vol. 3, no. 4, pp. 223–233, 1992.

[157] N. Svensson and R. Shishoo, "Manufacturing of Thermoplastic Composites from Commingled Yarns - A Review," *Journal of Thermoplastic Composite Materials*, vol. 11, pp. 22–56, 1998.

[158] N. Bernet, V. Michaud, P.-E. Bourban, and J.-A. E. Manson, "An Impregnation Model for the Consolidation of Thermoplastic Composites Made from Commingled Yarns," *Journal of Composite Materials*, vol. 33, no. 8, pp. 751–772, Apr. 1999.

[159] N. Svensson, R. Shishoo, and M. D. Gilchrist, "The Tensile and Flexural Properties of Textile Composites," *The Journal of The Textile Institute*, vol. 1, no. 4, pp. 635–646, 1998.

[160] R. Alagirusamy, "Development and Characterization of GF/PET, GF/Nylon, and GF/PP Commingled Yarns for Thermoplastic Composites," *Journal of Thermoplastic Composite Materials*, vol. 18, no. 3, pp. 269–285, May 2005.

[161] B. Choi, O. Diestel, and P. Offermann, "Commingled CF/PEEK Hybrid Yarns for Use in Textile Reinforced High Performance Rotors," in *ICCM12*, 1999.

[162] P. Mcdonnell, K. P. Mcgarvey, L. Rochford, and C. M. O Bradaigh, "Processing and Mechanical Properties Evaluation of a Commingled Carbon-Fibre/PA12 Composite," *Composites Part A: Applied Science and Manufacturing*, vol. 32, pp. 925–932, 2001.

[163] M. D. Wakeman, L. Zingraff, P.-E. Bourban, J.-A. E. Månson, and P. Blanchard, "Stamp forming of carbon fibre/PA12 composites – A comparison of a reactive impregnation process and a commingled yarn system," *Composites Science and Technology*, vol. 66, no. 1, pp. 19–35, Jan. 2006.

[164] K. Balaji Thattaiparthasarathy, S. Pillay, H. Ning, and U. K. Vaidya, "Process Simulation, Design and Manufacturing of a Long Fiber Thermoplastic Composite for Mass Transit Application," *Composites Part A: Applied Science and Manufacturing*, vol. 39, no. 9, pp. 1512–1521, Sep. 2008.

[165] D. D. L. Chung, *Composite Materials: Science and Applications*, 2nd ed. Springer Science & Business Media, 2010.

[166] P. K. Mallick, *Composites Engineering Handbook*, 1st ed. CRC Press, 1997.

[167] T. Hartness, G. Husman, J. Koenig, and J. Dyksterhouse, "The Characterization of Low Cost Fiber Reinforced Thermoplastic Composites Produced by the DRIFT Process," *Composites Part A: Applied Science and Manufacturing*, vol. 32, pp. 1155–1160, 2001.

[168] P. Nygard and C.-G. Gustafson, "Continuous Glass Fiber–Polypropylene Composites Made by Melt Impregnation: Influence of Processing Method," *Journal of Thermoplastic Composite Materials*, vol. 17, no. 2, pp. 167–184, Mar. 2004.

[169] R. Marissen, L. T. van der Drift, and J. Sterk, "Technology for Rapid Impregnation of Fibre Bundles with a Molten Thermoplastic Polymer," *Composites Science and Technology*, vol. 60, pp. 2029–2034, 2000.

[170] J. P. Nunes, F. W. J. van Hattum, C. A. Bernardo, J. F. Silva, and A. T. Marques, "Advances in Thermoplastic Matrix Towpregs Processing," *Journal of Thermoplastic Composite Materials*, vol. 17, no. 6, pp. 523–544, Nov. 2004.

[171] M. Rath, S. Kreuzberger, and G. Hinrichsen, "Manufacture of Aramid Fibre Reinforced Nylon-12 by Dry Powder Impregnation Process," *Composites Part A: Applied Science and Manufacturing*, vol. 29, no. 8, pp. 933–938, Aug. 1998.

[172] K. K. C. Ho, S.-R. Shamsuddin, S. Riaz, S. Lamorinere, M. Q. Tran, A. Javaid, and A. Bismarck, "Wet impregnation as route to unidirectional carbon fibre reinforced thermoplastic composites manufacturing," *Plastics, Rubber and Composites*, vol. 40, no. 2, pp. 100–107, Mar. 2011.

[173] M. Duvall and K. Ramani, "In-Situ Composite Manufacture using an Electrostatic Spray Process and Filament Winding," in *International Conference on Composite Materials 10*, 1995, pp. 469–492.

[174] A. C. Long, *Composites Forming Technologies*, 2nd ed. Elsevier, 2014.

[175] F. M. Schmidt, Y. Le Maoult, and S. Monteix, "Modelling of infrared heating of thermoplastic sheet used in thermoforming process," *Journal of Materials Processing Technology*, vol. 143–144, no. 1, pp. 225–231, 2003.

[176] G. Wypych, *Weathering of Plastics: Testing to Mirror Real Life Performance*, 1st ed. William Andrew, 1999.

References

[177] A. H. Miller, N. Dodds, J. M. Hale, and A. G. Gibson, "High speed pultrusion of thermoplastic matrix composites," *Composites Part A: Applied Science and Manufacturing*, vol. 29, no. 7, pp. 773–782, Jul. 1998.

[178] A. Abe, H. Kausch, M. M, and H. Pasch, *Polymer Composites - Polyolefin Fractionation - Polymeric Petidomimetic - Collagens*, 1st ed. Springer, 2012.

[179] T. A. Bullions, A. C. Loos, and J. E. Mcgrath, "Advanced Composites Manufactured via Dry Powder Impregnation," in *ICCM12*, 1999.

[180] M. Wilczek, J. Bertling, and D. Hintemann, "Optimised technologies for cryogenic grinding," *International Journal of Mineral Processing*, vol. 74, no. SUPPL., pp. 425–434, 2004.

[181] J. Xu, C. Yi, X. Wang, and H. Zeng, "Preparation of GF/PVC Composites Using Aqueous Suspension Impregnation Technique: the Interfacial Issues," in *ICCM12 Conference*, 1999.

[182] S. T. Peters, *Handbook of Composites*, 2nd ed. Springer Science & Business Media, 2013.

[183] F. C. Campbell, *Structural Composite Materials*, 1st ed. ASM International, 2010.

[184] P.-E. Bourban, N. Bernet, J.-E. Zanetto, and J.-A. E. Månson, "Material phenomena controlling rapid processing of thermoplastic composites," *Composites Part A: Applied Science and Manufacturing*, vol. 32, pp. 1045–1057, 2001.

[185] M. D. Wakeman and C. D. Rudd, "Compression Molding of Thermoplastic Composites," *Comprehensive Composite Materials*, pp. 915–963, 2000.

[186] H. Parton and I. Verpoest, "In situ polymerization of thermoplastic composites based on cyclic oligomers," *Polymer Composites*, vol. 26, no. 1, pp. 60–65, Feb. 2005.

[187] K. van Rijswijk, S. Lindstedt, D. P. N. Vlasveld, H. E. N. Bersee, and a. Beukers, "Reactive processing of anionic polyamide-6 for application in fiber composites: A comparitive study with melt processed polyamides and nanocomposites," *Polymer Testing*, vol. 25, no. 7, pp. 873–887, Oct. 2006.

[188] H. Parton, J. Baets, P. Lipnik, B. Goderis, J. Devaux, and I. Verpoest, "Properties of poly(butylene terephthatlate) polymerized from cyclic oligomers and its composites," *Polymer*, vol. 46, no. 23, pp. 9871–9880, Nov. 2005.

[189] K. van Rijswijk and H. E. N. Bersee, "Reactive processing of textile fiber-reinforced thermoplastic composites – An overview," *Composites Part A: Applied Science and Manufacturing*, vol. 38, no. 3, pp. 666–681, Mar. 2007.

[190] A. Burkhart and D. Cramer, "Feasibility of Continuous-Fibre Reinforced Thermoplastic Tailored Blanks for Automotive Applications," 2003.

[191] N. O. Cabrera, C. T. Reynolds, B. Alcock, and T. Peijs, "Non-isothermal stamp forming of continuous tape reinforced all-polypropylene composite sheet," *Composites Part A: Applied Science and Manufacturing*, vol. 39, no. 9, pp. 1455–1466, Sep. 2008.

[192] J. P. Nunes, A. M. Brito, A. S. Pouzada, and C. A. Bernardo, "Isothermal and Non-Isothermal Consolidation of Carbon Fiber Towpregs," *Polymer Composites*, vol. 22, no. 1, pp. 71 – 79, 2001.

[193] R. Törnqvist, P. Sunderland, and J. A. . Månson, "Non-isothermal process rheology of thermoplastic composites for compression flow moulding," *Composites Part A: Applied Science and Manufacturing*, vol. 31, no. 9, pp. 917–927, Sep. 2000.

[194] S. . Jespersen, F. Baudry, D. Schmäh, M. D. Wakeman, V. Michaud, P. Blanchard, R. E. Norris, and J. -a. E. Månson, "Rapid Processing of Net-Shape Thermoplastic Planar-Random Composite Preforms," *Applied Composite Materials*, vol. 16, no. 1, pp. 55–71, Jan. 2009.

[195] K. Giannadakis, M. Szpieg, and J. Varna, "Mechanical Performance of a Recycled Carbon Fibre/PP Composite," *Experimental Mechanics*, vol. 51, no. 5, pp. 767–777, Jun. 2010.

[196] B. Maringgal, K. Abdau, A. Ali, R. Janius, M. Faizal, and S. Kamaruddin, "Optimization of Compression Moulding Temperature for Polypropylene Materials," *Materials Testing*, vol. 53, no. 5, pp. 280–284, 2011.

[197] M. D. Wakeman, C. D. Rudd, T. A. Cain, R. Brooks, and A. C. Long, "Compression moulding of glass and polypropylene composites for optimised macro- and micro-mechanical properties . 4 : Technology demonstrator - a door cassette structure," *Composites Science and Technology*, vol. 60, pp. 1901 – 1918, 2000.

[198] C. Santulli, R. Brooks, C. D. Rudd, and A. C. Long, "Influence of microstructural voids on the mechanical and impact properties in commingled E-glass/polypropylene thermoplastic composites," *Proceedings of the Institution of Mechanical Engineers, Part L: Journal of Materials Design and Applications*, vol. 216, no. 2, pp. 85–100, Apr. 2002.

[199] C. Santulli, R. Brooks, A. C. Long, N. A. Warrior, and C. D. Rudd, "Impact properties of compression moulded commingled E-glass–polypropylene composites," *Plastics, Rubber and Composites*, vol. 31, no. 6, pp. 270–277, Jun. 2002.

[200] M. D. Wakeman, T. a. Cain, C. D. Rudd, R. Brooks, and a. C. Long, "Compression moulding of glass and polypropylene composites for optimised macro- and micro-mechanical properties II. Glass-mat-reinforced thermoplastics," *Composites Science and Technology*, vol. 59, no. 5, pp. 709–726, Apr. 1999.

[201] M. D. Wakeman, P. Blanchard, and J.-A. E. Månson, "Void Evolution During the Stamp-Forming of Thermoplastic Composites," in *ICCM15*, 2005, no. July.

[202] M. D. Wakeman, T. A. Cain, C. D. Rudd, R. Brooks, and A. C. Long, "Compression Moulding of Sandwich Structures of GMTs and Co-mingled Materials for Optimised Macro and Micro Mechanical Properties," in *ICCM11*, 1997.

[203] N. Bernet, V. Michaud, P.-E. Bourban, and J.-A. E. Månson, "Commingled yarn composites for rapid processing of complex shapes," *Composites Part A: Applied Science and Manufacturing*, vol. 32, pp. 1613–1626, 2001.

References

[204] C. D. Rudd, *Composites for Automotive Applications*, 1st ed. iSmithers Rapra Publishing, 2000.

[205] E. Haque, P. Bristow, and H. Giles, "Processing of Glass Fiber Mat Reinforced Thermoplastic COmposites," in *SPE/ANTEC 2001*, 2001.

[206] Y. Leterrier and C. G'Sell, "Formation and Elimination of Voids During the Processing of Thermoplastic Matrix Composites," *Polymer Composites*, vol. 15, no. 2, pp. 101–105, 1994.

[207] G. Jiang, S. J. Pickering, G. S. Walker, K. H. Wong, and C. D. Rudd, "Surface characterisation of carbon fibre recycled using fluidised bed," *Applied Surface Science*, vol. 254, no. 9, pp. 2588–2593, Feb. 2008.

[208] J. L. Thomason, "On the application of Weibull analysis to experimentally determined single fibre strength distributions," *Composites Science and Technology*, vol. 77, pp. 74–80, Mar. 2013.

[209] H. L. H. Yip, S. J. Pickering, and C. D. Rudd, "Characterisation of carbon fibres recycled from scrap composites using fluidised bed process," *Plastics, Rubber and Composites*, vol. 31, no. 6, pp. 278–282, Jun. 2002.

[210] I. J. Davies, "Empirical correction factor for the best estimate of Weibull modulus," *Journal of Materials Science Letters*, vol. 20, pp. 997–999, 2001.

[211] H. Viswanathan, M. A. Rooke, and P. M. A. Sherwood, "X-ray Photoelectron Spectroscopic Studies of Carbon Fiber Surfaces . 21 . Comparison of Carbon Fibers Electrochemically Oxidized in Acid using Achromatic and Monochromatic XPS," *Surface and Interface Analysis*, vol. 25, no. January, pp. 409–417, 1997.

[212] G. Jiang, S. Pickering, E. Lester, T. Turner, K. Wong, and N. Warrior, "Characterisation of carbon fibres recycled from carbon fibre/epoxy resin composites using supercritical n-propanol," *Composites Science and Technology*, vol. 69, no. 2, pp. 192–198, Feb. 2009.

[213] J.-C. Chen and C.-G. Chao, "Numerical simulation and experimental investigation for design of a carbon fiber tow pneumatic spreading system," *Carbon*, vol. 43, no. 12, pp. 2514–2529, Oct. 2005.

[214] M. S. Irfan, V. R. Machavaram, R. S. Mahendran, N. Shotton-Gale, C. F. Wait, M. a. Paget, M. Hudson, and G. F. Fernando, "Lateral spreading of a fiber bundle via mechanical means," *Journal of Composite Materials*, vol. 46, no. 3, pp. 311–330, Nov. 2011.

[215] A. Miller, C. Wei, and A. G. Gibson, "Manufacture of Polyphenylene Sulfide (PPS) Matrix Composites via the Powder Impregnation Route," *Composites Part A: Applied Science and Manufacturing*, vol. 27A, pp. 49–56, 1996.

[216] G. Jannerfeldt, R. Törnqvist, N. Rambert, L. Boogh, and J.-A. E. Månson, "Matrix Modification for Improved Reinforcement Effectiveness in Polypropylene / Glass Fibre Composites," *Applied Composite Materials*, vol. 8, pp. 327–341, 2001.

[217] L. Yang, J. L. Thomason, and W. Zhu, "The influence of thermo-oxidative degradation on the measured interface strength of glass fibre-polypropylene," *Composites Part A: Applied Science and Manufacturing*, vol. 42, no. 10, pp. 1293–1300, Oct. 2011.

[218] D. A. Biro, P. Mclean, and Y. Deslandes, "Characterization of Carbon Fiber-Epoxy Interfaces," *Polymer Engineering & Science*, vol. 37, no. 17, pp. 1250–1256, 1991.

[219] J. He, Y. Huang, L. Liu, and H. Cao, "Controlled interface between carbon fiber and epoxy by molecular self-assembly method," *Materials Chemistry and Physics*, vol. 99, pp. 388–393, 2006.

[220] L. Gonon, A. Momtaz, D. Van Hoyweghen, B. Chabert, J. F. Gérard, and R. Gaertner, "Physico-Chemical and micromechanical analysis of the interface in a poly(phenylene sulfide)/glass fiber composite—a microbond study," *Polymer Composites*, vol. 17, no. 2, pp. 265–274, 1996.

[221] W. B. Liu, S. Zhang, L. F. Hao, W. C. Jiao, F. Yang, X. F. Li, and R. G. Wang, "Properties of carbon fiber sized with poly(phthalazinone ether ketone) resin," *Journal of Applied Polymer Science*, pp. 3702–3709, 2012.

[222] X. Wang, D. Xu, H.-Y. Liu, H. Zhou, Y.-W. Mai, J. Yang, and E. Li, "Effects of thermal residual stress on interfacial properties of polyphenylene sulphide/carbon fibre (PPS/CF) composite by microbond test," *Journal of Materials Science*, pp. 1–10, 2015.

[223] L. P. Hann and D. E. Hirt, "Simulating the microbond technique with macrodroplets," *Composites Science and Technology*, vol. 54, no. 4, pp. 423–430, Jan. 1995.

[224] J. L. Thomason and L. Yang, "Interfacial Strength in Fibre Reinforced Thermoplastics," in *Interfaces and Interphases in Multicomponent Materials*, 2010, no. September.

[225] Z. Dai, F. Shi, B. Zhang, M. Li, and Z. Zhang, "Effect of sizing on carbon fiber surface properties and fibers/epoxy interfacial adhesion," *Applied Surface Science*, vol. 257, no. 15, pp. 6980–6985, May 2011.

[226] L. Yao, M. Li, Q. Wu, Z. Dai, Y. Gu, Y. Li, and Z. Zhang, "Comparison of sizing effect of T700 grade carbon fiber on interfacial properties of fiber / BMI and fiber / epoxy," *Applied Surface Science*, vol. 263, pp. 326–333, 2012.

[227] L. Chun, P. Chen, Q. Yu, Z. Ding, Z. Lin, and W. Li, "Interfacial Adhesion of PLasma-Treated Carbon Fiber/Poly(phthalazinone ether sulfone ketone) Composite," *Journal of Applied Polymer Science*, no. 106, pp. 1733–1741, 2007.

[228] Q. Bénard, M. Fois, and M. Grisel, "Roughness and fibre reinforcement effect onto wettability of composite surfaces," *Applied Surface Science*, vol. 253, no. 10, pp. 4753–4758, Mar. 2007.

[229] W. Song, A. Gu, G. Liang, and L. Yuan, "Effect of the surface roughness on interfacial properties of carbon fibers reinforced epoxy resin composites," *Applied Surface Science*, vol. 257, no. 9, pp. 4069–4074, 2011.

References

[230] Y. . Huang, L. Liu, J. . Qiu, and L. Shao, "Influence of ultrasonic treatment on the characteristics of epoxy resin and the interfacial property of its carbon fiber composites," *Composites Science and Technology*, vol. 62, no. 16, pp. 2153–2159, Dec. 2002.

[231] L. F. M. da Silva, *Handbook of Adhesion Technology*, 1st ed. Springer Science & Business Media, 2011.

[232] M. Szpieg, K. Giannadakis, and J. Varna, "Time-dependent Nonlinear Behavior of Recycled Polypropylene in High Tensile Stress Loading," *Journal of Thermoplastic Composite Materials*, vol. 24, no. 5, pp. 625–652, 2011.

[233] M. D. Wakeman, T. A. Cain, C. D. Rudd, R. Brooks, and A. C. Long, "Compression moulding of glass and polypropylene composites for optimised macro- and micro-mechanical properties 3. Sandwich structures of GMTS and commingled fabrics," *Composites Science and Technology*, vol. 59, no. 8, pp. 1153–1167, Jun. 1999.

[234] M. Chandra and S. K. Roy, *Plastics Technology Handbook*, 4th ed. CRC Press, 2006.

[235] L. Shibryaeva, "Thermal Oxidation of Polypropylene and Modified Polypropylene–Structure Effects," in *Polypropylene*, 1st ed., InTech, 2012.

[236] H. J. Oswald and E. Turi, "The Deterioration of Polypropylene," *Polymer Engineering and Science*, no. July, pp. 152–158, 1965.

[237] T. Bayerl, M. Brzeski, M. Martinez-Tafalla, R. Schledjewski, and P. Mitschang, "Thermal degradation analysis of short-time heated polymers," *Journal of Thermoplastic Composite Materials*, pp. 1–25, 2013.

[238] B. Singh and N. Sharma, "Mechanistic implications of plastic degradation," *Polymer Degradation and Stability*, vol. 93, no. 3, pp. 561–584, 2008.

[239] C. P. Beetz Jr, "The Analysis of Carbon Fibre Strength Distributions Exhibiting Multiple Modes of Failure," *Fibre Science and Technology*, vol. 16, no. 1, pp. 42–59, 1982.

[240] K. Naito, J. M. Yang, Y. Tanaka, and Y. Kagawa, "The effect of gauge length on tensile strength and Weibull modulus of polyacrylonitrile (PAN)- and pitch-based carbon fibers," *Journal of Materials Science*, vol. 47, no. 2, pp. 632–642, 2012.

[241] W. J. Padgett, S. D. Durham, and A. M. Mason, "Weibull Analysis of the Strength of Carbon Fibres Using Linear and Power Law Models for the Length Effect," *Journal of Composite Materials*, vol. 29, no. 14, pp. 1873–1884, 1995.

[242] P. Zinck, M. F. Pays, R. Rezakhanlou, J. F. Gerard, V. Cedex, and C. De Recherche, "Mechanical characterisation of glass fibres as an indirect analysis of the effect of surface treatment," vol. 4, pp. 2121–2133, 1999.

[243] L. Meng, D. Fan, Y. Huang, Z. Jiang, and C. Zhang, "Comparison studies of surface cleaning methods for PAN-based carbon fibers with acetone, supercritical acetone and subcritical alkali aqueous solutions," *Applied Surface Science*, vol. 261, pp. 415–421, 2012.

[244] K. L. Pickering and T. L. Murray, "Weak link scaling analysis of high-strength carbon fibre," *Composites Part A: Applied Science and Manufacturing*, vol. 30, no. December 1997, pp. 1017–1021, 1999.

[245] B. Gabbitas, J. Adams, and P. Marshall, "Failure characteristics in carbon / epoxy composite tows," *Composites Part A*, vol. 27A, pp. 1183–1194, 1996.

[246] E. M. Asloun, J. B. Donnet, G. Guilpain, M. Nardin, and J. Schultz, "On the Estimation of the Tensile Strength of Carbon Fibres at Short Lengths," *Journal of Materials Science*, vol. 24, no. 10, pp. 3504–3510, 1989.

[247] T. Jung, R. V Subramanian, and V. S. Manoranjan, "Prediction of Fiber Strength At the Critical Length - A Simulation Theory and Experimental-verification For Bimodally Distributed Carbon-fiber Strengths," *Journal of Materials Science*, vol. 28, no. 16, pp. 4489–4496, 1993.

[248] P. Zinck, M. F. Pays, R. Rezakhanlou, "Extrapolation techniques at short gauge lengths based on the weakest link concept for fibres exhibiting multiple failure modes," *Philosophical Magazine A*, vol. 79, no. 9, pp. 2103–2122, 1999.

[249] J. Watanabe, F. Tanaka, H. Okuda, and T. Okabe, "Tensile Strength Distribution of Carbon Fibres at Short Gauge Lengths," *Advanced Composite Materials*, vol. 23, pp. 535–550, 2014.

[250] C. Lu, R. Danzer, and F. D. Fischer, "Influence of Threshold Stress on the Estimation of Weibull Statistics," *Journal of American Ceramic Society*, vol. 42, pp. 1640–1642, 2002.

[251] A. P. Kettle, A. J. Beck, L. O'Toole, F. R. Jones, and R. D. Short, "Plasma polymerisation for molecular engineering of carbon-fibre surfaces for optimised composites," *Composites Science and Technology*, vol. 57, no. 8, pp. 1023–1032, Jan. 1997.

[252] S. M. Lee, *Handbook of Composite Reinforcements*, 1st ed. John Wiley & Sons, 1992.

[253] R. J. Diefendorf and E. W. Tokarsky, "The Relationship of Structure to Properties in Graphite Fibers, Part I," 1971.

[254] H. Zhang, Z. Zhang, and C. Breidt, "Comparison of short carbon fibre surface treatments on epoxy composites," *Composites Science and Technology*, vol. 64, no. 13–14, pp. 2021–2029, Oct. 2004.

[255] T. A. Langston and R. D. Granata, "Influence of nitric acid treatment time on the mechanical and surface properties of high-strength carbon fibers," *Journal of Composite Materials*, vol. 48, no. 3, pp. 259–276, Jan. 2013.

[256] C. A. Baillie, J. F. Watts, J. E. Castle, and M. G. Bader, "The Influence of Chemistry on the Adhesion at the Interface of Carbon/Epoxy Composites," *Composites Science and Technology*, vol. 48, no. 1–4, pp. 97–102, 1993.

[257] S. L. Gao and E. Mäder, "Characterisation of interphase nanoscale property variations in glass fibre reinforced polypropylene and epoxy resin composites," *Composites - Part A: Applied Science and Manufacturing*, vol. 33, no. 4, pp. 559–576, 2002.

References

[258] Y. Wang and T. H. Hahn, "AFM characterization of the interfacial properties of carbon fiber reinforced polymer composites subjected to hygrothermal treatments," *Composites Science and Technology*, vol. 67, no. 1, pp. 92–101, 2007.

[259] S. N. Magonov, V. Elings, and M.-H. Whangbo, "Phase imaging and stiffness in tapping-mode atomic force microscopy," *Surface Science*, vol. 375, no. 2–3. pp. L385–L391, 1997.

[260] G. Jiang, W. H. Wong, S. J. Pickering, C. D. Rudd, and G. S. Walker, "Study of a Fluidised Bed Process for Recycling Carbon Fibre From Polymer Composites," in *Proceedings of 7th World Congress for Chemical Engineering*, 2005.

[261] M. Li, Y. Gu, Y. Liu, Y. Li, and Z. Zhang, "Interfacial improvement of carbon fiber/epoxy composites using a simple process for depositing commercially functionalized carbon nanotubes on the fibers," *Carbon*, vol. 52, pp. 109–121, Feb. 2013.

[262] S. H. Han, H. J. Oh, and S. S. Kim, "Evaluation of the impregnation characteristics of carbon fiber-reinforced composites using dissolved polypropylene," *Composites Science and Technology*, vol. 91, pp. 55–62, Jan. 2014.

[263] P. E. McMahon and L. Ying, "Effects of Fiber/Matrix Interactions on the Properties of Graphite/Epoxy Composites," 1982.

[264] P. P. Parlevliet, H. E. N. Bersee, and A. Beukers, "Residual stresses in thermoplastic composites – a study of the literature. Part III: Effects of thermal residual stresses," *Composites Part A: Applied Science and Manufacturing*, vol. 38, no. 6, pp. 1581–1596, Jun. 2007.

[265] Y. Yang, Y. Zhao, Y. Li, Q. Dong, and D. Chen, "Effect of sizing on the interfacial shear strength of carbon fiber/epoxy resin monofilament composite," *Journal of Wuhan University of Technology-Mater. Sci. Ed.*, vol. 29, no. 3, pp. 483–487, 2014.

[266] R. L. Zhang, Y. D. Huang, D. Su, L. Liu, and Y. R. Tang, "Influence of sizing molecular weight on the properties of carbon fibers and its composites," *Materials and Design*, vol. 34, pp. 649–654, 2012.

[267] K. K. C. Ho, G. Kalinka, M. Q. Tran, N. V. Polyakova, and A. Bismarck, "Fluorinated carbon fibres and their suitability as reinforcement for fluoropolymers," *Composites Science and Technology*, vol. 67, no. 13, pp. 2699–2706, Oct. 2007.

[268] K. K. C. Ho, A. F. Lee, and A. Bismarck, "Fluorination of carbon fibres in atmospheric plasma," *Carbon*, vol. 45, no. 4, pp. 775–784, 2007.

[269] Y.-H. Lu, M.-S. Zhan, and W.-H. Zheng, "Preparation and Properties of M40 Carbon Fiber-Reinforced Thermoplastic Polyimide Composites," *Journal of Thermoplastic Composite Materials*, vol. 21, no. 6, pp. 525–542, Nov. 2008.

[270] C. Cazeneuve, J. E. Castle, and J. F. Watts, "The structure of the interface in carbon fibre composites by scanning Auger microscopy," *Journal of Materials Science*, vol. 25, no. 4, pp. 1902–1908, 1990.

[271] J. B. Donnet and R. C. Bansal, *Carbon Fibers*, 3rd ed. CRC Press, 1998.

[272] G. Ozkoc, G. Bayram, and E. Bayramli, "Effects of polyamide 6 incorporation to the short glass fiber reinforced ABS composites: An interfacial approach," *Polymer*, vol. 45, pp. 8957–8966, 2004.

[273] J. Li and C. L. Cai, "The carbon fiber surface treatment and addition of PA6 on tensile properties of ABS composites," *Current Applied Physics*, vol. 11, pp. 50–54, 2011.

[274] T. Ramanathan, A. Bismarck, E. Schulz, and K. Subramanian, "Investigation of the influence of acidic and basic surface groups on carbon fibres on the interfacial shear strength in an epoxy matrix by means of single-fibre pull-out test," *Composites Science and Technology*, vol. 61, pp. 599–605, 2001.

[275] W. D. Bascom, K.-J. Yon, R. M. Jensen, and L. Cordner, "The Adhesion of Carbon Fibers to Thermoset and Thermoplastic Polymers," *The Journal of Adhesion*, vol. 34, pp. 79–98, 1990.

[276] T. Ramanathan, A. Bismarck, E. Schulz, and K. Subramanian, "The use of a single-fiber pull-out test to investigate the influence of acidic and basic surface groups on carbon fibres on the adhesion to PPS and matrix morphology dependent fracture behaviour," *Composites Science and Technology*, 2001.

[277] H. P. Boehm, "Surface oxides on carbon and their analysis: A critical assessment," *Carbon*, vol. 40, no. 2, pp. 145–149, 2002.

[278] P. Mutjé, M. E. Vallejos, J. Gironès, F. Vilaseca, a. López, J. P. López, and J. a. Méndez, "Effect of maleated polypropylene as coupling agent for polypropylene composites reinforced with hemp strands," *Journal of Applied Polymer Science*, vol. 102, no. 1, pp. 833–840, 2006.

[279] E. Franco-Marques, J. A. Mendez, M. A. Pelach, F. Vilaseca, J. Bayer, and P. Mutje, "Influence of coupling agents in the preparation of polypropylene composites reinforced with recycled fibres.pdf," *Chemical Engineering Journal*, vol. 166, pp. 1170–1178, 2011.

[280] A. Grozdanov and G. Bogoeva-Gaceva, "Carbon Fibers/Polyamide 6 Composites Based on Hybrid Yarns," *Journal of Thermoplastic Composite Materials*, vol. 23, no. 1, pp. 99–110, Jun. 2009.

[281] S. Ryu, B. Park, and S. Park, "XPS Analysis of Carbon Fiber Surfaces-Anodized and Interfacial Effects in Fiber-Epoxy Composites.," *Journal of colloid and interface science*, vol. 215, no. 1, pp. 167–169, 1999.

[282] R. L. Zhang, Y. D. Huang, L. Liu, Y. R. Tang, D. Su, and L. W. Xu, "Effect of the molecular weight of sizing agent on the surface of carbon fibres and interface of its composites," *Applied Surface Science*, vol. 257, no. 6, pp. 1840–1844, Jan. 2011.

[283] W. H. Lee, J. G. Lee, and P. J. Reucroft, "XPS study of carbon fiber surfaces treated by thermal oxidation in a gas mixture of O 2 /(O 2 ‡ N 2)," *Applied Surface Science*, vol. 171, no. 1–2, pp. 136–142, 2001.

[284] S. Al-Malaika, *Reactive Modifiers for Polymers*, 1st ed. Springer Science & Business Media, 1997.

References

[285] F. W. J. van Hattum, J. P. Nunes, and C. A. Bernardo, "A theoretical and experimental study of new towpreg-based long fibre thermoplastic composites," *Composites Part A: Applied Science and Manufacturing*, vol. 36, no. 1, pp. 25–32, Jan. 2005.

[286] V. B. Gupta, R. K. Mittal, and P. K. Sharma, "Some Studies on Glass Fiber-Reinforced Polypropylene. Part II: Mechanical Properties and Their Dependence on Fiber Length, Interfacial Adhesion, and Fiber Dispersion," *Polymer Composites*, vol. 10, no. 1, 1989.

[287] H. A. Rijsdijk, M. Contant, and A. A. J. M. Peijs, "Continuous-Glass-Fibre-Reinforced Polypropylene Composites: I. Influence of Maleic-Anhydride-Modified Polypropylene on Mechanical Properties," *Composites Science and Technology*, vol. 48, pp. 161–172, 1993.

[288] H. Huang and R. Talreja, "Effects of void geometry on elastic properties of unidirectional fiber reinforced composites," *Composites Science and Technology*, vol. 65, no. 13, pp. 1964–1981, 2005.

[289] E. F. Olster, "Effect of Voids on Graphite Fiber Reinforced Composites," 1997.

[290] J. Lindhagen and L. Berglund, "Microscopical Damage Mechanisms in Glass Fiber," *Journal of Applied Polymer Science*, vol. 69, pp. 1319–1327, 1997.

[291] C. Subramanian and S. Senthilvelan, "Development and preliminary performance evaluation of discontinuous fibre reinforced thermoplastic leaf spring," *Proceedings of the Institution of Mechanical Engineers, Part L: Journal of Materials: Design and Applications*, vol. 223, no. 3, pp. 131–142, Jul. 2009.

[292] W. J. Cantwell and J. Morton, "The significance of damage and defects and their detection in composite materials: A review," *The Journal of Strain Analysis for Engineering Design*, vol. 27, no. 1, pp. 29–42, Jan. 1992.

[293] X. Xiao, "On the measurement of true fracture strain of thermoplastics materials," *Polymer Testing*, vol. 27, no. 3, pp. 284–295, May 2008.

[294] A. C. Long, C. E. Wilks, and C. D. Rudd, "Experimental characterisation of the consolidation of a commingled glass/polypropylene composite," *Composites Science and Technology*, vol. 61, no. 11, pp. 1591–1603, 2001.

[295] M. R. Piggott, "Mesomechanical Model for Fibre Composites: The Role of the Inerface," 1992.

[296] A. Levy and P. Hubert, "Interstrand void content evolution in compression moulding of randomly oriented strands (ROS) of thermoplastic composites," *Composites Part A: Applied Science and Manufacturing*, vol. 70, pp. 121–131, 2015.

[297] S. Pimenta, S. T. Pinho, P. Robinson, K. H. Wong, and S. J. Pickering, "Mechanical analysis and toughening mechanisms of a multiphase recycled CFRP," *Composites Science and Technology*, vol. 70, no. 12, pp. 1713–1725, Oct. 2010.

[298] C. Qian, L. T. Harper, T. A. Turner, and N. A. Warrior, "Notched behaviour of discontinuous carbon fibre composites: Comparison with quasi-isotropic non-crimp

fabric," *Composites Part A: Applied Science and Manufacturing*, vol. 42, no. 3, pp. 293–302, Mar. 2011.

[299] M. Szpieg, M. Wysocki, and L. Asp, "Mechanical performance and modelling of a fully recycled modified CF/PP composite," *Journal of Composite Materials*, vol. 46, no. 12, pp. 1503–1517, 2012.

[300] J. C. Halpin and J. L. Kardos, "The Halpin-Tsai Equations: A Review," *Polymer Engineering and Science*, vol. 16, no. 5, pp. 344–352, 1976.

[301] H. M. El-Dessouky and C. A. Lawrence, "Ultra-lightweight carbon fibre/thermoplastic composite material using spread tow technology," *Composites Part B: Engineering*, vol. 50, pp. 91–97, 2013.

[302] S. K. Garkhail, R. W. H. Heijenrath, and T. Peijs, "Mechanical Properties of Natural-Fibre-Mat- Reinforced Thermoplastics based on Flax Fibres and Polypropylene," *Applied Composite Materials*, vol. 7, pp. 351–372, 2000.

[303] K. Johanson, L. T. Harper, M. S. Johnson, and N. A. Warrior, "Heterogeneity of discontinuous carbon fibre composites: Damage initiation captured by Digital Image Correlation," *Composites Part a*, vol. 68, pp. 304–312, 2014.

[304] H. . Bijsterbosch and R. J. Gaymans, "Polyamide 6-Long Glass Fiber Injection Moldings," *Polymer Composites*, vol. 16, no. 5, p. 366, 1995.

[305] S. Y. Fu, B. Lauke, E. Mader, X. Hu, and C. Y. Yue, "Fracture resistance of short-glass-fiber-reinforced and short-carbon-fiber-reinforced polypropylene under Charpy impact load and its dependence on processing," *Jounral of Materials Processing Technology*, vol. 90, pp. 501–507, 1999.

[306] R. Luchoo, L. T. Harper, M. D. Bond, N. A. Warrior, and A. Dodworth, "Net shape spray deposition for compression moulding of discontinuous fibre composites for high performance applications," *Plastics, Rubber and Composites*, vol. 39, no. 3, pp. 216–231, 2010.

[307] J. K. Wells and P. W. R. Beaumont, "Debonding and pull-out processes in fibrous composites," *Journal of Materials Science*, vol. 20, no. 4, pp. 1275–1284, 1985.

[308] M. Ashby, "Material Indices," in *Materials Selection in Mechanical Design*, Butterworth-Heinemann, 2010, pp. 407–412.

[309] A. Güllü, A. Özdemir, and E. Özdemir, "Experimental investigation of the effect of glass fibres on the mechanical properties of polypropylene (PP) and polyamide 6 (PA6) plastics," *Materials & Design*, vol. 27, no. 4, pp. 316–323, Jan. 2006.

[310] F. Truckenmuller and H. G. Fritz, "Injection Molding of Long Fiber-Reinforced Thermoplastics: A Comparison of Extruded and Pultruded Materials With Direct Addition of Roving Strands," *Polymer Engineering and Science*, vol. 31, no. 18, pp. 1316–1329, 1991.

[311] J. Denault, T. Vu-Khanh, and B. Foster, "Tensile properties of injection molded long fiber thermoplastic composites," *Polymer Composites*, vol. 10, no. 5, pp. 313–321, Oct. 1989.

References

[312] P.A. Templeton, "Strength Predictions of Injection Moulded Compounds," *Journal of Reinforced Plastics and Composites*, vol. 9, pp. 210–225, 1996.

[313] S. Rahmanian, K. S. Thean, A. R. Suraya, M. A. Shazed, M. A. Mohd Salleh, and H. M. Yusoff, "Carbon and glass hierarchical fibers: Influence of carbon nanotubes on tensile, flexural and impact properties of short fiber reinforced composites," *Materials and Design*, vol. 43, pp. 10–16, 2013.

[314] N. Eguemann, L. Giger, K. Masania, C. Dransfeld, F. Thiebaud, and D. Perreux, "Processing and Characterisation of Carbon Fibre Reinforced PEEK with Discontinuous Architecture," in *16th European Conference on Composite Materials*, 2014.

[315] M. Li, X. Wen, J. Liu, and T. Tang, "Synergetic effect of epoxy resin and maleic anhydride grafted polypropylene on improving mechanical properties of polypropylene / short carbon fiber composites," *Composites Part A*, vol. 67, pp. 212–220, 2014.

[316] N. G. Karsli and A. Aytac, "Effects of maleated polypropylene on the morphology, thermal and mechanical properties of short carbon fiber reinforced polypropylene composites," *Materials & Design*, vol. 32, no. 7, pp. 4069–4073, Aug. 2011.

[317] C. Bowland, "A Formulation Study of Long Fiber Thermoplastic Polypropylene (Part 2): The Effects of Coupling Agent Type and Properties."

[318] R. Chaudhari, M. Reif, O. Geiger, F. Henning, A. Diehl, A. Terenzi, and C. Technologie, "E-Coat Sustainable Long-Fiber Thermoplastic Composites For Structural Automotive Applications."

[319] C. Bowland, "A Formulation Study of Long Fiber Thermoplastic Polypropylene (Part 1): The Effects of Coupling Agent Glass Content and Resin Properties on the Mechanical Properties," in *8th Annual Automotive Composites Conference and Exhibition*, 2008, no. Part 1.

[320] P. E. W. Krause, F. Henning, S. Troster, O. Geiger, "LFT-D – A Process Technology for Large Scale Production of Fiber Reinforced Thermoplastic Components," *Journal of Thermoplastic Composite Materials*, vol. 16, pp. 289–302, 2003.

[321] L. T. Harper, "Discontinuous Carbon Fibre Composites for Automotive Applications," 2006.

[322] T. A. Turner, L. T. Harper, N. A. Warrior, and C. D. Rudd, "Low cost carbon fibrebased automotive body panel systems: a performance and manufacturing cost comparison," *Proceedings of the Institution of Mechanical Engineers, Part D: Journal of Automobile Engineering*, vol. 222, no. 1, pp. 53–63, Jan. 2008.

[323] A. C. Caba, "Characterization of Carbon Mat Thermoplastic Composites : Flow and Mechanical Properties," Virginia Polytechnic Institute, 2005.

[324] K. Stoeffler, S. Andjelic, N. Legros, J. Roberge, and S. B. Schougaard, "Polyphenylene sulfide (PPS) composites reinforced with recycled carbon fiber," *Composites Science and Technology*, vol. 84, pp. 65–71, 2013.

[325] M. Such, C. Ward, and K. Potter, "Aligned Discontinuous Fibre Composites: A Short History," *Journal of Multifunctional Composites*, vol. 2, no. 3, 2014.

[326] H. Edwards and N.P. Evans, "A method for the production of high quality aligned short fibre mats and their composites," in *Proceedings of ICCM-3*, 1980.

[327] M. R. Piggott, M. Ko, and H. Y. Chuang, "Aligned Short-Fibre Reinforced Thermosets: Experiments and Analysis Lend Little Support for Established Theory," *Composites Science and Technology*, vol. 48, no. 1–4, pp. 291–299, 1993.

[328] Z. A. Mohd Ishak, Y. W. Leong, M. Steeg, and J. Karger-Kocsis, "Mechanical properties of woven glass fabric reinforced in situ polymerized poly(butylene terephthalate) composites," *Composites Science and Technology*, vol. 67, no. 3–4, pp. 390–398, Mar. 2007.

[329] A. Paesano, D. Cohee, and G. R. Palmese, "Composite Materials Carbon-Fiber Reinforced Thermoplastic Materials for Rigidizable Space Systems," *Journal of Thermoplastic Composite Materials*, vol. 16, 2003.